SYNTHESIS AND STRUCTURAL STUDIES OF SUPRAMOLECULES USING *N*-HETEROCYCLIC LIGANDS

Ph.D. THESIS

by

SHIKHA NARANG

DEPARTMENT OF CHEMISTRY
INDIAN INSTITUTE OF TECHNOLOGY ROORKEE
ROORKEE-247 667 (INDIA)
JUNE, 2014

SYNTHESIS AND STRUCTURAL STUDIES OF SUPRAMOLECULES USING *N*-HETEROCYCLIC LIGANDS

A THESIS

Submitted in partial fulfilment of the requirements for the award of the degree of

DOCTOR OF PHILOSOPHY

in

CHEMISTRY

by

SHIKHA NARANG

DEPARTMENT OF CHEMISTRY
INDIAN INSTITUTE OF TECHNOLOGY ROORKEE
ROORKEE-247 667 (INDIA)
JUNE, 2014

INDIAN INSTITUTE OF TECHNOLOGY ROORKEE
ROORKEE

CANDIDATE'S DECLARATION

I hereby certify that the work which is being presented in the thesis entitled '**SYNTHESIS AND STRUCTURAL STUDIES OF SUPRAMOLECULES USING *N*-HETEROCYCLIC LIGANDS**' in partial fulfilment of the requirements for the award of the Degree of Doctor of Philosophy and submitted in the Department of Chemistry of the Indian Institute of Technology Roorkee, Roorkee is an authentic record of my own work carried out during a period from July, 2009 to June, 2014 under the supervision of Dr. Udai P. Singh, Professor, Department of Chemistry and Dr. Shailly Tomar, Associate Professor, Department of Biotechnology, Indian Institute of Technology Roorkee, Roorkee.

The matter presented in this thesis has not been submitted by me for the award of any other degree of this or any other Institute.

(SHIKHA NARANG)

This is to certify that the above statement made by the candidate is correct to the best of my knowledge.

(Shailly Tomar)
Supervisor

(Udai P. Singh)
Supervisor

Dated:

The Ph.D. Viva-Voce Examination of **Ms. Shikha Narang**, Research Scholar, has been held on..... .

Signature of Supervisors Chairman, SRC Signature of External Examiner

Head of the Department/Chairman, ODC

ABSTRACT

Design and supramolecular synthesis of the functional solid materials through non-covalent interaction could lead the prospect to find new supramolecular synthons which triggers the construction of potential intriguing architecture. It results in enhancing the physical properties of the bulk material without chemically modifying themselves.

Well known *N*-heterocyclic compounds such as pyrazole and pyridyl based ligands have attracted the researchers for the synthesis of new functional solid materials. The propensity of pyrazole and pyridine to acquire hydrogen from the acidic component has allowed these molecules to interact with H-donor as well as acceptor moieties in the multi-component system. Moreover, these molecules are potential ditopic ligands, which display diversity of coordination modes in the formation of metal complexes and distinct Supramolecular Organic Frameworks (SOFs) with different dimensionality (0D, 1D, 2D and 3D).

In the realm of crystal engineering, the component with both proton donor and acceptor might display an array of non-covalent interactions. In this context, the phosphonic acid which is less exploited as compare to carboxylic acid, possesses tetrahedral geometry with two ionisable hydrogen atoms and one acceptor atom has been employed in this thesis. Both coformers with H-donor and H-acceptor in *N*-heterocyclic ligands and phosphonic acid may lead to intriguing and potential architecture.

The **first** chapter of the thesis includes the brief introduction and literature survey regarding crystal engineering involved in the system acquiring *N*-heterocyclic ditopic ligand, phosphonic acid and metal complexes representing CO_2 adsorption followed by the brief description of the goal behind the presented work.

In **second** chapter of the thesis, a family of bispyrazole-phosphonate was synthesized and assessed the competitive hydrogen bonding interactions between different phosphonic acids possessing diverse functional group on it. The main aim for this work is to obtain the degree of control and reliability of the non-covalent interactions involved between the resulted series of bispyrazole-phosphonate system. Overall fourteen molecular complexes were obtained from two conformational flexible and one rigid bispyrazole separated by different groups present between two complementary pyrazoles i.e., 3,3',5,5'-tetramethyl-1H,1'H-4,4'-bipyrazole (BPz), methylenebis(3,5-dimethylpyrazole) (MBPz) and 1,2-bis(3,5-dimethyl-1H-pyrazol-4-yl)diazene,

(BPaz) with variety of phosphonic acids i.e., phenylphosphonic acid (H_2PPA), phosphonoacetic acid (H_2PAA), 3-phosphonopropionic acid (H_2PPRA), *tert*-butylphosphonic acid (H_2tBPA), etidronic acid (H_4EA), (1,4-phenylenebis(methylene))diphosphonic acid (H_4DPA) via synthon approach, among which twelve were salts and two were the co-crystals. X-ray analysis revealed that all compounds result in different supramolecular architecture with the formation of cyclic hydrogen bond motif as a structural motif. It was significant to note that instead of presence of carboxylic group on phosphonic acid in some salts, the synthon formation was observed merely by the phosphonic group and no synthon was formed by carboxylic group. However, besides the dimer formation, the most interesting feature of the supramolecular network of phosphonate salts of pyrazole is the formation of trimeric and extended trimeric (tetrameric) heterosynthons. Furthermore, the analysis of theoretically obtained interaction and synthon energy in the solid state for all the compounds deduced that the stability for salt involving the (1,4-phenylenebis(methylene))diphosphonic acid (DPA) is largest among all the salts. It was also pointed out that the occurrence of particular synthon having the higher stability is more. On the other hand, the thermal study revealed that the phosphonate salts of pyrazole analogues are stable upto 280 ºC which might be due to the presence of more strong interactions. As a consequence, it was concluded that the stability of all the compounds observed from DFT level energy was in agreement with the stability provided by TG analysis. Hence, the present study provides an enhanced understanding about the effects of substituents on the resulted supramolecular assembly and ended in the designing of new synthons.

The **third** chapter of the thesis deals with the formation of the molecular salts composed of (anthracen-9-ylmethyl)phosphonic acid (H_2APa) and 3,3',5,5'-tetramethyl-1H,1'H-4,4'-bipyrazole (BPz) and an assessment of formation of their several psuedopolymorphs (solvates) and ternary complexes was carried out. In other words, further enhancing the understanding of potential structural effect of different solvent molecules on phosphonic-pyrazole system was studied. To gain the profound knowledge of consistency of the non-covalent interactions, numerous solvates were synthesized to control the deprotonation of ionisable proton in presence of particular solvent molecule. Interestingly, all resulted in a salt formation with four type of different frameworks revealing host-guest hydrogen bonded assemblies where APaBPz assembled into a host and diversity of solvent molecules such as tetrahydrofuran (THF), dioxane, benzene, thiophene, nitromethane, nitrobenzene, thiophenol and

toluene remains inside the cavity as the guests. It is worth noting that all solvates retained the acid dimer even with the change in functional group present on the solvent molecule which substantiates that it is a robust synthon for the formation of the host-guest assembly. Besides, variety of new synthons was also observed. Notably, the bulky and aromatic moiety of the phosphonic acid with conformational flexibility changes its conformation in small magnitude depending upon the upcoming guest and probably be the reason for the different host-guest assemblies. Hence, X-ray data analysis showed the formation of π···π and C–H···π interactions were also responsible for the change in framework. Few ternary supramolecules were also produced from phenol, 2-nitrophenol, 4-nitrophenol and *p*-cresol with the guest molecule resided inside the cavity. However in presence of water molecule, the hydrated APaBPz system involves water molecules as the constituent of the framework; hence no such host-guest assembly is resulted. Therefore, the thermal study showed that the hydrated APaBPz system was found to be more stable solvate which decomposes at higher temperature. Additionally, a 0D Cu(II) based molecular complex, $[Cu_2(\mu_2\text{-}C_{15}H_{12}PO_3)_2(^{2,2'\text{-}}BPy)_2(H_2O)_2]((NO_3)_2.X)$ was also envisioned using newly synthesized ethyl hydrogen (anthracen-9-ylmethyl)phosphonate and 2,2'-bipyridine as an auxillary base in presence of triethylamine. Single crystal X-ray characterized metal complex revealed that the dinuclear assembly is comprised of two CuN_2O_3 square pyramidal at the two opposite corner connected through bridged CPO_3 tetrahedra of the phosphonate. However, the π-electron cloud of 2,2'-bipyridine and phosphonate ligands in the dinuclear assembly are chiefly accountable for the extension of 0D to 3D structure with a 1D channel. It is interested to note that the resulted metal complex undergo an important aspect of solid state transformation (crystal-amorphous-crystal transformation) which led to the formation of $Cu_2(\mu_2\text{-}C_{15}H_{12}PO_3)_2(^{2,2'\text{-}}BPy)_2(NO_3)_2]$.MeOH), neutral coordination complex from cationic coordination complex on external stimuli. Hence, the transformation of cationic metal complex to neutral metal complex based on anthracene-phosphonomonoester may show tunable luminescent behavior.

Besides pyrazole ligands, some pyridyl based ditopic ligands such as 2,2'-bipyridine, 4,4'-bipyridine, 1,10-phenanthroline and 4,2':6',4''-terpyridine were used for deducing its supramolecular behavior with tripodal phosphonic acid i.e., ((2,4,6-trimethylbenzene-1,3,5-triyl)tris(methylene))triphosphonic acid in **fourth** chapter. Overall total five different packing motifs were observed, mainly defined by the columns of tripodal phosphonic acid in all these resulted salts. Remarkably, this phosphonic acid showed two different conformations in the salts

depending upon the ditopic ligands used. On the other hand, X-ray data analysis disclosed that the two of the resulted salts showed an important feature of polymorphism in which one of the polymorph displays hydrogen bonded chain formed by triphosphonic and water via O–H···O interaction whereas in another polymorph, hydrogen bond is found between triphosphonic acid and water molecules ensuing in a continuous chain of water and one of the OH of the phosphonic acid. After analysis, it has been predicted that the latter complex permits the continuous proton transfer in the infinite chain of phosphonic and water molecules; hence it was presumed that it might show proton conductivity. Moreover, the resulted salts acquiring 4,4'-bipyridine, 1,10-phenanthroline showed the tendency to transform into another solid complex via SCSC transformation. Furthermore, some 2D MOFs were also ascertained with the newly synthesized conformationally flexible ditopic pyridine based ligand which may have appealing structural properties for the generation of soft porous materials, hence, eight isostructural 2D MOFs were successfully synthesized with variation in anions (NO_3^-, Cl^-, Br^-, I^-, SCN^-, ClO_4^-) coordinated to the metal ion M(II) (M = Cd^{2+}, Co^{2+}, Zn^{2+}, Eu^{2+}). Depending upon their particular size, the tuned pore size of MOFs can be used as the absorber for selective gases. Single crystal X-ray diffraction study reveals that all metal complexes possess similar structural features such as metal-coordination environments, network topologies, π···π interactions and exhibits a 2D uninodal of 4^4**-sql** topology with slightly tuned cavity. All complexes except the complex with ClO_4^- anion exhibited [[$M(dmpt)_2(A)_2$]·X] as the secondary building unit (SBU), building the 2D layer which is extended into three-dimensional (3D) framework. On the other hand, the effect of weak interactions involved in the structural dynamics of the systems has also been studied. While the MOF with ClO_4^- anion displayed the extended supramolecular large rectangular cavities of dimension 13.9 X 6.4 $Å^2$, accommodated by uncoordinated ClO_4^- anions, $CHCl_3$ molecule and coordinated DMSO molecule from Cd(II). Moreover, gas adsorption study of these complexes demonstrated that the resulted complexes showed the selective adsorption of CO_2 gas over N_2 gas. Albeit, the CO_2 uptake shown by these compounds is modest but comparatively the complexes with anion NO_3^- and SCN^- shows the higher CO_2 uptake.

The material and reagents, synthetic procedures, experimental details, some spectroscopic measurements for all the compounds including the salts, co-crystals and metal complexes reported in chapter 2-4 have been provided in chapter **five** of the thesis.

ACKNOWLEDGEMENT

It's the gracious blessing of Almighty God that has provided me the opportunity to do this work, strength to overcome all the difficulties and helped me in preceding the right path to acquire few pebbles of knowledge from its seashore.

In the beginning, I would like to express my great indebtedness and sincere thanks to **Prof. Udai P. Singh**, Department of Chemistry, IIT Roorkee, for his valuable guidance, advices and time for making my PhD life go so smoothly. I am really thankful for his steady support, encouragement and enthusiasm for the work. The freedom and complete faith that he bestowed on me throughout, has inculcated a deep sense of responsibility to achieve the desired objectives of the project. No words articulate to acknowledge for his helpful discussions and ideas throughout my PhD work. I am also thankful to my co-guide **Dr. Shailly Tomar**, Department of Biotechnology, IIT Roorkee, for her constant support and encouragement throughout my PhD tenure.

I am highly grateful to **Prof. Anil Kumar** (the present), **Prof. V. K. Gupta** and **Prof. Kamaluddin**, the former Heads of the Department of Chemistry, Indian Institute of Technology Roorkee, for providing the necessary equipments, various facilities and environment of research in the department.

I heartily acknowledge **Mr. Madan Pal** for his technical assistance in various instruments. I would also like to thank to all members of Institute Instrumentation Center and department of chemistry for their kind co-operation and help throughout my research work.

I express my wholehearted gratitude to esteemed **Dr. Rahul Banerjee**, NCL Pune, for not merely providing the instrumental help. But, I will always be grateful to him throughout my life for providing the mental support and useful suggestions, which has made my things simpler during my PhD tenure.

This strenuous task would not be possible without my senior's, **Dr. Sujata Singh**, **Dr. Nidhi Goel**, **Dr. Sandeep Singh**, **Dr. Kapil Tomar**, **Dr. Sushil Kumar** and **Radha Raman Maurya**, discerning guidance, moral and mental support as it will not be exaggerating fact to mention here that without their help, this work would have never been accomplished so successfully. With great happiness, I would like to thank my lab mates **Neetu Singh**, **Suman**, **Rajan sir**, **Ovender**, **Sweety**, **Chaitanya** and **Sandipan** for their support and cooperation.

Special thanks must go to all my best buddies, **Khushboo**, **Shafique**, **Anirudh**, **Amita**, **Jyotima** and **Stuti** who have always helped me in every need. I am contented to have friends like you all, who have given me the courage to carry out my goals smoothly and always tried to make me happy through my bad times. I am greatly thankful to Mrs. **Reeta madam**, **Ravi** and **Akhand** for providing me the homely atmosphere.

My loving siblings **Nitin bhaiya**, **Manish bhaiya**, **Himanshu**, **Harman**, **Manveer and Viraj**, who have been patient, understanding and supportive not just over the past five years but throughout my life and always stood by my side through my good and bad times. The last but not the least I would like to express my love and regards to my beloved **grandparents** and **parents** for providing me the strength and motivation to complete all the difficult tasks throughout my life. I love and cherish you all.

The financial assistance by Council of Scientific and Industrial Research (CSIR), New Delhi for this investigation is thankfully acknowledged.

At the end, I am thankful to those people, whose names have been mistakenly left, thank you very much for your support and prayers. Finally, I want to apologize with all sincerity from my heart to each one of you, if knowingly or unknowingly I have ever hurt you and believe that you will always be there for all the support and help as you have provided in times of need.

(**Shikha Narang)**

LIST OF PUBLICATIONS

1. Udai P. Singh, **Shikha Narang**, Pradip Pachfule and Rahul Banerjee, "Variation of CO_2 adsorption in isostructural Cd(II)/Co(II) based MOFs by anion modulation", *CrystEngComm*, **16** (23), 5012 – 5020 (2014).
2. Udai P. Singh and **Shikha Narang**, "A supramolecular approach towards the construction of molecular salts using phosphonic acid and pyrazole", *CrystEngComm*, (accepted).
3. Ashok Kumar Singh, Manoj K. Sahani, Ajay K. Jain, Anjali Upadhyay, Amit Kumar, U. P. Singh, **Shikha Narang**, "Fabrication of novel coated pyrolytic graphite electrodes for the selective nano-level monitoring of Cd^{2+} ions in biological and environmental samples using polymeric membrane of newly synthesized macrocycle", *Anal. Chim. Acta*, (Second revision).
4. Udai P. Singh and **Shikha Narang**, "Construction of two phosphomonoester based metal supramolecular isomer: Solid state transformation and solid state emission studies", (Manuscript under preparation).
5. Udai P. Singh and **Shikha Narang**, "Rational analysis of pseudo-polymorphs, ternary salts of flexible anthracene based phosphonic acid with pyrazole: Effect of solvate on its luminescence", (Manuscript under preparation).

CONFERENCES / SYMPOSIUM

1. Participated in International Workshop on "Chemical evolution and origin of life", Indian Institute of Technology Roorkee, India (2010).
2. **Shikha Narang** and Udai P. Singh, "Synthesis of Structural Trends in Supramolecular Networks of Phosphonic Acid and Analogues of Pyrazole", P-149, Symposium on Modern Trends in Inorganic Chemistry-XIV, School of Chemistry, University of Hyderabad, Hyderabad, December 10-13 (2011).
3. Participated in 7th RSC-CRSI Symposium in Chemistry, Banaras Hindu University, Varanasi, January 31 (2013).

4. **Shikha Narang,** Shailly Tomar and Udai P. Singh, "Single-Crystal to Single-Crystal Transformation: Solvent controlled Synthesis of some Supramolecules", P-80, 15th CRSI National Symposium in Chemistry (NSC-15), Banaras Hindu University, Varanasi, February 1-3 (2013).
5. **Shikha Narang** and Udai P. Singh, presented paper on "Crystal Engineering with phosphonic acid and pyrazole: competitive effect of Functional Group on Supramolecular Organic Framework (SOF)", 42nd National Seminar on Crystallography (NSC-42) and International Workshop on Application of X-Ray Diffraction for Drug Discovery, Jawaharlal Nehru University, New Delhi, November 21-23 (2013).
6. Neetu Singh, **Shikha Narang** and Udai P. Singh, "Synthesis, Structural Trends and Biological Activity of Salts/Co-crystals of Different Sulfonic Acid with Natural and Unnatural Nucleobases", P-164, Symposium on Modern Trends in Inorganic Chemistry-XV, Indian Institute of Technology Roorkee, Roorkee, Uttarakhand, December 13-16 (2013).
7. **Shikha Narang**, Udai P. Singh and Rahul Banerjee, "Architecture of Isostructural Cd^{2+}/Co^{2+} Coordination Polymer and its CO_2 Sorption Properties Modulated by Different Anions", P-15, 16th CRSI National Symposium in Chemistry (NSC-16), Indian Institute of Technology Bombay, Bombay, February 7-9 (2014).

CONTENTS

Chapter 1

General Introduction

Supramolecular chemistry [1-2] is described as “chemistry beyond the molecule” [3]. It is an important branch of chemistry which has rendered substantial role in various fields such as material technology [4], catalysis [5], medicine [6], data storage and processing [7] etc. Basically, it involves the association of supramolecular reagents impelled by various intermolecular interactions such as hydrogen bonds, halogen bonds, Vander Waals interactions and coordination bonds [8] resulting in the formation of well organized supramolecule [9]. In last few decades, it has proven that the controlled self-assembly of the molecular components via supramolecular approach could generate potential materials [10] which have consequently led to the blooming results in enormous diversity such as inclusion complexes, vesicles, liquid crystals, co-crystals etc. In particular, the pre-designed molecular components (building block) with various functional moieties govern the molecular assembly involving various intermolecular interactions. However, the complete understanding of the interactions involved led to another section of supramolecular chemistry i.e., crystal engineering.

‘Crystal engineering’ as illustrated by Desiraju [11], involves the implementation of the information regarding the forces responsible for assembling the molecules to produce solid-state materials. It was made clear that the physiochemical properties of the solid material resulted by the assembly of the molecules, depends upon the internal molecular arrangement of the molecules in the solid state.

This concept has been broadened by the recent advancement into fields as diverse as supramolecular synthesis [12], crystal structure investigation and prediction [3]. Supramolecular synthesis provides novel insights into the establishment of strategies for the facile design of supramolecular complexes. These supermolecules are held together by ‘supramolecular synthons’, a structural unit formed by known synthetic operations such as hydrogen-bonding, π-π stacking, Vander Waals forces etc and have been categorized as homosynthon and heterosynthon [13] (Fig. 1.1). It is well known that conventional hydrogen bonding for instance O–H···O, N–H···O interactions are primarily responsible for building the supramolecular framework besides this, some non-conventional weak H-bonding interactions i.e., C–H···O, C–H···π interactions also take part in further stabilizing the framework [14-15]. In fact, the hydrogen bonds are formed in hierarchical fashion (according to the Etter’s rule), which leads to the crystal stability on the basis of specific intermolecular interactions [16].

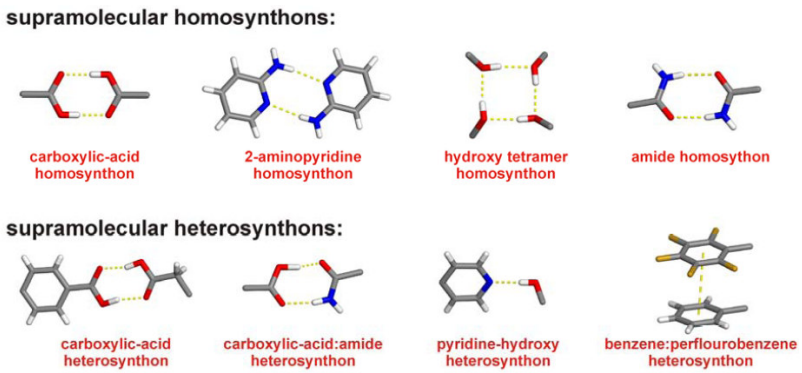

Fig. 1.1: An overview of reported homosynthons and heterosynthons

Researchers have devoted all their effort that has spawned and incited an exponential growth in the field of crystal design and crystal engineering. Furthermore, these concepts have been imposed beyond material sciences since structure-property relationship in the solid state has given the opportunity to produce various potential materials [17-18].

The crystal form landscape is vast for an organic molecular compound (Fig. 1.2). Being a single component, it has the ability to exist in more than one network with same chemical composition termed as polymorphs [19], which may be generated as a consequence of producing different synthons by the same molecular units i.e., supramolecular synthon isomerism. On the other hand, the molecule also has the tendency to crystallize with the solvent molecule and generally, the solvent molecules reside inside the pores formed by the molecules. Such inclusion compounds have also given the name, pseudo-polymorphism [20]. However, it can form multi-component molecular crystals with variety of different molecular compounds which are solid at ambient temperature generating binary, ternary and quaternary co-crystals [21]. Although the term co-crystal was familiarized by Margret Etter [22] in 1990's but the formation of co-crystal began in 1844. Thereby, it was introduced by some other names till 1990's such as molecular complexes [23], addition compounds [24], organic molecular compounds [25] and solid state complexes [26].

Apparently, the choice of the constituents for the formation of the crystalline form inherently depends upon the requirement (desired material) since the physiochemical property of the resulted multi-component system intrinsically based on the chemical nature of the blocks chosen [27].

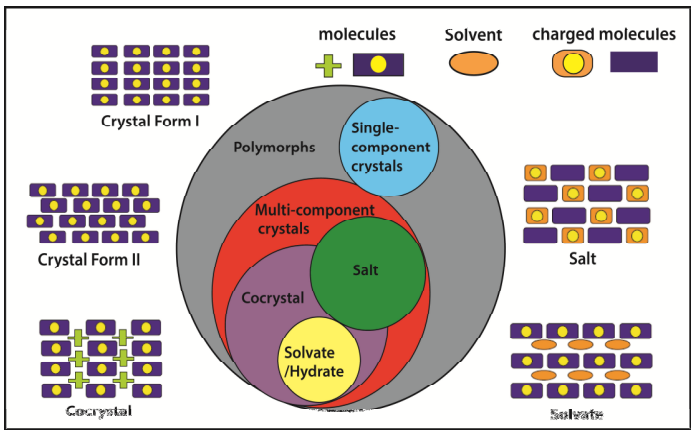

Fig. 1.2: The crystal form landscape and variety of crystalline form of a molecule

N-heterocyclic ligands have received considerable interest in the synthesis of diverse potential new materials [28-29]. In last few decades, several *N*-based ditopic heterocyclic ligands have been used for the construction of supramolecular assembly. In this context, pyrazole and pyridine based ligands such as bispyrazole, bis- and tris- pyridine have been rationalized in this thesis. These ligands have been chosen as it possess (a) an aromatic ring which will aid in formation of π···π interactions; (b) flexibility in the ligand- variation in conformation which may lead to the variety of distinct Supramolecular Organic Frameworks (SOFs).

Pyrazole possesses lone pairs on the nitrogen atom and proton-donor NH group, which could ensure the formation of cyclic complexes involving the acidic group of second component, as well as more complex cyclic associates consisting of more than one molecule of one or another component. Owing to the presence of both N and –NH, pyrazole can act as

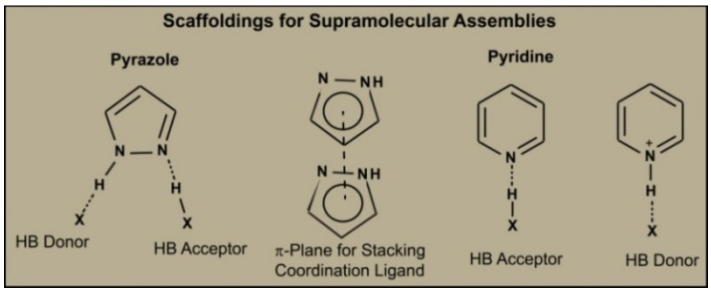

Fig. 1.3: Various scaffoldings involved in supramolecular assembly constituting pyrazole and pyridine

both H-donor as well as acceptor which increase the possibility of formation of various scaffolds that aids in the supramolecule assemblage. Similarly in case of pyridine, the Lewis base N atom interacts easily with the other component and, it can easily be protonated in presence of acidic

component hence, it contribute in various favorable N–H/N–pyridine hydrogen bonding synthon (Fig. 1.3).

Pyrazole analogues possess a distinctive propensity to form various self-associates (linear chains, cyclic dimers, trimers, and tetramers) owing to the presence of a proton donor and acceptor N atom in the gaseous phase, in crystal, and in solution [30-32].

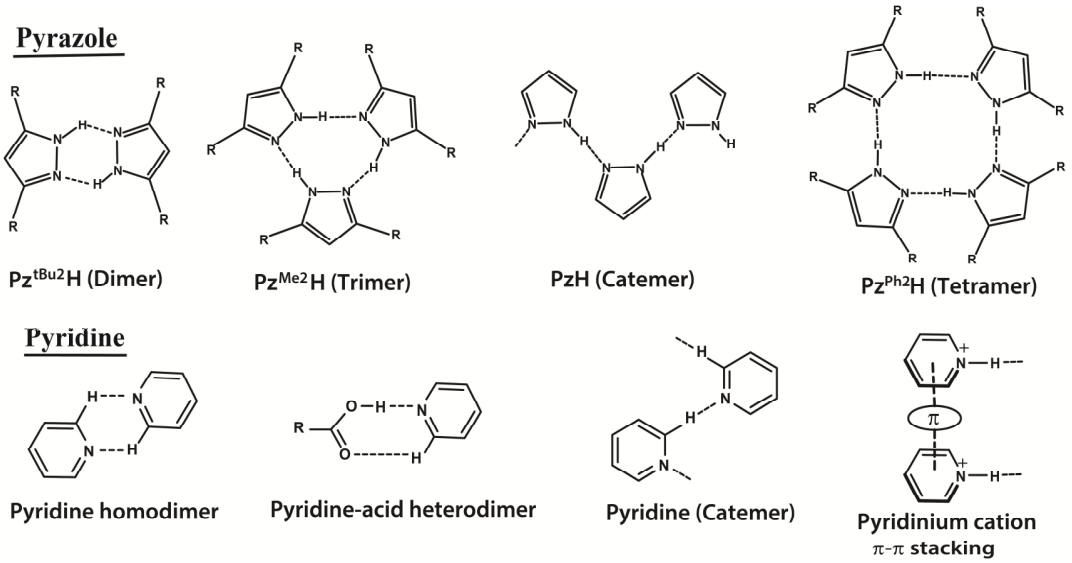

Fig. 1.4: Various synthons reported by substituted pyrazole and pyridine in literature

For instance, the parent pyrazole forms linear chains via N–H···N hydrogen bonds, however significant variation in the network were reported when pyrazole is substituted at 3, 4 and 5 positions, e.g., 3,5-dimethylpyrazole forms cyclic trimers, 3,5-ditertbutylpyrazole forms cyclic dimers, 3,5-diphenylpyrazole and 3,5-bis(trifluoromethyl)-1H-pyrazole forms cyclic tetramers (Fig. 1.4).

Water soluble and biologically important phosphonic acid ($–PO_3H_2$) display an additional H-bonding in contrast to carboxylic and sulfonic acid as it possess an extra ionisable hydrogen atom. Notably, phosphonates are less studied relative to carboxylic acids which being planar molecule resulted in robust and potential network. However, the former display tetrahedral geometry which give rise to a complex network and devoid of a robust network and high yielding synthetic procedure. Synthetically, phosphonic acid can easily be introduced on any halogenated precursor, when allowed to undergo Michaelis-Arbuzov reaction followed by the acid hydrolysis of the phosphonate to form phosphonic acid [33] (Fig. 1.5).

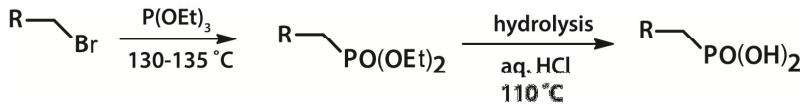

Fig. 1.5: General reaction of synthesis of phosphonic acid by Michaelis-Arbuzov reaction

The phosphonic acid moiety, $R–PO_3H_2$ exist in two deprotonated forms, $R–PO_3H^-$ and $R–PO_3^{2-}$ depending upon basicity of the ligand used (pH dependent) (Fig. 1.6). Usually the first proton deprotonates very easily as it is very acidic, while the second proton being less acidic requires more basic condition in order to get deprotonated.

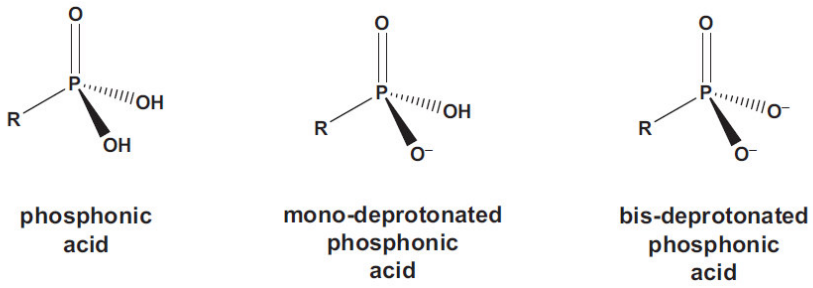

Fig. 1.6: Three forms of the phosphonic acid group

Pyrazole with complementary group, has a Lewis acid pyrolic N–H group and a Lewis base pyridinic N-donor adjacent to it, makes it an excellent ligand. Moreover, bispyrazole with two pyrolic N–H group and two pyridinic N-donor *trans* to each other, acts as the potential linker in the formation of a new solid material. It was anticipated that supramolecular assembly of these conformational flexible bispyrazole with other component will exhibit potential intriguing architectures. Variety of phosphonic acids have been chosen as the second component because it can exist in two deprotonated forms, which can lead to the formation of diverse supramolecular organic frameworks with bispyrazole. Additionally, the supramolecular assembly of flexible phosphonic acid with pyridyl analogues was also envisaged to show polymorphism.

There are various reports on ditopic pyrazole and pyridine based supramolecules. Some of the relevant literature has been discussed below.

Boldog et al. [34] reported a range of binary compounds involving monofunctional 3,5-dimethylpyrazole (Me_2pz) and bifunctional 3,3',5,5'-tetramethyl-4,4'-bipyrazole (Me_4bpz) with phenol (PhOH), resorcinol, hydroquinone (p-$C_6H_4(OH)_2$) and phloroglucinol. They revealed that the prospect of self-complementary molecules to display cooperative association resulted in the formation of binary compounds. After analyzing the results, they found that the common features

are applicable for the preparation of binary compounds of monofunctional and bifunctional components (Fig. 1.7). They observed that the binary system with resorcinol indispensably form an unprecedented N–H···π pyrazole hydrogen bonding.

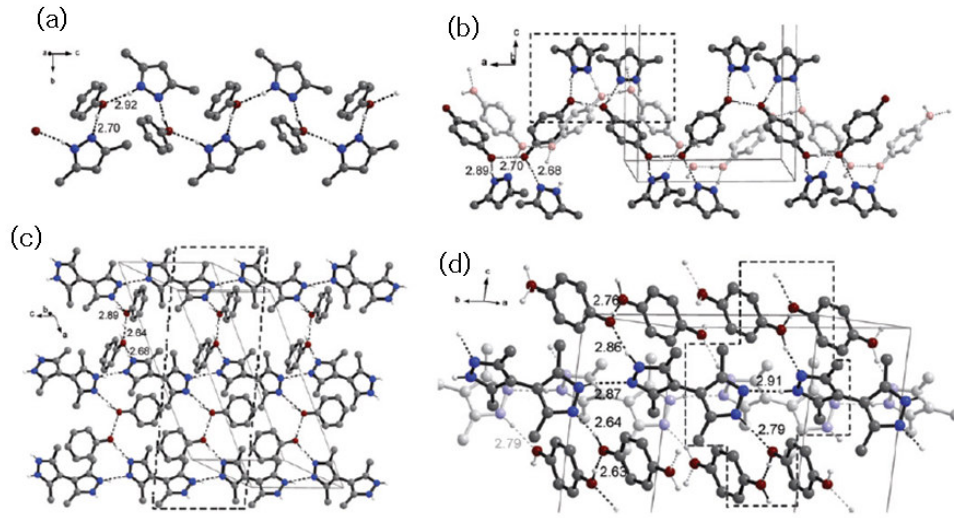

Fig. 1.7: Crystal structures of $Me_2pz.PhOH$ (a); $Me_2pz.(p\text{-}C_6H_4(OH)_2)$ (b); $Me_4bpz.2PhOH$ (c) and $Me_4bpz.(p\text{-}C_6H_4(OH)_2)$ (d)

Sanz et al. [35] reported the synthesis and deduced the crystal structure of two pyrazole analogues *viz*., 3,3'-(1,3-phenylene)bis-1H-pyrazole and 3,3'-(1,4-phenylene)bis-1H-pyrazole. They showed that the former form a trimer sustained by N–H···O hydrogen bond and resulted in the formation eaves gutter-like structure as two parallel strands of pyrazole is linked by the third one. However in latter, the framework is resulted by hydrogen bonded tetramer which led to a remarkable framework possessing double stranded *zig-zag* chain (Fig. 1.8).

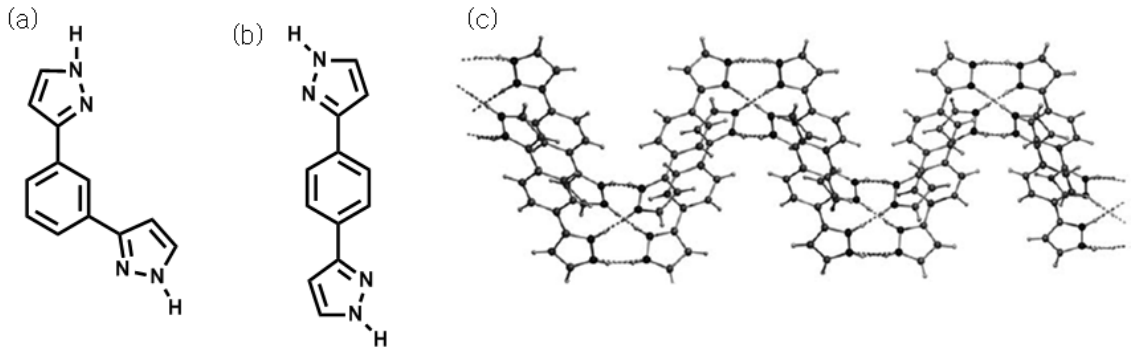

Fig. 1.8: Molecular structure of (a) 3,3'-(1,3-phenylene)bis-1H-pyrazole; (b) 3,3'-(1,4-phenylene)bis-1H-pyrazole and (c) details of an isolated *zig-zag* chain formed in the solid-state structure of *para*-derivative

Aakeröy et al. [36] correlated the structural and spectroscopic study of the N-heterocyclic complex of phenyloximes R–C=N–OH. They investigated the potential and versatility of phenyloximes by reacting it with variety of N-heterocyclic hydrogen bonded acceptors including five to six membered, monotopic-ditopic and symmetric-asymmetric ligands (Fig. 1.9). Theoretically, they found that these ligands display significant selectivity towards the best hydrogen bond acceptor moiety in ditopic molecule.

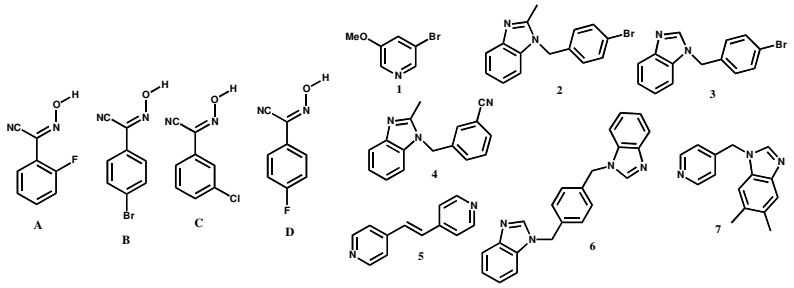

Fig. 1.9: Chemical structure of phenyloximes (A-D) and list of various monotopic and ditopic ligands used in this study (1-7)

Boldog et al. [37] synthesized and reported the crystal structure of 4,4'-bipyrazolyl (4,4'-bpz) and 3,3',5,5'-tetramethyl-4,4'-bipyrazolyl (4,4'-Me_4bpz). The structural study further revealed that the latter analogue exists in two acentric polymorphic forms and exhibit the helical motif whereas the former is centrosymmetric (Fig. 1.10). They demonstrated that the properties of the crystal can be designed at the molecular level by various conformations of the molecular unit in the context of inducing bulk property. Various isomorphous pseudopolymorphs have also resulted by crystallizing 4,4'-Me_4bpz in different solvents such as acetone, ethylacetate and THF.

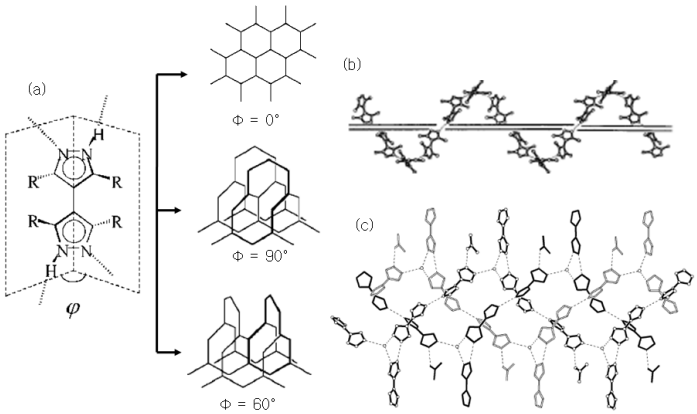

Fig. 1.10: (a) Pathways for the self assembly of bipyrazolyls and nature of the supramolecular isomerism in 4,4'-Me_4bpz; (b) helicate motif in the structure of the hexagonal polymorph of 4,4'-Me_4bpz and (c) triple-helicate motif of the structure in [3(4,4'-Me_4bpz).H_2O.acetone]

Boldog et al. [38] reported a new crystal structure of 3,3',5,5'-tetramethyl-4,4'-bipyrazolyl (4,4'-Me_4bpz) crystallized from absolute chloroform. They found that a highly interpenetrated 3D framework is resulted and display unique hydrogen bonded trimeric motif (Fig. 1.11). They reported the first example of catemer/trimer supramolecular isomerism of pyrazoles and six-fold interpenetrated network with topology (10,3)-a. They also demonstrated the control over the degree of interpenetration.

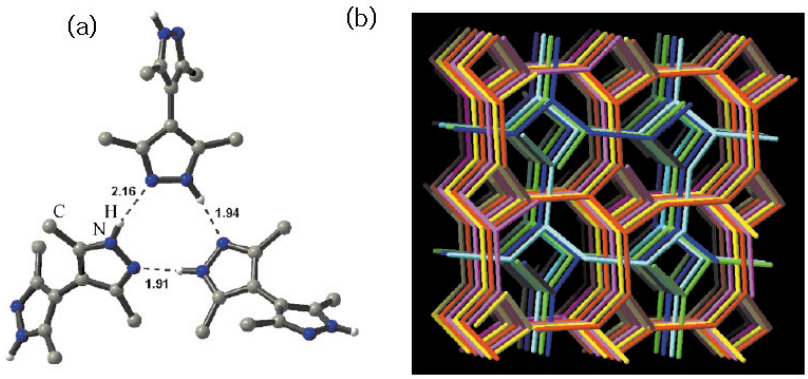

Fig. 1.11: (a) Trimeric pyrazole motif that dominates self-association of Me_4bpz and (b) view of interpenetration of six nets of (10,3)-a topology (the nodes are the pyrazole trimers) in the crystal structure of Me_4bpz

Aakeröy et al. [39] systematically studied the high yielding supramolecular assembly of ditopic imidazoles/benzimidazoles with dicarboxylic acids. They demonstrated that O–H···N hydrogen bond is the robust intermolecular interaction resulted in COOH–Im and COOH–BIm synthons (Fig. 1.12). However, secondary C–H···O interactions present in the motif as well as between neighboring chains have also been proved to be equally important on a structural aspect. They also revealed that neutral hydrogen-bond interaction is the main driving force for directed assembly of carboxylic-ditopic benzimidazole binary complex.

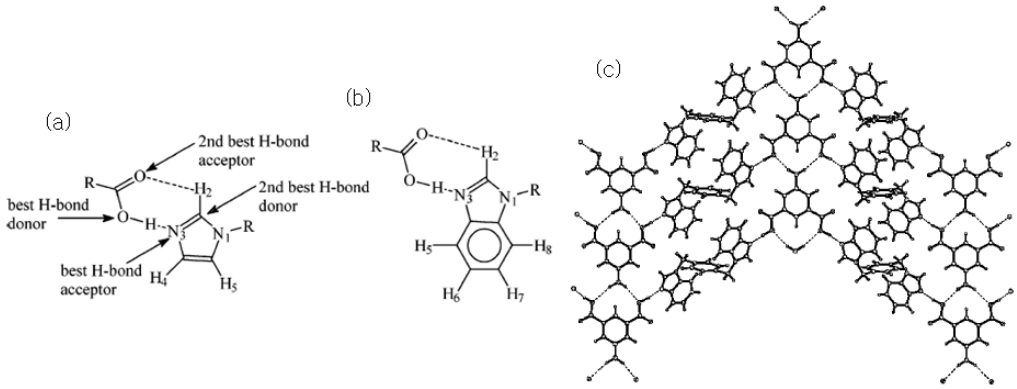

Fig. 1.12: (a) COOH···Im; (b) COOH···BzIm synthons indicating the best and second-best hydrogen-bond donor/acceptor couples and (c) infinite 2D sheet in [1,4-bis[(benzimidazol-1-yl)methyl]benzene:5-aminoisophthalic acid:$EtOH_{0.5}$] resulting from N–H···O interaction

Aakeröy et al. [40] further synthesized two ditopic symmetric ligands, 1,4-bis[(pyrazol-1-yl)methyl]benzene and 1,4-bis[(3,5-dimethylpyrazol-1-yl)methyl]benzene and

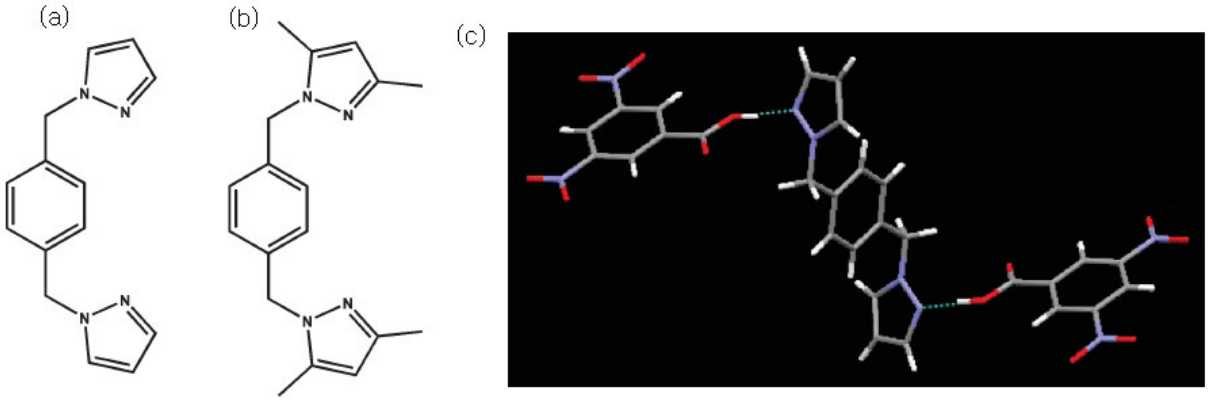

Fig. 1.13: Chemical structure of (a) 1,4-bis[(pyrazol-1-yl)methyl]benzene; (b) 1,4-bis[(3,5-dimethylpyrazol-1-yl)methyl]benzene and (c) 1:2 binary co-crystal of 1,4-bis[(pyrazol-1-yl)methyl]benzene and 3,5-dinitrobenzoic acid

co-crystallized them with various aromatic acids. They compared the success rate of crystallization of these ditopic ligands depending upon their basicity (Fig. 1.13). They found that the latter ligand exhibited higher success rate owing to the electronic influence of electron donating group present on the ligand. Structural analysis revealed that no proton transfer takes place from acid to base; as a result, the COOH–Pz assembly is driven by the formation of O–H···N interaction between OH of COOH group and N of pyrazole group.

Aakeröy et al. [41] also reported the systematic co-crystallization of pyrazole analogues and library of aromatic carboxylic acids by using melt and solution-based experiments. They screened the solid by IR spectroscopy in order to observe whether the resulted solid is salt/co-crystal. Moreover, they reported the correlation between the electrostatic charges on hydrogen-bond donor/acceptor site and the supramolecular yield of ensuing co-crystallizations. Hence, they studied the effect of the different substituents present on the pyrazole and observed that NO_2 group showed the noticeable change than the halo groups depending upon their electrostatic nature (Fig. 1.14).

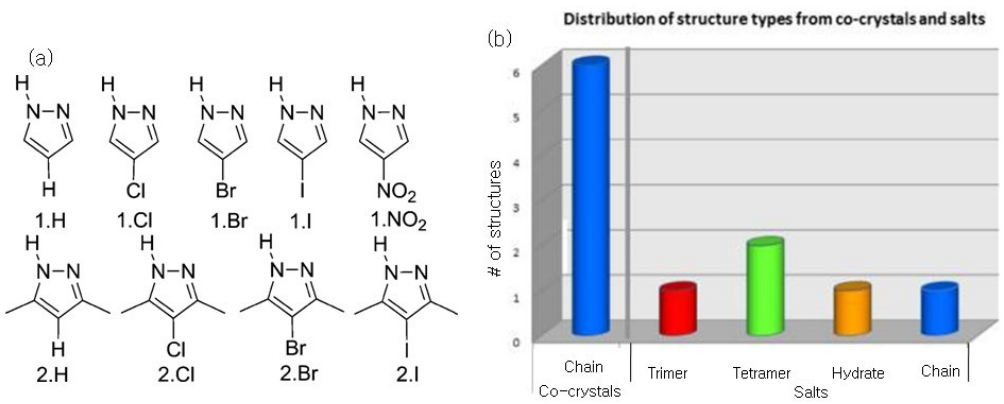

Fig. 1.14: (a) The nine pyrazoles used in this study and (b) distribution of structure type from co-crystals and salts

Goswami et al. [42] reported two polymorphs (A and B) of a pyrazole based ditopic ligand molecule, methylenebis(3,5-dimethylpyrazole) (H_2MDP) resulted by small conformational change in the ligand. They found that both of the two forms give rise to (6,3) net. The coordination of the ligand was found to be similar in both the forms but with the subtle difference. One form led to a staircase-like architecture due to perpendicular arrangement of the nets, while the crystal structure of another form ended in a wave-like undulated topology (Fig. 1.15). Furthermore, they observed that the framework has the tendency to show unique framework i.e., anion assisted helix interweaved into another helix network (anion-assisted 'helix inside a helix' network) involving strong hydrogen bond, π-stacking and anion-π interactions in presence of acid such as perchloric and trifluroacetic acid.

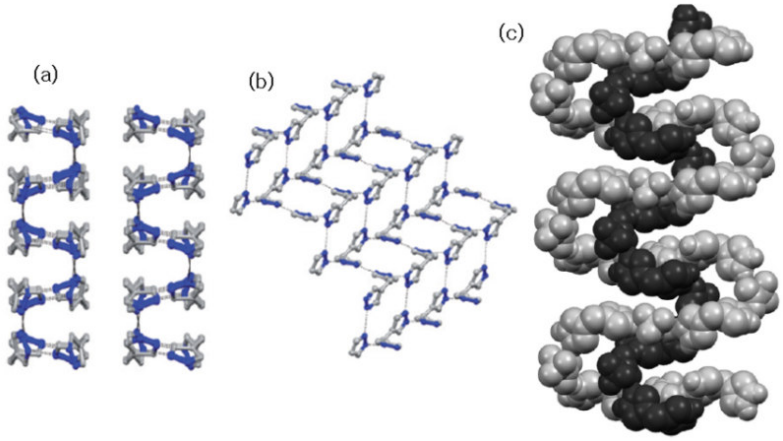

Fig. 1.15: A comparative depiction of crystal structures of polymorphs (a) form-A; (b) form-B, illustrating the wave-like undulated and staircase topology, respectively and (c) a space-filled model showing two interweaving helices of different pitch lengths

Basu et al. [43] synthesized coordination polymer from the same flexible exoditopic methylenebis(3,5-dimethylpyrazole) (H_2MDP) and V-shaped polycarboxylic acids, such as

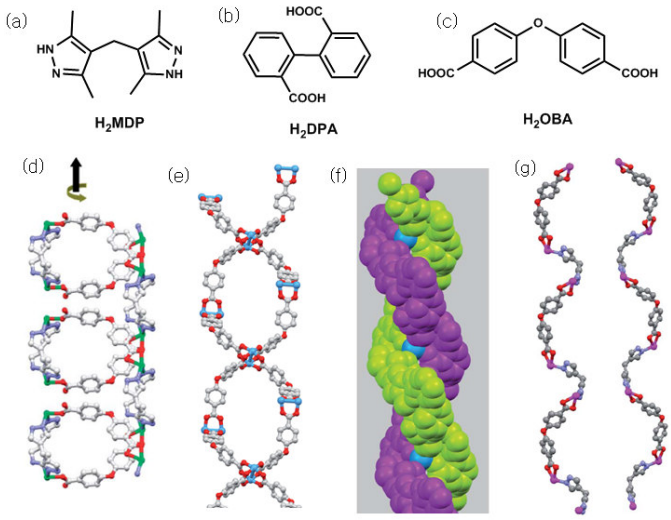

Fig. 1.16: Chemical structure of (a) methylenebis(3,5-dimethylpyrazole) (H_2MDP); (b) diphenic acid (H_2DPA); (c) 4,4'-oxybis(benzoic acid) (H_2OBA); view of double helical strand in (d) $[Ni(OBA)(H_2MDP)(H_2O)].(DMF)_{1.625}\}_n$; (e) $[Cu_2(OBA)_2(H_2MDP)].(DMF)_5\}_n$; (f) $\{[Zn(DPA)(H_2MDP)].2(H_2O)\}_n$ and (g) $[Cd(OBA)(H_2MDP)]_n$

diphenic acid (H_2DPA), 4,4'-oxybis(benzoic acid) (H_2OBA), used as the bridging ligand. They also reported a series of helical coordination polymers based on two mixed flexible and V-shaped ligands showing metal dependent topology. Primarily, the presence of flexibility owing to the change in conformation of the ligand is the driving force for the formation of helical network (Fig. 1.16).

Mukherjee et al. [44] reported the polymorphs from co-crystallization of 4,4'-bipyridine-4-hydroxybenzoic acid system with varied structural landscape i.e., synthon polymorphism, which could be attributed due to the analogous acidity of the phenolic and acidic functionalities in the acid molecule (Fig. 1.17). They found that the resulted polymorphs displayed the relationship between close packing and intermolecular interactions in the molecular system and they concluded that the subsistence of polymorphism is due to the interplay between geometrical and chemical models for crystallization.

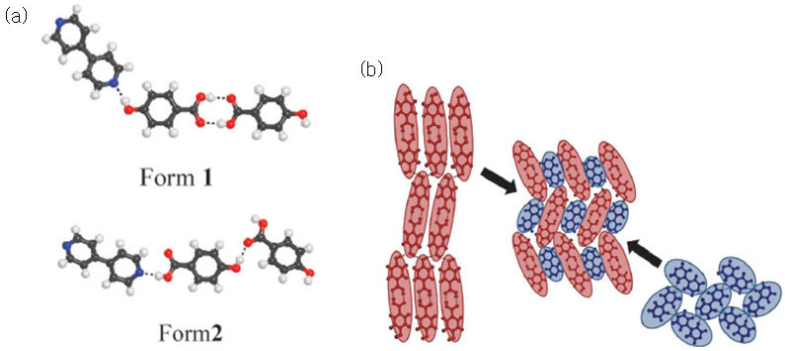

Fig. 1.17: (a) Hydrogen bonding schemes in two polymorphs and (b) mutual topological relationships of 4,4'-bipyridine and 4-hydroxybenzoic acid molecules in form 1 of the 1:2 co-crystal

Roy et al. [45] demonstrated the supramolecular reactions of 2,2',6,6'-tetracarboxybiphenyl with bis(4-pyridyl)ethylene (bpe) and 4,4'-bipyridine (bpy). The reaction directed transfer of the molecular symmetry (pseudo-S4) into supramolecular symmetry (8-fold interpenetrated diamondoid network) only in case of co-crystals (Fig. 1.18). They successfully found the condition to form co-crystal over salt for instance the addition of phenol promoted the growth of crystals as co-crystal. However, this strategy was not successful in case of bpy, which usually resulted in a salt. Structural study revealed that all salts exhibits the formation of monoanion acid being as a square building block and proliferate the framework as the layer structure.

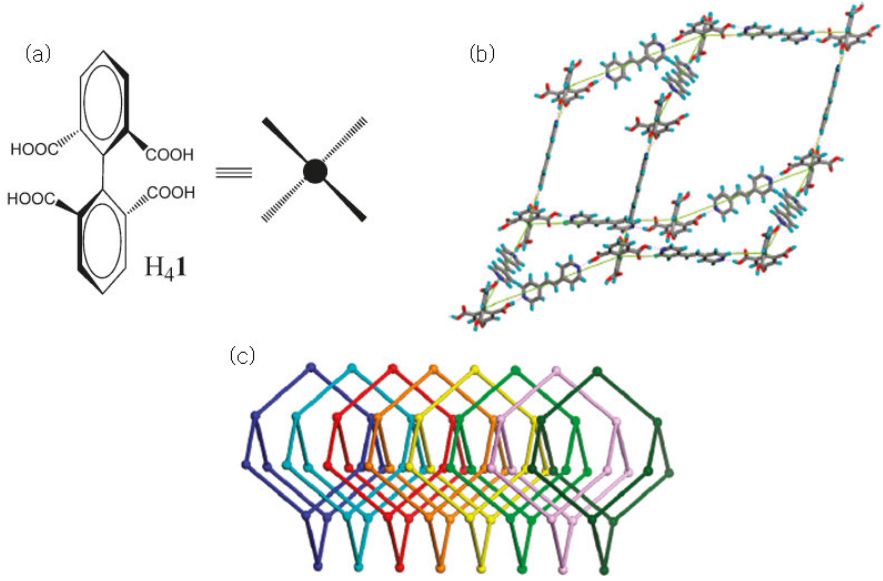

Fig. 1.18: (a) Molecular structure of 2,2',6,6'-tetracarboxybiphenyl displaying its molecular symmetry pseudo-S4; (b) single supramolecular adamantanoid cage, 8-fold interpenetrated adamantanoid network and (c) side view of 8-fold interpenetrated network

Du et al. [46] demonstrated the potentiality of pamoic acid (H_2PA), which has the ability to produce a supramolecular triple helix via charge-assisted N^+–H···O interactions when allowed to crystallize with piperazine (PIPO) in $[(PA)\cdot(H_2PIPO)]\cdot 3H_2O$ (Fig. 1.19). However, it represented the formation of first co-crystal, $[(H_2PA)\cdot(BIPY)]$ with ditopic 4,4'-

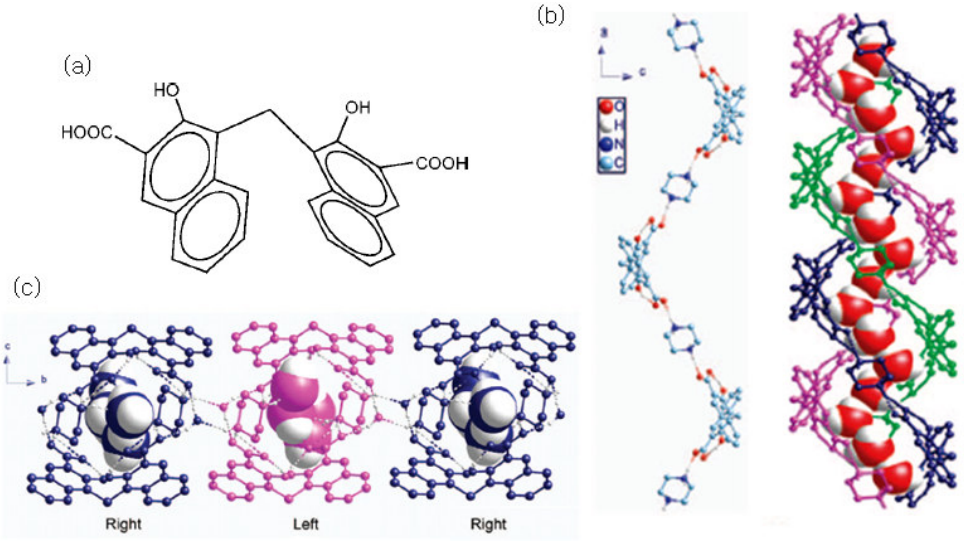

Fig. 1.19: (a) Molecular structure of pamoic acid (H_2PA); (b) left: a single H-bonding helical chain and right: the triple-helix framework with the inclusion of a helical water chain (in space-filling model) and (c) top view of triple-helix arrays with lattice water molecules

bipyridyl (BIPY) sustaining well known carboxyl-pyridyl H-bonding synthons. Therefore, they concluded that the judicial choice of the building block is essential for accomplishment of a local helical or zonal motif. It was found that the former compound is stable as on dehydration its crystallinity retains.

Aakeröy et al. [47] also synthesized two ditopic amide based ligands (N-(4-pyridin-2-yl)-isonicotinamide) and (N-(3-pyridin-2-yl)nicotinamide) and thereafter rationally constructed the co-crystals with an odd/even number of carbon atoms of aliphatic dicarboxylic acids using the principle of crystal engineering. They have demonstrated that number of carbon atoms in the acid with the defined orientation of the coformer; indeed manage the resulting supramolecular assembly (Fig. 1.20). They illustrated the remarkable difference between the bipy-system and newly synthesized amide ligands, is the relative orientation of the binding sites on the molecule. Hence, they found that difference in the geometry of the binding sites controls the overall outcome of the assembly process as evident from the results. It is well known that the structural

packing and solid-state derived properties are connected but interestingly such fundamental differences extend from homomeric solids to heteromeric co-crystals.

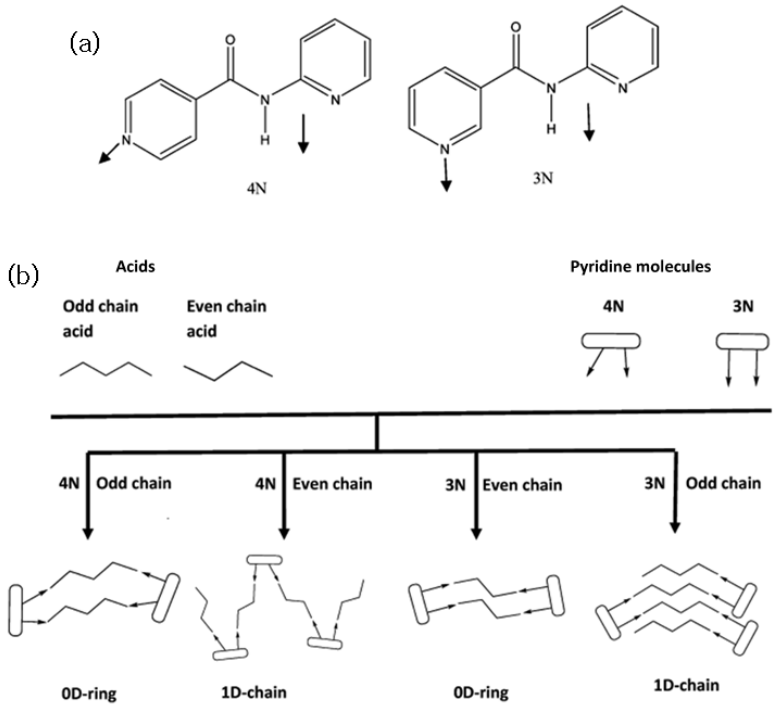

Fig. 1.20: (a) View of ditopic amide ligands involved and (b) possible architectures resulted

Nauha et al. [48] reported the conventional co-crystallization of agrochemical actives thiophanate-methyl and thiophanate-ethyl with 2,2'-bipyridine (22bp), 4,4'-bipyridine (44bp) and 1,2-bis(4-pyridyl)ethane (44bpe) by the slurry method and liquid-assisted grinding (Fig. 1.21). They found that co-crystals with 2,2'-bipyridine is resulted by the combination of weak interactions, whereas in case of thiophanate-methyl, caused moderately due to motivational force of close packing. On the other hand, favorable N–H/N–pyridine hydrogen bonding synthon is the main reason for the formation of 4,4'-bipyridine and 1,2-bis(4-pyridyl)ethane co-crystals. Moreover, they discussed the influence of molecular size on further involvement of particular hydrogen bond moieties in H-bonding and concluded that due to more conformational freedom of the larger molecules, these molecules have shown the tendency to pack well even with more hydrogen bonds in use.

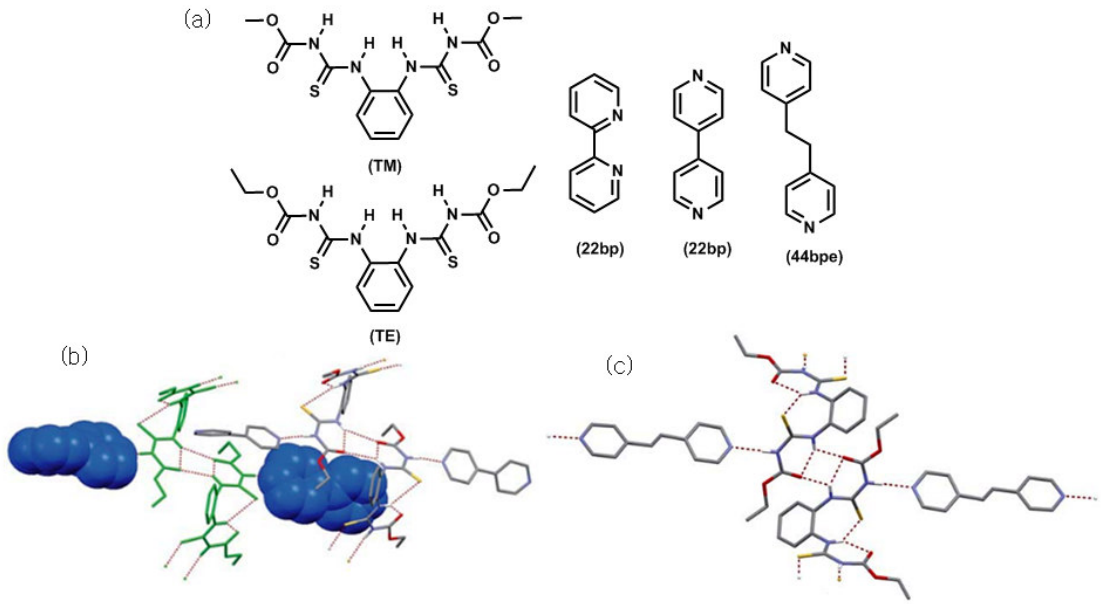

Fig. 1.21: (a) Molecular structures of thiophanate-methyl (TM), thiophanate-ethyl (TE), 2,2'-bipyridine (22bp) and 4,4'-bipyridine (44bp), and 1,2-bis(4-pyridyl)ethane (44bpe); (b) hydrogen bonding and packing in the TE–44bp co-crystals and (c) hydrogen bonded pairs in TE.1,2-bis(4-pyridyl)ethane co-crystals

Bhogala et al. [49] reported some ternary and quaternary host-guest co-crystals of 1,3-*cis*,5-*cis*-cyclohexanetricarboxylic acid (H_3CTA) with variety of 4,4'-bipyridine (bpy) based component (Fig. 1.22). The $–CH_2–$ chain between two bpy showed conformational and structural role in resulting diverse supramolecular architectures via O–H···N hydrogen bonds such as helix or chain or loop, which eventually led to the square/hexagonal nets (Fig. 1.23).

On structural study, they revealed that helices of acid-bipy molecules involve the small/rigid bipy partner whereas these helices/loops are interlinked through the longer/flexible bipy base. Hence, they found that the flexible longer ditopic pyridyl ligand played an important role in deducing the multi-component system leading to the construction of distinct architectures which sustains robust known acid-pyridine synthons.

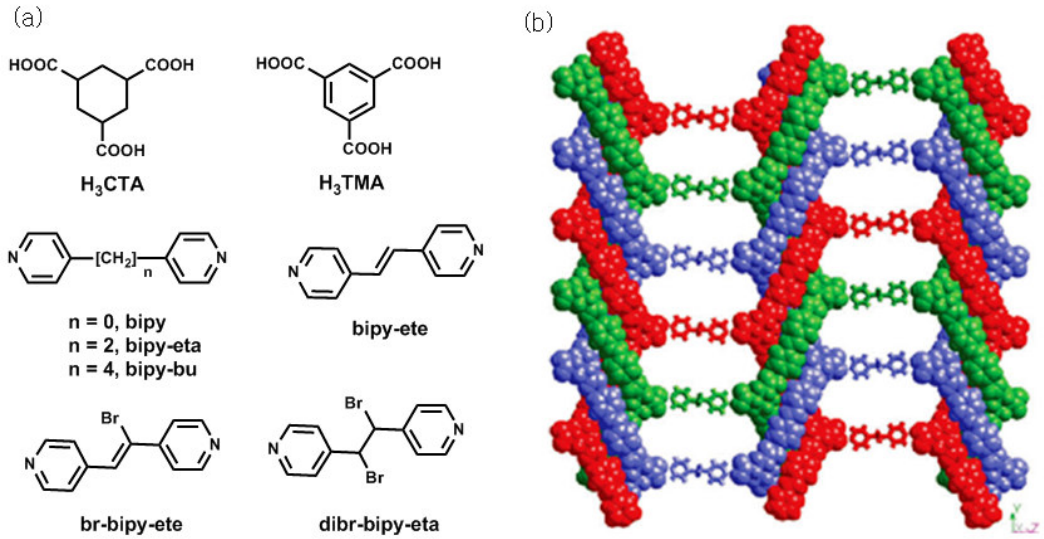

Fig. 1.22: (a) Carboxylic acid and bipyridine bases used in co-crystallization and (b) three-fold parallel-interpenetration of (6,3) nets in $H_3CTA.bipy\text{-}ete.(bipy\text{-}eta)_{0.5}$

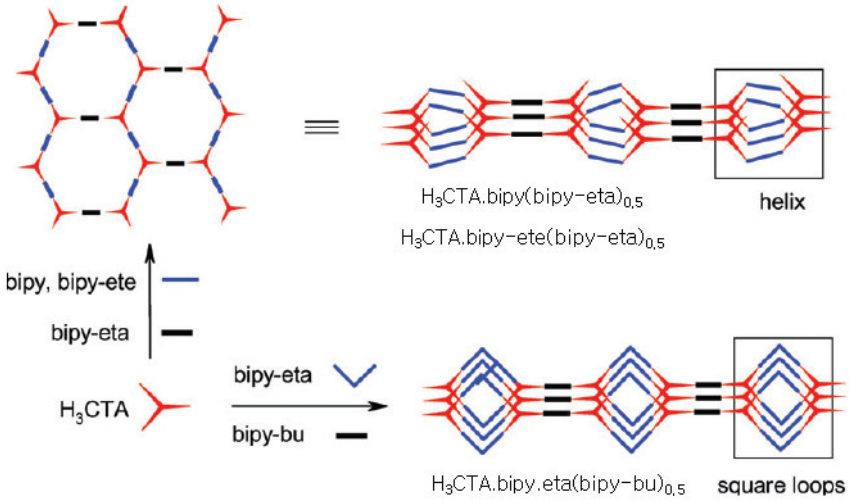

Fig. 1.23: Formation of hexagonal nets in structure $H_3CTA.bipy(bipy\text{-}eta)_{0.5}$ and $H_3CTA.bipy\text{-}ete(bipy\text{-}eta)_{0.5}$ and square loops in $H_3CTA.bipy.eta(bipy\text{-}bu)_{0.5}$ occurs via similar molecular components but the difference is in the infinite helix/chain vs closed loop motifs

The utilization of the various carboxylate as well as nitrogen rich ligands for the coordination complex/MOFs construction is usual [50]. In this regard, rigid multipyridyl ligands have received considerable attention as their rigidity and trigonal geometry can lead to the formation of nanosized cages and porous frameworks enclosing cavities, chambers and channels [51-52]. Some of the relevant literatures related to this work have been discussed below.

Yoshida et al. [53] examined two bis(β-diketonato) Co(II) complexes with a polypyridyl ligand, 2',4',6'-tri(4-pyridyl)pyridine (L), resulted in the coordination polymers i.e., $[Co(acac)_2](L)(CHCl_3)$ and $[Co(acacCN)_2]_3(L)_2(MeOH)_4$ where acac = pentane-2,4-

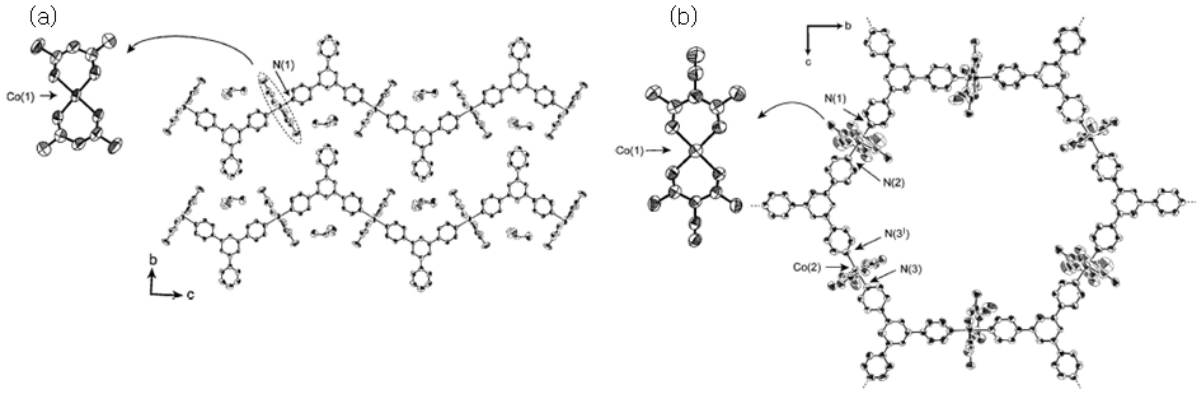

Fig. 1.24: (a) 1D zigzag structure of $[Co(acac)_2](L)(CHCl_3)$ and (b) 2D (6,3) hexagonal network of $[Co(acacCN)_2]_3(L)_2(MeOH)_4$

dionato and acacCN = 3-cyano-pentane-2,4-dionato. On structural analysis of these complexes, they deduced that polymeric structure with 1D zigzag chain and 2D hexagonal net were found respectively (Fig. 1.24).

Heine et al. [54] reported a polycatenane, $[(ZnCl_2)_{12}(pytpy)_8]_n.xCHCl_3$ assembled by $ZnCl_2$ and 2,4,6-tris(4-pyridyl)pyridine (pytpy) possessing unprecedented strand of interlocking icosahedral cage which acquires volume greater than 2700 $Å^3$ (Fig. 1.25). They gauge the contents of the icosahedral cage with the help of solid-state NMR spectroscopy and discussed the factors involved for its synthesis. They found that this complex incorporated the guest molecule of appropriate size and polarity in its cage and gave a defined three-dimensional array of solvent nanodroplets.

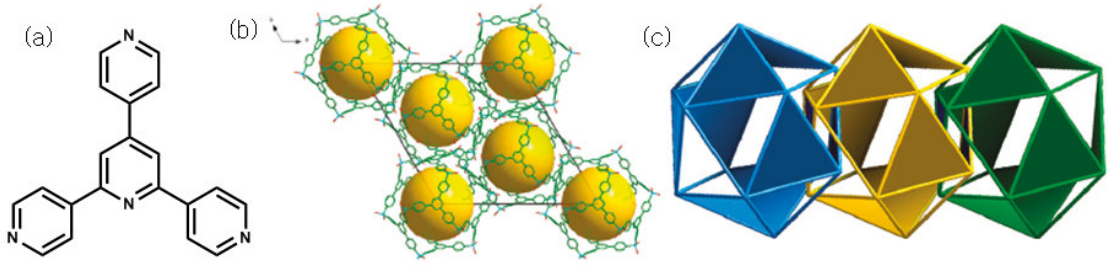

Fig. 1.25: (a) Chemical structure of 2,4,6-tris(4-pyridyl)pyridine (pytpy); (b) packing of the strands of interlaced coordination icosahedra in $[(ZnCl_2)_{12}(pytpy)_8]_n.xCHCl_3$, along *c*-axis and (c) structural fragment containing three interlaced icosahedral cages

Zhang et al. [55] reported two isomeric supramolecular porous metal bipyrazolates isomers $[M_2(bpz)]$ (M = Ag, Cu) $[Ag(NH_3)_2]^+$ or $[Cu(NH_3)_2]^+$ formed by the template-controlled reactions of 3,3',5,5'-tetramethyl-4,4'-bipyrazole (H_2bpz) each with Ag^+ and Cu^+ (Fig. 1.26). On structural analysis, they depicted that one isomer possesses four-fold interpenetrated (10,3)-a coordination network, two-fold interpenetrated (10,3)-a channel networks, and porous metal clusters, however, the second isomer show eight-fold interpenetrated $(6^2.10)(6.10^2)$ coordination networks with small pores. They have also done the N_2 and CO_2 adsorption study for all the coordination networks. In addition, they found that the resulted isomers are thermally stable and flexible as it allowed the reversible uptake/release of larger molecule, such as benzene, toluene and mesitylene. Therefore, the first isomer of Ag and Cu displays the higher N_2 and CO_2 adsorption (Fig. 1.27).

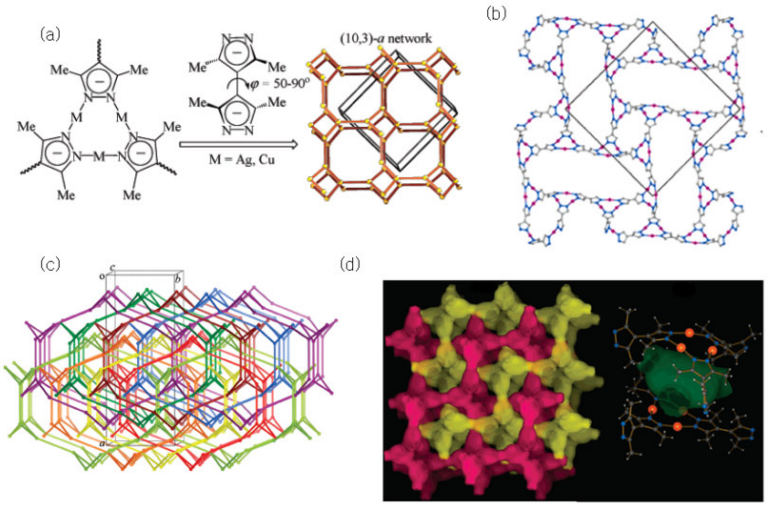

Fig. 1.26: (a) Synthetic scheme for binary metal bipyrazolate; (b) view of a single $[Ag_2(bpz)]$ network of one isomer Ag; (c) eight-fold interpenetrated coordination networks of second isomer Ag and (d) two-fold interpenetrated channels

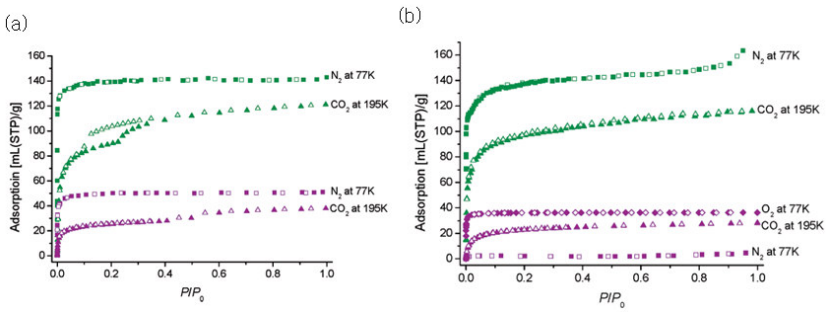

Fig. 1.27: Nitrogen and carbon dioxide adsorption (solid) and desorption (open) isotherms of (a) 1-Ag (green) and 2-Ag (purple) and (b) 1-Cu (green) and 2-Cu (purple)

Mitra et al. [56] demonstrated that anion plays an important role in controlling the architecture of MOFs. They synthesized a non-interpenetrated square grid Zn(II) based MOF with linear N,N''-di(4-pyridyl)-1,4,5,8-naphthalenediimide (DPNDI) ligand in presence of ClO_4^- ion, which resided inside the cavity interacted via C–H···anion interactions (Fig. 1.28). However in presence of NO_3^- anion, the formation of linear coordination polymer was resulted. They observed that the porous non-interpenetrated network displays high stability with large pore dimensions (20×20 Å). As a consequence, they assumed that the resulted MOF would show potential application in exchanging and sequester hazardous anions (ClO_4^-, TcO_4^-, ReO_4^-, CrO_4^{2-}, SO_4^{2-}) inside the cavities.

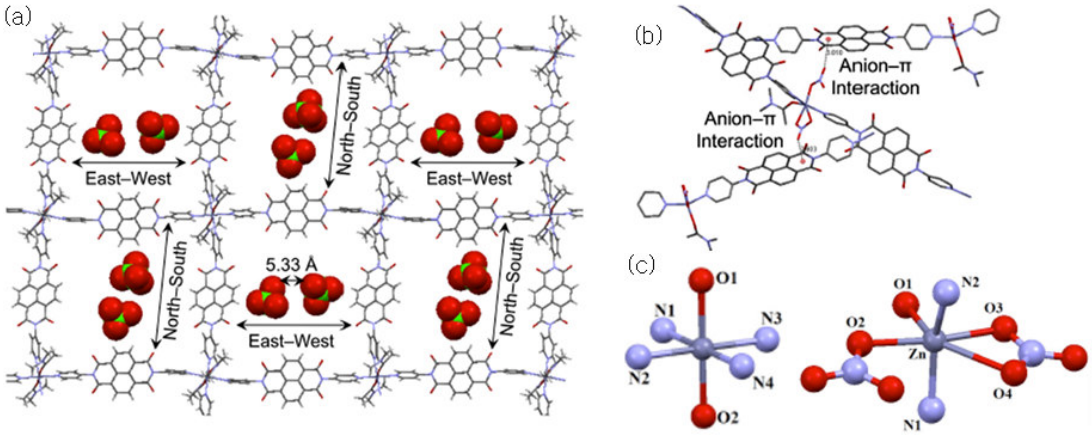

Fig. 1.28: (a) Two ClO_4^- ions occupy each cavity via C–H···O in $[Zn(DPNDI)_2(DMAc)_2.2ClO_4]_n$; (b) representing anion-π interactions with π-acidic DPNDI ligand in $[Zn(DPNDI)(DMAc)(NO_3)_2]_n$ and (c) coordination environment of Zn(II) in case of ClO_4^- and NO_3^-

Ma et al. [57] hydrothermally synthesized two Cu(II) coordination polymers (CPs), $[Cu_3(HL)_2(Hpyterpy)_2].2H_2O$ and $[Cu_4(HL)_2(4,4'\text{-bipy})(H_2O)_5]$ using *N*-heterocyclic ligands such as 4'-(4-pyridyl)-4,2':6',4''-terpyridine (pyterpy) and 4,4'-bipyridyl (4,4'-bipy) and 1-hydroxyethylidenediphosphonic acid ($H_5L = CH_3C(OH)(PO_3H_2)_2$). They characterized the CPs by powder X-ray diffraction, elemental analysis, IR and TG-DSC. Structural data analysis disclosed that $[Cu_3(HL)_2(Hpyterpy)_2].2H_2O$ exhibited trinuclear units $[Cu_3(HL)_2]_n^{2-}$ forming 1D fish-bone like chain with three five-coordinated Cu(II) ions. However, the second CP $[Cu_4(HL)_2(4,4'\text{-bipy})(H_2O)_5]$ displayed tetranuclear units $[Cu_4O_{10}]_n$ forming 2D inorganic-organic alternate arrangement layer with four five coordinated Cu(II) ions (Fig. 1.29).

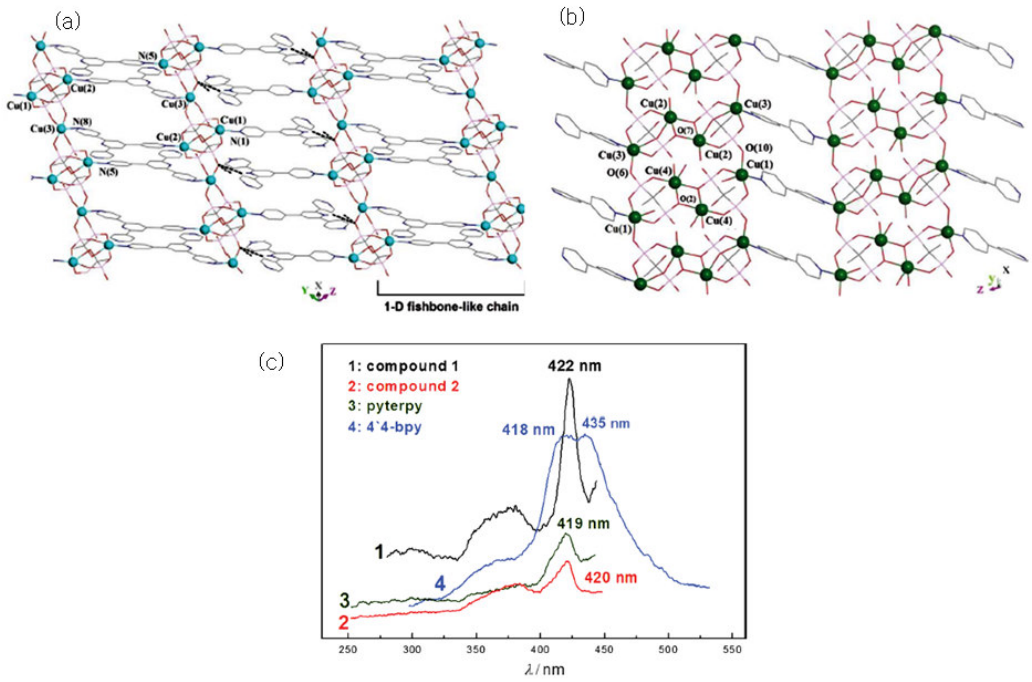

Fig. 1.29: (a) 2D H-bonded layer by linking 1D fishbone-like chain with H-bond interactions in *ab*-plane; (b) 2D *zig-zag* layer structure with inorganic-organic alternate arrangement in the *ac*-plane and (c) solid-state emission spectra of complexes

Furthermore, they confirmed their potential use in optics field by obtaining the electrochemical studies for both compounds. They carried out the emission studies for these CPs and observed that the emission for complex bearing pyterpy display higher intensity due to intraligand π*-π emission state of organic *N*-heterocyclic amine. They also reported their magnetism data, which revealed that the former compound demonstrated ferrimagnetic interactions between metal centers, whereas the latter has antiferromagnetic property.

Yucesan et al. [58] hydrothermally synthesized materials of Cu(II)-terpy/oxovanadium organophosphonate family from the reaction of $CuSO_4.5H_2O$, Na_3VO_4, 2,2':6:2''-terpyridine (terpy), and the appropriate organophosphonate ligand. They explained that the aforementioned family showed the propensity to display diverse oxovanadium building blocks. Hence, the reported complexes $[\{Cu(terpy)\}\text{-}(V_2O_4)(O_3PPh)(HO_3PPh)_2]$, $[\{Cu(terpy)\}VO(O_3PCH_2PO_3)]$, $[\{Cu(terpy)\}_2(V_4O_{10})(O_3PCH_2CH_2PO_3)]$ and $[\{Cu\text{-}(terpy)\}(V_2O_4)\{O_3P(CH_2)_3PO_3\}].2.5H_2O$ are one dimensional, $[\{Cu(terpy)\}(V_2O_4)\{O_3P(CH_2)_3PO_3\}]$ and $[\{Cu(terpy)(H_2O)\}(V_3O_6)\{O_3P(CH_2)_4PO_3\}]$ are three- and two-dimensional, respectively (Fig. 1.30). Furthermore, they found that the oxovanadium subunits showed diverse geometry around

vanadium range from square pyramid to tetrahedra with distinct oxidation state of metal ion including the formation of mixed oxidation state metal ion in one of the complex i.e., square pyramid V(IV) and binuclear units of corner-sharing V(V) tetrahedra in [{Cu(terpy)(H_2O)}(V_3O_6){$O_3P(CH_2)_4PO_3$}].

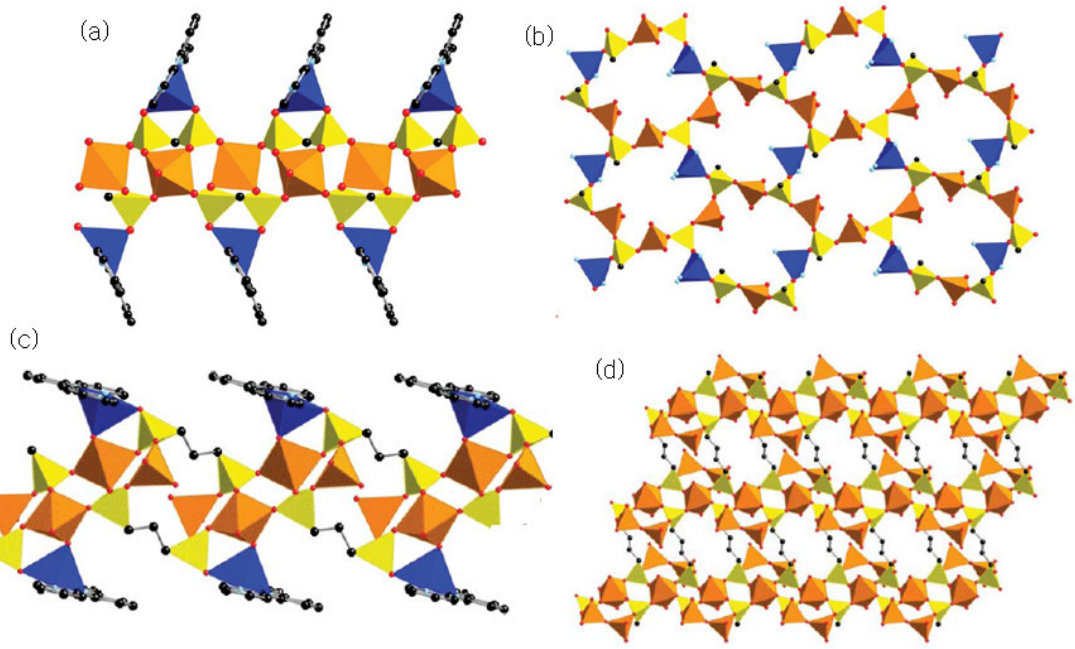

Fig. 1.30: A polyhedral representation of (a) 1D structure of [Cu(terpy)VO-($O_3PCH_2PO_3$)]; (b) bimetallic copper vanadophosphonate network of [{Cu(terpy)}(V_2O_4){$O_3P(CH_2)_3PO_3$}] in the *ab*-plane; (c) 1D structure of [{Cu(terpy)}(V_2O_4){$O_3P(CH_2)3PO_3$}].2.5H_2O and (d) the vanadophosphonate layer structure of [{Cu(terpy)(H_2O)}(V_3O_6){$O_3P(CH_2)_4PO_3$}] in the *ab*-plane

Constable et al. [59] reported the synthesis of Zn(II) based discrete molecular metallohexacycle constituted from 4'-(4-ethynylphenyl)-4,2':6',4"-terpyridine, polycatenated, triply interlocked metallocapsules from 4'-(4-pyridyl)-4,2':6',4"-terpyridine, and 1-dimensional coordination polymers from 4'-{4-(3-chloropyridyl)}-4,2':6',4"-terpyridine (Fig. 1.31).

However, they observed that an incorporation of the chloro-substituent into the ligand changes the assembly from the discrete cage to a 1-D polymer in which the 4'-(3-chloropyridyl) group is non-coordinated. They found diverse architectures with the use of different crystallization conditions of the complexes.

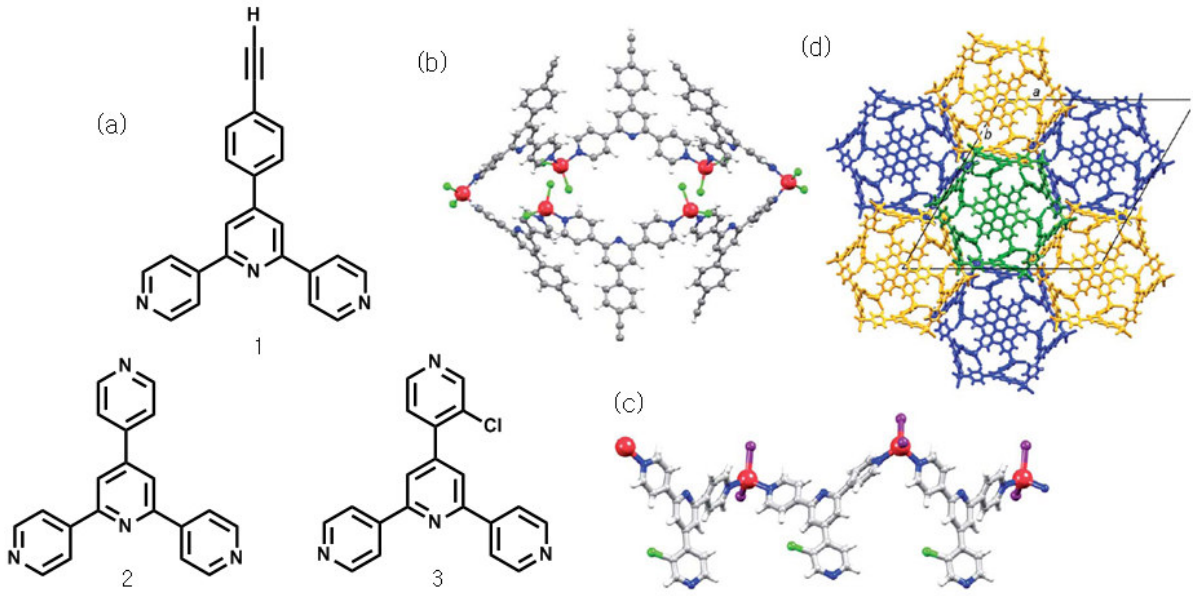

Fig. 1.31: (a) Structures of ligands 1-3; (b) view of hexametallic macrocycle in $[\{ZnCl_2(1)\}_6]$; (c) part of 1D chain of $[\{ZnI_2(3)\}_n]$ in $[\{ZnI_2(3)\}_n].0.25H_2O$ and (d) packing of $[Zn_{12}I_{24}(2)_8]$ molecules along *c*-axis; the color codes highlight the 3-fold symmetry

Chen et al. [60] solvothermally synthesized Cu(I) MOF, $\{[Cu(pytpy)].NO_3.CH_3OH\}_\infty$ exhibiting 4-fold interpenetrating 3D framework with (10,3)-b topology by assembling $Cu(NO_3)_2 \cdot 3H_2O$ with 2,4,6- tris(4-pyridyl)-pyridine (pytpy) in MeOH-dimethylacetamide (DMA) solvent mixture. Moreover, they showed the dynamic behavior of the MOF by allowing it to exchange the MeOH molecule from water molecule via single-crystal-to-single-crystal (SC–SC) process. Thereby, they observed that exchanging the anions possessing different geometries such as spherical, linear, and trigonal planar anions was easily documented visually by change in color corresponding to the anion. Hence, the hydrated complex found to be a sensor for these anions (Fig. 1.32). Furthermore, the dehydrated complex displayed the selective adsorption of CO_2 over N_2 remarkably with the variation in anions at ambient temperature.

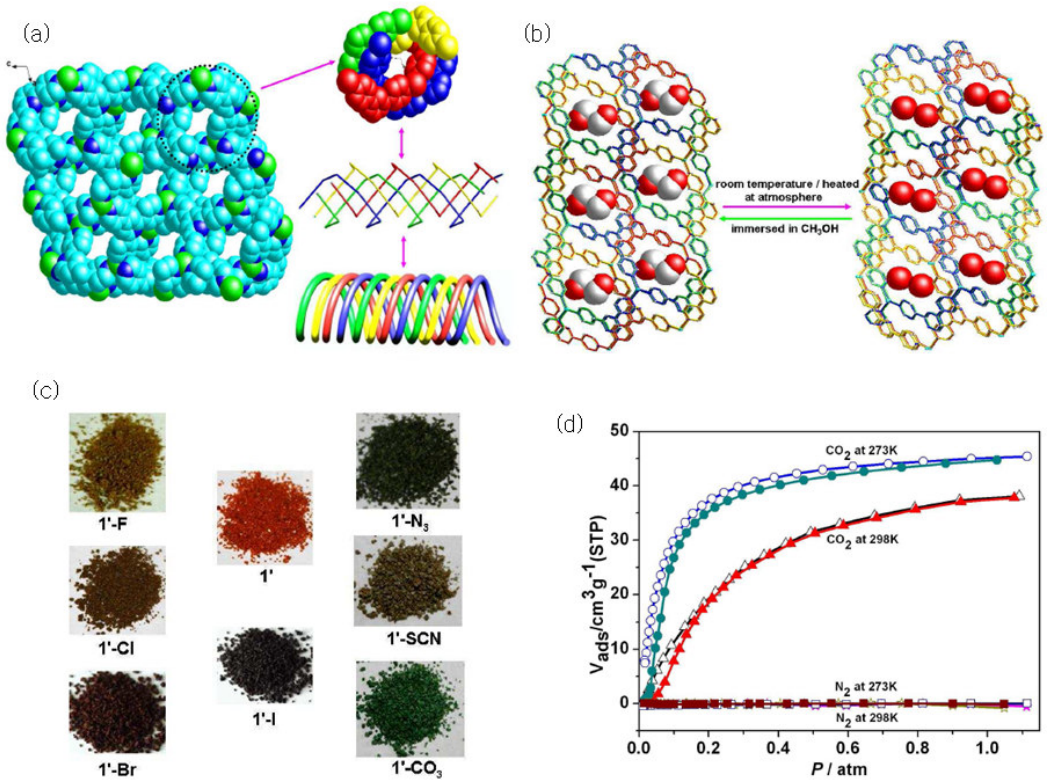

Fig. 1.32: (a) A space–filling diagram of the 4-fold interpenetration in $\{[Cu(pytpy)].NO_3.CH_3OH\}_\infty$ and view of the single 4-fold helical channel; (b) representation of SC-SC transformation; (c) the color of dehydrated complex and different anion-exchanged complexes and (d) sorption isotherms of CO_2 and N_2 measured at 273 and 298 K

Choi et al. [61] synthesized 3D porous MOFs, $[Zn_4O.(NTN)_2]\cdot 10DMA\cdot 7H_2O$ (SNU-150) and $[Zn_5.(NTN)_4.(DEF)_2][NH_2\text{-}(C_2H_5)_2]_2\cdot 8DEF\cdot 6H_2O$ (SNU-151) in different solvent systems, particularly, in absence and presence of acid. The authors reported that the former MOF displayed neutral doubly interpenetrated framework while latter formed an anionic non-interpenetrated framework with diethylammonium cations in the pores. Though with smaller surface area and different framework structure, the desolvated charged framework (SNU-151') showed higher gas storage capacity than the desolvated neutral MOF (SNU-150'). Hence, they suggested that the charged framework is found to be potential for gas storage and gas separation applications (Fig. 1.33).

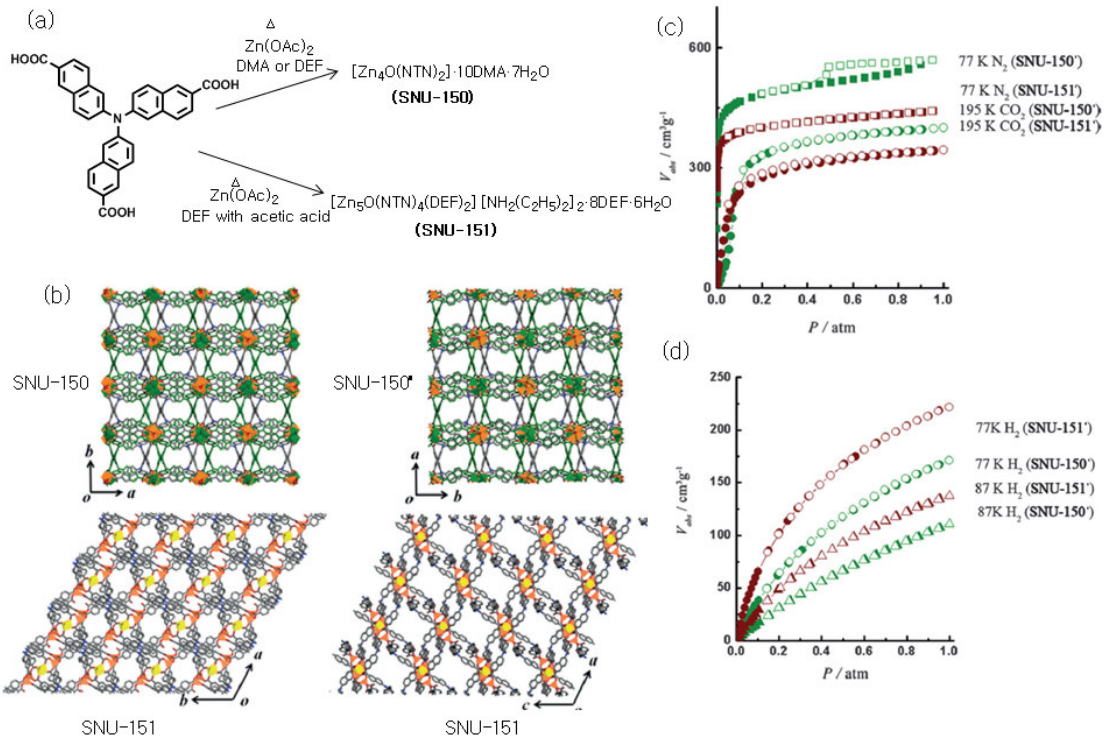

Fig. 1.33: (a) Synthetic scheme of SNU-150 and SNU-151; (b) crystal packing of SNU-150, SNU-150' in *ab*-plane whereas SNU-151 and SNU-151' in the *ab* and *ac*-plane; gas sorption isotherms for SNU-150' and SNU-151'; (c) N_2 and CO_2 and (d) H_2 at 77 K and 87 K

Liu et al. [62] synthesized six anthracene based Cu(II), Co(II), and Ni(II) complexes i.e., $[Cu_2(L1)_4(CH_3OH)_2](CH_3OH)$, $[Cu_4(L1)_6(L2)_4](NO_3)_2(H_2O)_2$, $\{[Cu_2(L1)_4(L3)](CH_3OH)_{0.25}\}_\infty$, $[Co_2(L1)_4(L4)_2(\acute{\imath}\text{-H2O})](CH_3OH)$, $\{[Co(L1)_2(L5)(CH_3OH)_2]\}_\infty$, and $\{[Ni(L1)_2(L5)(CH_3OH)_2]\}_\infty$ involving anthracene-9-carboxylic acid (HL1) with different auxiliary ligands *viz.*, (L2) 2,2'-bipyridine, (L3) 1,4-diazabicyclo[2.2.2]octane, (L4) 1,10-phenanthroline, and (L5) 4,4'-bipyridine). They systematically investigated that the influence of bulky π-ring of anthracene on the properties of the complex with respect to the auxillary ligand chosen (Fig. 1.34). The complexes showed various secondary intermolecular interactions such as π-π stacking and C–H···π interactions mainly responsible for the formation of metal complexes. Additionally, they have reported the magnetic study for all the complexes and found that the complexes with long intermetallic link led to the weak magnetic coupling while Cu complexes found to be strongly coupled owing to the presence of paddle-wheel structure of copper acetate.

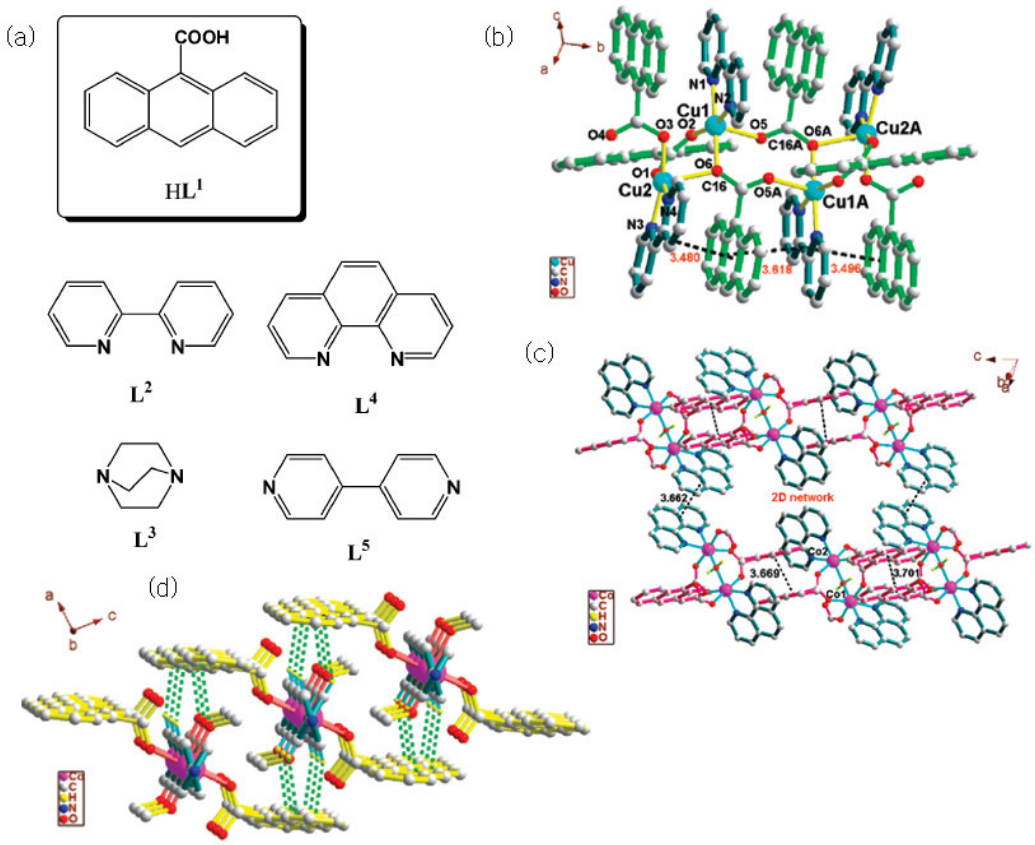

Fig. 1.34: (a) Chemical structure of the molecules; (b) view of the coordination environment of Cu(II) in the tetranuclear unit of $[Cu_4(L1)_6(L2)_4](NO_3)_2(H_2O)_2$; (c) 2D network in $[Co_2(L1)_4(L4)_2(\acute{\imath}\text{-}H_2O)](CH_3OH)$ and (d) interchain C–H$\cdots\pi$ interactions in $\{[Co(L1)_2(L5)(CH_3OH)_2]\}_\infty$

Dong et al. [63] solvothermally synthesized Mn(II) based supramolecular isomers, $[Mn_2(pbt)_2(H_2O)_2.2H_2O]_n$ and $[Mn_2(pbt)_2(H_2O)_2.DMF]_n$ (H_2pbt = 5'-(pyridin-2-yl)-2H,4'H-3,3'-bis(1,2,4-triazole) in different solvent system. They observed that the former isomer showed a new (3,4)-connected topology whereas the latter is a 4-connected 'lvt' net (Fig. 1.35). They concluded that the solvent plays an important role in governing the structure of the complex. Additionally, they also obtained that irreversible solid state transformation of one isomer to another isomer and also illustrated that both isomers show weak antiferromagnetic interactions as revealed by their magnetic measurement.

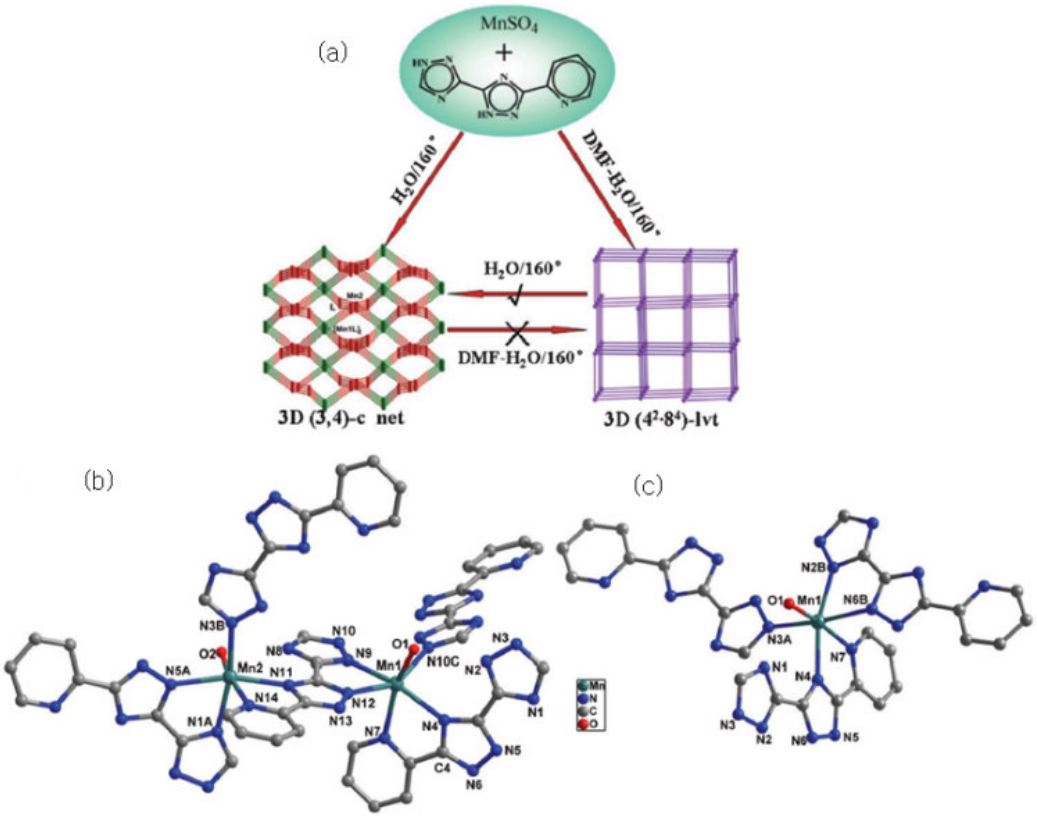

Fig. 1.35: (a) Synthetic procedures and structural transformations of both isomers; coordination environments for Mn(II) in (a) $[Mn_2(pbt)_2(H_2O)_2.2H_2O]_n$ and (b) $[Mn_2(pbt)_2(H_2O)_2.DMF]_n$

The above literatures revealed that there is no systematic study on the co-crystal/salt formation using phosphonic acid and pyrazole.

Goals

A profound understanding of the fundamental interactions involved in the construction of multi-component non-covalently bound architectures is requisite, thereafter; the knowledge is further transcript to produce novel potential materials. Computational tools endow with a convenient means to rank and correlate the strength of co-crystal/salts formed by the acknowledgement of the strength of synthons formed.

The present work of the thesis aims to-

- Study the effects of covalent modification on the supramolecular behavior of ditopic ligands and variety of phosphonic acids comprising different functional group including the search for new synthons formed by pyrazole and phosphonic acid.

- Construction of several pseudo-polymorphs and ternary systems from newly synthesized anthracene based phosphonic acid and conformationally flexible bispyrazole, to analyze the effect of various guests on the supramolecular architecture. In addition, study of Cu(II) metal complex of newly synthesized monoester of phosphonic acid and solid state transformation of Cu(II) metal complex to new another Cu(II) metal complex

- Besides pyrazole, evaluation of structural analysis and synthons in ditopic pyridine analogues with triphosphonic acid were carried out using crystal engineering tools. The investigation of the variable anion effect on CO_2 gas adsorption was also envisaged by ditopic terpyridine based isomorphous MOFs.

- The predictions based on computational results were compared with experimental results to explore their stability.

References:

1. Lehn, J. M., Atwood, J. L., Davies, J. E. D., MacNicol, D. D. and Vögtle, F., "*Comprehensive Supramolecular Chemistry*", Pergamon/Elsevier Oxford (1996).
2. Vögtle, F., "*Supramolecular Chemistry*", John Wiley & Sons, Ltd, Chichester (1991).
3. Lehn, J. M., "*Supramolecular Chemistry: Concepts and Perspectives*", Wiley-VCH Verlag GmbH, Weinheim, (1995).
4. Gale, P. A. and Steed, J. W., "*Supramolecular Chemistry: From Molecules to Nanomaterials*", (Eds), John Wiley & Sons, Chichester (2012).
5. Kornecki, K. P. and Berry, J. F., "Introducing a mixed-valent dirhodium(II,III) catalyst with increased stability in C-H amination", *Chem. Commun*., **48**, 12097 (2012).
6. Bertrand, N., Gauthier, M. A., Bouvet, C., Moreau, P., Petitjean, A., Leroux, J. C. and Leblond, J., "New pharmaceutical applications for macromolecular binders", *J. Control. Release*, **155**, 200 (2011).
7. Sauvage, J.-P., "Molecular Machines & Motors. *Struct. Bond.*", Springer, **99** (2001).
8. Maitland, G. C., Rigby, E. B., Smith, E. B. and Wakeham, W. A., "*Intermolecular Forces: Their Origin and Determination*", Clarendon press, Oxford (1981).
9. Dunitz, J. D., "*Thoughts on Crystals as Supermolecules*", John Wiley & Sons, Ltd., 1-30 (2007).
10. Steed, J. W. and Atwood, J. L., "*Supramolecular Chemistry*", 2 ed., John Wiley & Sons, Ltd., Hoboken, New Jersey (2009).
11. Desiraju, G. R., "*Crystal Engineering: The Design of Organic Solids*", Elsevier, Amsterdam, (1989).
12. Desiraju, G. R., "Supramolecular synthons in crystal engineering—A new organic synthesis", *Angew. Chem., Int. Ed.*, **34**, 2311 (1995).
13. Walsh, R. D. B., Bradner, M. W., Fleischman, S., Morales, L. A., Moulton, B., Rodríguez-Hornedo, N. and Zaworotko, M. J., "Crystal engineering of the composition of pharmaceutical phases", *Chem. Commun*., 186 (2003).
14. Shen, Q. J., Pang, X., Zhao, X. R., Gao, H. Y., Sun, H.-L. and Jin, W. J., "Phosphorescent co-crystals constructed by 1,4-diiodotetrafluorobenzene and polyaromatic hydrocarbons based on C–I$\cdots\pi$ halogen bonding and other assisting weak interactions", *CrystEngComm*, **14**, 5027 (2012).

15. Nishio, M., "*In Weak Hydrogen Bonds in Encyclopedia of Supramolecular Chemistry*", Atwood, J. L. and Steed, J. W., Eds., Marcel Dekker, New York, 1576–1585 (2004).
16. Etter, M. C., "Hydrogen bonds as design elements in organic chemistry", *J. Phys. Chem.***, 95**, 4601 (1991).
17. Braga, D., Grepioni, F. and Desiraju, G. R., "Crystal engineering and organometallic architecture", *Chem. Rev*., **98**, 1375 (1998).
18. Chui, S. S. Y., Lo, S. M. F., Charmant, J. P. H., Orpen, A. G. and Williams, I. D., "A chemically functionalizable nanoporous material", *Science*, **283**, 1148 (1999).
19. Bernstein, J., "*Polymorphism in Molecular Crystals*", Oxford University Press, United States, 352 (2002).
20. Sarma, J. A. R. P. and Desiraju, G. R., "*Polymorphism and Pseudopolymorphism in Organic Crystals: A Cambridge Structural Database Study*", Kluwer, Dordrecht, 325–356 (1999).
21. Almarsson, Ö. and Zaworotko, M. J., "Crystal engineering of the composition of pharmaceutical phases. Do pharmaceutical co-crystals represent a new path to improved medicines?", *Chem. Commun.*, 1889 (2004).
22. Etter, M. C. and Panunto, T. W., "1,3-bis(m-nitrophenyl)urea: An exceptionally good complexing agent for proton acceptors", *J. Am. Chem. Soc*., **110**, 5896 (1988).
23. Vanniekerk, J. N. and Saunder, D. H., "The crystal structure of the molecular complex of 4:4'-dinitrodiphenyl with diphenyl", *Acta Crystallogr.*, **1**, 44 (1948).
24. Buck, J. S. and Ide, W. S., "Mixed benzoins. VI. Further examples of reversibility. The formation of addition compounds", *J. Am. Chem. Soc.*, **53**, 2784 (1931).
25. Anderson, J. S., "Structure of organic molecular compounds", *Nature*, **140**, 583 (1937).
26. Hall, B. and Devlin, J. P., "2:1 solid-state complex of hexamethylbenzene:tetracyanoethylene", *J. Phys. Chem.*, **71**, 465 (1967).
27. Du, M., Zhang, Z.-H. and Zhao, X.-J. "Co-crystallization of bent dipyridyl type compounds with aromatic dicarboxylic acids: Effect of the geometries of building blocks on hydrogen-bonding supramolecular patterns", *Cryst. Growth Des*., **5**, 1199 (2005).
28. Baylies, C. J., Riis-Johannessen, T., Harding, L. P., Jeffrey, J. C., Moon, R., Rice, C. R. and Whitehead, M., "Allosteric-controlled metal specificity of a ditopic ligand", *Angew. Chem., Int. Ed*., **44**, 6909 (2005).

29. Kennedy, A. R., Brown, K. G., Graham, D., Kirkhouse, J. B., Kittner, M., Major, C., McHugh, C. J., Murdoch, P. and Smith, W. E., "Chromophore containing bipyridyl ligands: Part 1, supramolecular solid-state structure of Ag(I) complexes", *New J. Chem.*, **29**, 826 (2005).
30. Klein, O., Aguilar-Parrilla, F., Lopez, J. M., Jagerovic, N., Elguero, J. and Limbach, H.-H., "Dynamic NMR study of the mechanisms of double, triple, and quadruple proton and deuteron transfer in cyclic hydrogen bonded solids of pyrazole derivatives", *J. Am. Chem. Soc.*, **126**, 11718 (2004).
31. Claramunt, R. M., Lopez, C., Garcia, M. A., Denisov, G. S., Alkorta, I. and Elguero, J., "Protonation and phase effects on the NMR chemical shifts of imidazoles and pyrazoles: Experimental results and GIAO calculations", *New J. Chem.*, **27**, 734 (2003).
32. Detering, K., Tolstoi, P. M., Golubev, N. S., Denisov, G. S. and Limbakh, Kh.-Kh., "Vicinal H/D isotope effects in NMR spectra of complexes with coupled hydrogen bonds: Phosphoric acids", *Dokl. Ross. Akad. Nauk.*, **379**, 353 (2001).
33. Bhattacharya, A. K. and Thyagarajan, G. "Michaelis–Arbuzov rearrangement", *Chem. Rev.*, **81**, 415 (1981).
34. Boldog, I., Rusanov, E. B., Sielerb, J. and Domasevitch, K. V., "Cooperative association of pyrazoles and phenols: A versatile binary system", *New J. Chem.*, **28**, 756 (2004).
35. Sanz, D., Claramunt, R. M., Alkorta, I., Elguero, J., Thielc, W. R. and Rüfferd, T., "A theoretical and experimental NMR study of the tautomerism of two phenylene-bis-C-substituted pyrazoles", *New J. Chem.*, **32**, 2225 (2008).
36. Aakeröy, C. B., Salmon, D. J., Smith, M. M. and Desper, J., "Cyanooximes as effective and selective co-crystallizing agents", *CrystEngComm*, **11**, 439 (2009).
37. Boldog, I., Rusanov, E. B., Chernega, A. N., Sieler, J. and Domasevitch, K. V., "Acentric extended solids by self assembly of 4,4'-bipyrazolyls", *Angew. Chem., Int. Ed.*, **40**, 3435 (2001).
38. Boldog, I., Rusanov, E. B., Sieler, J., Blaurock, S. and Domasevitch, K. V., "Construction of extended networks with a trimeric pyrazole synthon", *Chem. Commun.*, 740 (2003).
39. Aakeröy, C. B., Desper, J., Leonard, B. and Urbina, J. F., "Toward high-yielding supramoleculars synthesis: Directed assembly of ditopic imidazoles/benzimidazoles and

dicarboxylic acids into co-crystals via selective O–H···N hydrogen bonds", *Cryst. Growth Des*., **5**, 865 (2005).

40. Aakeröy, C. B., Desper, J., and Fasulo, M. E., "Improving success rate of hydrogen-bond driven synthesis of co-crystals", *CrystEngComm*, **8**, 586 (2006).
41. Aakeröy, C. B., Hurley, E. P. and Desper, J., "Modulating supramolecular reactivity using covalent 'switches' on a pyrazole platform", *Cryst. Growth Des*., **12**, 5806 (2012).
42. Goswami, A., Sengupta, S. and Mondal, R., "Construction of helical networks by using multiple V-shaped mixed ligand systems", *CrystEngComm*, **14**, 561 (2012).
43. Basu, T. and Mondal, R., "Construction of first anion-assisted helix inside a helix network", *CrystEngComm*, **12**, 366 (2010).
44. Mukherjee, A. and Desiraju, G. R., "Synthon polymorphism and pseudopolymorphism in co-crystals. The 4,4'-bipyridine–4-hydroxybenzoic acid structural landscape", *Chem. Commun*., **47**, 4090 (2011).
45. Roy, S., Mahata, G. and Biradha, K., "Co-crystal and salts of 2,2',6,6'-tetracarboxybiphenyl with bis(pyridyl) derivatives: Eight-fold interpenetrated diamondoid and layered networks", *Cryst. Growth Des*., **9**, 5006 (2009).
46. Du, M., Zhang, Z.-H., Guo, W. and Fu, X.-J., "Multi-component hydrogen-bonding assembly of a pharmaceutical agent pamoic acid with piperazine or 4,4'-bipyridyl: A channel hydrated salt with multiple-helical motifs vs a bimolecular co-crystal", *Cryst. Growth Des*., **9**, 1655 (2009).
47. Aakeröy, C. B., Panikkattu, S. V., DeHaven, B. and Desper, J., "Establishing supramolecular control over solid-state architectures: A simple mix and match strategy", *Cryst. Growth Des*., **12**, 2579 (2012).
48. Nauha, E., Kolehmainen, E. and Nissinen, M., "Packing incentives and a reliable N–H/N–pyridine synthon in co-crystallization of bipyridines with two agrochemical actives", *CrystEngComm*, **13**, 6531 (2011).
49. Bhogala, B. R. and Nangia, A., "Ternary and quaternary co-crystals of 1,3-cis,5-ciscyclohexanetricarboxylic acid and 4,4'-bipyridines", *New J. Chem*., **32**, 800 (2008).
50. Song, Y.-F., Berry, J. F., Bill, E., Bothe, E., Weyhermüller, T. and Wieghardt, K., "Iron complexes of new pentadentate ligands containing the 1,4,7-triazacyclononane-1,4-diacetate motif. Spectroscopic, electro-, and photochemical studies", *Inorg. Chem.*, **46**, 2208 (2007).

51. Abrahams, B. F., Batten, S. R., Hamit, H., Hoskins, B. F. and Robson, R., "A cubic (3,4)-connected net with large cavities in solvated $[Cu_3(tpt)_4](ClO_4)_3$ (tpt = 2,4,6-tri(4-pyridyl)-1,3,5-triazine)", *Angew. Chem., Int. Ed.*, **35**, 1690 (1996).
52. Li, M.-X., Miao, Z.-X., Shao, M., Liang, S.-W. and Zhu, S.-R., "Metal-organic frameworks constructed from 2,4,6-tris(4-pyridyl)-1,3,5-triazine", *Inorg. Chem.*, **47**, 4481 (2008).
53. Yoshida, J., Nishikiori, S.-I. and Kuroda, R., "Construction of supramolecular complexes by use of planar bis(β-diketonato)cobalt(II) complexes as building blocks", *Chem. Lett.*, **36**, 678 (2007).
54. Heine, J., Schmedt auf der Günne, J. and Dehnen, S., "Formation of a strandlike polycatenane of icosahedral cages for reversible one-dimensional encapsulation of guests", *J. Am. Chem. Soc*., **133**, 10018 (2011).
55. Zhang, J.-P. and Kitagawa, S., "Supramolecular isomerism, framework flexibility, unsaturated metal center, and porous property of Ag(I)/Cu(I) 3,3',5,5'-tetrametyl-4,4'-bipyrazolate", *J. Am. Chem. Soc*., **130**, 907 (2008).
56. Mitra, A., Hubley, C. T., Panda, D. K., Clark, R. J. and Saha, S., "Anion-directed assembly of a non-interpenetrated square-grid metal-organic framework with nanoscale porosity", *Chem. Commun.*, **49**, 6629 (2013).
57. Ma, K.-R., Ma, F., Zhu, Y.-L., Yu, L.-J., Zhao, X.-M., Yang, Y. and Duan, W.-H., "*N*-heterocyclic amine-directed structures and properties of two Cu(II) diphosphonates", *Dalton Trans*., **40**, 9774 (2011).
58. Yucesan, G., Golub, V., O'Connor, C. J. and Zubieta, J., "Solid state coordination chemistry of the copper(II)-terpyridine/oxovanadium organophosphonate system: Hydrothermal syntheses, structural characterization and magnetic properties", *Dalton Trans*., 2241 (2005).
59. Constable, E. C., Zhang, G., Housecroft, C. E. and Zampese, J. A., "Zinc(II) coordination polymers, metallohexacycles and metallocapsules—Do we understand self-assembly in metallosupramolecular chemistry: Algorithms or serendipity?", *CrystEngComm*, **13**, 6864 (2011).
60. Chen, Y.-Q., Li, G.-R., Chang, Z., Qu, Y.-K., Zhang, Y.-H. and Bu, X.-H., "A Cu(I) metal-organic framework with 4-fold helical channels for sensing anions", *Chem. Sci.*, **4**, 3678 (2013).

61. Choi, M.-H., Park, H. J., Hong, D. H. and Suh, M. P., "Comparison of gas sorption properties of neutral and anionic metal-organic frameworks prepared from the same building blocks but in different solvent systems", *Chem. Eur. J.*, **19**, 17432 (2013).
62. Liu, C.-S., Wang, J.-J., Yan, L.-F., Chang, Z., Bu, X.-H., Sañudo, E. C. and Ribas, J., "Copper(II), cobalt(II), and nickel(II) complexes with a bulky anthracene-based carboxylic ligand: Syntheses, crystal structures, and magnetic properties", *Inorg. Chem.*, **46**, 6299 (2007).
63. Dong, W.-W., Li, D.-S., Zhao, J., Ma, L.-F., Wua, Y.-P. and Duana, Y.-P., "Two solvent-dependent manganese(II) supramolecular isomers: Solid-state transformation and magnetic properties", *CrystEngComm*, **15**, 5412 (2013).

Chapter 2

Synthesis and Structural Studies of Supramolecular Organic Frameworks (SOFs) using Pyrazole

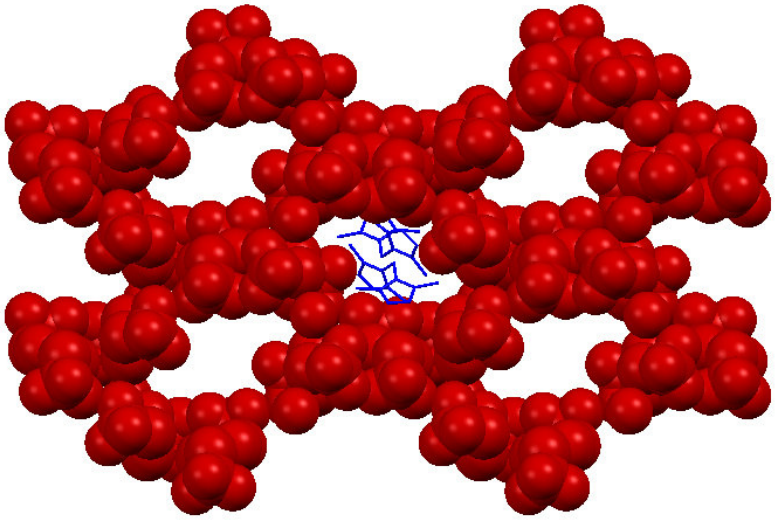

Crystal engineering targets its goal in finding robust supramolecular synthons that has led to the design of new potential materials through synthon approach with the potential to exhibit specific chemical/physical properties [1-3]. To this end, the building blocks of different dimensions and functionalities have been synthesized by different workers as its conformation/orientation [4-7] directs the construction of diverse supramolecular organic frameworks (SOFs). Notably, the rigid ligand with inadequate conformation decreases the anticipation of obtaining distinct topology however, the inclusion of flexible unit in the ligand may aid in fabrication of supramolecular architecture with guest breathing potential. Hence, the orientation of the ligand plays a vital role in the formation of potential intriguing architecture.

The pyrazole with presence of proton donor and acceptor capability represents a very fascinating class of heterocyclic compounds and has many biological and pharmaceutical importances [8-9]. Several groups employed number of pyrazole analogues with diversity in substituents for the formation of their solid molecular structures in which proton tautomerism was comprehensively examined [10-12] and [Ref. [34] from chapter 1]. Moreover, the choice of building block possessing the potential hydrogen bonding moieties is indispensable for the generation of new synthons [13-16]. In past decades, researchers have exploited synthons involving carboxylic acids [17-20] for designing co-crystals, which led to the profound knowledge of the intermolecular interactions between two constituents possessing hydrogen bond donors and acceptors. Therefore, it was assumed that the tetrahedral geometry would give rise to distinct networks in contrast to the planar carboxylic acid. In this regard, the tetrahedral geometry of phosphonate group possessing two hydrogen donors and one acceptor has been utilized, which gives complex and diverse supramolecular patterns. Although phosphonate salts have got less recognition as compare to carboxylic acids, however, some of the phosphonate supramolecular patterns with amines and pyridyls analogues have been reported in last decade. Notably, many researchers have also reported various ammonium salts of alkane phosphonic acids [21], diphosphonic acids [22-23], some mixed phosphono-carboxylic acids [24-26] and have illustrated an array of two- or three-dimensional hydrogen bonded supramolecular organic frameworks (SOFs). It is considerably familiar that the hydrogen bond such as O–H···O, N–H···O, N–H···N etc., which through recurrently occurring synthons is the main driving force for the formation of intriguing and potential supramolecular network. Therefore, formation of two repeating units i.e., catemeric chain of phosphonic group (P–O–H···O–P) bonds and its

dimer have been illustrated among all diversity of 2D- or 3D- hydrogen bonded networks. Subsequently, the formation of dimeric or catemeric phosphonate synthon governs the construction of crystal structure of phosphonic acid. Recently, our group has reported the formation of phosphonate salts with pyrazole and has focused on impact of electron donating substituent possessed by pyrazole on supramolecular structures [27].

The thrust for the rational synthesis of supramolecular structure under deliberate control via intermolecular interactions with the better understanding of the process of self-assembly and the consequently synthesis of a premeditated crystal structure, remains the main goal of these sort of studies. Some of the relevant literatures involving pyrazole and phosphonic acid have been discussed below.

Plabst et al. [28] synthesized the bisphosphonic acid C_6H_5-$CH(PO_3H_2)_2$ (H_4L) and the tetrakisphosphonic acid $(PO_3H_2)_2CH$-C_6H_4-$CH(PO_3H_2)_2$ (H_8L) and reported the collection of hydrogen bonded networks of these phosphonic acids with a library of amines (Fig. 2.1) for instance guanidine, aniline, benzylamine, piperidine etc. using catemeric hydrogen bond [P–O–H···O–P] and the dimeric $R^2_2(8)$ ring motif.

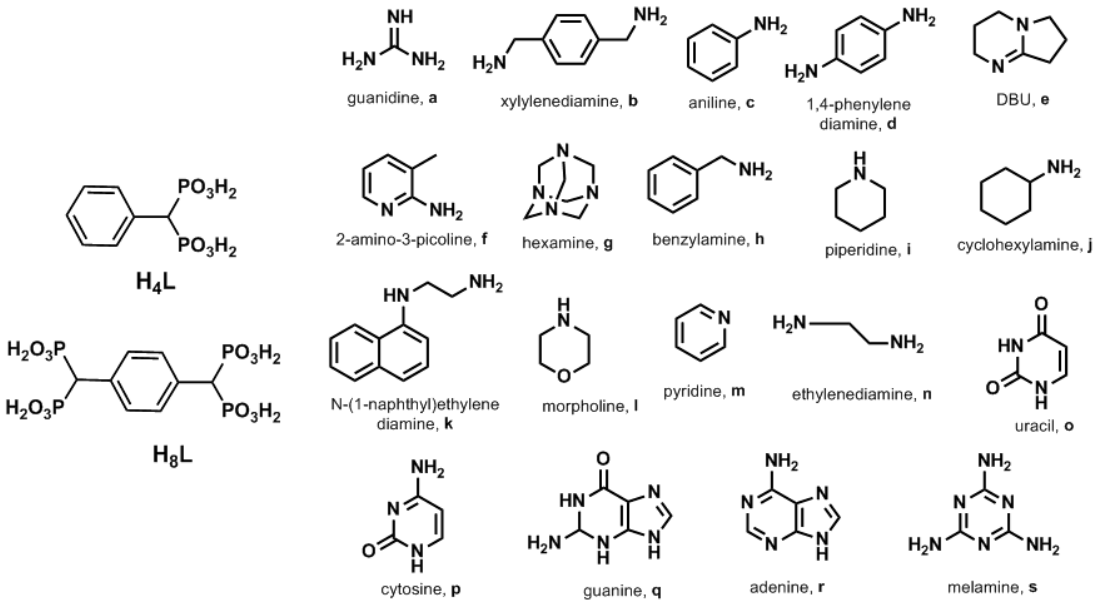

Fig. 2.1: Left: chemical structure of bisphosphonic acid (H_4L) and the tetrakisphosphonic acid (H_8L) and right: amine library used for the synthesis of molecular complex

López et al. [29] reported two co-crystals [(dmpz)$(sa)_2$] and [$(dmpz)_2$(sa)] formed from controlled supramolecular reaction of 3,5-dimethyl-1*H*-pyrazole (dmpz) and salicylic acid (sa) affording two different trimers (Fig. 2.2). They concluded that the hydrogen-bond interactions between dmpz and sa were responsible for offering the sufficient driving force to direct molecular recognition and crystal packing.

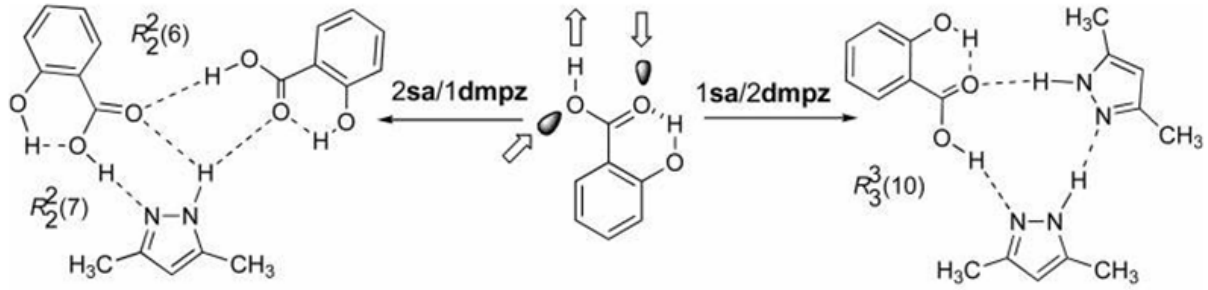

Fig. 2.2: Supramolecular synthesis of aggregates [(dmpz)$(sa)_2$] and [$(dmpz)_2$(sa)]

Basu et al. [30] investigated six molecular networks in co-crystals formed by self-complementary ditopic flexible molecule, methylenebis(3,5-dimethylpyrazole) (H_2MDP) and variety of common benzene polycarboxylic acids such as isophthalic (H_2IPA), trimesic (H_3TMA), pyromellitic acid (H_4PMA), terephthalic acid (H_2TPA), and acetic acid (Fig. 2.3). They have significantly accomplished that the observed heterosynthons are remarkably similar, both from the view point of H-bond directionality and size of the synthons (Scheme 2.1). They have also reported that the acid component apparently shows a systematic level of ionization based on their pKa values.

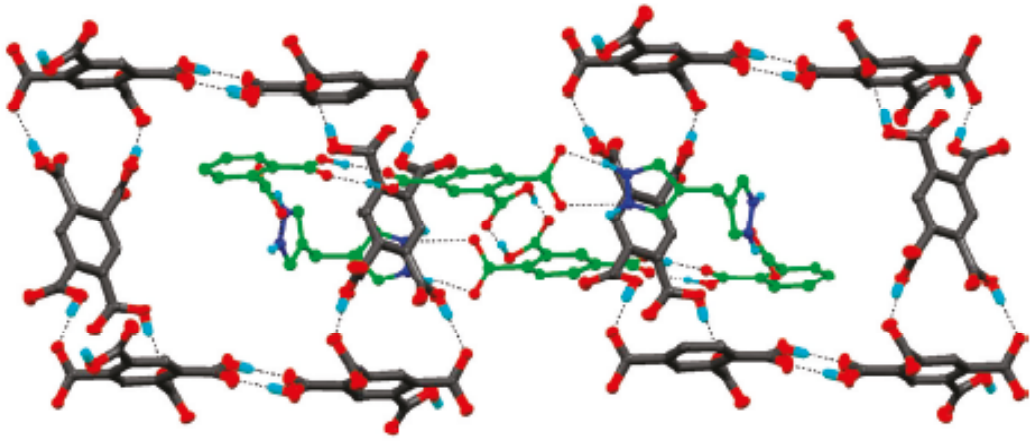

Fig. 2.3: View of two interpenetrating grids in complex [$(H_4MDP)^{2+}$.$(H_2PMA)^{2-}$.(H_4PMA)]

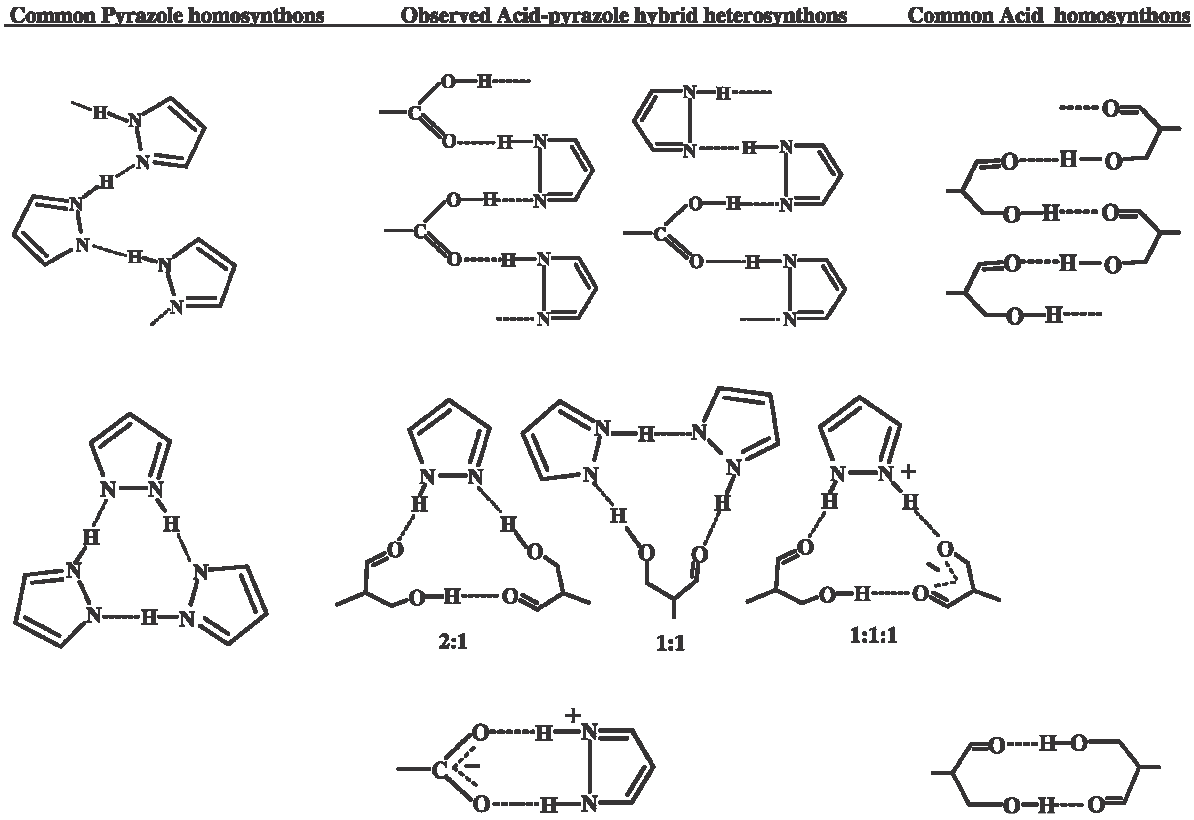

Scheme 2.1: Various homo- and hetero-synthons observed in supramolecular solid formed between pyrazole and carboxylic acid

Bureiko et al. [31] examined hydrogen molecular complexes composed of 3,5-dimethylpyrazole and a number of strong carboxylic acids: trifluoroacetic acid, trichloroacetic acid and dichloroacetic acid. They studied the structure, spectral and thermodynamic parameters of molecular complexes in solution using IR and low-temperature ^{1}H and ^{15}N NMR spectroscopy as well as quantum-chemical calculations.

Ugono et al. [32] emphasized on the steric factor which is considered to be one of the structure-directing factor and controls the type of architecture resulted from ammonium salts of 3,5-pyrazole dicarboxylic acid (PzDCA). They found that depending upon the bulkiness of amine used for co-crystallization, the assemblies of PzDCA adjust itself in order to accommodate the amine. In case of anilinium ions, *ortho*-substitution resulted in HPzDCA hydrogen-bonded chains (Fig. 2.4). However, ammonium counterions having < 6.0 Å width led to a bilayered architecture even in the presence of *ortho*-substituents.

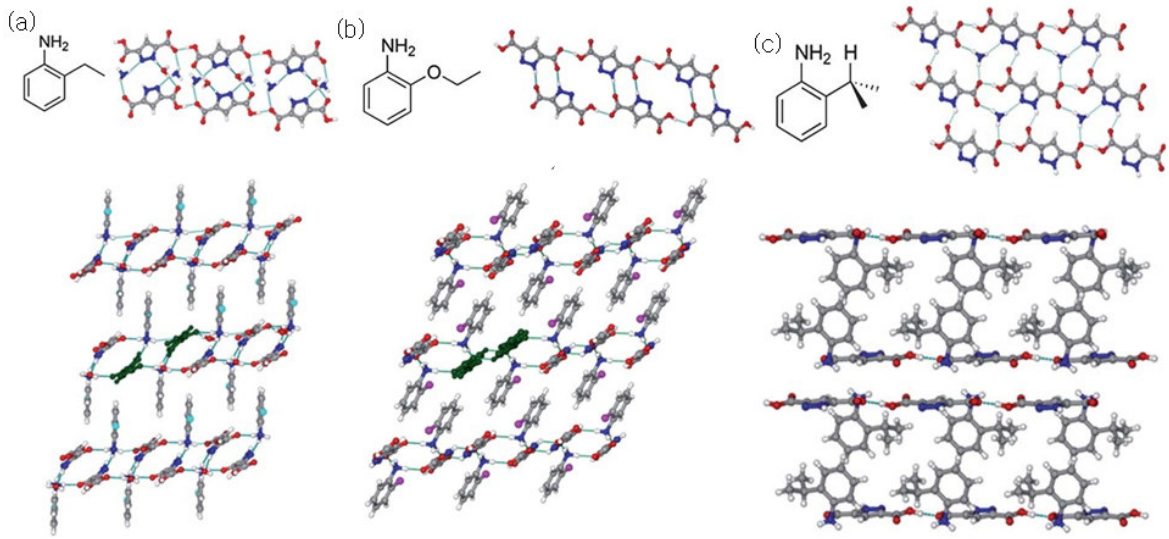

Fig. 2.4: Structural features of (a) o-ethoxyanilinium:HPzDCA - ribbons formed from hydrogen-bonded antiparallel HPzDCA chains; (b) o-ethylanilinium:HPzDCA.H_2O - ribbons formed from antiparallel HPzDCA chains and (c) 2-isopropylanilinium:HPzDCA - hydrogen-bonded layer network

Singh et al. [33] reported the anion directed supramolecular architectures formed by the association of 3,5-diphenyl-1H-pyrazole ($Pz^{Ph2}H$), with different inorganic anions such as Cl^-, SO_4^{2-}, NO_3^-, ClO_4^- and PO_4^{3-} (Fig. 2.5). They found variety of supramolecular frameworks with different anions as deduced by single crystal X-ray study. They also estimated the hydrogen bond interaction energy of these salts and concluded that rise in hydrogen bond interaction energy is caused by increase in the strength of the inorganic acid.

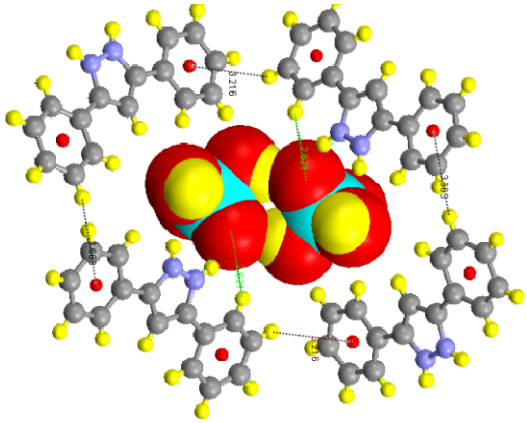

Fig. 2.5: Formation of the cavity between $Pz^{Ph2}H$ trapping the two $H_2PO_4^-$ anions in $Pz^{Ph2}H_2^+ \cdot H_2PO_4^-$

Han et al. [34] co-crystallized 3,3',5,5'-tetramethyl-4,4'-bipyrazole (tmbpz) with aliphatic dicarboxylic acid: suberic acid (H_2sub) and sebacic acid (H_2seb) with variable carbon chain length and formed two solids [(tmbpz)$_2$·(H_2sub)] and [(tmbpz)$_2$·(H_2seb)] by both solid-solid grinding and crystallization from solutions. They observed that the frameworks manifest 4-fold and 5-fold parallel interpenetration of 6^3-**hcb** networks respectively depending on the carbon chain length via formation of heterotrimer synthon as revealed by structural analysis (Fig. 2.6 and 2.7). Furthermore, authors concluded that co-crystallization could be utilized to alter the emission of the single component.

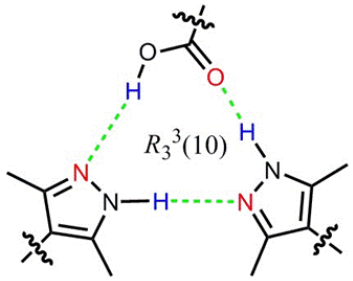

Fig. 2.6: Supramolecular heterosynthon involved in supramolecular solid of tmbpz and aliphatic carboxylic acid

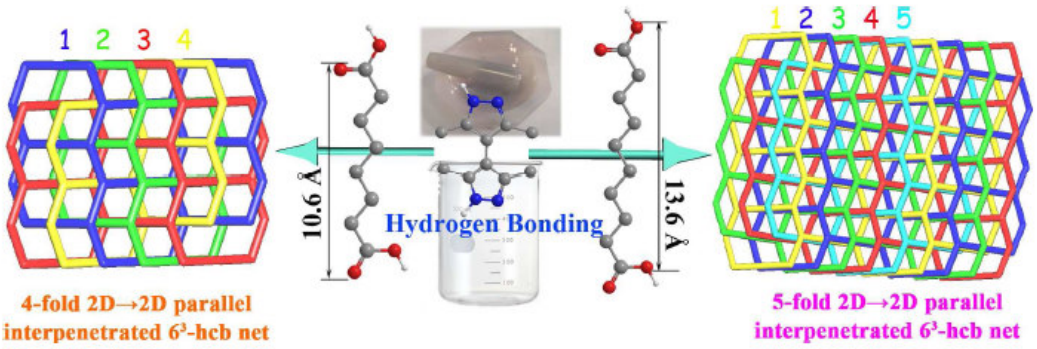

Fig. 2.7: Scheme for the synthesis of two supramolecular solids

Mahmoudkhani et al. [22] reported the concomitant polymorphs of 1,4-butanebisphosphonic acid and formation of its salts with aniline and *p*-phenylazoaniline. They demonstrated the potential use of 1,4-butanebisphosphonic acid for the generation of extended supramolecular hydrogen-bonded networks (Fig. 2.8). They concluded that the approach of using already reported phosphonate ammonium synthons formed via (P–)O–H···O–P and N–H···O–P hydrogen bonds leads to the formation of new solid material.

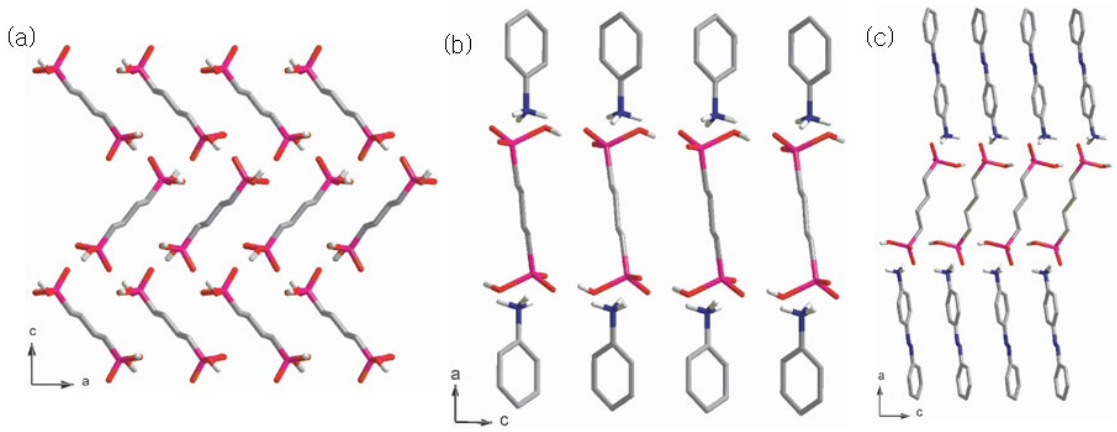

Fig. 2.8: Representation of the (a) pillared-layered structure of polymorph of 1,4-butanebisphosphonic acid; (b) pillared-bilayered structure of salt with aniline and (c) pillared-bilayered structure of salt with *p*-phenylazoaniline

Mahmoudkhani et al. [35] also reported hydrogen bonded supramolecular assemblies of phenylphosphonic acid and its salts *viz.*, anilinium phenylphosphonate, *p*-phenylazoanilinium phenylphosphonate, ethylenediammonium phenylphosphonate hydrate, and hexamethylenediammonium phenylphosphonate hydrate. On analysis, they found that self assembly of phenylphosphonic led to the formation of 2D hydrogen bonded supramolecular array (Fig. 2.9). Further, they have analyzed the crystal structures that would aid in designing new materials by understanding the structural association of organic and inorganic salts of phenylphosphonic.

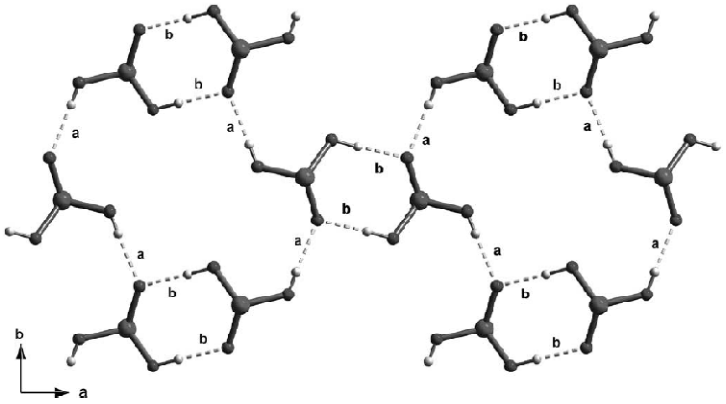

Fig. 2.9: Hydrogen bonded network in the crystal structure of phenylphosphonic acid (Note: phenyl groups are not shown for clarity)

Mahmoudkhani et al. [36] further reported extended hydrogen bonded network of diammonium salts of 1,4-butanebisphosphonic acid. They concluded that the crystal structure of

aforementioned salt can be regarded as model to design a new class of organic nanoporous materials (Fig. 2.10).

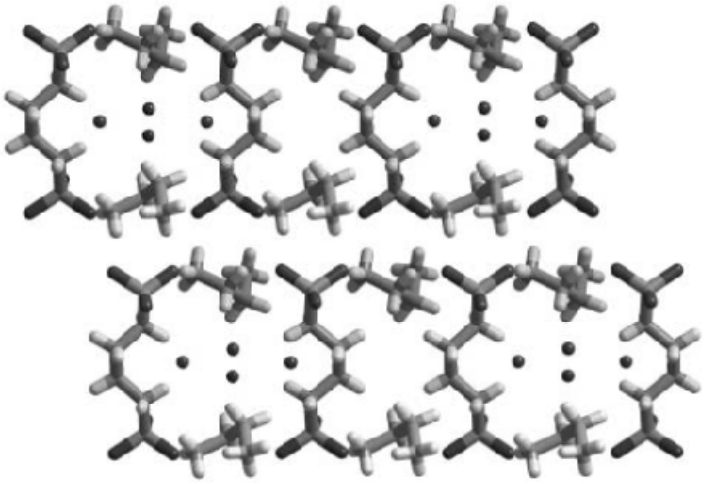

Fig. 2.10: Representation of a pillared bilayered unit for bis(ethylenediammonium).butanebisphosphonate hydrate including water molecules

Singh et al. [27] co-crystallized phenylphosphonic acid (PPA) with a diversity of ditopic pyrazoles, $Pz_{R1,R2}H$ (where R1 = R2 = H; R1 = R2 = Me; R1 = Ph, R2 = Me; and R1 = R2 = iPr). They reported that the different substituted pyrazole leads to the formation of diverse supramolecular architectures by providing sufficient non-covalent interactions as deduced by single crystal X-ray data (Fig. 2.11). They have also calculated the hydrogen bond interaction energy theoretically for all the salts and concluded that it mainly depends upon the functional group involved in the interaction. Authors also confirmed the structures in both solid and gaseous state are same.

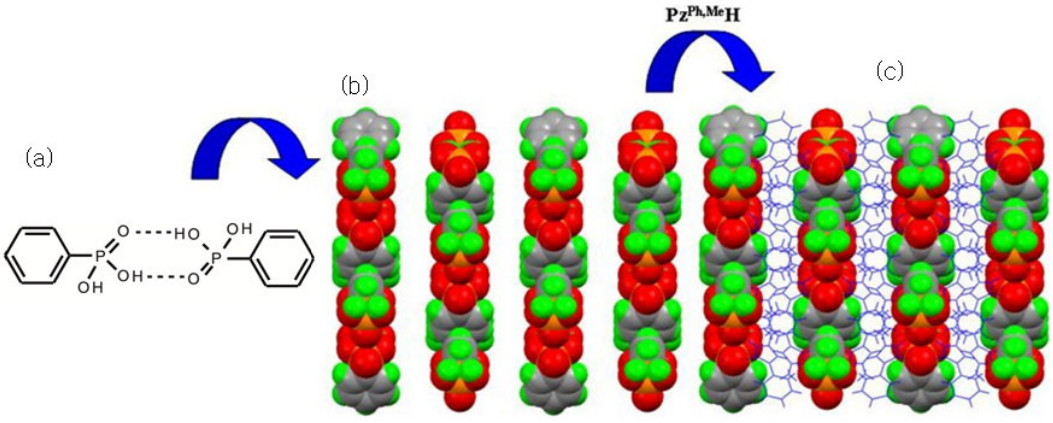

Fig. 2.11: (a) Dimeric analogue of benzoic acid; (b) alternate channels of host framework formed by phosphonic acid and (c) host with guest 3-phenyl-5-methylpyrazole

The implementation of supramolecular synthon approach has led the researchers to comprehend the intermolecular interactions between two components and utilize them to tailor new desired solids. The main target was to explore the synthon formed and structural link between phosphonic acid and rigid/flexible pyrazole analogue i.e., 3,3',5,5'-tetramethyl-1H,1'H-4,4'-bipyrazole (BPz), methylenebis(3,5-dimethylpyrazole) (MBPz) and 1,2-bis(3,5-dimethyl-1H-pyrazol-4-yl)diazene, (BPaz) and that may assist to design solid architectures with desired properties. Though, the exploitation of structural interaction pattern of phosphonic acid [37-38], pyrazole [Ref. [37-38] from chapter 1] and pyrazole as a coformer [30] have been done individually and resulted in various robust supramolecular synthons but the structural chemistry of both these components via synthon approach has not been reported yet.

The present chapter has reported the construction of four phosphonate salts of 3,3',5,5-tetramethyl-1H,1'H-4,4'-bipyrazole (BPz), conformationally flexible ligand; seven phosphonate salts of methylenebis(3,5-dimethylpyrazole) (MBPz), the bent core molecule and, three phosphonate salts/co-crystals of 1,2-bis(3,5-dimethyl-1H-pyrazol-4-yl)diazene (BPaz), rigid ligand with different range of phosphonic acids on the basis of supramolecular synthon approach.

Result and discussion

It was endeavored to achieve the effect on H-bonded supramolecular domain produced by various substituted phosphonic acids with bent and flexible pyrazole by raising our understanding of competing molecular interactions in order to obtain detailed knowledge of a supramolecular organization. The potential of bispyrazole as a rigid and flexible component mixed with the variety of phosphonic acids, that ranges from monophosphonic acid to mixed hydroxyl phosphonic acid for the construction of extended supramolecular organic frameworks (SOFs) was envisaged. In this context, the four phosphonate salts of 3,3',5,5'-tetramethyl-1H,1'H-4,4'-bipyrazole (BPz) (Scheme 2.2) *viz*., $[(HPPA^{-})_2.H_2BPz^{2+}]$ (**2a**), $[HtBPA^{-}.HBPz^{+}]$ (**2b**), $[(HPPRA^{-})_2.H_2BPz^{2+}.(MeOH)_2.H_2O]$ (**2c**), $[H_2DPA^{2-}.(HBPz^{+})_2.H_2O]$ (**2d**) were constructed, where H_2PPA = phenylphosphonic acid, H_2PAA = phosphonoacetic acid, H_2PPRA = 3-phosphonopropionic acid, H_2tBPA = *tert*-butylphosphonic acid, H_4EA = etidronic acid, H_4DPA = (1,4-phenylenebis(methylene))diphosphonic acid. The main emphasis was on the interaction patterns resulted from the molecular salts of pyrazole and phosphonic acid to evaluate the stability of the same and the occurrence of persistent synthons in the crystal structure (Scheme 2.3). The crystallographic data and non-covalent interactions for salts/co-crystals **2a**-**2n** have been tabulated in Table 2.1-2.4 and Table 2.15 respectively. Moreover, theoretical calculation was performed for all molecular complexes **2a**-**2n** using B3LYP/6-31G basis set [39-41] in order to evaluate their stability.

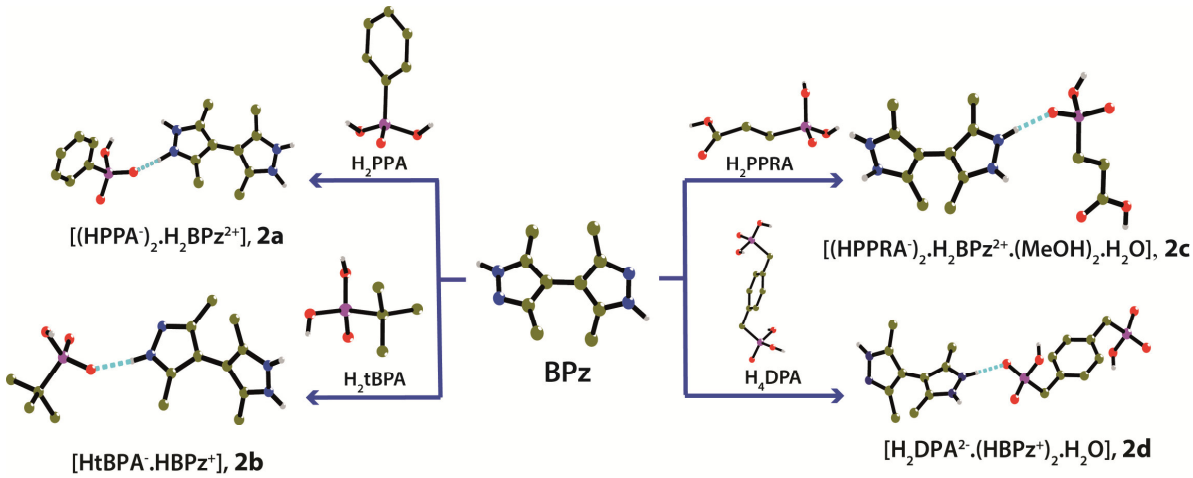

Scheme 2.2

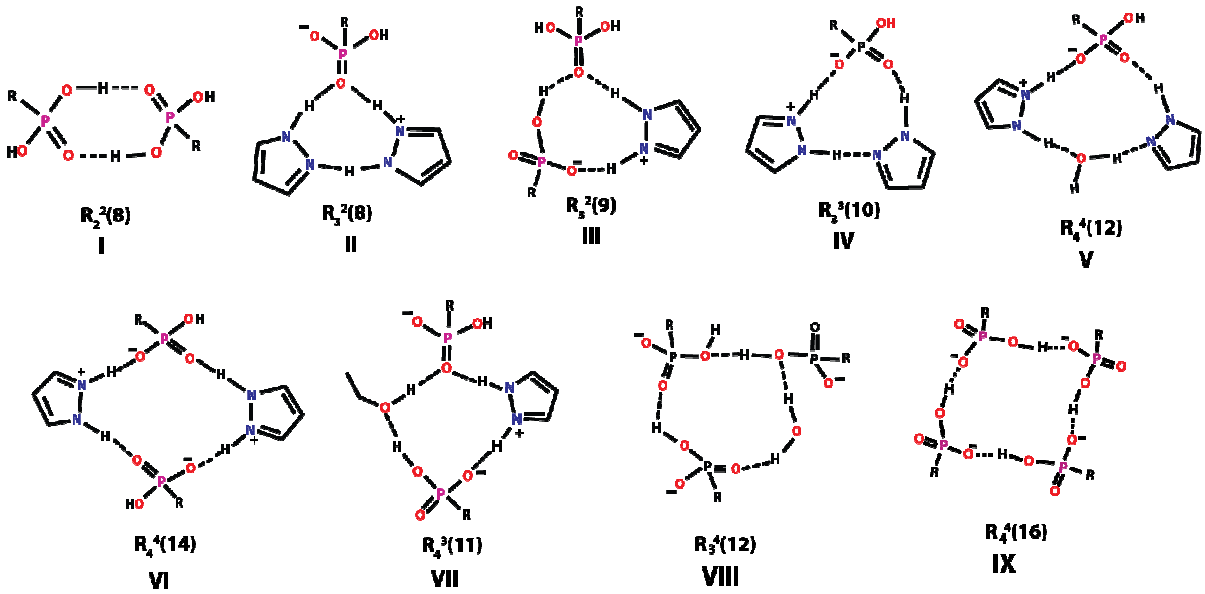

Scheme 2.3: Various heterosynthons **I**-**IX** found in **2a**-**2n**

Structural analysis with conformationally flexible 3,3',5,5'-tetramethyl-1H,1'H-4,4'-bipyrazole (BPz) (Scheme 2.2)

Crystal structure of $[(HPPA^{-})_2.H_2BPz^{2+}]$ (2a)

The crystal data analysis of **2a** revealed that asymmetric unit is comprised of one phosphonate anion and half molecule of the bispyrazole cation, resulted by the transfer of one acidic proton from phosphonic acid to pyrazole (Fig. 2.12). The $HPPA^{-}$ molecules are connected with each other through O–H···O interaction (O1E–H1E···O2, 1.850 Å) and form a 1D infinite chain along *c*-axis. These chains are further interlinked through the bipyrazole linker via trimer synthon **III** ($R_3^2(9)$) involving various N–H···O and O–H···O interactions (N2–H2D···O3, 1.594 Å; O1E–H1E···O2, 1.850 Å; N1–H1D···O2, 1.782 Å), resulted in a ten (eight acid and two base units) membered rectangular cavity. These supramolecular cavities with dimensions, 15.5 X 10.9 $Å^2$ can be regarded as a composite building block (CBB). These cavities are joined together to form a 2D sheet structure with brick wall topology as shown in Fig. 2.13. Interestingly, the anionic moieties are tied in such a way that the consecutive phenyl groups are arranged ≈ 78° to each other, mainly responsible for extension of sheet in all four directions (Fig. 2.14). Moreover in three dimensions, a porous framework with rectangular grids was resulted when these sheets are further connected by BPz linkers (Fig. 2.15). As a consequence, the resulted grid has adequate space in between to allow another grid to pass through it, ensuing in an interpenetrated

two fold 3D supramolecular framework (Fig. 2.16), which displays π-π interaction (3.828 Å) between the phenyl group and the pyrazole nuclear.

Crystal structure of [$HtBPA^{-}.HBPz^{+}$] (2b)

The X-ray structural determination disclosed that the asymmetric unit consisted of one molecule each of *tert*-butylphosphonate anion and bispyrazole cation resulted by the transfer of one proton to BPz (Fig. 2.17). In **2b**, the $HtBPA^{-}$ afforded the ubiquitous phosphonic homodimer synthon, **I** (R_2^2 (8)) (O1–H1E···O2, 1.757 Å). Unlike in **2a**, the infinite chains of cationic pyrazole associated through N–H···N interaction (N1–H1D···N4, 1.982 Å), runs along *c*-axis, which are interlinked to each other through the homodimer synthon, **I**. This arrangement led to the formation of an eight membered circular grid (four BPz and a pair of homodimer moiety) as depicted in Fig. 2.18. Extension of these circular grids in one dimension via a heterosynthons, **IV** (R_3^3 (10)) involving various N–H···O and N–H···N interactions (N1–H1D···N4, 1.982 Å; N2–H2D···O3, 1.709 Å; N3–H3D···O2, 1.920 Å) resulted in a double tape like structure. Further, these double tapes led to a 2D sheet, connected through phosphonate moieties as shown in Fig. 2.19. Subsequently, the 2D framework is extended to 3D layered supramolecular network via edge-edge π-π interactions (3.456 Å) between pyrazole cations from two adjacent sheets along *a*-axis (Fig. 2.20). It may be noted that the bulky *tert*-butyl group of the phosphonate moieties pointed towards the empty space of the cavity.

Crystal structure of [$(HPPRA^{-})_2.H_2BPz^{2+}.(MeOH)_2.H_2O$] (2c)

The crystal structure **2c** is crystallized in centrosymmetric monoclinic space group, *C2/c* and its asymmetric unit consisted of half molecule of H_2BPz^{2+} and water molecule lie at the inversion centre in addition to the one molecule each of $HPPRA^{-}$ and methanol as displayed in Fig. 2.21. On probing the structure, it was found that the monodeprotonation occurred from more acidic phosphonic group, whereas the bond length of C–O (1.252 Å) and C=O (1.177 Å) of carboxylic group, ascertained that the proton of carboxylic acid remains intact. Interestingly, due to presence of carboxylic group in addition to phosphonic acid in **2c**, surplus hydrogen bonded interactions were observed in the chain, leaving two P–O of phosphonate anion available for shaping the homodimer **I** (O3–H3E···O2, 1.821 Å) and subsequently extends into a 1D anionic molecular tape in *ab*-plane (Fig. 2.22). It was also observed that the pair of molecular tapes in *ab*-plane are bridged by H_2BPz^{2+} and the other half of the same H_2BPz^{2+} group generated by

symmetry, bridges another pair of the same perpendicularly via N–H···O interaction, 1.771 Å; 1.769 Å owing to the twisting of the conformational flexible bispyrazole cation (Fig. 2.82) (dihedral angle ≈ 108°). As a result, the eight membered cyclic hydrogen bonded cavity ring motif was formed by six phosphonate anions and two pyrazole cations (Fig. 2.23). This cyclic assembly extends into a porous three dimensional supramolecular assembly with the help of an array of N–H···O and O–H···O interactions (Fig. 2.24). Hence, this accomplished in the formation of 3D supramolecular hydrogen bonded network involving various fused heterotetramer **VI**, (R_4^4(14)) and homodimer **I** synthons along *a*-axis which consequently begets the channel, occupied by methanol and water molecules as shown in the crystal packing (Fig. 2.25). Interestingly, the water oxygen (O7) detected in difference Fourier map lies on the special position with inversion centre hence, it has been refined with 0.5 site occupancy isotropically. Unfortunately, the position of the hydrogen atoms germane for hydrogen bond interactions on solvent molecules was not detected due to poor quality of the data set.

Crystal structure of [H_2DPA^{2-}.($HBPz^+$)$_2$.H_2O] (2d)

Co-crystallization of bifunctional molecules i.e., diphosphonic acid and bispyrazole resulted in 1:2 adduct. The asymmetric unit of salt is composed of one dideprotonated diphosphonate anion, two monoprotonated BPz cations and a water molecule (Fig. 2.26). Structural analysis revealed that the wreath of the $HBPz^+$ moieties and water molecule interconnected to an adjacent wreath, which propagates parallelly along *a*-axis using bifunctional diphosphonate moiety and give rise to a larger circular grid of dimensions 14.58 X 15.97 $Å^2$. The seven membered circular grid is comprised of four molecules of $HBPz^+$, two molecules of H_2DPA^{2-} and one water molecule (Fig. 2.27) sustained together by various N–H···N and N–H···O interactions (N7–H7D···O4, 2.048 Å; N2–H2D···O2, 1.936 Å; N3–H3D···N8, 2.067 Å; N5–H5D···O1, 1.824 Å; N4–H4D···O5, 1.708 Å; O7–H8W···N1, 2.086 Å). These cyclic cavities are fused together through two types of heterosynthons acting as a gluing factor: trimeric synthon, **IV** (R_3^3 (10)) (N7–H7D···O4; N4–H4D···O5; N3–H3D···N8) and extended trimeric synthon, **V** (R_4^4(14)) (O7–H8W···N1; N6–H6D···O7, 1.873 Å; N5–H5D···O1; N2–H2D···O2) to form an undulated 2D sheet structure (Fig. 2.28). Each ring is comprised of a water molecule, which facilitates the formation of the ring motif along with two $HBPz^+$ molecules and a phosphonic acid. Due to availability of such big dimensional grids, the 2D sheet allows another

2D sheet to interpenetrate into it and the interpenetrated sheet is drifted by 7.913 Å to the adjacent sheet. These sheets are interconnected via a homosynthon **I** (O3–H3E···O4, 1.816 Å; O6–H6E···O1, 1.758 Å) (Fig. 2.29). Notably, due to various possible binding modes of diphosphonic acid and larger hydrogen bonded ring size, the 3D packing is found to be very complicated. Hence, the three dimensional framework has been represented in simplified form as produced by TOPOS [42] (Fig. 2.30).

As literature revealed phosphonic acid generally shows layered structure. The above studies with conformationally flexible 3,3',5,5'-tetramethyl-1H,1'H-4,4'-bipyrazole (BPz), phosphonic acid displayed diverse architectures such as interpenetrated and host-guest assembly depending upon the substituent present on the phosphonic acid. Each supramolecular assembly exhibited the hydrogen bonded ring, considered as the structural unit.

Structural analysis with conformationally flexible methylenebis(3,5-dimethylpyrazole) (MBPz) (Scheme 2.4)

In order to gain the complete knowledge of the intermolecular interactions and synthons involved in phosphonic-pyrazole system, the further exploration of these phosphonic acids moieties with flexible as well as bent bispyrazole i.e., methylenebis(3,5-dimethylpyrazole) (MBPz) was carried out. Hence, seven phosphonate salts of MBPz were formed *viz*., [$HPPA^-$.H_2PPA.$HMBPz^+$.MBPz] (**2e**), [$(HtBPA^-)_2$.H_2MBPz^{2+}.EtOH] (**2f**), [$HPAA^-$.$HMBPz^+$.MBPz.MeOH] (**2g**), [$HPPRA^-$.$HMBPz^+$] (**2h**), [H_2EA^{2-}.H_2MBPz^{2+}.S] (**2i**), [H_2EA^{2-}.H_2MBPz^{2+}] (**2j**), [H_3DPA^-.$(H_2DPA^{2-})_{0.5}$.H_2MBPz^{2+}.$(H_2O)_{0.4}$] (**2k**) (Scheme 2.4). Moreover, the change in conformation of flexible MBPz in salts **2e**-**2k** was also monitored with different phosphonic acids, which has governed the supramolecular assembly and resulted in distinct SOFs (Table 2.20; Fig. 2.82). It may be noted that the molecular salt **2i** has some disordered solvent molecule; therefore, the solvent electron density has been removed by SQUEEZE program in PLATON [43]. The crystallographic data and non-covalent interactions for salts **2e**-**2k** have been tabulated in Table 2.5-2.11 and Table 2.15 respectively.

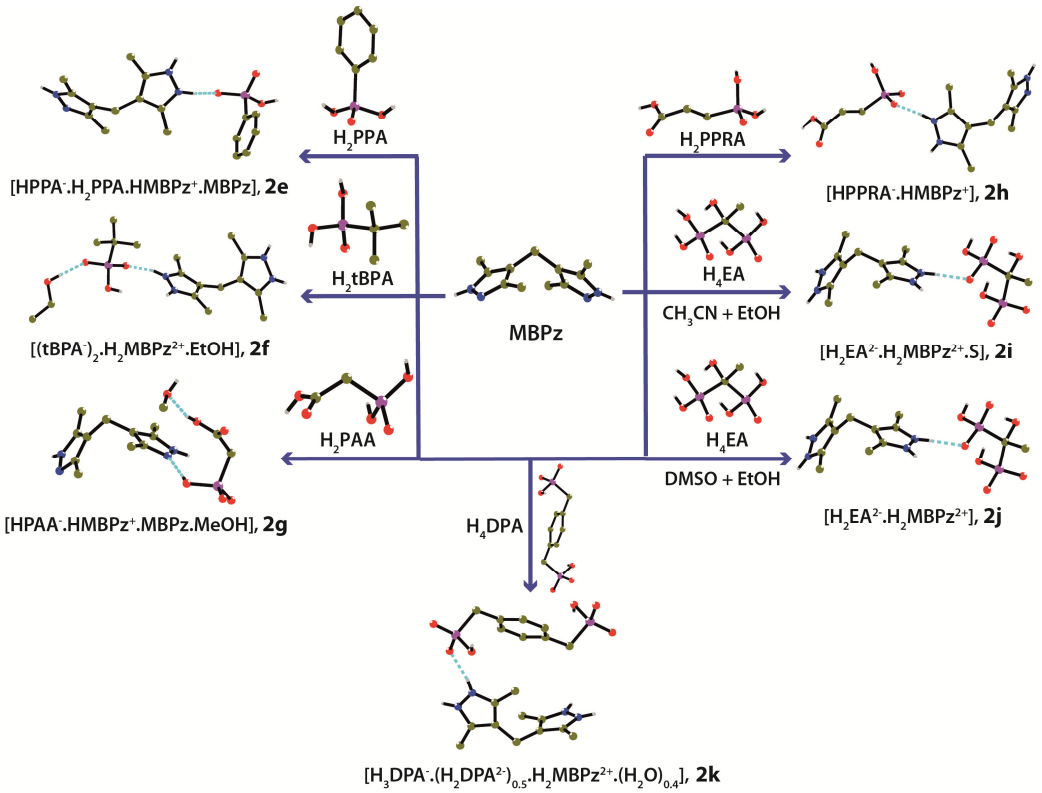

Scheme 2.4

Crystal structure of [HPPA$^-$.H$_2$PPA.HMBPz$^+$.MBPz] (2e)

The salt **2e** with two molecules each of H_2PPA (monodeprotonated and neutral H_2PPA) and MBPz (monoprotonated and neutral MBPz) in asymmetric unit crystallized in tetragonal space group, *Pca*2$_1$ (Fig. 2.31). The proton transfer between one of the phosphonic acid to one of the two symmetry independent methylene bispyrazole, MBPz, led to the formation of a salt, which is further disclosed by the reduced P–O bond length of the resulted phosphonate.

Structural analysis deduced that the acid homodimer **I** (O2–H2E···O4, 1.729 Å; O6–H6E···O3, 1.748 Å) and two different heterotrimer synthons **IV** involving various N–H···O, N–H···N and O–H···N interactions (N8–H8D···N1, 2.094 Å; N2–H2D···O3, 1.929 Å; O1–H1E···N7, 1.713 Å and N4–H4D···O5, 1.681 Å; N3–H3D···N5, 2.037 Å; N6–H6D···O4, 1.948 Å) are fused together and form a H-bonded pattern resulting in a eight membered (four MBPz and a pair of homodimer) cyclic hydrogen bonded unit involving N–H···N and N–H···O interactions (Fig. 2.32). A myriad of concerted arrays of these fused homo- and heterosynthons led to the formation of 2D corrugated sheet.

On examining the molecular system of **2e**, it was found that the two symmetry independent MBPz and $HMBPz^+$ constructs an infinite one-dimensional undulated molecular chain via N–H···N intermolecular interactions. The parallel infinite wavy chain of pyrazole propagate along *b*-axis and these parallel chains are sustained together by the phosphonic homodimer and resulted in 2D corrugated sheet as shown in Fig. 2.3.

Furthermore, due to the possible flexibility in MBPz, the 2D parallel stacked sheets increases its dimensionality from 2D to 3D via interaction between methylene hydrogen of one MBPz molecule and π-electron cloud of another molecule present in the neighboring sheet along *c*-axis (Fig. 2.34(b), (c)). These 2D sheets are arrangement as such that the rings in one sheet are at the medial of the two rings in the next sheet (Fig. 2.34(a)) therefore, no channel formation was observed in the resulted 3D SOF. On the other hand, the refinement of salt **2e** was carried out successfully with the TWIN instruction and Flack parameter [44] was found to be 0.33(10) with highest peak and deepest hole as 0.182 and -0.265 respectively, surmised from XShell [45] program.

Crystal structure of [$(HtBPA^-)_2.H_2MBPz^{2+}.EtOH$] (2f)

It is crystallized in a polar and non-centrosymmetric space group, $P2_1$ with eight molecules of $HtBPA^-$, four molecules each of H_2MBPz^{2+} and ethanol in the asymmetric unit (Fig. 2.35) bearing high Z' value (Z'=8) [46-47]. Here, merely one oxygen of the phosphonic acid is deprotonated; hence in the asymmetric unit, all MBPz are doubly protonated and all phosphonate anions are singly deprotonated. Crystal structure study of **2f** exemplified an intriguing stacked arrangement of a pair of infinite 2D undulated sheet. The 2D sheet of the pair is further composed of alternate catemeric arrangement of two heterosynthons i.e., heterotrimers **III** formed via different N–H···O, O–H···O and O–H···O interactions (O15–H15E···O17, 1.764 Å; N9–H9D···O14, 1.674 Å; N10–H10D···O17, 1.947 Å) & (O21–H21E···O22, 1.777 Å; N4–H4D···O22, 1.929 Å; N3–H3D···O20, 1.681 Å) and inclusion of an ethanol molecule in heterotrimer led to heterotetramer (extended trimer) **VII** (R_4^3 (11)) (O25–H25E···O13, 1.920 Å; O24–H24E···O25, 1.848 Å; N1–H1D···O23, 1.644 Å; N2–H2D···O13, 1.825 Å) & (O27–H27E···O19, 1.875 Å; N12–H12D···O19, 1.819 Å; N11–H11D···O18, 1.647 Å; O16–H16E···O27, 1.807 Å) (Fig. 2.36). The other sheet of the same pair is also composed of heterotrimers (N8–H8D···O6, 1.844 Å; N7–H7D···O2, 1.681 Å; O1–H1E···O6; 1.826 Å) &

(O7–H7E···O12, 1.821 Å; N14–H14D···O12, 1.844 Å; N13–H13D···O8, 1.687 Å) (Fig. 2.37) and heterotetramers (O26–H26E···O9, 1.905 Å; N6–H6D···O9, 1.806 Å; N5–H5D···O5, 1.696 Å, O4–H4E···O26, 1.865 Å) & (O28–H28E···O3, 1.907 Å; N16–H16D···O3, 1.823 Å; N15–H15D···O11, 1.689 Å, O10–H10E···O28, 1.834 Å), assisted by H_2MBPz^{2+} and $HtBPA^-$. The sheets in a pair are further interlinked by alternate face to face π-π (3.535 Å) and edge to edge π-π (3.720 Å) interactions (Fig. 2.39). Basically, the sheet comprised a string of phosphonate and an ethanol molecule, which contributes in the formation of a seven membered ring motif (four $HtBPA^-$ and three H_2MBPz^{2+}) involving N–H···O and O–H···O interactions (N11–H11D···O18, 1.646 Å; N9–H9D···O14, 1.674 Å; N2–H2D···O13, 1.825 Å, N4–H4D···O22, 1.929 Å; N1–H1D···O23, 1.644 Å; O15–H15E···O17, 1.765 Å) and thereafter, formed a hydrogen bond directed porous network, which suspends an ethanol molecule in its pores in *ab*-plane (Fig. 2.38). The 2D undulated sheets of two different pairs are further interconnected via weak interlayer C–H···O interaction (2.632 Å) between H_2MBPz^{2+} methylene C–H and oxygen of phosphonate of above layer. The adjacent layers are stacked in such a way that the *tert*-butyl group lies in between the stacked layers along *b*-axis (Fig. 2.40). On the other hand, the crystal structure was refined with the TWIN instruction and Flack parameter refined to 0.03(5) for the selected crystal with highest peak and deepest hole as 0.388 and -0.241 respectively.

Crystal structure of [$HPAA^-$.$HMBPz^+$.MBPz.MeOH] (2g)

The asymmetric unit is consisted of two symmetry independent molecules of MBPz, one molecule of $HPAA^-$ and a methanol molecule as a solvent of crystallization (Fig. 2.41). Formation of **2g** is aided by the transfer of one proton from P–O of H_2PAA to N of one MBPz, which afforded one cation, one anion and a neutral molecule. The hydrogen atom of carboxylic group present in phosphonic acid remains intact with carboxylate group.

The 2D network resulted from the stacking of infinite 1D undulated sheets was ascertained as observed in **2e**. The 1D sheet is further composed of the parallel wavy chains, formed by intermolecular hydrogen bonding between MBPz and $HMBPz^+$ through N–H···N interaction (N5–H5D···N4, 2.073 Å; N2–H2D···O3, 1.873 Å), propagating along *a*–axis. These parallel chains are arrested together by two different synthons i.e., heterotrimer **II** (N8–H8D···O3, 1.954 Å; N1–H1D···O3, 1.785 Å; N2–H2D···O3, 1.873 Å) constituted by a

bifurcated hydrogen bonding with a phosphonic acid on one side and **IV** (N5–H5D···N4, 2.073 Å; N3–H3D···O2, 1.900 Å; O1–H1E···N6, 1.821 Å) on another side (Fig. 2.42(a)). Subsequently, the stacking of these wavy parallel chains is retained as in **2e** along *b*–axis but via an infinite linear chain directed by the bifunctional phosphonic acid and the solvent molecule involving O–H···O interaction (O4–H4Z···O6, 1.780 Å; O6–H6C···O2, 1.851 Å) as represented in Fig. 2.42(b).

Eventually, the resulted 2D sheet with heterosynthons aggregates into larger hydrogen bonded cavity of dimensions 10.9 X 8.2 $Å^2$ (Fig. 2.43). Therefore, the large hydrogen bonded cavity and corrugated feature of the system allowed another network to interpenetrate further leading to a 3D two-fold interpenetrated network (Fig. 2.44). Unlikely as **2e**, salt **2g** involved $HPAA^-$ along with the solvent molecule, methanol, which plays a significant role in the formation of polythreading corrugated architecture. Moreover, the comprehensive H-bonding interactions in 2D sheets acquired parallel packing in the solid, further helped in achieving a non-centrosymmetric arrangement [48] in ABAB pattern (Fig. 2.45). Initially, an attempt was also made in order to solve the same structure in centrosymmetric space group *Pbcm* as suggested by ADDSYM [49] but it ended up in high R values. Therefore, it was solved in non-centrosymmetric space group, $Pca2_1$ and was refined with twin and the Flack parameter was determined to be 0.35(12) with highest peak and deepest hole as 0.366 and -0.333 respectively.

Crystal structure of [$HPPRA^-$.$HMBPz^+$] (2h)

X-ray data reveals that the compound **2h** is crystallized in centrosymmetric space group, $P2_1/c$ and its asymmetric unit contained each molecule of $HMBPz^+$ and $HPPRA^-$ with monodeprotonation of phosphonic functionality (Fig. 2.46), further confirmed by the reduced bond length of P–O. The C–O bond length in carboxylic acid of $HPPRA^-$ remains unchanged (C3–O4 = 1.196; C3–O5 = 1.323 Å) and thereby, it clarifies that proton of carboxylic remains intact with its parent molecule. On probing the crystal packing, it was deduced that the infinite 1D *zig-zag* chain constituted from continuous $HMBPz^+$ involving N–H···N (N2–H2D···N4; 1.934 Å) along *b*-axis (Fig. 2.47) and is further interlinked to the next 1D *zig-zag* parallel chain along *c*-axis by π-π interaction (≈ 4.489 Å) (Fig. 2.50(b)). The parallel chains of $HMBPz^+$ are sandwiched between the 2D corrugated sheets (Fig. 2.48) generated by bifunctional and the longer phosphonic acid i.e. $HPPRA^-$ (Fig. 2.49). In *ab*-plane, this corrugated sheet seems to have

the form of alternate hydrogen bonded troughs and crest. The interaction responsible for the formation of troughs and crests from $HPPRA^-$ is O5–H5Z···O3, 1.804 Å between carboxylic group of $HPPRA^-$ and phosphonic group of another $HPPRA^-$ whereas these two humps are interconnected by the phosphonic dimer **I** (O1–H1E···O2, 1.796 Å) as shown in Fig. 2.50(a). Eventually, the interlayer interaction between the sheets formed by $HMBPz^+$ and $HPPRA^-$ followed the ABAB trend, which resulted in the formation of 3D centrosymmetric bulk hydrogen bonded solid (Fig. 2.51). The various interlayer interactions involved between the alternate sheet of phosphonic and MBPz are N1–H1D···O3, 1.781; N3–H3D···O2, 1.982; C9–H9B···O4, 2.669; C8–H8C···O4, 2.423 Å.

Crystal structure of [H_2EA^{2-}.H_2MBPz^{2+}.S] (2i) and [H_2EA^{2-}.H_2MBPz^{2+}] (2j)

The molecular salts **2i** and **2j** formed from bisphosphonate anion and diprotonated MBPz cation but crystallized in different solvent medium. Salt **2i** was crystallized from acetonitrile and ethanol, whereas salt **2j** was crystallized from DMSO and ethanol. The structural analysis of molecular salts **2i** and **2j** revealed that the former is crystallized in monoclinic space group, $P2_1/c$ while the latter is crystallized in triclinic space group, *P*-1. Both salts are comprised of one molecule each of anion and cation in its asymmetric unit along with one molecule of ethanol in former (Fig. 2.52) but in latter, no solvent was found in lattice (Fig. 2.58). In **2i**, it was envisaged that a chain of phosphonate anion is generated along *a*-axis due to presence of multifunctional group on it i.e. hydroxy group in addition to bisphosphonic functionality (Fig. 2.54). These chains are found to be arranged parallel to each other in *ac*-plane and are interlinked by two H_2MBPz^{2+} (Fig. 2.53) from both sides via various N–H···O interactions (N1–H1D···O2, 1.886; N2–H2D···O4, 1.720; N3–H3D···O6, 1.945; N4–H4D···O1, 1.739 Å), which ultimately led to the formation of 1D channel along *b*-axis filled by the disorder solvent molecules with internal dimensions of 6.509 X 5.759 $Å^2$ (Fig. 2.55). The column is further cross-linked with the adjacent column parallel to *b*-axis through multiple hydrogen bonds due to presence of multifunctional group on phosphonic acid resulting in a 2D infinite sheet. The interlinked H_2MBPz^{2+} molecules further extended the sheet from other side in *ac*-plane. Subsequently, the 2D supramolecular network widens to 3D supramolecular organization (Fig. 2.56) along *c*-axis via C–H···O interaction (C8–H8A···O4, 2.436 Å) between methylene C–H with phosphonate from the adjacent layer while the solvent molecule sits along 1D channel. Moreover during

refinement, some extra electron density was located in the difference Fourier map but it was difficult to model the molecule due to the disorder hence the residual electron density was extruded using the SQUEEZE program in PLATON. The extruded solvent molecule was tentatively found to be ethanol with the help of squeeze calculation and TGA analysis. Similarly in **2j**, the parallel chains of phosphonate anion interlinked by the H_2MBPz^{2+} molecules propagates along *b*-axis resulting in a 2D sheet (Fig. 2.60). Nevertheless, the chain of bisphosphonate in this case, encompassed an array of alternate homodimer (Fig. 2.59) involving O–H···O interactions (O4–H4E···O3, 1.772; O1–H1E···O6, 1.829; O7–H7E···O5, 2.018 Å). These sheets are in turn linked through N–H···O interaction (N3–H3D···O6, 1.801 Å) between pyrazole N–H from one sheet and phosphonic acid O–H from next sheet in three dimensions (Fig. 2.61).

It was clearly shown that the solvent plays an important role in modifying the crystal structure as with change in solvent medium, molecular salt **2j** exemplified narrow channels than in **2i**. Although, the number of components involved in the hydrogen bond ring motif is same in both cases but the number of acceptors involved in the ring is different. In **2i**, both bisphosphonic groups was involved in the ring, whereas **2j** displayed bifurcated hydrogen bond, which further upsurge the torsion angle of H_2MBPz^{2+} from 78.20 to 127.41. Hence, the insertion of solvent molecule in the lattice changes the conformation of the flexible molecule and thereby, led to the porous organic supramolecular organization from non–porous.

Crystal structure of $[H_3DPA^{-}.(H_2DPA^{2-})_{0.5}.H_2MBPz^{2+}.(H_2O)_{0.4}]$ (2k)

Complex **2k** crystallized in centrosymmetric space group, $P2_1/c$. Its asymmetric unit contained half a molecule of H_2DPA^{2-} lying about an inversion center and one molecule each of H_2MBPz^{2+} and H_3DPA^{-} along with the water molecule. The salt formation is aided by monodeprotonation from each H_4DPA (Fig. 2.62). The crystal structure analysis of **2k** disclosed that the diphosphonate with water molecule forms a supramolecular pouch in *bc*-plane via synthon **VIII**, R_4^4 (12) considered as a building unit (Fig. 2.63), occupied by two H_2MBPz^{2+} molecules, which produced a hydrogen bonded module with the phosphonic acid involved in the formation of pouch via synthon **III**, R_3^2 (9) (Fig. 2.64). The two H_2MBPz^{2+} molecules were also interacted to each other via π-π interaction (Cg—Cg distance, 3.554 Å) leading to the formation of hydrogen bonded host-guest assembly. The larger hydrogen bonded supramolecular pouch

formed by DPA involves an array of hydrogen bonded interactions such as O–H···O, N–H···O interactions (O2–H2E···O7, 1.795; O8–H8E···O6, 1.791; O10–H···O3, O10–H···O5). The guest molecules present in the channels are interacted to the host assembly via diverse N–H···O interactions (N2–H2D···O7, 1.786; N4–H4D···O6, 1.789 Å; N3–H3D···O9, 1.786 Å). It can be concluded that salt **2k** is formed by conformational flexible H_4DPA molecule and somehow the length of H_4DPA in addition to number of hydrogen bond forming moieties might also be responsible for the formation of larger hydrogen bonded cavities as compare to other salts. In 2D, each of the pouches in the crystal packing is packed over each other in such a way that it generated the rectangular shaped tunnels involving O–H···O interactions (O5–H5E···O9, 1.749; O3–H3E···O4, 1.655 Å) (Fig. 2.65) along *a*-axis. In 3D, these tunnels are arranged as such that the two tunnels shared a common wall, which attributed to the formation of synthon **IX**, $R_4^4(16)$ and thereby resulting in a formation of infinite parallely arranged tunnels of rectangular shaped (Fig. 2.66). The water oxygen detected in difference Fourier map lies on the special position with inversion centre hence, it has been refined with 0.5 site occupancy isotropically. But the addition of hydrogen on the oxygen of the water molecule was not accomplished due to disorder.

The above studies revealed that the conformation of conformationally flexible methylenebis(3,5-dimethylpyrazole) (MBPz) is influenced by the substituents present on different phosphonic acid which led to the formation of diverse architectures such as interpenetrated, supramolecular porous framework and host-guest. Similarly here, each supramolecular assembly exhibited hydrogen bonded ring, considered as the structural unit.

Structural analysis with rigid 1,2-bis(3,5-dimethyl-1H-pyrazol-4-yl)diazene, (BPaz) (Scheme 2.5)

After the results with conformationally flexible ligand, the rigid bispyrazole ligand was also employed with these phosphonic acids. Three phosphonate salts of 1,2-bis(3,5-dimethyl-1H-pyrazol-4-yl)diazene, (BPaz) (Scheme 2.5) were formed *viz*., [H_2PPA.BPaz] (**2l**), [(H_2tBPA)$_2$.BPaz] (**2m**) and [H_2DPA^{2-}.($HBPaz^+$)$_2$.(BPaz)$_2$.DMSO.H_2O] (**2n**). The crystallographic data and non-covalent interactions for salts/co-crystals **2l**-**2n** have been tabulated in Table 2.12-2.14 and Table 2.15 respectively.

Crystal structure of [H_2PPA.BPaz] (2l) and [(H_2tBPA)$_2$.BPaz] (2m)

The molecular compounds **2l** and **2m** of BPaz crystallized with H_2PPA and H_2tBPA in triclinic space group, *P*-1. The asymmetric unit of **2l** is consisted of one molecule of H_2PPA and two half molecules of BPaz (Fig. 2.67) while **2m** is comprised of one molecule of H_2tBPA and half molecule of BPaz (Fig. 2.71). Unlike in all molecular crystals aforementioned, both **2l** and **2m** were found to be co-crystals i.e., no hydrogen transfer take place in this instance from acid to pyrazole. In **2l**, the crystal packing is similar to **2e**. The

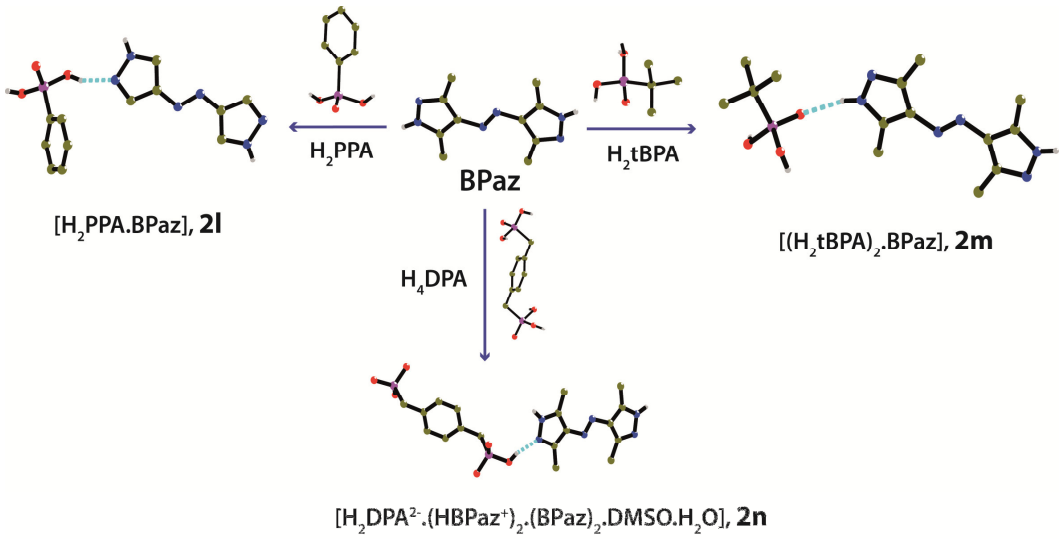

Scheme 2.5

eight membered circular ring is formed by BPaz and a pair of phosphonic homodimer involving different N–H···N, N–H···O and O–H···O interactions (N4–H4D···O3, 2.224; N1–H1D···N5, 2.031; O2–H2E···O3, 1.754; O1–H1E···N2, 1.789 Å). An array of these circular rings resulted in a 2D sheet spread along *c*-axis (Fig. 2.68).

Further, the 2D supramolecular sheet is extended to 3D supramolecular network via C–H···π, interaction (3.113 Å) between C–H of methyl group in BPaz and its nuclei in adjacent layer (Fig. 2.70(b)). Notably, the two parallel sheets are offset by 7.34 Å along *b*-axis and the intersheet distance is 3.11 Å (Fig. 2.70).

While in **2m**, the structural analysis revealed that the formation of two types of oval shaped grids i.e., **A** and **B** (Fig. 2.73). The previous one involved two molecules each of BPaz and H_2tBPA (N2–H2D···O1, 1.936; O2–H2E···N1, 1.769 Å) and second grid, **B** is comprised of two peripheries of BPaz and a pair of phosphonic dimer (O3–H3E···O1, 1.749 Å) as shown in Fig. 2.73. On probing, it was found that the BPaz are stacked over each other along *a*-axis and

the stacking of BPaz is bridged between the phosphonic homodimer. Hence, the piles of BPaz via homodimer are extended into a sheet in *bc*-plane. Furthermore, the 2D sheet is interlinked via weak C–H···O, (C5–H5A···O2, 2.632 Å) between methyl group of BPaz and phosphonic group in the next layer (Fig. 2.74).

Crystal structure of [H_2DPA^{2-}.$(HBPaz^+)_2$.$(BPaz)_2$.DMSO.H_2O] (2n)

In the crystal structure of **2n**, the bisphosphonic acid and BPaz crystallized in centrosymmetric space group, $P2_1/c$ with one molecule of bisphosphonate dianion, two symmetry independent molecules each of BPaz and $HBPaz^+$ in its asymmetric unit along with one water molecule and one disordered molecule of DMSO as a crystallizing solvent (Fig. 2.75). It may be noted that in this case the proton was transferred from diphosphonic to BPaz unlike in other molecular compounds of BPaz.

On analysis of the crystal structure, it was found that the 2D association derived from the parallel 1D rippled alternate chains of BPaz and $HBPaz^+$ along *b*-axis produced two 2D sheets *viz*., **A** and **B**. In sheet **A**, the two different parallel wavy chains, framed by N–H···N interactions (N13–H13D···N16, 1.952 Å and N4–H4D···N1, 2.132 Å), are hinged together by two different heterotrimer synthons, **II** (N13–H13D···N16, 1.952 Å; N15–H15D···O4, 1.880 Å; N14–H14D···O4, 1.752 Å) devised by a bifurcated hydrogen bonding with one phosphonic group of the bifunctional molecule on one side and **IV** (R_3^3 (10)) involving N–H···N, N–H···O and O–H···N interactions (N4–H4D···N1, 2.132 Å; N2–H2D···O5, 1.846 Å; O6–H6E···N3, 1.895 Å) on another side (Fig. 2.76). However, the other phosphonic group of the same bifunctional molecule extended the network to 3D supramolecular framework through robust hydrogen bonds along *a*-axis. Consequently, the 2D sheet displayed the hydrogen bond cavity similar to the salt **2g**, accommodated by DMSO and a water molecule. Likely in sheet **A**, sheet **B** also possesses two different heterotrimers, **II** (N20–H20D···N21, 1.982 Å; N19–H19D···O1, 1.766 Å; N22–H22D···O1, 1.898 Å) and **IV** (N7–H7D···N10, 2.123 Å; N9–H9D···O2, 1.871 Å; O3–H3E···N8, 1.905 Å). Moreover, it acquired hydrogen bonded cavity that allows the bifunctional moiety to pass through it, hence it led to an interpenetrated architecture (Fig. 2.77). Notably, the pair of sheet **B** is sandwiched between sheets **A** from both sides (Fig. 2.78) and interconnected together via diphosphonic moiety (Fig. 2.79). Eventually, it led to the formation of a pack of four sheets in ABBA way of pattern and the interaction involve between two sets of

the pack is C–H···π interaction (2.906 Å) between the C–H (methyl group) of BPaz from one set and the π- electrons of another BPaz from neighboring set (Fig. 2.80).

Thermal stability and powder X-ray diffraction:

To ascertain the thermal stability of the molecular complexes **2a**-**2n**, thermogravimeteric analysis was performed (Fig. 2.86). It was investigated that all salts are stable upto 260-280 °C. In contrast to salts **2a**-**2d**, salt **2d** was found to be most stable as it represented the stable framework and hence, decomposes around 300 °C. First mass loss relates to the loss of a water molecule around 120 °C with mass loss of 2.56 % (experimental) and 2.70 % (observed). Later, mass loss nearly 300 °C corresponds to the loss of the organic part of the phosphonic acid. In salts **2a**-**2c**, all are stable upto 270 °C, however in case of **2c**, the first mass loss corresponds to the discharge of methanol molecule which starts around 90 °C and completes around 120 °C with mass loss of 8.78 % (experimental) and 10.69 % (observed). Second mass loss accounts for the release of water molecule around 140 °C with mass loss of 5.78 % (experimental) and 6.74 % (observed). The next weight loss at 262 °C attributed to the loss of the organic component of the phosphonic acid at 262 °C for **2a** and at 268 °C for **2b**.

In **2e**-**2k**, the primary mass loss of 33.45 %, 4.81 %, 9.81 % and 2.56 % starts about 80 °C and continues upto 130 °C, which attributed to the loss of four molecules of ethanol for **2f**, one molecule of methanol for **2g**, one ethanol for **2i** and one molecule of water for **2k** respectively. Furthermore, loss of the framework occurs in the range of 250-280 °C accounting for the loss of the organic part of the phosphonic molecule. Among all, **2k** manifests to be the stable salt as it decomposes around 280 °C. It can be ascertained that the collectively non-covalent interaction between the two components is anticipated to be strong such that these salts are stable around 280 °C.

In **2l**-**2n**, salt **2n** illustrates first mass loss of 1.6 % starts around 105 °C and continues upto 115 °C, followed by the second mass loss of 6.8 % about 135 °C, which corresponds to the loss of water molecule and DMSO molecule. Later, the organic part of the compound was lost nearly 300 °C however, in case of **2l** and **2m** the framework was stable about 260-270 °C. The structural homogeneity of bulk samples **2a**-**2k** was scrutinized through a comparison of as-synthesized and simulated powder X-ray diffraction (XRD) patterns. The experimental patterns correlated favorably with the simulated ones generated from single-crystal X-ray diffraction (Fig. 2.83-2.85).

Computational study

In order to have a preview of ideal geometries of salts **2a**-**2n**, the optimized geometries and energy were calculated at DFT level [50] using (B3LYP)/6-31G(d,p) basis set on Gaussian 03 suite of program. Recently, Singh et al. [33] reported the hydrogen bond interaction energy of various inorganic acids in the presence of pyrazole analogue and has suggested that in gaseous and the solid phase, the orientation and interaction between the components remain almost the same. In this chapter, the effect of an organic acid i.e., variety of phosphonic acid, on the pyrazole ligand was strived to predict the hydrogen bond interaction energy. Henceforth, single point energy calculations and zero point corrected total energy for varied species were evidenced. Besides, the hydrogen bond interaction energy was calculated using the following equation:

$$\Delta E = E_{salt} - (E_{pyrazole} + E_{acid})$$

where E_{salt}, $E_{pyrazole}$ and E_{acid} are the zero point corrected total energy of salt, pyrazole and acid respectively. All through the calculations, the solvent molecules were not deemed to ascertain the relative stability.

On probing the empirical energy calculation for broad range of hydrogen bonded system, it has been ascertained that the interaction energy is governed by various factors such as (a) substituents present on the molecule, i.e., electron donating group will tend to increase the stability as it increases the electron density, whereas electron withdrawing group will decrease the stability; (b) number of interactions involved in the molecule; (c) presence of stable synthon in the framework; (d) steric hindrance caused by the substituents. Amongst salts **2a**-**2d**, salts **2a** and **2b** encompasses synthons **I** & **III** and, **IV** respectively. The tertiary group in later is liable for providing the higher stability to the framework. Further in **2c** and **2d**, the latter flaunted the highest stability by keeping all the factors under consideration. The substituents present on the phosphonic acid i.e., bifunctionality and the synthons involved in the interpenetrated framework might be responsible for its higher stability among others. The energy is less for former although barely perceptible from **2a**, perhaps due to presence of electron withdrawing group.

In salts **2e**-**2k**, the interaction energy is mainly influenced by the upsurge in number of interactions involved in the salts. Perhaps, the presence of large number of molecules in the hydrogen bonded ring in the system is responsible for higher stability in salts **2e**-**2f** comprising synthons **I** & **IV** and, **III** & **V** respectively. While, the *tert*-butyl group in salt **2f** being the

electron donating group is responsible for its stability [51]. Further, the decrease in stability in salts **2g**-**2h** was envisaged due to -I effect of the carboxylic group, which decreases the interaction energy though the difference is subtle but the latter has the higher stability than the former as the inductive effect is significant only over the short distance. On the other hand, the salts **2i** and **2k** displayed the lowest and the highest stability correspondingly as in former number of interactions was found to be less and the steric hindrance caused by the rigid phosphonic acid, EA in **2i**. In contrast, the upsurge in interactions was scrutinized in salt **2k** due to presence of two phosphonic acid groups, which later led to increase in stability. Among salts **2l**-**2n**, **2n** illustrates highest stability than **2l** and **2m** attributable to the aforementioned reason.

Interaction energy for salts **2a**-**2d**, **2e**-**2k** and **2l**-**2n** has been summarized in Table 2.16, 2.17 and 2.18 respectively. For all salts, the stability was remarked to be harmonious with the number of increase in intermolecular interactions. It was ascertained that among all pyrazole ligands, BPaz is assumed to be a rich member comparatively as it may provide more stability to the salt due to presence of –N=N– having lone pair of electrons. Further, the trend is followed by MBPz as it has $–CH_2–$ group that could also be liable for providing high stability as compare to BPz salts. Considering together, it was found that phosphonate salts/complexes of BPaz illustrated highest interaction energy than salts of BPz and MBPz.

The frequency of occurrence and robustness of the synthons in the salts **2a**-**2n** has been evaluated at DFT level using (B3LYP)/6-31G(d,p) basis set. In addition to the occurrence of dimer **I**, synthons **III** and **IV** were found to be mostly found synthons in case of pyrazole salts of phosphonate due to their higher stability (Table 2.19), which is further due to increase in interactions involved in the salts. The probable reason for this trend may be the number of molecules involved in the interaction, hence more is the stability.

On probing thoroughly, it was investigated that the theoretical interaction energy which ultimately illustrated the stability of the salts deduced from DFT level calculation was in agreement with the stability attained by TG analysis of salts **2a**-**2n**.

Summary

Fourteen molecular salts/co-crystals were effectively constructed using pyrazole analogues with variety of phosphonic acids via synthon approach resulted in an intriguing robust supramolecular synthons. Variety of SOFs was adequately observed depending upon the functionality on phosphonic acids, used in the building block and the flexible/rigid analogue of

pyrazole BPz, MBPz and BPaz. The details of the **2a**-**2n** have been summarized in Table 2.21. The most interesting characteristic of the supramolecular network of phosphonate salts of pyrazole could be attributed to the formation of trimeric and tetrameric heterosynthons. Notably in each case, hydrogen bonded supramolecular ring, considered as the structural unit, is ascertained depending upon the type of phosphonic moiety used, which consequently display variety of supramolecular networks in presence of flexible/rigid pyrazole analogues (Scheme 2.6-2.8). On probing all the salts, it was found that salts **2a**-**2n** showed N–H···O, N–H···N, O–H···O types of interactions mostly and π-π interactions as well. It is important to point out that in the formation of hydrogen bonded ring, the shape and size of the ring depends on (a) substituents present on the phosphonic acid [52]; (b) the orientation of the molecules; (c) the conformation of the flexible pyrazole; and (d) short range interactions among them. It is worthwhile to notice that in presence of different phosphonic acid or the substituent(s) present on it, has affected the conformation of conformationally flexible BPz and MBPz with different torsion angles in each salt (Fig. 2.82, Table 2.20). Significantly, instead of presence of carboxylic group on phosphonic acid in salt **2c**, **2g**-**2h**, as anticipated, the dimerisation of phosphonic acid is raised along with the generation of robust synthons without any hindrance from competing dimer of carboxylic group present on the building block. The interaction energy of salts and synthons in the solid state of salts **2a**-**2n** were calculated to evaluate their occurrence by DFT calculation. It was observed that the interaction energy for salt involving DPA is largest among all salts and the occurrence of synthon **III**, having the higher stability is more. Furthermore, the thermal study revealed that the phosphonate salts of pyrazole analogues are stable upto 280 ºC, which might be on account of more stable interactions present. Moreover, the stability of salts **2a**-**2n** observed from DFT level energy was found to be in agreement with the stability provided by TGA. Hence, the present study provides an enhanced understanding about the effects of substituents on the resulted supramolecular assembly.

Table 2.1: Crystal Data and Collection Details of $[(HPPA^-)_2.H_2BPz^{2+}]$ (2a)

Emprical formula	$C_{22}H_{28}N_4O_6P_2$
Formula weight	506.42
Crystal system	Tetragonal
Space group	$I4_1/a$
a/ Å	16.344(5)
b/ Å	16.344(5)
c/ Å	18.856(8)
α/ °	90
β/ °	90
γ/ °	90
V / Å^3	5037.2(4)
Z	8
D_{calc} (g cm^{-3})	1.336
μ/mm^{-3}	0.217
θ range/ °	1.65 - 27.57
Reflections collected	28820
Independent reflections	2911
Parameters/ Restraints	168/0
GOF (F^2)	1.136
R_1; wR_2 [I>2σ(I)]	0.0399; 0.1319
R_1; wR_2 (all data)	0.0553; 0.1537
$\Delta\rho_{max}$; $\Delta\rho_{min}$	0.461; -0.450

Table 2.2: Crystal Data and Collection Details of [$HtBPA^{-}.HBPz^{+}$] (2b)

Emprical formula	$C_{14}H_{25}N_4O_3P$
Formula weight	328.35
Crystal system	Monoclinic
Space group	$P2_1/c$
a/ Å	10.127(6)
b/ Å	11.392(8)
c/ Å	16.319(11)
α/ °	90
β/ °	100.97(3)
γ/ °	90
V / Å^3	1848.5(2)
Z	4
D_{calc} (g cm^{-3})	1.180
μ/mm^{-3}	0.165
θ range/ °	2.05 - 25.00
Reflections collected	34222
Independent reflections	3247
Parameters/ Restraints	208/0
GOF (F^2)	1.094
R_1; wR_2 [I>2σ(I)]	0.0522; 0.1387
R_1; wR_2 (all data)	0.0677; 0.1637
$\Delta\rho_{max}$; $\Delta\rho_{min}$	0.694; -0.628

Table 2.3: Crystal Data and Collection Details of $[(HPPRA^{-})_2.H_2BPz^{2+}.(MeOH)_2.H_2O]$ (2c)

Emprical formula	$C_{18}H_{28}N_4O_{13}P_2$
Formula weight	570.38
Crystal system	Monoclinic
Space group	*C2/c*
a/ Å	11.221(5)
b/ Å	12.915(6)
c/ Å	23.006(12)
α/ °	90
β/ °	95.67(2)
γ/ °	90
V / Å^3	3318.0(3)
Z	4
D_{calc} (g cm^{-3})	1.158
μ/mm^{-3}	0.187
θ range/ °	1.78 - 26.36
Reflections collected	4820
Independent reflections	2396
Parameters/ Restraints	172/0
GOF (F^2)	1.091
R_1; wR_2 [I>2σ(I)]	0.0752; 0.2254
R_1; wR_2 (all data)	0.1107; 0.2566
$\Delta\rho_{max}$; $\Delta\rho_{min}$	0.677; -0.420

Table 2.4: Crystal Data and Collection Details of $[H_2DPA^{2-}.(HBPz^{+})_2.H_2O]$ (2d)

Emprical formula	$C_{28}H_{42}N_8O_7P_2$
Formula weight	664.64
Crystal system	Monoclinic
Space group	$P2_1/c$
a/ Å	7.912(9)
b/ Å	23.750(3)
c/ Å	17.518(19)
α/ °	90
β/ °	90.21(6)
γ/ °	90
V / Å^3	3292.3(7)
Z	4
D_{calc} (g cm^{-3})	1.341
μ/mm^{-3}	0.189
θ range/ °	2.07 - 26.38
Reflections collected	34146
Independent reflections	6630
Parameters/ Restraints	424/0
GOF (F^2)	1.015
R_1; wR_2 [I>2σ(I)]	0.0540;0.1124
R_1; wR_2 (all data)	0.1217; 0.1379
$\Delta\rho_{max}$; $\Delta\rho_{min}$	0.283; -0.282

Table 2.5: Crystal Data and Collection Details of [$HPPA^-.H_2PPA.HMBPz^+.MBPz$] (2e)

Emprical formula	$C_{34}H_{46}N_8O_6P_2$
Formula weight	724.73
Crystal system	Orthorhombic
Space group	$Pca2_1$
a/ Å	26.167(10)
b/ Å	16.091(8)
c/ Å	8.629(4)
α/ ^{o}	90
β/ ^{o}	90
γ/ ^{o}	90
V / Å^3	3633.8(3)
Z	4
D_{calc} (g cm^{-3})	1.325
μ/mm^{-3}	0.175
Flack parameter	0.33(10)
θ range/ ^{o}	1.27 - 28.29
Reflections collected	62864
Independent reflections	8834
Parameters/ Restraints	462/1
GOF (F^2)	1.000
R_1; wR_2 [I>2σ(I)]	0.0494; 0.1125
R_1; wR_2 (all data)	0.1077; 0.1441
$\Delta\rho_{max}$; $\Delta\rho_{min}$	0.182; -0.265

Table 2.6: Crystal Data and Collection Details of [$(HtBPA^-)_2.H_2MBPz^{2+}$.EtOH] (2f)

Emprical formula	$C_{21}H_{44}N_4O_7P_2$
Formula weight	526.51
Crystal system	Monoclinic
Space group	$P2_1$
a/ Å	11.698(5)
b/ Å	19.793(8)
c/ Å	25.474(11)
α/ ^{o}	90
β/ ^{o}	92.01(2)
γ/ ^{o}	90
V / Å^3	5894.8(4)
Z	8
D_{calc} (g cm^{-3})	1.186
μ/mm^{-3}	0.189
Flack parameter	0.03(5)
θ range/ ^{o}	1.30 - 25.00
Reflections collected	65075
Independent reflections	19847
Parameters/ Restraints	1270/1
GOF (F^2)	0.995
R_1; wR_2 [I>2σ(I)]	0.0485; 0.1033
R_1; wR_2 (all data)	0.0888; 0.1211
$\Delta\rho_{max}$; $\Delta\rho_{min}$	0.388; -0.241

Table 2.7: Crystal Data and Collection Details of [$HPAA^{-}.HMBPz^{+}.MBPz.MeOH$] (2g)

Emprical formula	$C_{25}H_{41}N_8O_6P$
Formula weight	580.63
Crystal system	Orthorhombic
Space group	$Pca2_1$
a/ Å	15.269(3)
b/ Å	8.820(2)
c/ Å	21.635(5)
α/ ^{o}	90
β/ ^{o}	90
γ/ ^{o}	90
V / Å^3	2913.6(11)
Z	4
D_{calc} (g cm^{-3})	1.324
μ/mm^{-3}	0.148
Flack parameter	0.35(12)
θ range/ ^{o}	1.88 - 28.46
Reflections collected	47141
Independent reflections	7288
Parameters/ Restraints	374/1
GOF (F^2)	0.933
R_1; wR_2 [I>2σ(I)]	0.0541; 0.1342
R_1; wR_2 (all data)	0.0858; 0.1532
$\Delta\rho_{max}$; $\Delta\rho_{min}$	0.366; -0.333

Table 2.8: Crystal Data and Collection Details of [$HPPRA^{-}.HMBPz^{+}$] (2h)

Emprical formula	$C_{14}H_{23}N_4O_5P$
Formula weight	358.33
Crystal system	Monoclinic
Space group	$P2_1/c$
a/ Å	10.364(3)
b/ Å	16.227(4)
c/ Å	11.093(3)
α/ ^{o}	90
β/ ^{o}	102.84(12)
γ/ ^{o}	90
V / Å^3	1818.9(9)
Z	4
D_{calc} (g cm^{-3})	1.309
μ/mm^{-3}	0.182
θ range/ ^{o}	2.02 - 25.00
Reflections collected	22721
Independent reflections	3197
Parameters/ Restraints	223/0
GOF (F^2)	1.082
R_1; wR_2 [I>2σ(I)]	0.0368; 0.1236
R_1; wR_2 (all data)	0.1719; 0.1534
$\Delta\rho_{max}$; $\Delta\rho_{min}$	0.518; -0.650

Table 2.9: Crystal Data and Collection Details of [$H_2EA^{2-}.H_2MBPz^{2+}.S$] (2i) (squeezed)

Emprical formula	$C_{15}H_{30}N_4O_8P_2$
Formula weight	456.37
Crystal system	Monoclinic
Space group	$P2_1/c$
a/ Å	11.491(9)
b/ Å	9.472(7)
c/ Å	22.752(18)
α/ ^{o}	90
β/ ^{o}	118.24(4)
γ/ ^{o}	90
V / Å^3	2181.8(3)
Z	4
D_{calc} (g cm^{-3})	1.249
μ/mm^{-3}	0.237
θ range/ ^{o}	2.01 - 26.41
Reflections collected	31105
Independent reflections	4462
Parameters/ Restraints	241/0
GOF (F^2)	1.056
R_1; wR_2 [I>2σ(I)]	0.0759; 0.2319
R_1; wR_2 (all data)	0.1032; 0.2439
$\Delta\rho_{max}$; $\Delta\rho_{min}$	0.900; -0.359

Table 2.10: Crystal Data and Collection Details of $[H_2EA^{2-}.H_2MBPz^{2+}]$ (2j)

Emprical formula	$C_{13}H_{24}N_4O_7P_2$
Formula weight	410.30
Crystal system	Triclinic
Space group	*P*-1
a/ Å	9.245(3)
b/ Å	10.426(3)
c/ Å	10.607(3)
α/ °	74.17(10)
β/ °	70.48(10)
γ/ °	84.10(10)
V / Å^3	927.1(5)
Z	2
D_{calc} (g cm^{-3})	1.470
μ/mm^{-3}	0.278
θ range/ °	2.03 - 28.29
Reflections collected	15303
Independent reflections	4542
Parameters/ Restraints	243/0
GOF (F^2)	1. 049
R_1; wR_2 [I>2σ(I)]	0.0338; 0.0998
R_1; wR_2 (all data)	0.0380; 0.0958
$\Delta\rho_{max}$; $\Delta\rho_{min}$	0.361; -0.334

Table 2.11: Crystal Data and Collection Details of $[H_3DPA^{-}.(H_2DPA^{2-})_{0.5}.H_2MBPz^{2+}.(H_2O)_{0.4}]$ (2k)

Emprical formula	$C_{23}H_{34.8}N_4O_{9.4}P_3$
Formula weight	610.66
Crystal system	Monoclinic
Space group	$P2_1/c$
a/ Å	11.376(9)
b/ Å	21.236(15)
c/ Å	12.425(9)
α/ ^{o}	90
β/ ^{o}	100.76(4)
γ/ ^{o}	90
V / Å^3	2949.2(4)
Z	2
D_{calc} (g cm^{-3})	1.377
μ/mm^{-3}	0.258
θ range/ ^{o}	1.82 - 26.47
Reflections collected	35500
Independent reflections	6042
Parameters/ Restraints	364/0
GOF (F^2)	0.924
R_1; wR_2 [I>2σ(I)]	0.0589; 0.1359
R_1; wR_2 (all data)	0.1475; 0.1836
$\Delta\rho_{max}$; $\Delta\rho_{min}$	0.565; -0.489

Table 2.12: Crystal Data and Collection Details of [H_2PPA.BPaz] (2l)

Emprical formula	$C_{16}H_{21}N_6O_3P$
Formula weight	376.36
Crystal system	Triclinic
Space group	*P*-1
a/ Å	8.435(5)
b/ Å	8.776(5)
c/ Å	13.778(8)
α/ °	103.57(3)
β/ °	101.27(4)
γ/ °	104.45(3)
V / Å^3	924.6(10)
Z	2
D_{calc} (g cm^{-3})	1.352
μ/mm^{-3}	0.178
θ range/ °	1.58 - 28.33
Reflections collected	12417
Independent reflections	4408
Parameters/ Restraints	241/0
GOF (F^2)	1.030
R_1; wR_2 [I>2σ(I)]	0.0575; 0.1630
R_1; wR_2 (all data)	0.0831; 0.1887
$\Delta\rho_{max}$; $\Delta\rho_{min}$	0.411; -0.566

Table 2.13: Crystal Data and Collection Details of [(H_2tBPA)$_2$.BPaz] (2m)

Emprical formula	$C_{18}H_{36}N_6O_6P_2$
Formula weight	494.47
Crystal system	Triclinic
Space group	*P*-1
a/ Å	5.856(3)
b/ Å	10.251(4)
c/ Å	11.698(5)
α/ ^{o}	94.719(2)
β/ ^{o}	102.46(2)
γ/ ^{o}	102.04(2)
V / Å^3	664.7(5)
Z	1
D_{calc} (g cm^{-3})	1.235
μ/mm^{-3}	0.205
θ range/ ^{o}	1.80 - 28.35
Reflections collected	9744
Independent reflections	3220
Parameters/ Restraints	152/0
GOF (F^2)	1.055
R_1; wR_2 [I>2σ(I)]	0.0419; 0.1159
R_1; wR_2 (all data)	0.0514; 0.1284
$\Delta\rho_{max}$; $\Delta\rho_{min}$	0.279; -0.315

Table 2.14: Crystal Data and Collection Details of [H_2DPA^{2-} .$(HBPaz^+)_2$.$(BPaz)_2$.DMSO.H_2O] (2n)

Emprical formula	$C_{50}H_{68}N_{24}O_8P_2S$
Formula weight	1227.29
Crystal system	Monoclinic
Space group	$P2_1/c$
a/ Å	14.695(7)
b/ Å	22.606(10)
c/ Å	20.204(8)
α/ ^{o}	90
β/ ^{o}	109.31(13)
γ/ ^{o}	90
V / Å^3	6334.0(5)
Z	4
D_{calc} (g cm^{-3})	1.287
μ/mm^{-3}	0.170
θ range/ ^{o}	1.47 - 25.00
Reflections collected	11121
Independent reflections	5497
Parameters/ Restraints	802/3
GOF (F^2)	0.953
R_1; wR_2 [I>2σ(I)]	0.0687; 0.1972
R_1; wR_2 (all data)	0.1522; 0.2598
$\Delta\rho_{max}$; $\Delta\rho_{min}$	0.607; -0.309

Table 2.15 Non-covalent interactions for 2a-2n (Å and ^{o})

D-H···A	d(D-H)	d(H-A)	d(D-A)	<(DHA)>	Symmetery codes
$[(HPPA^{-})_2.H_2BPz^{2+}]$ (2a)					
N1–H1D···O2	0.908(28)	1.782(28)	2.657(2)	161.0	x,+y,+z+1
O1–H1E···O2	0.755(38)	1.850(39)	2.596(2)	169.7	x+1/4+1,y+1/4,+z+1/4
N2–H2D···O3	0.980(28)	1.594(28)	2.564(2)	170.0	+x-1/4,-y+1/4+1,+z+3/4
$[HtBPA^{-}.HBPz^{+}]$ (2b)					
N1–H1D···N4	0.860(2)	1.982(2)	2.823(3)	165.5	x,-y+1/2+1,+z+1/2
N2–H2D···O3	0.860(2)	1.709(2)	2.548(3)	164.6	-x+1,-y+1,-z+1
N3–H3D···O2	0.861(2)	1.920(3)	2.756(4)	163.4	-x+1,+y+1/2,-z+1/2
O1–H1E···O2	0.820(2)	1.757(2)	2.564(3)	167.7	-x+2,y+1,-z
$[(HPPRA^{-})_2.H_2BPz^{2+}.(MeOH)_2.H_2O]$ (2c)					
N1–H1D···O2	0.860(5)	1.769(4)	2.622(6)	170.6	-x+1/2+1,-y+1/2,-z
N2–H2D···O1	0.860(9)	1.771(18)	2.628(25)	173.9	x-1,+y,+z
O3–H3E···O2	0.820(5)	1.821(6)	2.623(9)	165.8	-x+2,-y+1,-z
O5–H5Z···O1	0.820(7)	1.848(5)	2.631(8)	159.4	x-1/2,+y-1/2,+z
$[H_2DPA^{2-}.(HBPz^{+})_2.H_2O]$ (2d)					
N2–H2D···O2	0.860(3)	1.936(5)	2.731(18)	153.2	x+1,-y+1/2+1,+z-1/2
N3–H3D···N8	0.860(3)	2.067(2)	2.835(7)	148.2	-x+1,-y+1,-z
N4–H4D···O5	0.861(3)	1.708(5)	2.505(7)	152.9	x-1,+y,+z-1

N5–H5D···O1	0.861(3)	1.824(4)	2.677(6)	168.4	-x,+y-1/2,-z+1/2+1
N6–H6D···O7	0.820(2)	1.873(3)	2.693(4)	158.8	-
N7–H7D···O4	0.859(3)	2.408(4)	2.887(6)	165.0	-x+2,-y+1,-z+1
O3–H3E···O4	0.820(2)	1.816(2)	2.628(3)	170.4	x-1,+y,+z
O6–H6E···O1	0.820(2)	1.758(2)	2.570(3)	170.5	x+1,+y,+z
O7–H8W···N1	0.842(51)	2.086(52)	2.906(7)	164.2	-x+1,-y+1,-z+1
O7–H7W···O2	0.834(49)	1.932(49)	2.764(4)	175.3	x,-y+1/2+1,+z-1/2

[$HPPA^{-}$.H_2PPA.$HMBPz^{+}$.MBPz] (2e)

N2–H2D···O3	0.859(3)	1.929(2)	2.773(3)	169.1	x,+y,+z-1
N3–H3D···N5	0.860(2)	2.037(2)	2.881(3)	168.6	-
N4–H4D···O5	0.859(3)	1.681(3)	2.520(4)	164.6	-
N6–H6D···O4	0.860(3)	1.948(2)	2.780(4)	165.5	-
N8–H8D···N1	0.860(2)	2.094(2)	2.924(3)	162.2	x,+y+1,+z
O1–H1E···N7	0.821(3)	1.713(3)	2.517(4)	165.6	x,+y-1,+z+1
O2–H2E···O4	0.821(2)	1.729(2)	2.541(3)	170.6	x-1/2,-y+1,+z+1
O6–H6E···O3	0.820(2)	1.748(2)	2.564(3)	175.1	x+1/2,-y+1,+z+1

[($HtBPA^{-}$)$_2$.H_2MBPz^{2+}.EtOH] (2f)

N1–H1D···O23	0.859(4)	1.644(4)	2.492(6)	168.8	-x+2,+y+1/2,-z+1
N2–H2D···O13	0.860(3)	1.825(3)	2.638(4)	156.9	x+1,+y,+z
N3–H3D···O20	0.860(3)	1.681(3)	2.522(5)	165.1	-x+1,+y+1/2,-z+1
N4–H4D···O22	0.860(4)	1.929(4)	2.720(6)	152.3	-x+1,+y+1/2,-z+1

N5–H5D···O5	0.860(4)	1.696(4)	2.517(5)	158.5	-
N6–H6D···O9	0.860(3)	1.806(3)	2.605(4)	153.5	-
N7–H7D···O2	0.861(3)	1.681(3)	2.532(4)	169.6	-
N8–H8D···O6	0.861(3)	1.844(3)	2.678(5)	162.7	x-1,+y,+z
N9–H9D···O14	0.860(3)	1.674(3)	2.521(5)	167.8	x+1,+y,+z
N10–H10D···O17	0.859(4)	1.947(4)	2.735(6)	151.7	x+1,+y,+z
N11–H11D···O18	0.860(4)	1.647(4)	2.506(5)	177.5	-
N12–H12D···O19	0.860(3)	1.819(3)	2.648(4)	161.3	- x+1,+y-1/2,-z+1
N13–H13D···O8	0.860(3)	1.687(3)	2.531(4)	166.4	-
N14–H14D···O12	0.860(3)	1.844(3)	2.657(5)	162.3	-
N15–H15D···O11	0.860(3)	1.687(3)	2.513(5)	160.2	x-1,+y,+z
N16–H16D···O3	0.860(3)	1.823(3)	2.616(4)	152.5	x,+y-1,+z
O1–H1E···O6	0.820(3)	1.826(2)	2.629(4)	165.8	x-1,+y,+z
O4–H4E···O26	0.819(3)	1.865(3)	2.663(4)	164.4	-
O7–H7E···O12	0.820(3)	1.821(2)	2.627(4)	167.2	-
O10–H10E···O28	0.820(3)	1.834(3)	2.643(4)	168.5	x,+y-1,+z
O15–H15E···O17	0.819(3)	1.765(3)	2.570(4)	166.9	-
O16–H16E···O27	0.820(3)	1.807(3)	2.580(4)	156.5	x,+y-1,+z
O21–H21E···O22	0.820(3)	1.777(3)	2.571(4)	162.5	-
O24–H24E···O25	0.820(3)	1.848(3)	2.653(4)	166.6	-x+1,+y-1/2,-z+1
O25–H25E···O13	0.820(4)	1.920(3)	2.738(5)	175.7	-

O26–H26E···O9	0.820(4)	1.905(3)	2.719(5)	171.3	-
O27–H27E···O19	0.821(4)	1.875(3)	2.669(5)	162.4	-x+1,+y+1/2,-z+1
O28–H28E···O3	0.819(4)	1.907(3)	2.726(4)	178.0	x+1,+y,+z
C19–H19B···O17	0.960(6)	2.715(3)	3.498(7)	139.1	-
C25–H25A···N12	0.959(6)	2.644(4)	3.489(7)	147.1	-x+1,+y+1/2,-z+1
C38–H38A···O5	0.971(4)	2.630(3)	3.501(5)	149.5	-
C44–H44B···O8	0.960(4)	2.407(3)	3.354(4)	169.0	-
[HPAA^{-}.HMBPz^{+}.MBPz.MeOH] (2g)					
N1–H1D···O3	0.860(2)	1.785(2)	2.602(3)	158.0	x+1,+y,+z
N2–H2D···O3	0.860(3)	1.873(3)	2.969(4)	160.4	-x+1/2+1,+y,+z-1/2
N3–H3D···O2	0.860(2)	1.900(2)	2.744(3)	166.8	-
N5–H5D···N4	0.860(3)	2.073(3)	2.921(4)	168.5	-
N8–H8D···O3	0.861(2)	1.954(2)	2.723(3)	148.1	-x+1/2,+y,+z-1/2
O1–H1E···N6	0.821(2)	1.821(2)	2.630(3)	158.0	-
O4–H4Z···O6	0.820(2)	1.780(2)	2.571(3)	161.6	x,+y+1,+z
O6–H6C···O2	0.820(2)	1.851(2)	2.637(3)	160.6	-
[HPPRA^{-}.HMBPz^{+}] (2h)					
N1–H1D···O3	0.860(4)	1.781(5)	2.638(8)	174.1	x,-y+1/2,+z-1/2
N2–H2D···N4	0.859(4)	1.934(4)	2.764(8)	162.0	-x,+y-1/2,-z+1/2
N3–H3D···O2	0.860(3)	1.982(2)	2.800(4)	158.4	x,+y+1,+z
O1–H1E···O2	0.820(3)	1.796(7)	3.569(9)	173.7	-x+1,-y,-z+1

O5–H5D···O3	0.820(2)	1.804(6)	2.598(7)	162.7	x,-y+1/2,+z-1/2
C8–H8C···O4	0.960(4)	2.423(9)	3.356(12)	163.7	-x,-y+1,-z+1
C9–H9B···O4	0.969(3)	2.669(3)	3.638(5)	178.1	-x,-y+1,-z+1
$[H_2EA^{2-}.H_2MBPz^{2+}.S]$ (2i)					
N1–H1D···O2	0.860(4)	1.886(6)	2.701(9)	156.9	x-1,+y+1,+z
N2–H2D···O4	0.860(5)	1.720(5)	2.550(7)	161.4	-x,+y+1/2,-z+1/2
N3–H3D···O6	0.859(4)	1.945(6)	2.774(8)	161.5	-x+1,-y+1,-z+1
N4–H4D···O1	0.860(4)	1.739(5)	2.580(7)	165.5	x,-y+1/2+1,+z+1/2
O3–H3E···O6	0.820(4)	1.813(3)	2.633(5)	177.3	-x+1,+y+1/2,-z+1/2
O5–H5E···O2	0.820(4)	1.733(3)	2.541(5)	167.8	-x+1,+y+1/2,-z+1/2
O7–H7Z···O6	0.820(3)	2.032(3)	2.774(5)	150.3	-x+1,+y+1/2,-z+1/2
C1–H1B··· O5	0.960(6)	2.617(5)	3.434(7)	143.0	-x+1,+y-1/2,-z+1/2
C8–H8A···O4	0.969 (6)	2.436(5)	3.352(7)	157.3	x,+y+1,+z
$[H_2EA^{2-}.H_2MBPz^{2+}]$ (2j)					
N1–H1D···O5	0.860(2)	1.775(2)	2.632(2)	173.5	x+1,+y,+z
N2–H2D···O2	0.860(1)	2.059(1)	2.865(2)	155.7	-x+1,-y+1,-z+1
N3–H3D···O6	0.860(1)	1.801(2)	2.655(2)	172.0	x+1,+y,+z-1
N4–H4D···O2	0.860(2)	1.727(2)	2.580(2)	171.1	x,+y,+z-1
O1–H1E···O6	0.820(1)	1.829(1)	2.625(2)	163.3	-x,-y+2,-z+1
O4–H4E···O3	0.820(1)	1.772(1)	2.567(2)	162.9	-x,-y+2,-z+1
O7–H7E···O5	0.820(1)	2.018(1)	2.760(2)	150.1	-x,-y+1,-z+1

$[H_3DPA^{-}.(H_2DPA^{2-})_{0.5}.H_2MBPz^{2+}.(H_2O)_{0.4}]$ (2k)					
N1–H1D···O1	0.860(3)	1.789(3)	2.604(5)	157.3	-
N2–H2D···O7	0.860(4)	1.786(5)	2.643(7)	154.8	-
N3–H3D···O9	0.860(4)	1.786(4)	2.632(6)	167.3	x+1,+y+1,+z
N4–H4D···O6	0.861(4)	1.789(5)	2.616(6)	160.7	-x+2,+y+1/2,-z+1/2+1
O2–H2E···O7	0.821(3)	1.795(3)	2.596(4)	164.8	-
O3–H3E···O4	0.821(3)	1.655(3)	2.424(5)	155.0	x-1,+y,+z
O5–H5E···O9	0.820(3)	1.749(3)	2.549(5)	164.5	x+1,-y+1/2,+z+1/2
O8–H8E···O6	0.820(3)	1.791(3)	2.577(4)	159.9	-x+1,+y-1/2,-z+1/2+1
C8–H8B···O10	0.969(5)	2.329(14)	3.231(15)	154.5	-
C9–H9B···O4	0.971(5)	2.710(4)	3.584(5)	149.9	x-1,-y+1/2,+z-1/2
C13–H13B···O8	0.960(5)	2.666(4)	3.570(7)	157.1	-
C18–H18B···O1	0.970(4)	2.608(3)	3.553(5)	164.7	-x+1,-y+1,-z+2
C17–H17B···O8	0.960(5)	2.395(4)	3.328(6)	163.6	-x+1,-y+1,-z+2
C23–H23B···O3	0.959(5)	2.684(4)	3.405(6)	132.4	-x+1,-y,-z+2
O10–O3	-	-	2.737(14)	-	-
O5–O10	-	-	2.857(13)	-	-
$[H_2PPA.BPaz]$ (2l)					
N1–H1D···N5	0.860(3)	2.031(3)	2.859(5)	161.2	-x+1,-y+1,-z+1
N4–H4D···O3	0.860(3)	2.224(2)	3.015(4)	152.6	-x+1,-y+1,-z+1
O1–H1E···N2	0.820(3)	1.789(4)	2.557(6)	155.5	-

O2–H2E···O3	0.820(3)	1.754(4)	2.558(6)	166.1	-
[(H_2tBPA)$_2$.BPaz] (2m)					
O2–H2E···N1	0.820(2)	1.769(2)	2.565(3)	163.0	-x+1,-y,-z+1
N2–H2D···O1	0.860(2)	1.936(3)	2.770(5)	163.0	-x,-y,-z+1
O3–H3E···O1	0.820(2)	1.749(2)	2.548(3)	164.7	-
[H_2DPA^{2-}.($HBPaz^{+}$)$_2$.(BPaz)$_2$.DMSO.H_2O] (2n)					
N2–H2D···O5	0.860(4)	1.846(4)	2.704(6)	175.0	x,-y+1/2,+z-1/2
N4–H4D···N1	0.859(4)	2.132(4)	2.983(6)	170.5	x,-y+1/2,+z+1/2
N7–H7D···N10	0.859(4)	2.123(4)	2.962(6)	165.2	x,-y+1/2,+z-1/2
N9–H9D···O2	0.860(4)	1.817(4)	2.707(6)	163.3	-x+1,+y+1/2,-z+1/2+1
N13–H13D···N16	0.814(6)	1.952(4)	2.716(5)	162.8	x,-y+1/2,+z-1/2
N14–H14D···O4	0.860(3)	1.752(4)	2.573(5)	165.2	-x+1,+y+1/2,-z+1/2
N15–H15D···O4	0.861(3)	1.880(4)	2.695(5)	157.5	-x+1,-y,-z+1
N19–H19D···O1	0.860(3)	1.766(5)	2.576(6)	156.3	x,+y,+z-1
N20–H20D···N21	0.860(3)	1.982(4)	2.806(5)	159.7	x,-y+1/2,+z-1/2
N22–H22D···O1	0.860(3)	1.898(4)	2.700(5)	154.6	x,-y+1/2,+z-1/2
O3–H3E···N8	0.820(4)	1.904(4)	2.683(5)	158.1	-x+1,-y,-z+1
O6–H6E···N3	0.819(3)	1.895(5)	2.661(6)	155.4	-

*Note: The disorder in the system causes the failure in addition of hydrogen atoms on water molecule in salt **2k**, O–O interactions have been shown instead of O–H···O interaction.

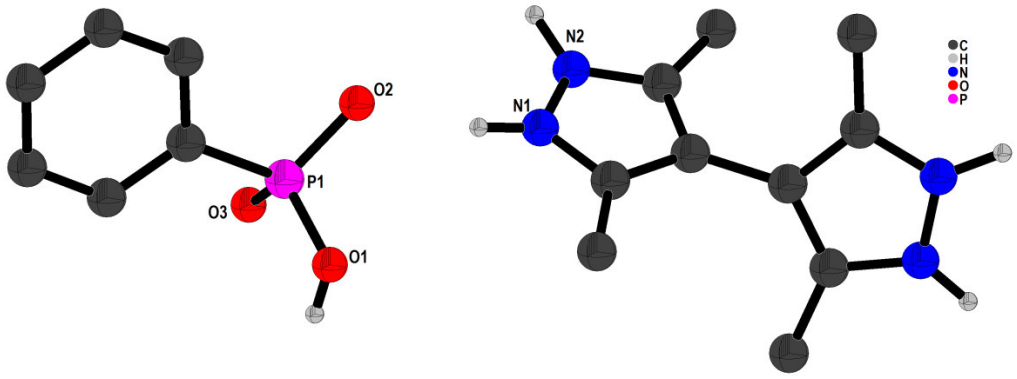

Fig. 2.12: Crystal Structure of [$(HPPA^{-})_2.H_2BPz^{2+}$] (**2a**). (C–H bonds are not shown for clarity)

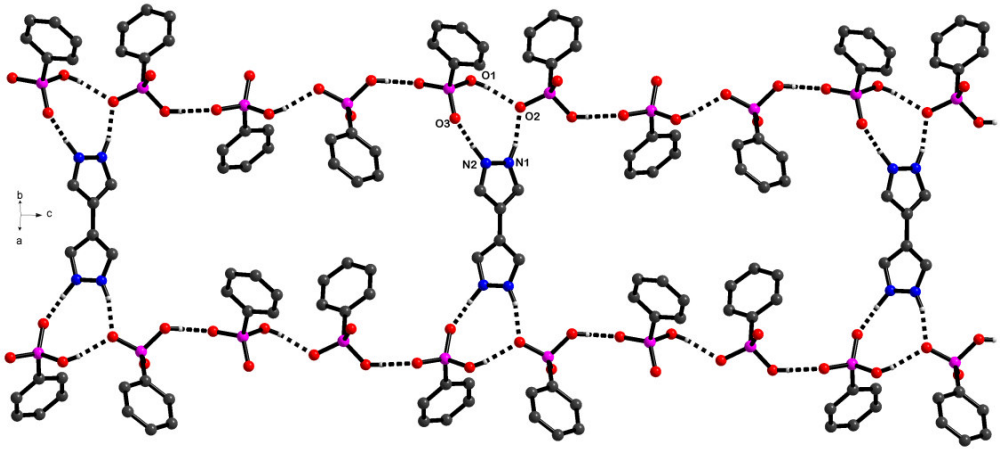

Fig. 2.13: View of 2D sheet structure with brick wall topology via formation of heterotrimer **III**, in **2a**. (Hydrogen atoms and methyl groups present on BPz are not shown for clarity)

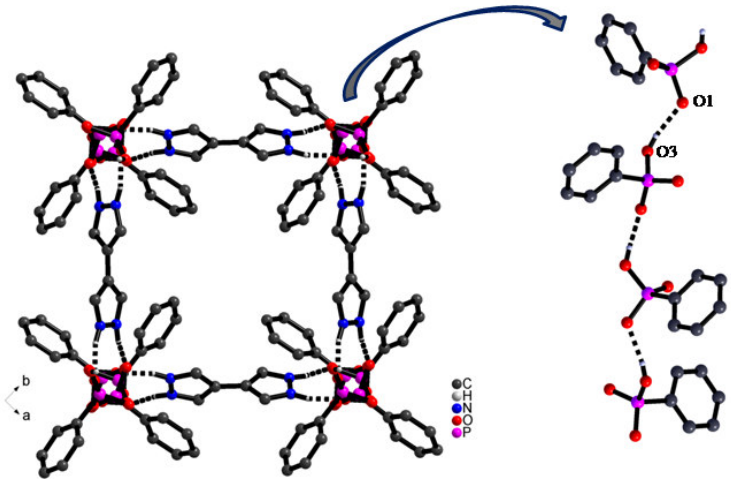

Fig. 2.14: a) Square grid formation in *ab*-plane extended by BPz linker and b) anionic thread of phenylphosphonate at 78° to each other in **2a**

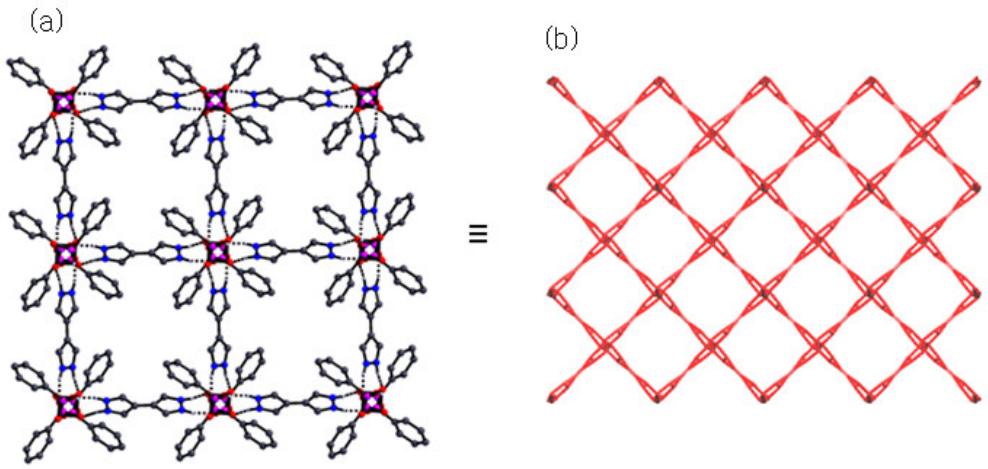

Fig. 2.15: 3D supramolecular framework in **2a** and (b) simplified representation of 3D supramolecular framework in **2a** produced by TOPOS

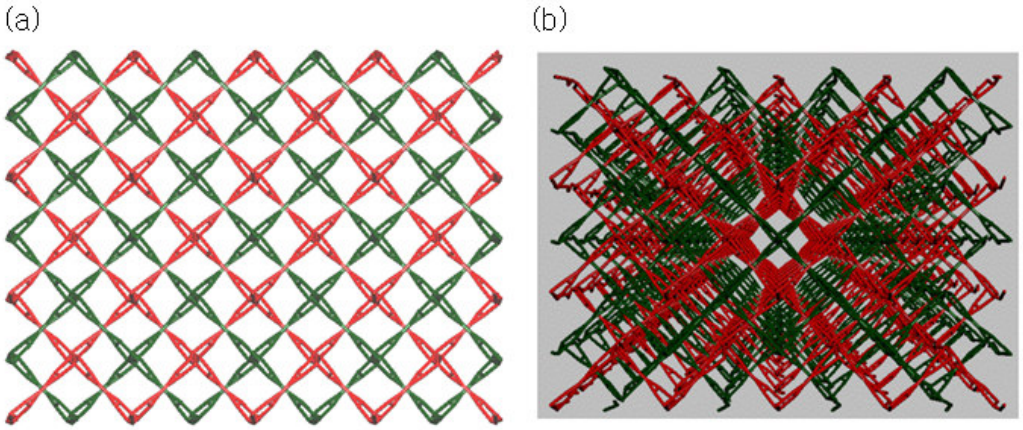

Fig. 2.16 (a) View of an interpenetrated two fold 3D supramolecular framework and (b) perspective view of **2a**

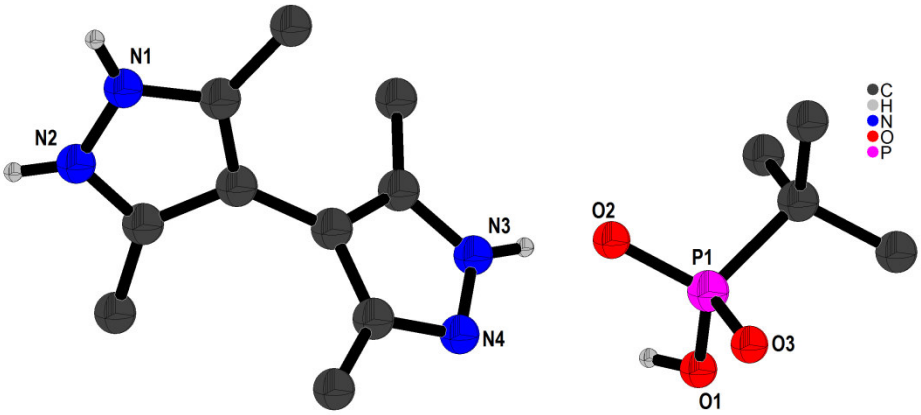

Fig. 2.17: Crystal Structure of [$HtBPA^{-}$.$HBPz^{+}$] (**2b**). (C–H bonds are not shown for clarity)

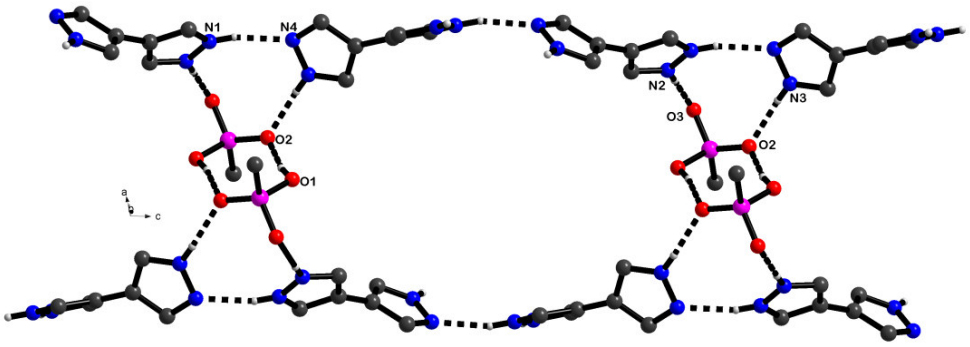

Fig. 2.18: Formation of an eight membered circular grid in **2b**. (Hydrogen atoms and methyl groups present on BPz are not shown for clarity)

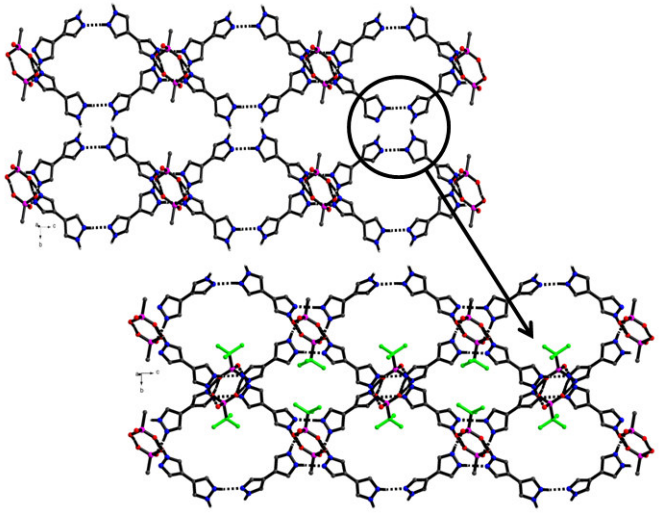

Fig. 2.19: 2D sheet formed with the help of homodimer of phosphonic acid in **2b**

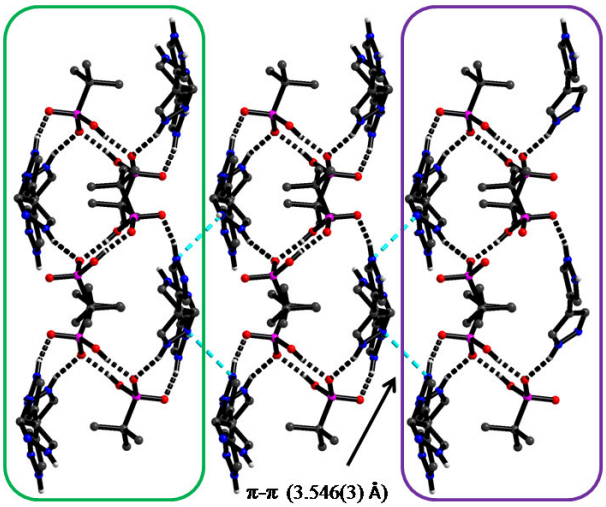

Fig. 2.20: 3D extended supramolecular framework formed via π···π interaction in **2b**

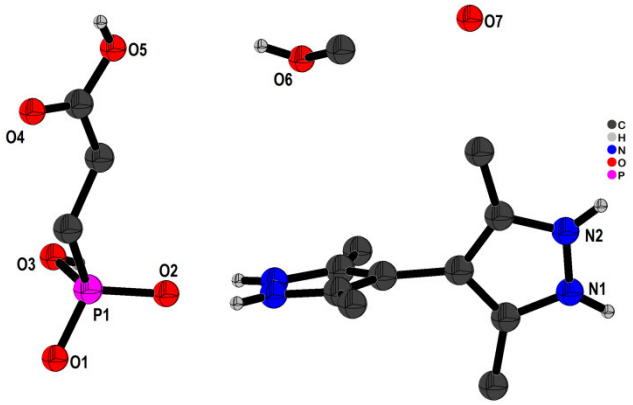

Fig. 2.21: Crystal Structure of [$(HPPRA^{-})_2.H_2BPz^{2+}.(MeOH)_2.H_2O$] (**2c**). (C–H bonds are not shown for clarity)

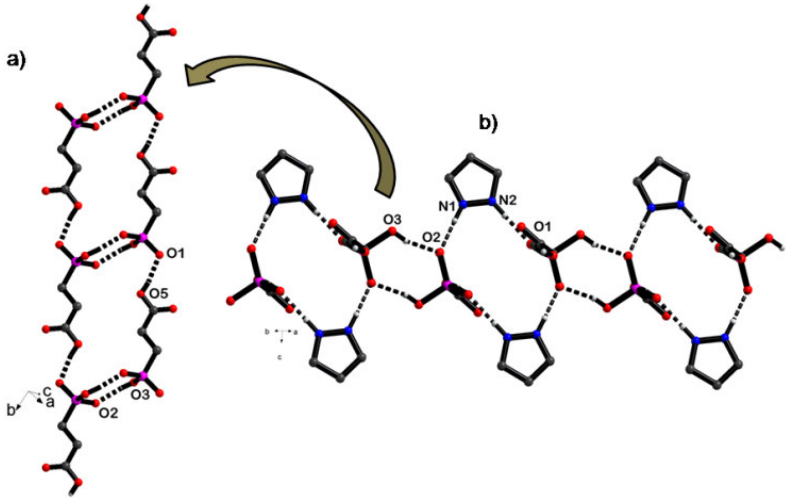

Fig. 2.22: (a) View of 1D tape and (b) extension of 1D tape to 2D supramolecular framework via BPz linker in **2c**. (Hydrogen atoms and methyl groups present on BPz are not shown for clarity)

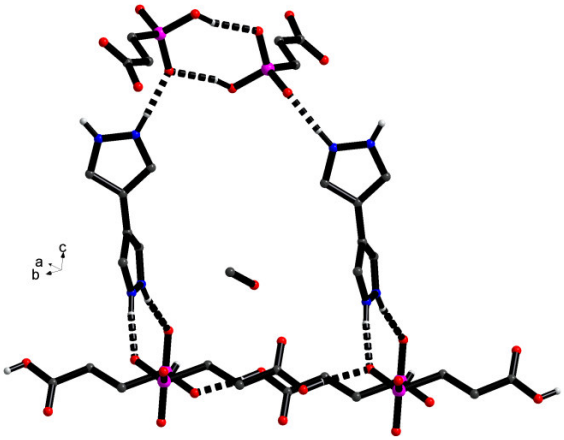

Fig. 2.23: Formation of hydrogen bonded ring motif in **2c**

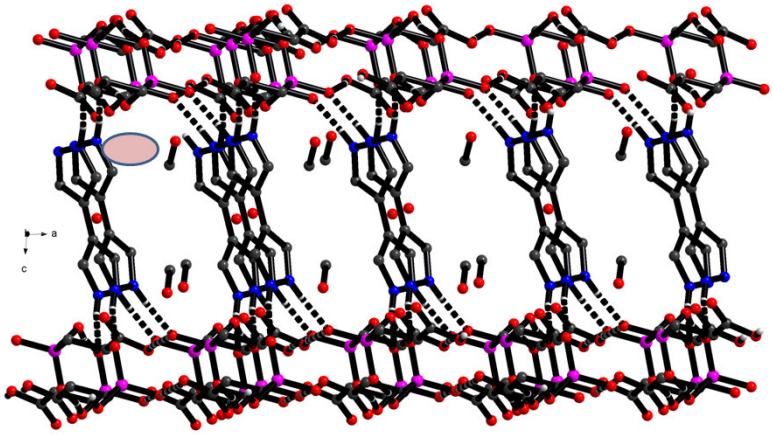

Fig. 2.24: 3D supramolecular organic framework along *b*-axis in **2c**

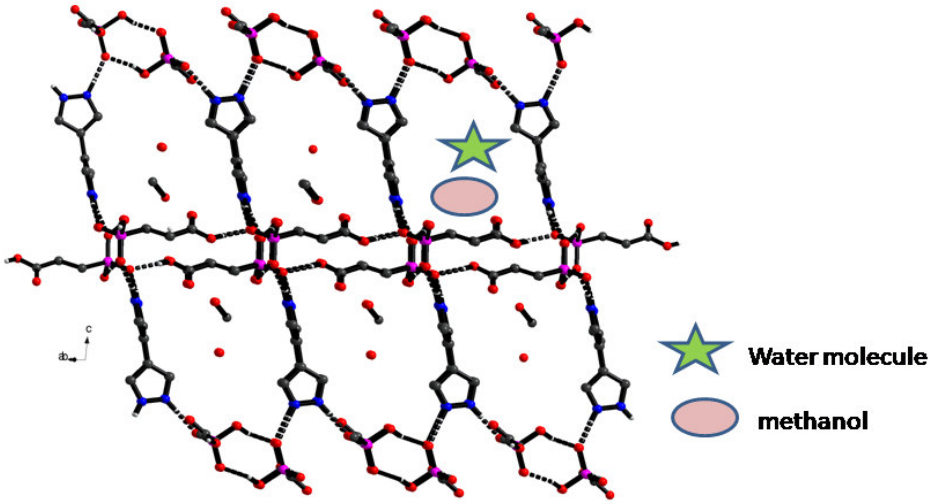

Fig. 2.25: 3D supramolecular organic framework along *a*-axis with water and methanol molecule occupying the channel formed in **2c**

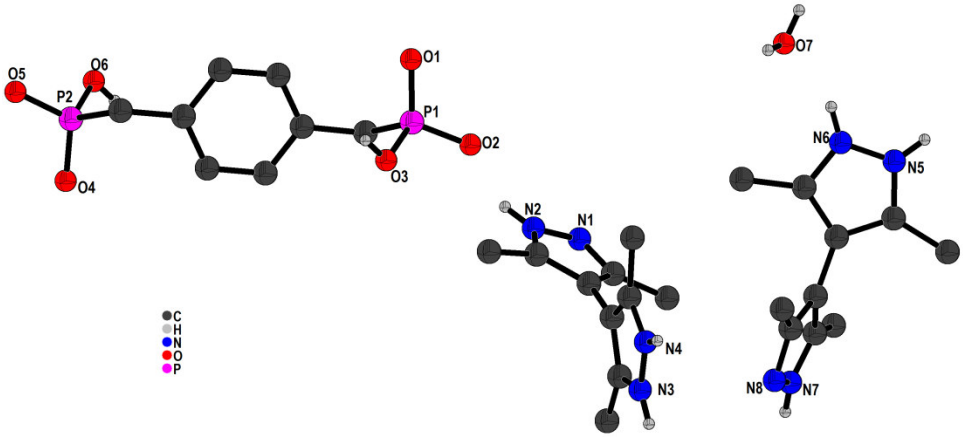

Fig. 2.26: Crystal structure of $[H_2DPA^{2-}.(HBPz^{+})_2.H_2O]$ (**2d**). (C–H bonds are not shown for clarity)

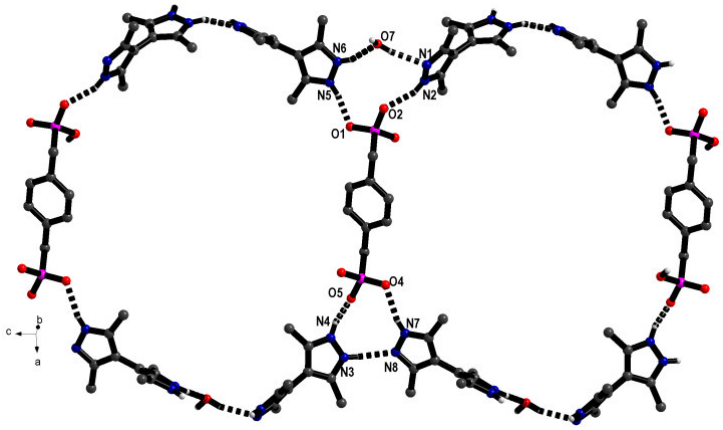

Fig.2.27: View of seven membered circular grid in **2d**

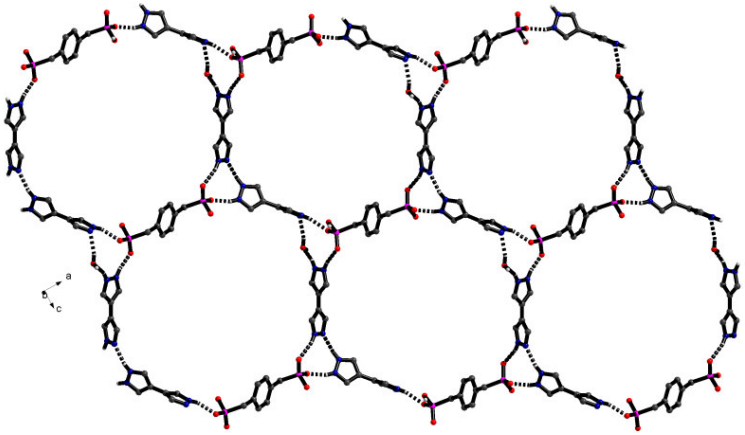

Fig. 2.28: View of 2D supramolecular network using heterotetramer synthon, **V** in **2d**. (Hydrogen atoms and methyl groups present on BPz are not shown for clarity)

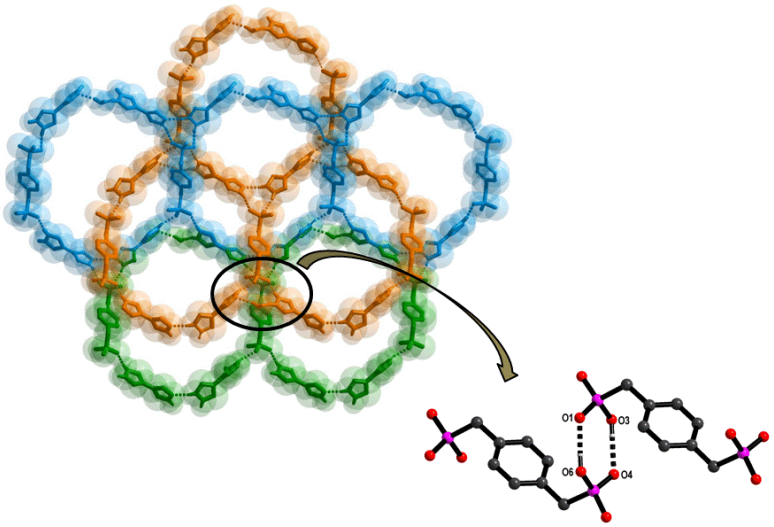

Fig. 2.29: Representation of interpenetrated supramolecular network linked by homodimer, **I** of phosphonic acid in **2d**

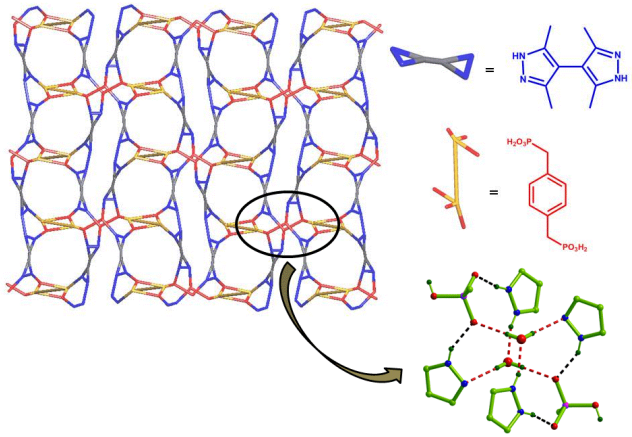

Fig. 2.30: Simplified representation of 3D supramolecular framework in **2d**

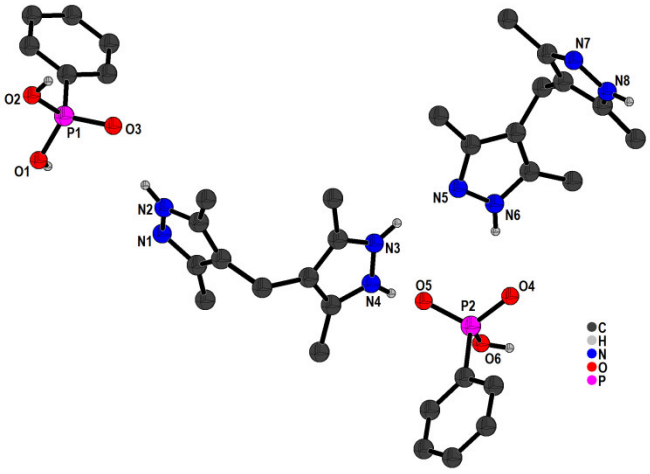

Fig. 2.31: Crystal structure of [$HPPA^-$.H_2PPA.$HMBPz^+$.MBPz] (**2e**). (C–H bonds are not shown for clarity)

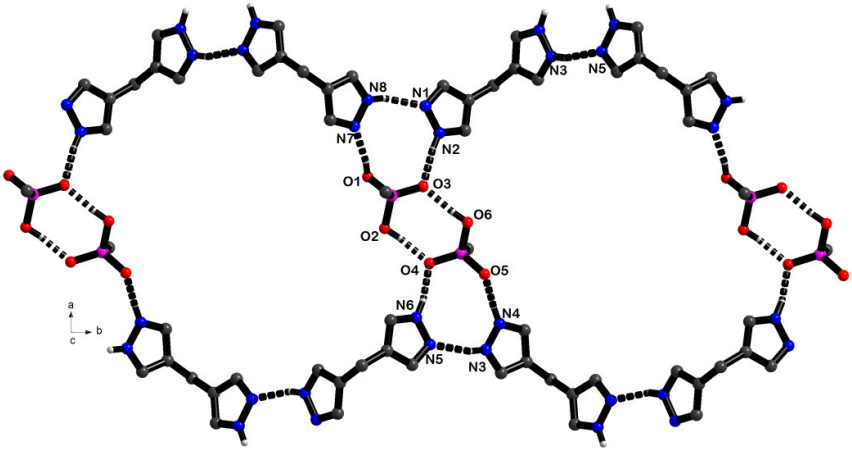

Fig. 2.32: Structural unit representing parallel undulated chains of MBPz and $HMBpz^+$ glued together by the homodimer **I** (Hydrogen atoms and methyl groups present on MBPz are not shown for clarity) in **2e**

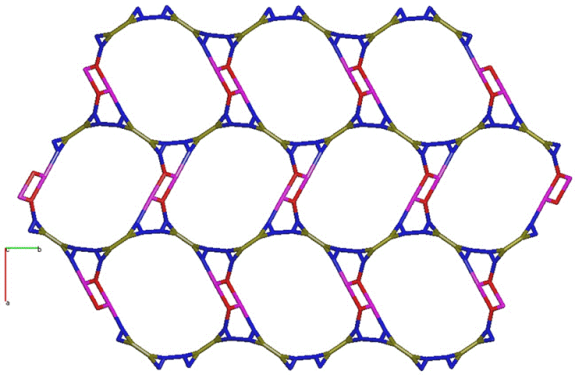

Fig. 2.33: Simplified representation of 2D layer produced by TOPOS in **2e**

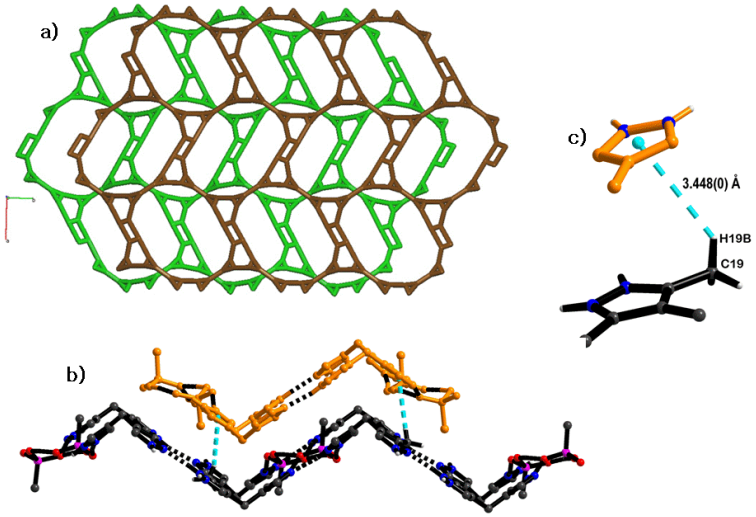

Fig. 2.34: (a) Packing of adjacent layers by TOPOS (top view); (b) side view and (c) C–H···π (3.448 Å) interaction between two adjacent layers in **2e**

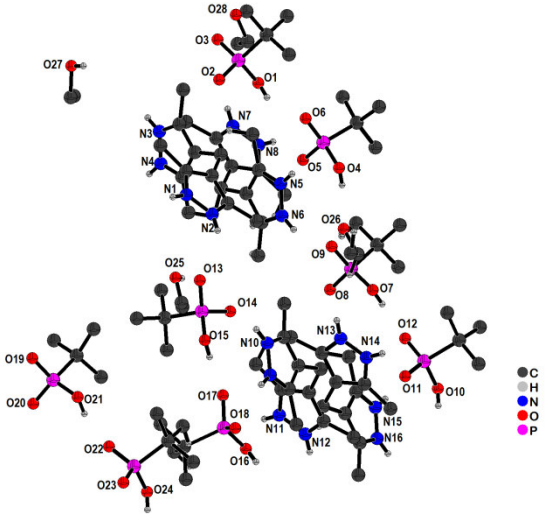

Fig. 2.35: Crystal structure of [$(HtBPA^-)_2.H_2MBPz^{2+}$.EtOH] (**2f**). (C–H bonds are not shown for clarity)

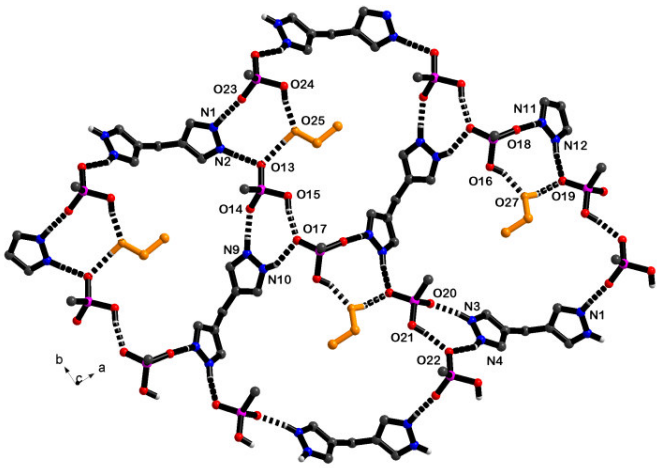

Fig. 2.36: 2D sheet produced by synthons: heterotrimer **III** and heterotetramers **VII** along *c*-axis with ethanol molecule shown in orange in **2f**. (Hydrogen atoms and methyl groups present on MBPz are not shown for clarity)

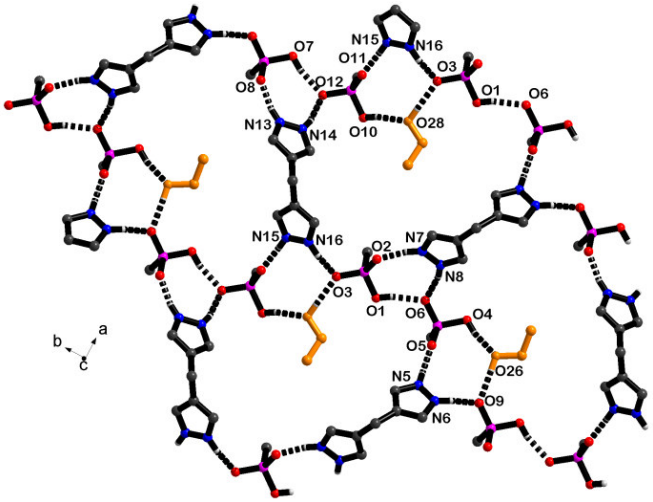

Fig. 2.37: Another 2D sheet produced by heterotrimer **III** and heterotetramer **VII** in **2f**

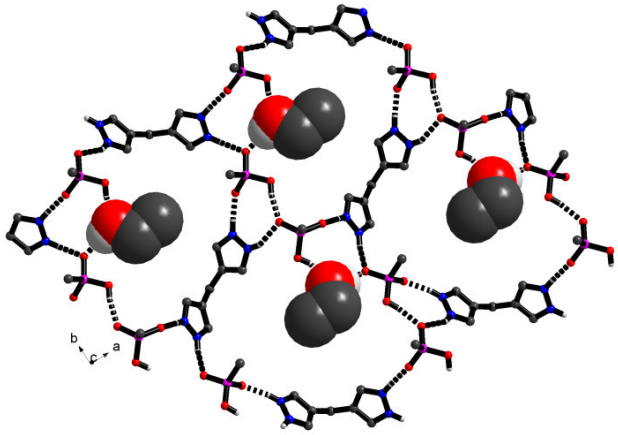

Fig. 2.38: 2D sheet hydrogen bonded porous sheet residing ethanol molecule in the cavity in **2f**

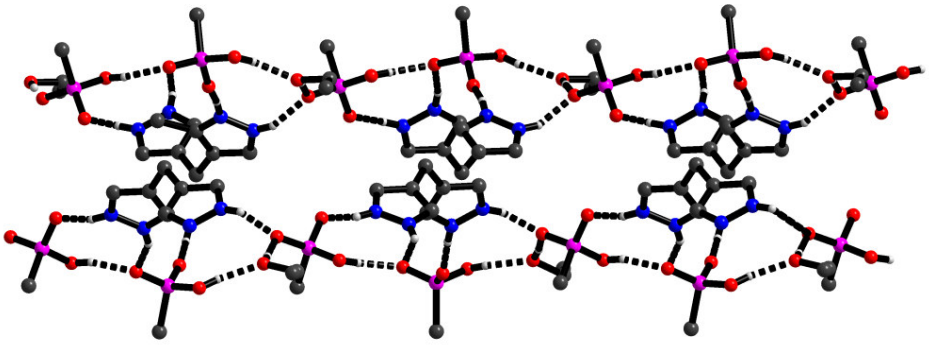

Fig. 2.39: Two stacked 2D sheets together along *a*-axis in **2f**

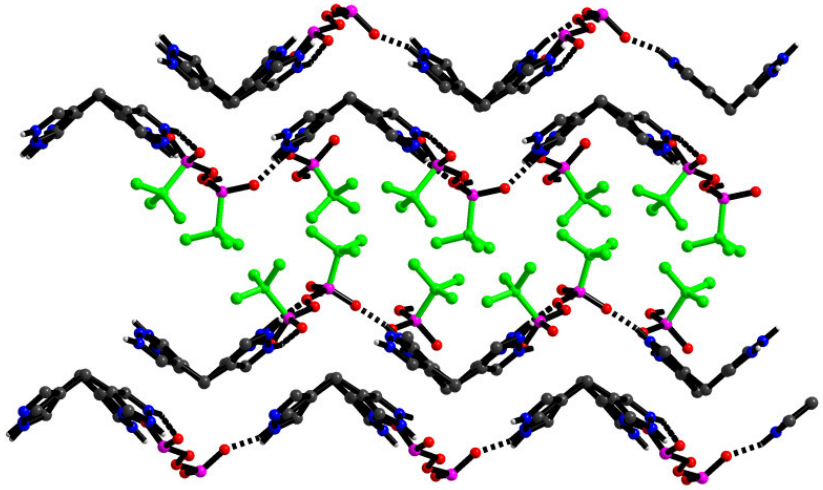

Fig. 2.40: Stacking of the adjacent layer of 2D sheets with tertiary butyl group in between the stacked layers along *b*-axis (*tert*-butyl groups are shown in green color) in **2f**

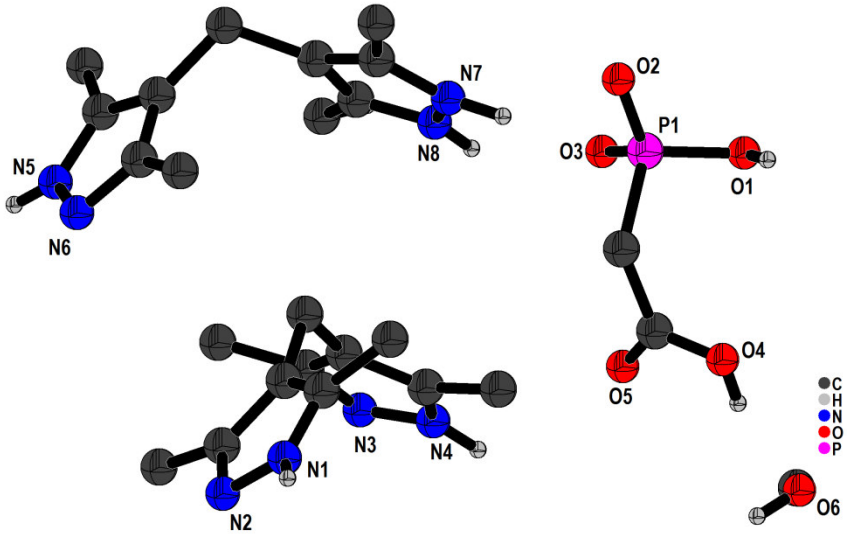

Fig. 2.41: Crystal structure of [HPAA^{-}.HMBPz^{+}.MBPz.MeOH] (**2g**). (C–H bonds are not shown for clarity)

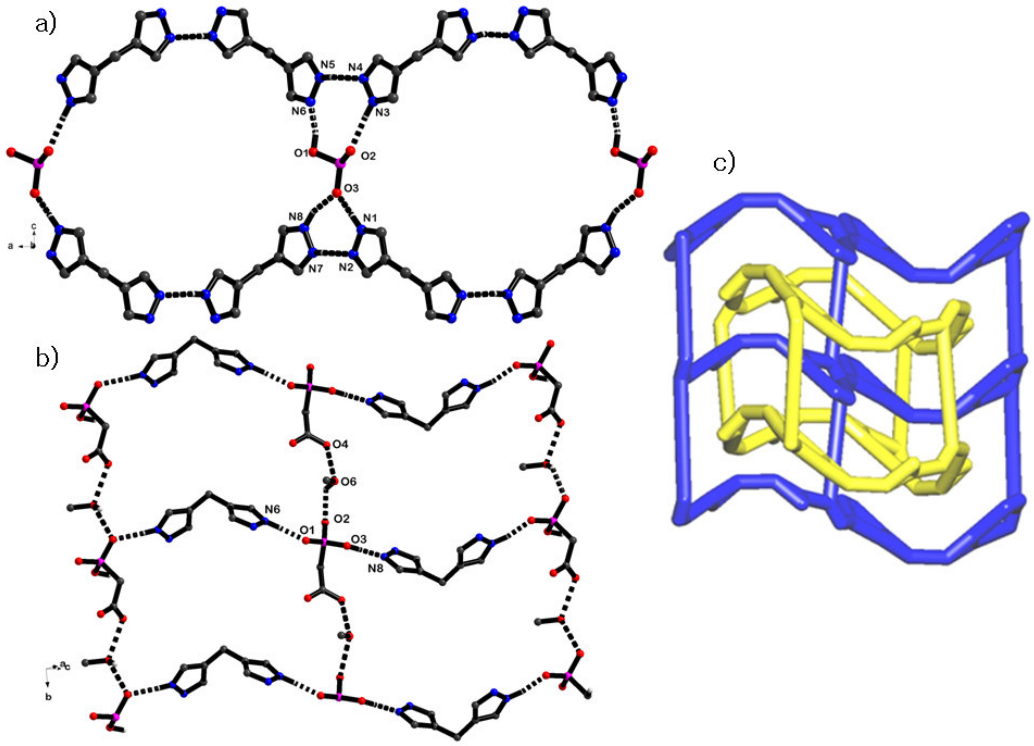

Fig. 2.42: (a) Structural unit representing involving two different trimer heterosynthons **II** and **IV** perpendicular to *b*-axis forming 2D sheet. (Hydrogen atoms and methyl groups present on MBPz are not shown for clarity); (b) cross-section of the structure representing the chain of $HPAA^-$ and methanol molecule O4–O6 and O6–O2 connecting the structural unit parallel to *b*-axis and (c) simplified representation of entanglement of two adjacent 2D sheets produced by TOPOS in **2g**

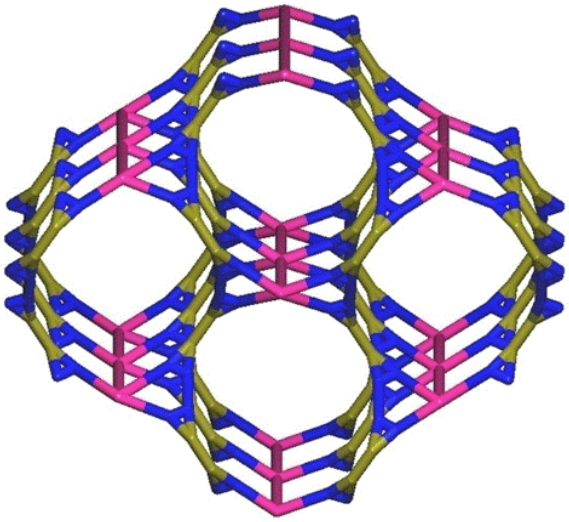

Fig. 2.43: 3D packing of a network along *b*-axis by TOPOS (top view) in **2g**

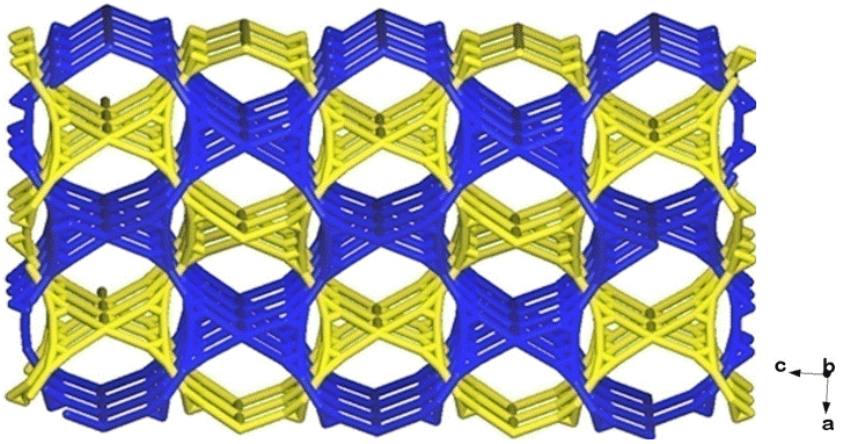

Fig. 2.44: Simplified representation of entanglement of two networks due to slipped packing of adjacent layers, the two networks are shown in blue and yellow color (top view) produced by TOPOS in **2g**

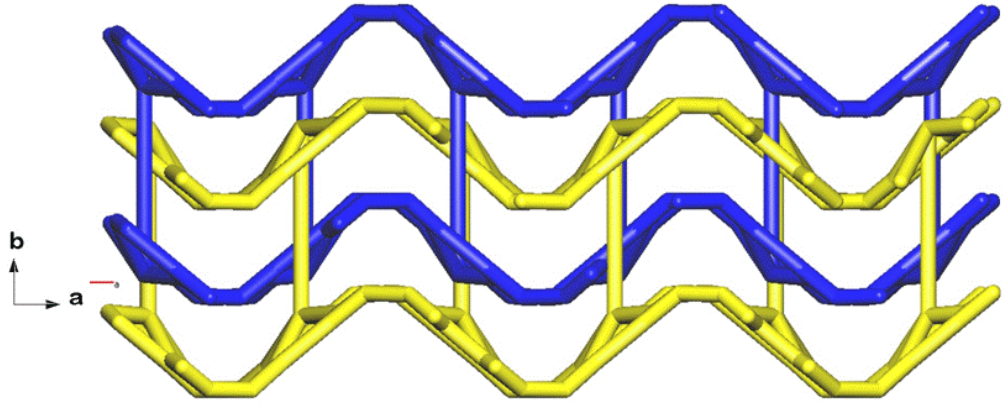

Fig. 2.45: Side view of the two networks representing ABAB pattern along *c*-axis in **2g**

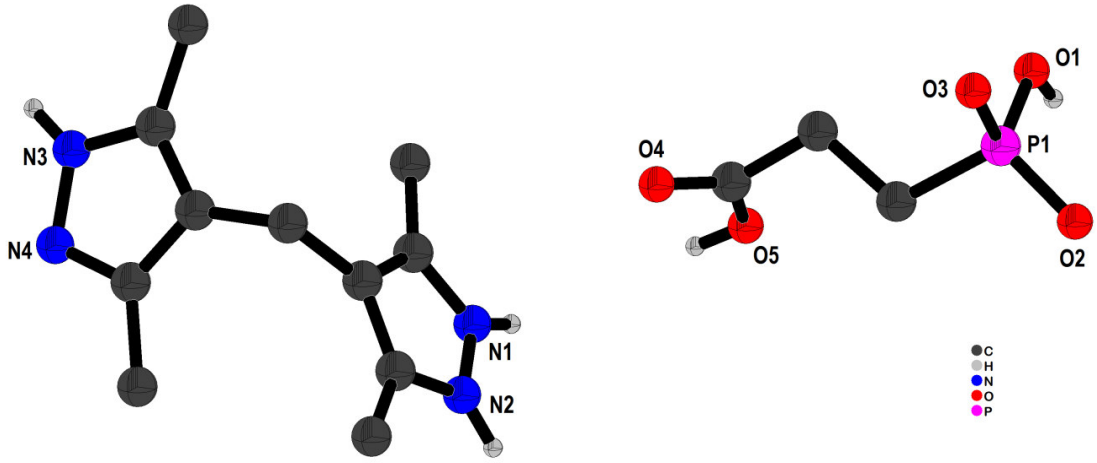

Fig. 2.46: Crystal structure of [HPPRA^{-}.HMBPz^{+}] (**2h**). (C–H bonds are not shown for clarity)

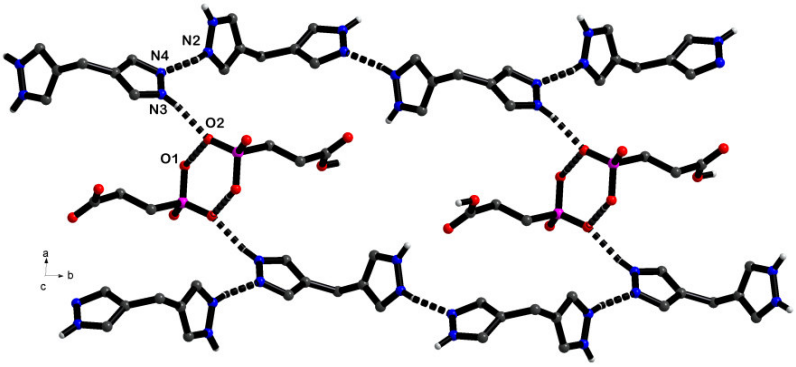

Fig. 2.47: Structural unit representing parallel *zig-zag* chains of $HMBpz^{+}$ glued together by homosynthon I in *ab*-plane in **2h**. (Hydrogen atoms and methyl groups present on MBPz are not shown for clarity)

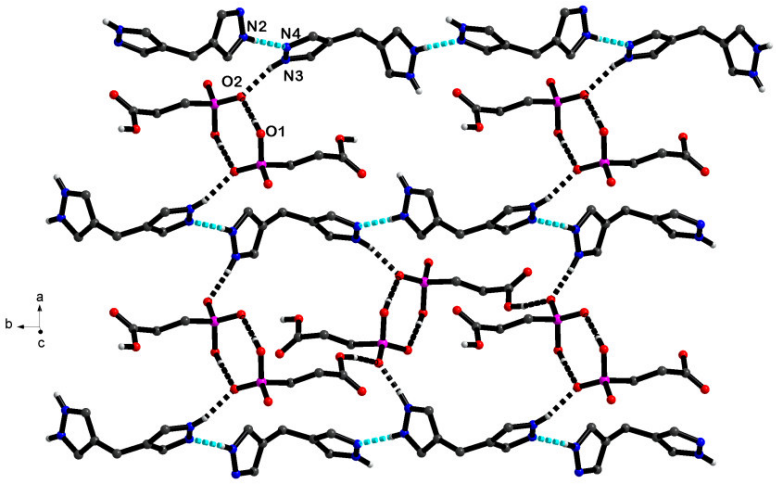

Fig. 2.48: Representation of 2D sheet in *ab*-plane in **2h**

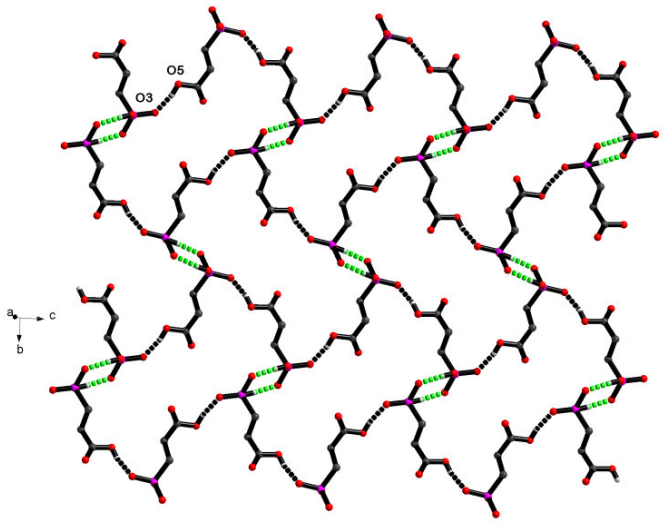

Fig. 2.49: Herringbone layer of $HPPRA^{-}$ molecules perpendicular to *a*-axis, phosphonic homodimer is shown in green colored hydrogen bond in **2h**

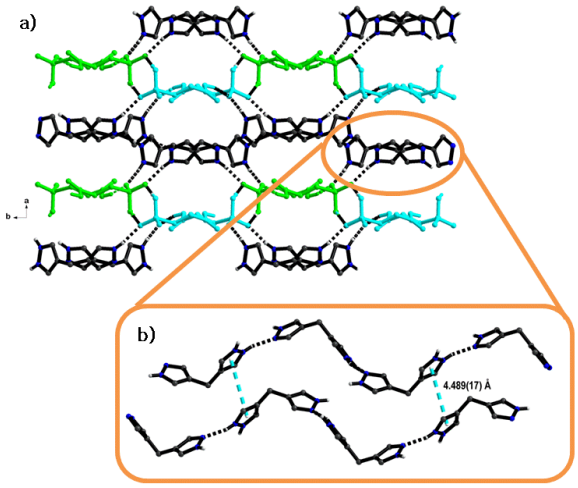

Fig. 2.50: 3D supramolecular hydrogen bonded network representing troughs (in green) and crests (in blue) and (b) π···π interaction between two $HMBPz^{+}$ along *c*-axis in 3D network in **2h**

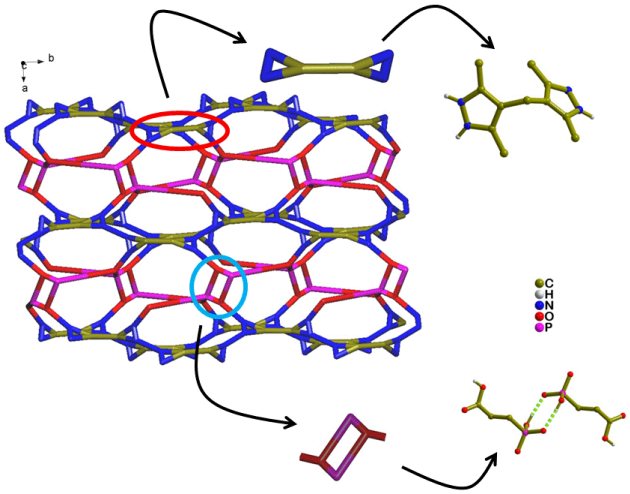

Fig. 2.51: 3D network in **2h**

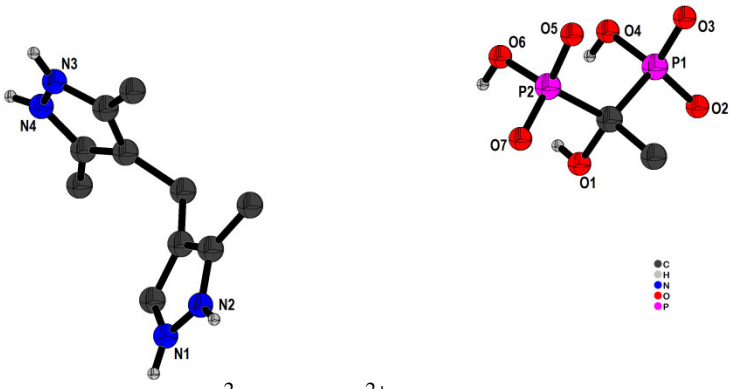

Fig. 2.52: Crystal structure of $[H_2EA^{2-}.H_2MBPz^{2+}.S]$ (**2i**). (C–H bonds are not shown for clarity)

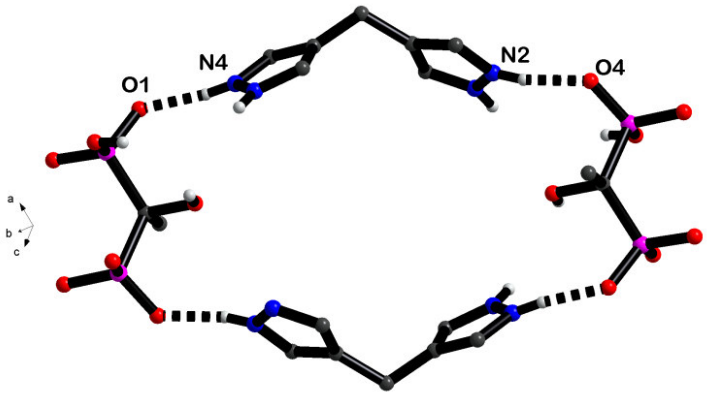

Fig. 2.53: Chain of bisphosphonic acid interlinked by H_2MBPz^{2+} linker in **2i**. (Hydrogen atoms and methyl groups present on MBPz are not shown for clarity)

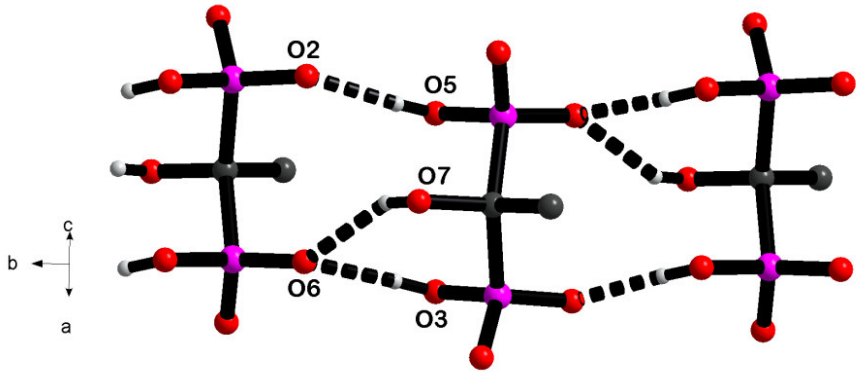

Fig. 2.54: View of 1D chain of phosphonate anion along *a*-axis in **2i**

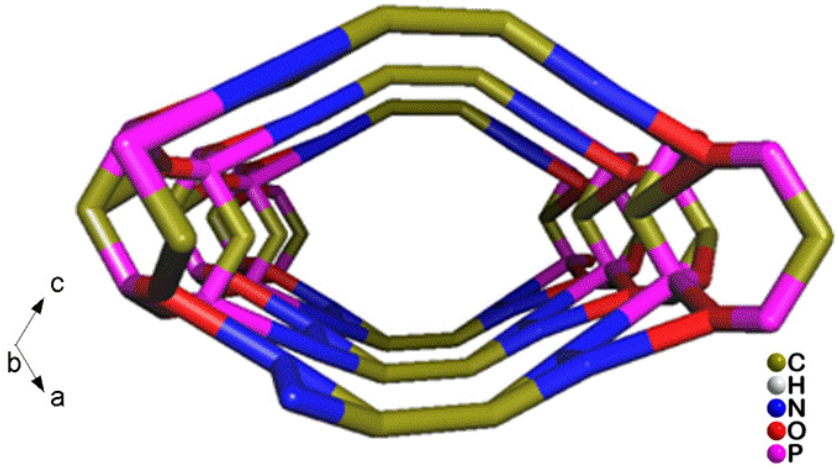

Fig. 2.55: Simplified perspective view of 1D columnar along *b*-axis in **2i**

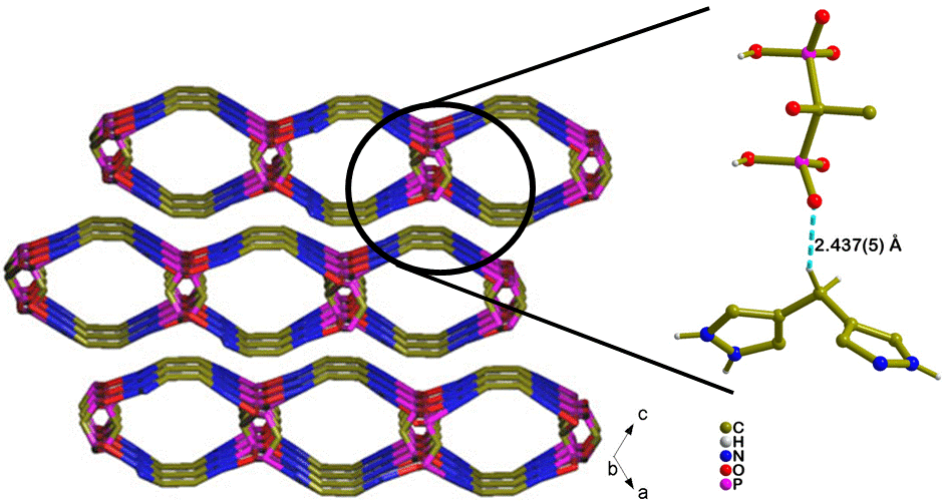

Fig. 2.56: Extended 3D supramolecular hydrogen bonded porous network in **2i**

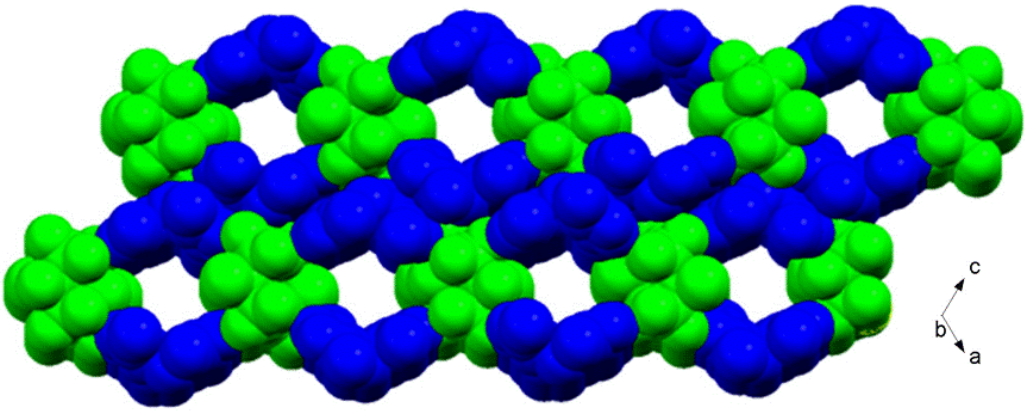

Fig. 2.57: Space-fill representation of 3D supramolecular network in **2i**

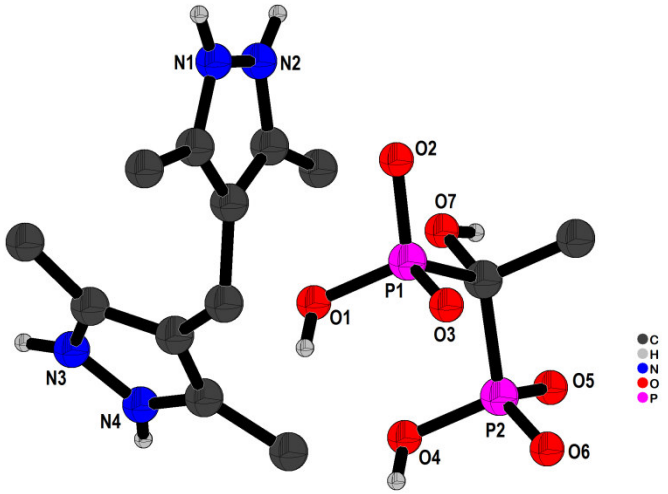

Fig. 2.58: Crystal structure of $[H_2EA^{2-}.H_2MBPz^{2+}]$ (**2j**). (C–H bonds are not shown for clarity)

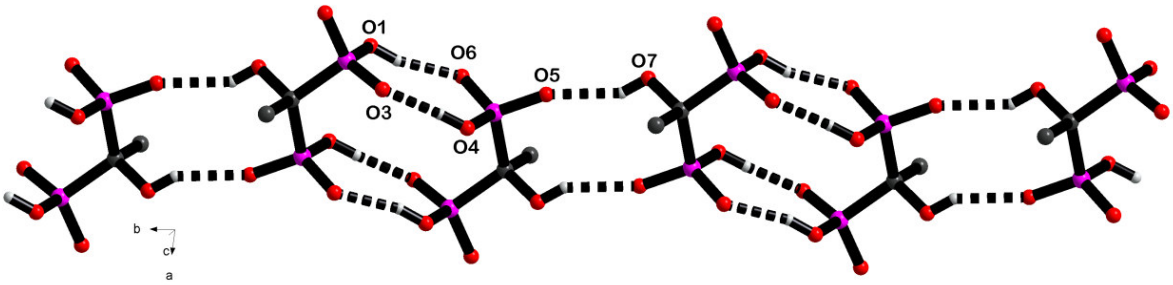

Fig. 2.59: 1D chain of bisphosphonate along *b*-axis with alternate array of homodimer in **2j**

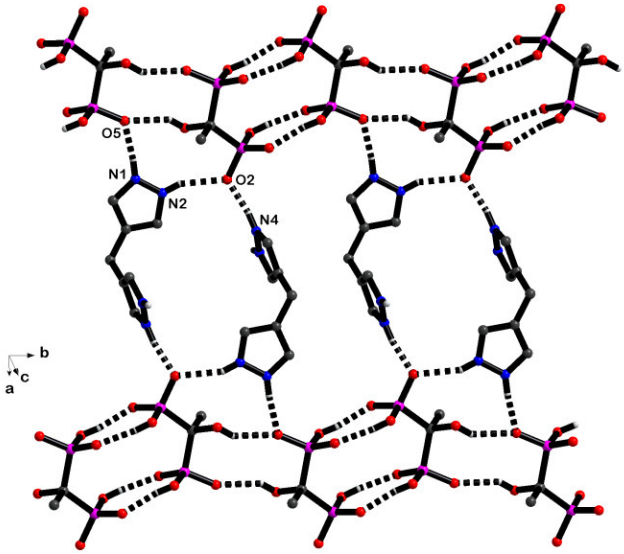

Fig. 2.60: Representation of 2D sheet in *ab*-plane formed by linking the 1D chain of phosphonic acid with H_2MBPz^{2+} in **2j**. (Hydrogen atoms and methyl groups present on MBPz are not shown for clarity)

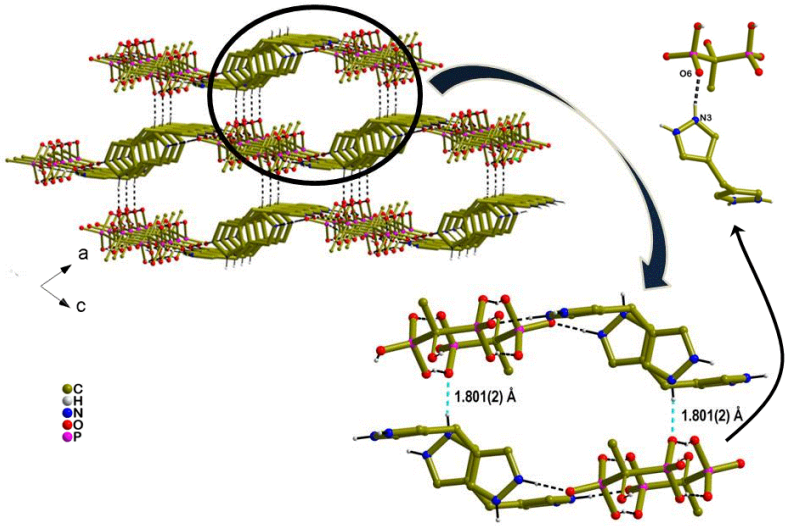

Fig. 2.61: Extended 3D supramolecular network in **2j**

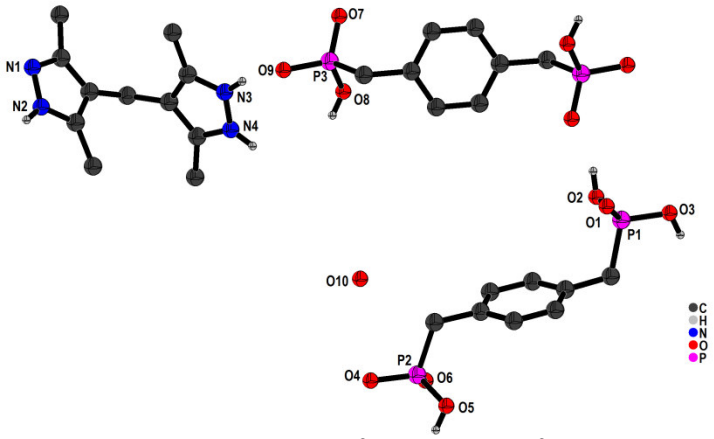

Fig. 2.62: Crystal structure of $[H_3DPA^{-}.(H_2DPA^{2-})_{0.5}.H_2MBPz^{2+}.(H_2O)_{0.4}]$ (**2k**). (C–H bonds are not shown for clarity)

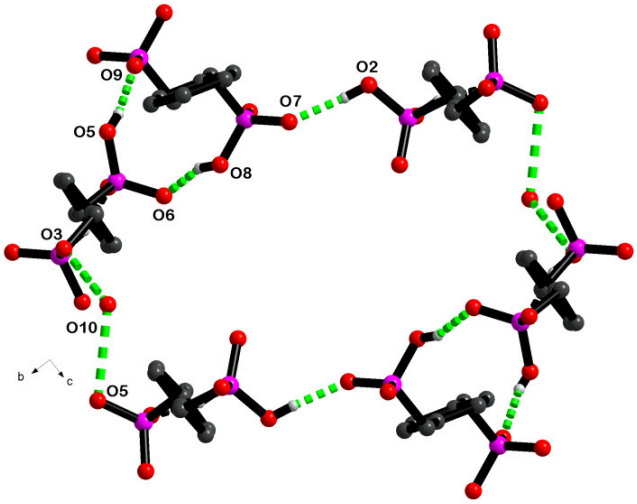

Fig. 2.63: Illustration of top view of hydrogen bonded supramolecular pouch as a building unit in **2k**

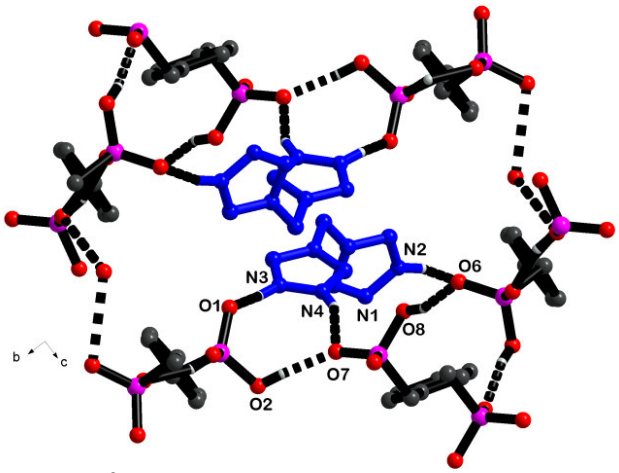

Fig. 2.64: Inclusion of H_2MBPz^{2+} (in blue) inside the tunnel along *a*-axis (Hydrogen atoms and methyl groups present on MBPz are not shown for clarity) in **2k**

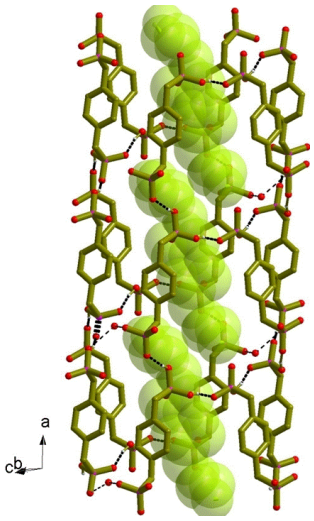

Fig. 2.65: Space-fill representation of H_2MBPz^{2+} in the hydrogen bonded supramolecular tunnel of DPA along *a*-axis in **2k**

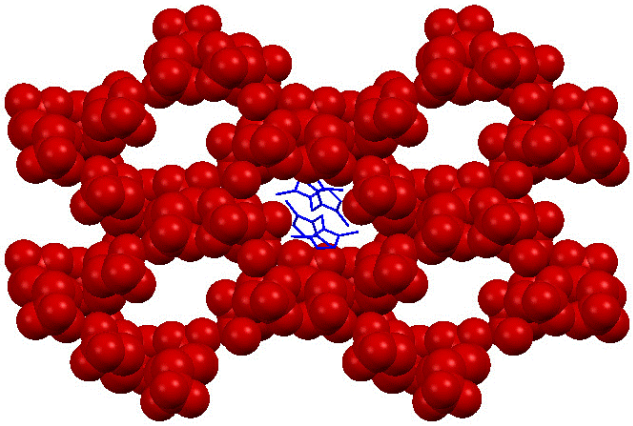

Fig. 2.66: 3D supramolecular hydrogen bonded network illustrating the host formed by DPA and water molecules, H_2MBPz^{2+} (in blue) as guest along *a*-axis in **2k**

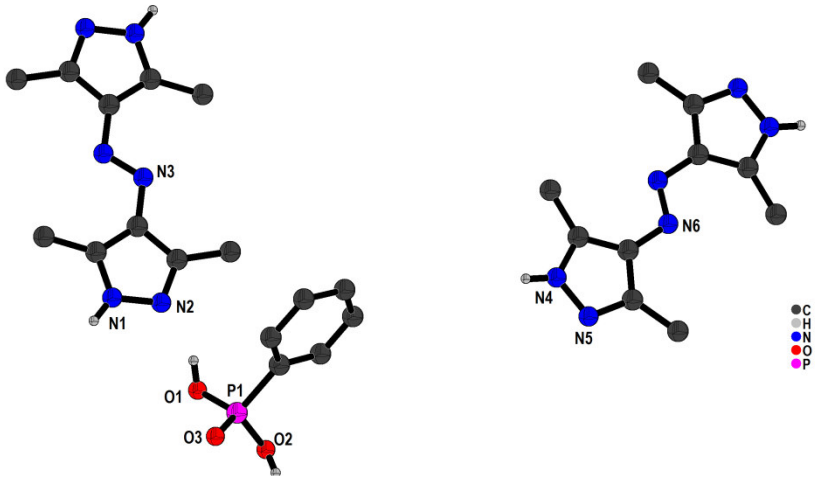

Fig. 2.67: Crystal structure of [H_2PPA.BPaz] (**2l**). (C–H bonds are not shown for clarity)

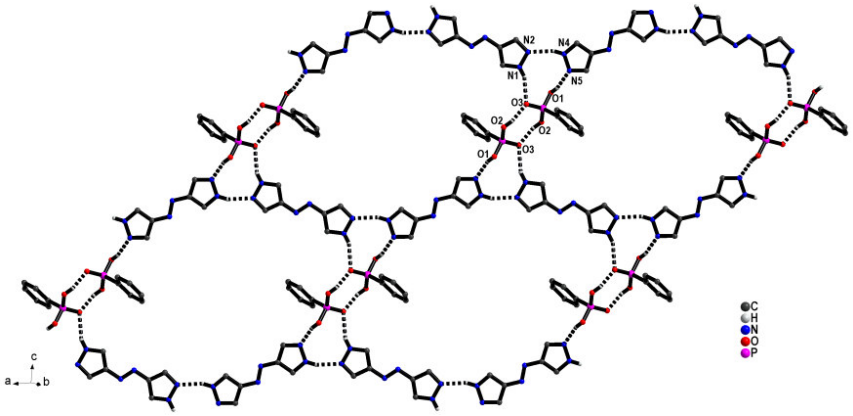

Fig. 2.68: Illustration of 2D supramolecular network formed via heterotrimer and homodimer in **2l**. (Hydrogen atoms and methyl groups present on MBPz are not shown for clarity)

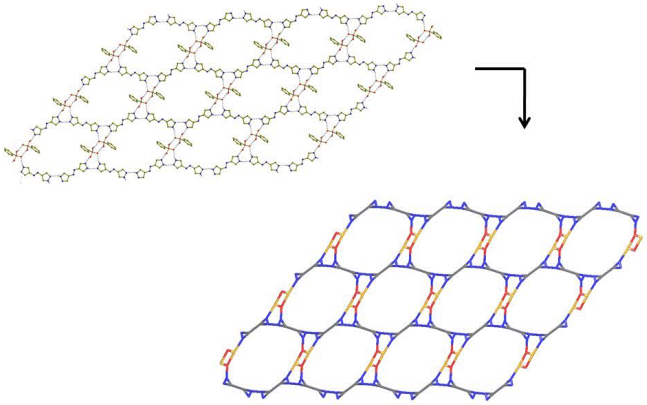

Fig. 2.69: Simplified representation of 2D sheet in **2l**

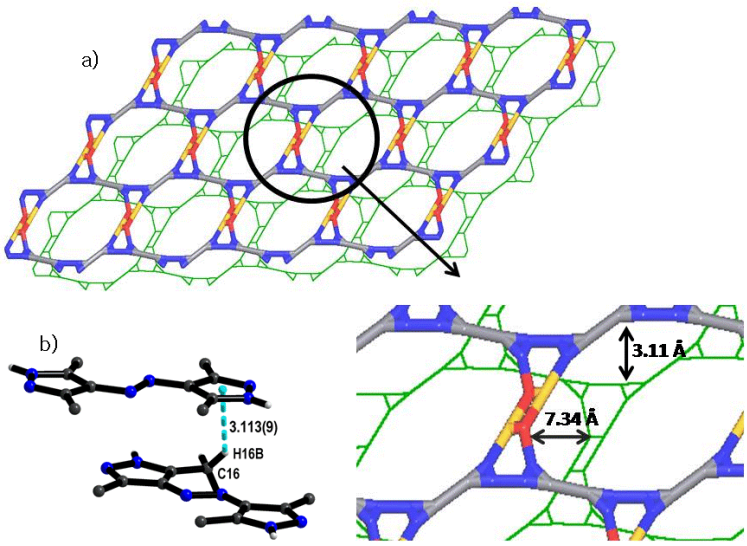

Fig. 2.70: (a) Stacking of two parallel simplified sheets showing offset distance of 7.34 Å along *b*-axis and (b) C–H···π interaction between C–H(CH_3) of one BPaz and π electron of another BPaz molecule in **2l**

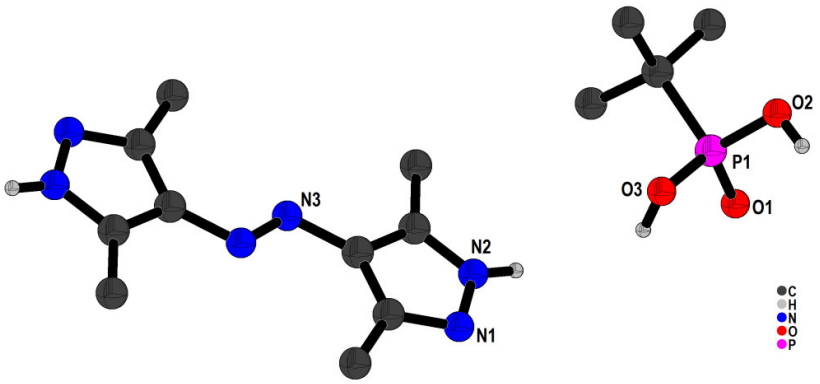

Fig. 2.71: Crystal structure of [(H_2tBPA)$_2$.BPaz] (**2m**). (C–H bonds are not shown for clarity)

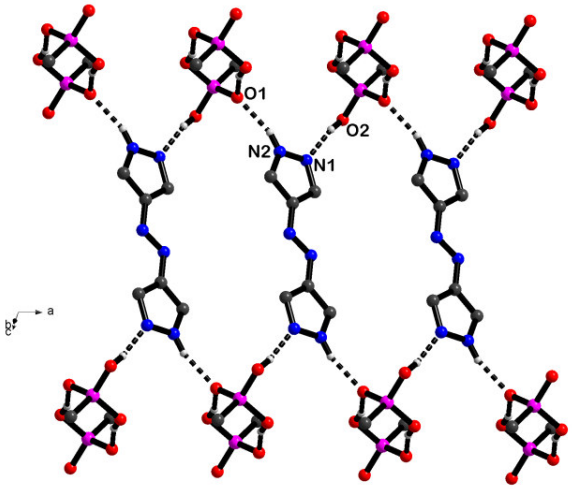

Fig. 2.72: Illustration of 2D sheet in *ac*-plane formed by bridging homodimer with BPaz in **2m**. (Hydrogen atoms and methyl groups present on MBPz are not shown for clarity)

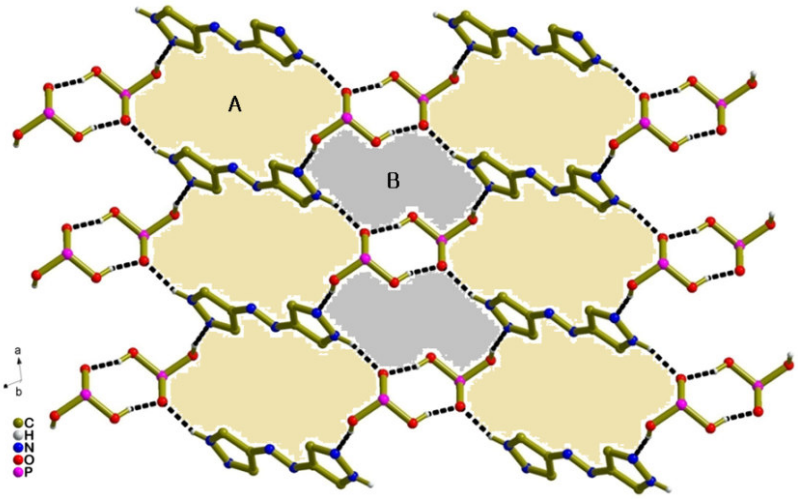

Fig. 2.73: Illustration of two types of oval shaped cavities A and B in **2m**

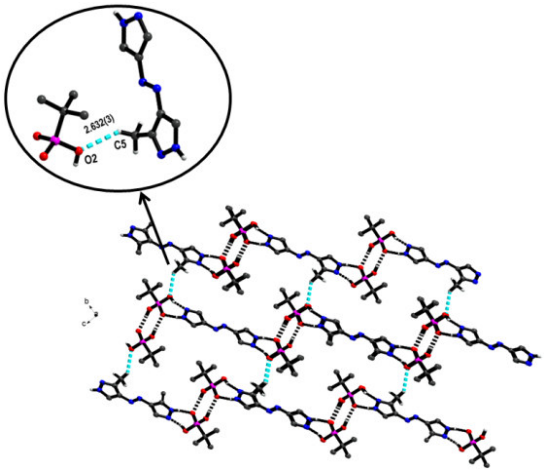

Fig. 2.74: Extended 3D supramolecular framework along *bc*-plane involving the C–H···π interaction between two neighboring sheets in **2m**

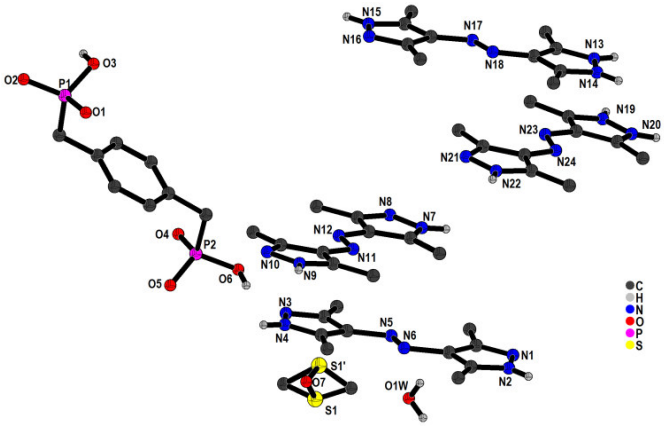

Fig. 2.75: Crystal structure of $[H_2DPA^{2-}.(HBPaz^{+})_2.(BPaz)_2.DMSO.H_2O]$ (**2n**). (C–H bonds are not shown for clarity)

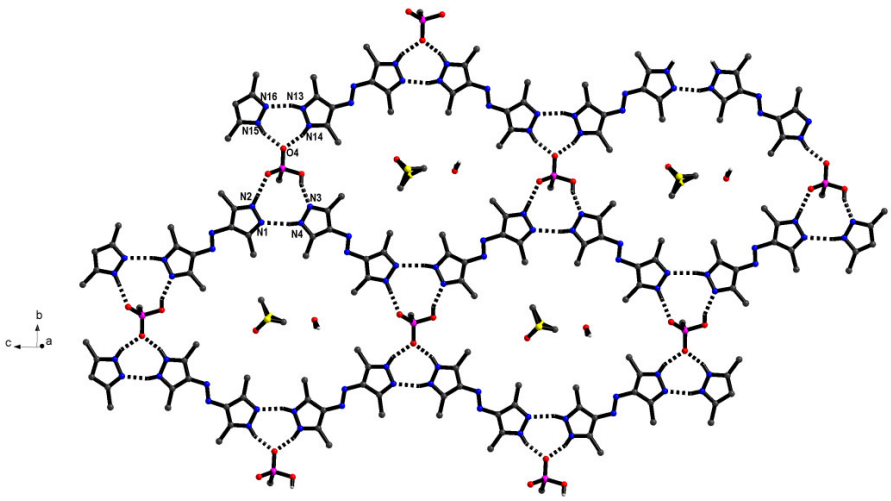

Fig. 2.76: Representation of 2D supramolecular sheet A with DMSO and water molecule residing in the cavity in **2n**

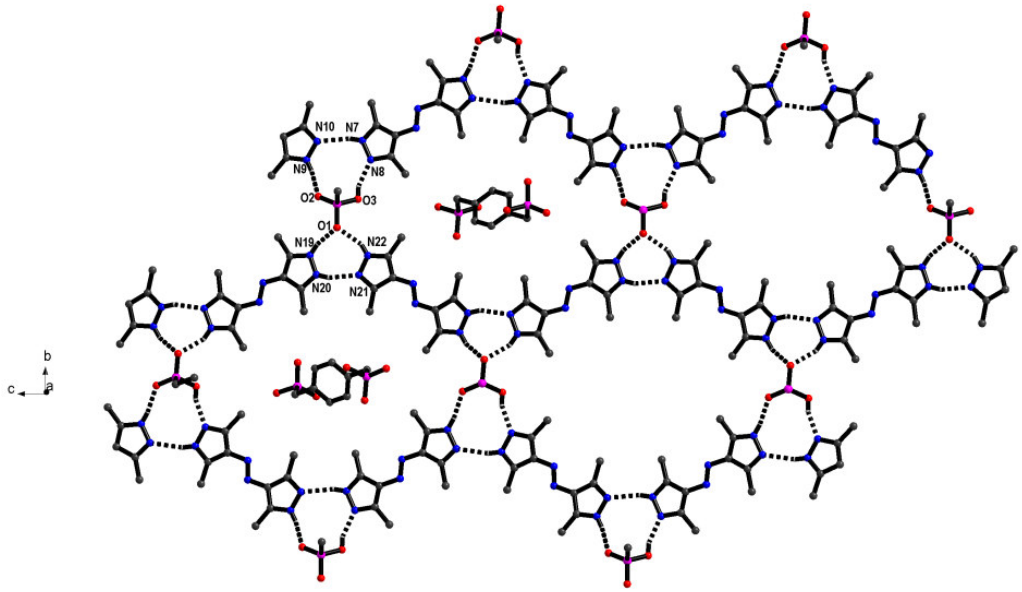

Fig. 2.77: Representation of 2D supramolecular sheet B with passage of diphosphonic molecule into the cavity in **2n**

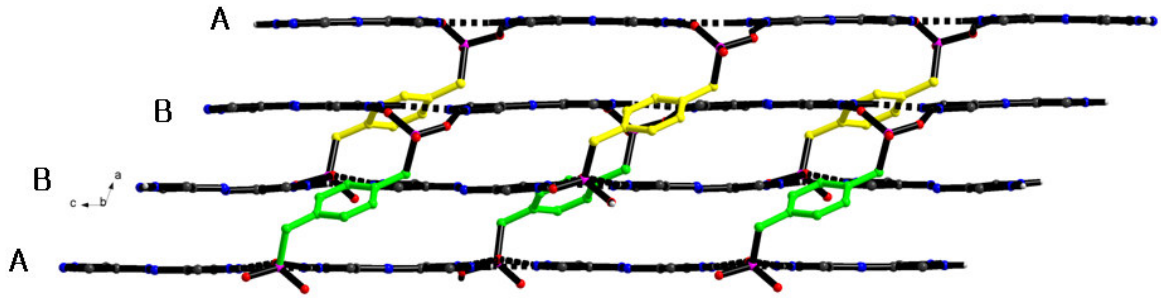

Fig. 2.78: Illustration of a pack of four sheets in ABBA way of pattern in **2n**

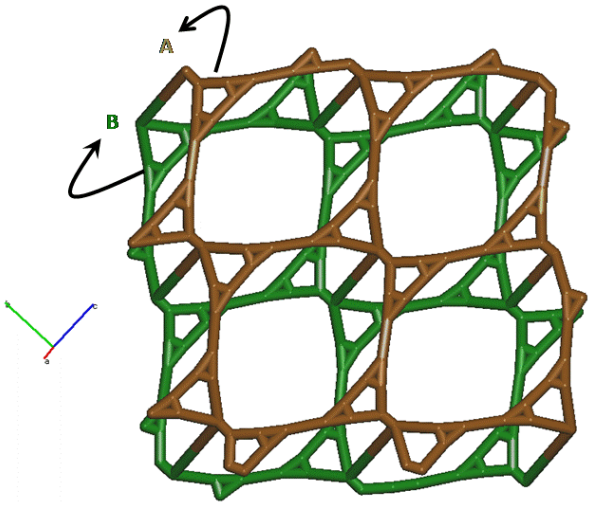

Fig. 2.79: Simplified view of 2D sheets A (brown colored) and B (green colored) linked together by diphosphonic acid in **2n**

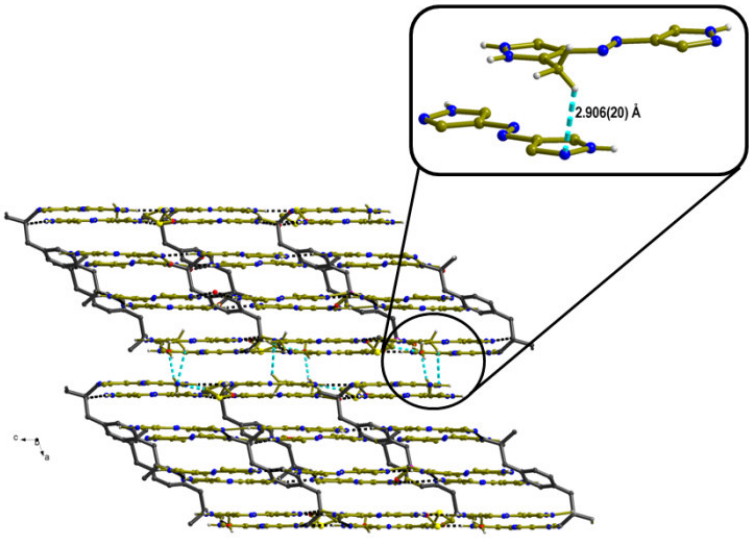

Fig. 2.80: 3D supramolecular framework extended by C–H(CH_3) and π electrons of BPaz in **2n**

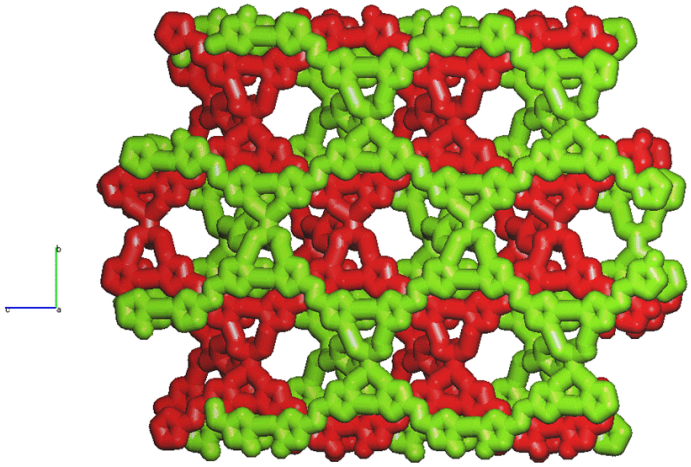

Fig. 2.81: Space-filled representation of two fold interpenetrated supramolecular network differentiated by red and green color in **2n**

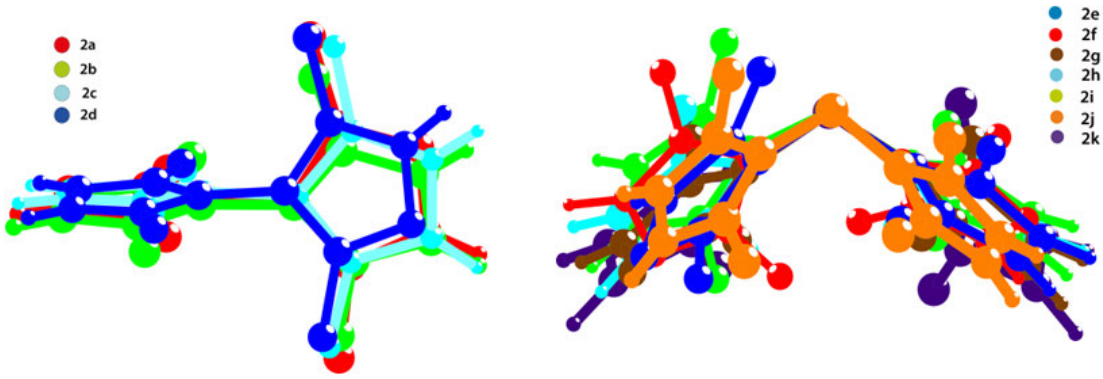

Fig. 2.82: Conformations of BPz and MBPz in salts **2a**-**2d** and **2e**-**2k**, respectively

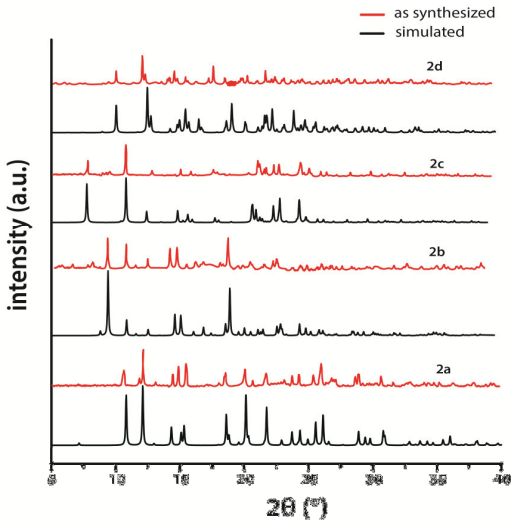

Fig. 2.83: PXRD pattern of salts **2a**-**2d**

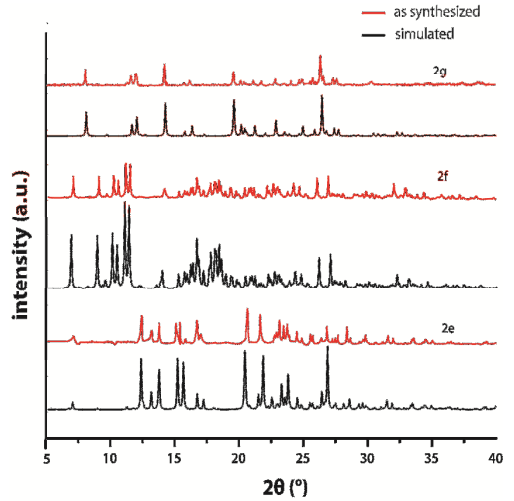

Fig. 2.84: PXRD pattern of salts **2e**-**2g**

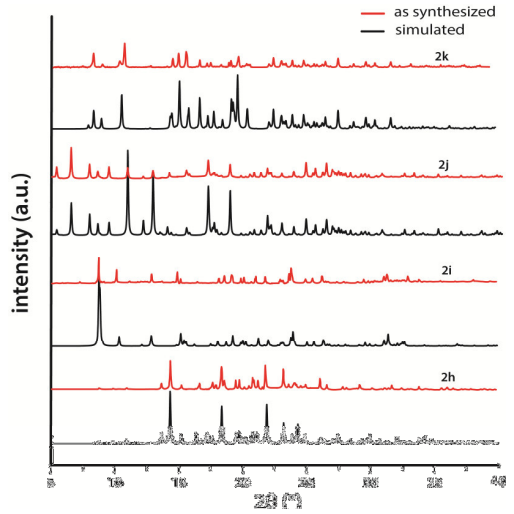

Fig. 2.85: PXRD pattern of salts **2h**-**2k**

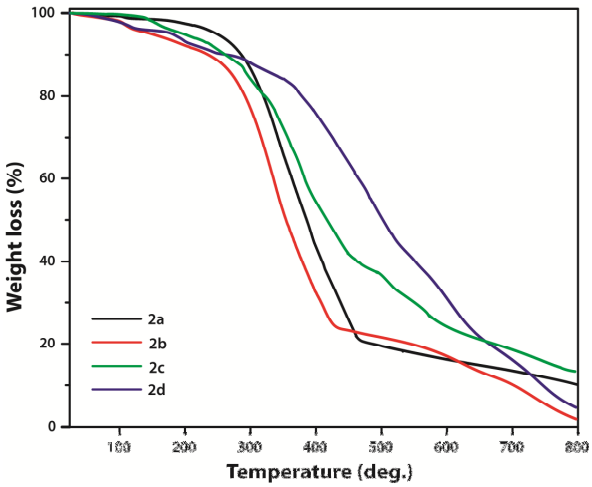

Fig. 2.86: Thermogravimetric curves for salts **2a**-**2d**

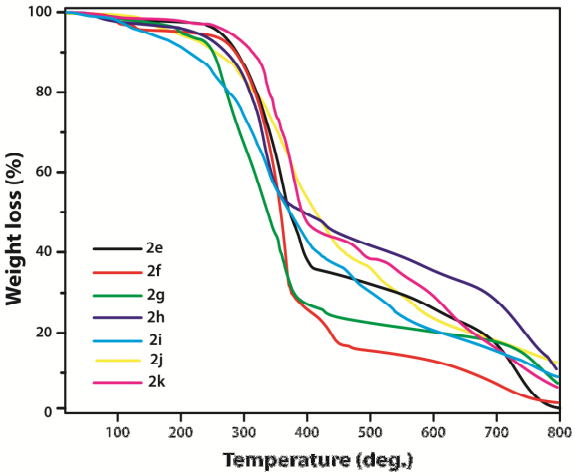

Fig. 2.87: Thermogravimetric curves for salts **2e**-**2k**

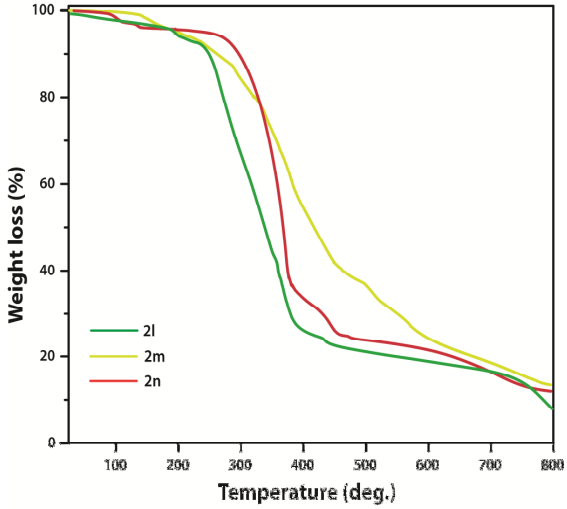

Fig. 2.88: Thermogravimetric curves for co-crystal/salt **2l**-**2n**

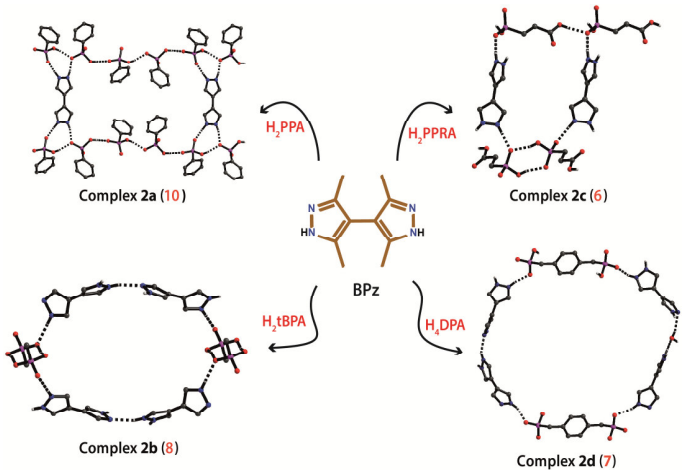

Scheme 2.6: Illustration of structural unit (hydrogen bonded ring) formed in salts **2a**-**2d**. Note: the number in bracket represents the number of molecules involved in the ring

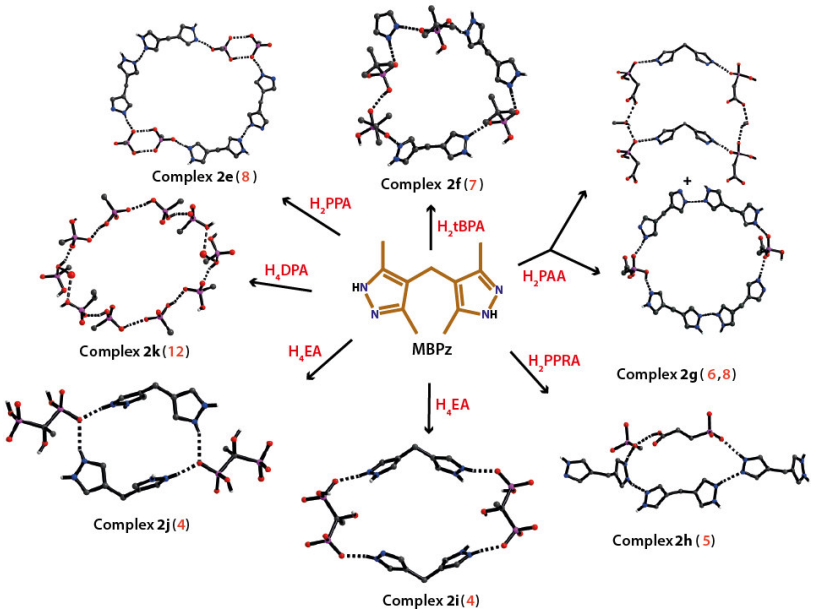

Scheme 2.7: Illustration of structural unit (hydrogen bonded ring) formed in salts **2e**-**2k**

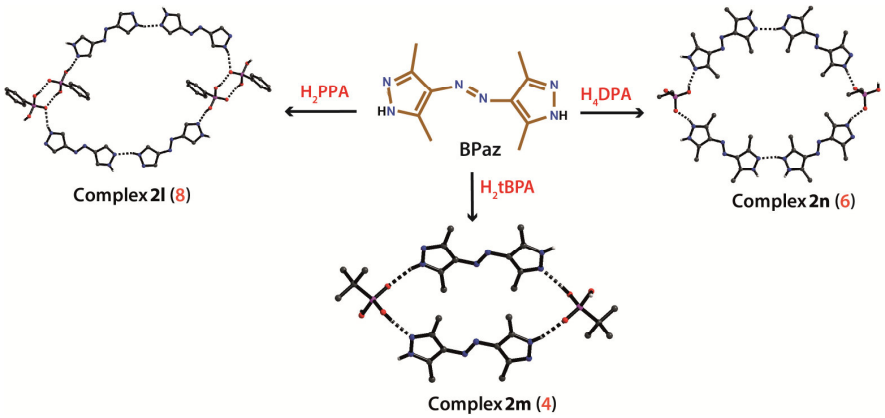

Scheme 2.8: Illustration of structural unit (hydrogen bonded ring) formed in salts **2l**-**2n**

Table 2.16: Trend of hydrogen bond interaction energy in salts 2a-2d (Kcal/mol)

Sl No.	Salt	Hydrogen bond interaction energy (Kcal/mol)
1.	$[(HPPA^-)_2.H_2BPz^{2+}]$ (**2a**)	-21.23
2.	$[HtBPA^-.HBPz^+]$ (**2b**)	-22.22
3.	$[(HPPRA^-)_2.H_2BPz^{2+}.(MeOH)_2.H_2O]$ (**2c**)	-21.08
4.	$[H_2DPA^{2-}.(HBPz^+)_2.H_2O]$ (**2d**)	-24.63

Table 2.17: Trend of hydrogen bond interaction energy in salts 2e-2k (Kcal/mol)

Sl No.	Salt	Hydrogen bond interaction energy (Kcal/mol)
1.	$[HPPA^-.H_2PPA.HMBPz^+.MBPz]$ (**2e**)	-21.96
2.	$[(HtBPA^-)_2.H_2MBPz^{2+}.EtOH]$ (**2f**)	-22.59
3.	$[HPAA^-.HMBPz^+.MBPz.MeOH]$ (**2g**)	-21.34
4.	$[HPPRA^-.HMBPz^+]$ (**2h**)	-21.96
5.	$[H_2EA^{2-}.H_2MBPz^{2+}.S]$ **(2i)**	-20.08
6.	$[H_3DPA^-.(H_2DPA^{2-})_{0.5}.H_2MBPz^{2+}.(H_2O)_{0.4}]$ (**2k**)	-27.80

Table 2.18: Trend of hydrogen bond interaction energy in salts 2l-2n (Kcal/mol)

Sl No.	Salt	Hydrogen bond interaction energy (Kcal/mol)
1.	$[H_2PPA.BPaz]$ (**2l**)	-22.45
2.	$[(H_2tBPA)_2.BPaz]$ (**2m**)	-22.62
3.	$[H_2DPA^{2-}.(HBPaz^{+})_2.(BPaz)_2.DMSO.H_2O]$ (**2n**)	-28.23

Table 2.19: Trend of hydrogen bond interaction energy in synthons (Kcal/mol)

Synthon	Description, $R_d^a(n)$	Hydrogen bond interaction energy (Kcal/mol)
I	Dimer of phosphonic acid, $R_2^2(8)$	-27.17
II	Two pyrazoles and one phosphonic group, $R_3^2(8)$	-30.67
III	Two phosphonic groups and one pyrazole, $R_3^2(9)$	-40.79
IV	Two pyrazoles and one phosphonic group, $R_3^3(10)$	-36.41
VI	Two pyrazoles and two phosphonic groups, $R_4^4(14)$	-45.68

Table 2.20: Trend of Torsion angle in MBPz in salts 2e-2k (º)

Salt	Torsion angle in MBPz (º)
Salt **2e**	76.88(0.38)
Salt **2f**	63.02(0.49)/120.69(0.42)
Salt **2g**	74.19(0.37)
Salt **2h**	69.92(0.30)
Salt **2i**	77.93(0.83)
Salt **2j**	119.31(0.43)
Salt **2k**	60.11(0.49)

Table 2.21: Summary of molecular complexes 2a-2n

Salts	Hydrogen bonded ring size	Synthons present	Framework
2a	10	III	Interpenetrated
2b	8	I, IV	Layered structure
2c	6	I, VI	Host-guest framework
2d	7	I, IV	Interpenetrated
2e	8	I, IV	Layered structure
2f	7	III, V	Layered structure
2g	8 and 6	II, IV	Interpenetrated
2h	5	I	3D H-bonded supramolecular network
2i	4	III	2D H-bonded porous framework

2j	6	I	Layered structure
2k	12	III, VI	Host-guest framework
2l	8	I, IV	Layered structure
2m	4	I	Layered structure
2n	6	IV	Interpenetrated

References:

1. Desiraju, G. R., "Supramolecular synthons in crystal engineering - A new organic synthesis", *Angew. Chem., Int. Ed.*, **34**, 2311 (1995).
2. Braga, D., Brammer, L. and Champness, N. R., "New trends in crystal engineering", *CrystEngComm*, **7**, 1 (2005).
3. Reddy, D. S., Craig, D. C. and Desiraju, G. R., "Supramolecular synthons in crystal engineering .4. Structure simplification and synthon interchangeability in some organic diamondoid solids", *J. Am. Chem. Soc.*, **118**, 4090 (1996).
4. Pigge, F. C., "Losing control? 'Design' of crystalline organic and metal-organic networks using conformationally flexible building blocks", *CrystEngComm*, **13**, 1733 (2011).
5. Du, M., Zhang, Z.-H., Wang, X.-G., Wu, H.-F. and Wang, Q., "Flexible building blocks of N,N'-Bis(picolinoyl)hydrazine for hydrogen-bonding directed co-crystallization: Structural diversity, concomitant polymorphs, and synthon prediction", *Cryst. Growth Des.*, **6**, 1867 (2006).
6. Aakeröy, C. B., Beatty, A. M. and Zou, M., "Building organic assemblies with 2-pyridone and dicarboxylic acids: Relating molecular conformation and synthon stability to crystal structure", *Cryst. Eng*., **1**, 225 (1998).
7. Aakeröy, C. B., Beatty, A. M. and Lorimer, K., "Syntheses and crystal structures of (*N*-pyridylmethylene)aminobenzamides: New building blocks for binary and ternary co-crystals", *Mol. Cryst. Liq. Cryst*., **456**, 163 (2006).
8. Bandgar, B. P., Gawande, S. S., Bodade, R. G., Gawande, N. M. and Khobragade, C. N., "Synthesis and biological evaluation of a novel series of pyrazole chalcones as anti-inflammatory, antioxidant and antimicrobial agents", *Bioorg. Med. Chem*., **17**, 8168 (2009).
9. Keter F. K. and Darkwa, J., "Perspective: The potential of pyrazole-based compounds in medicine", *Biometals*, **25**, 9 (2012).
10. Foces-Foces, C., Echevarría, A., Jagerovic, N., Alkorta, I., Elguero, J., Langer, U., Klein, O., Minguet-Bonvehí, M. and Limbach, H.-H., "A solid-state NMR, X-ray diffraction, and ab initio computational study of hydrogen-bond structure and dynamics of pyrazole-4-carboxylic acid chains", *J. Am. Chem. Soc*., **123**, 7898 (2001).

11. Gong, H. and Krische, M. J., "Hydrogen-bond-mediated self-assembly of aminopyrazolones: Macrocyclic quartets—Single and stacked one-dimensional motifs", *Angew. Chem., Int. Ed*., **44**, 7069 (2005).
12. Rusanov, E. B., Ponomarova, V. V., Komarchuk, V. V., Evans, H. S., Ibanez, E. F., Stoeckli, F., Sieler J. and Domasevitch, K. V., "A topology paradigm for metal-organic zeolites", *Angew. Chem., Int. Ed*., **42**, 2499 (2003).
13. Reddy, L. S., Babu, N. S. and Nangia, A., "Carboxamide–pyridine *N*-oxide heterosynthon for crystal engineering and pharmaceutical co-crystals", *Chem. Commun.*, 1369 (2006).
14. Allen, F. H., Lommerse, J. P. M., Hoy, V. J., Howard, J. A. K. and Desiraju, G. R., "Halogen···O(nitro) supramolecular synthon in crystal engineering: A combined crystallographic database", *Acta Cryst*., **B53**, 1006 (1997).
15. Sander, J. R. G., Bučar, D.-K., Henry, R. F., Giangiorgi, B. N., Zhang, G. G. Z. and MacGillivray, L. R., "'Masked synthons' in crystal engineering: Insulated components in acetaminophen co-crystal hydrates", *CrystEngComm*, **15**, 4816 (2013).
16. Paisner, K., Zakharov, L. N. and Doxsee, K. M., "A robust thiourea synthon for crystal engineering", *Cryst. Growth Des*., **10**, 3757 (2010).
17. Rajput, L. and Biradha, K., "Design of co-crystals via new and robust supramolecular synthon between carboxylic acid and secondary amide: Honeycomb network with jailed aromatics", *Cryst. Growth Des*., **9**, 40 (2009).
18. Rajput, L., Jana, N. and Biradha, K., "Carboxylic acid and phenolic hydroxyl interactions in the crystal structures of co-crystals/clathrates of trimesic acid and pyromellitic acid with phenolic derivatives", *Cryst. Growth Des*., **10**, 4565 (2010).
19. Wang, W.-H., Xi, P.-H., Su, X.-Y., Lan, J.-B., Mao, Z.-H., You, J.-S. and Xie, R.-G., "Supramolecular assemblies of multifunctional diimidazole and dicarboxylic acids via various hydrogen bonds and X···π (X = π, CH) interactions", *Cryst. Growth Des*., **7**, 741 (2007).
20. Braga, D., Maini, L., Polito, M., Rossini, M. and Grepioni, F., "Tunable supramolecular synthons and versatile, water-soluble building blocks for crystal engineering: $[(\eta^5\text{-}C_5H_4COOH)_2Co^{III}]^+$ and its zwitterionic form $[(\eta^5\text{-}C_5H_4COOH)(\eta^5\text{-}C_5H_4COO)Co^{III}]$", *Chem. Eur. J*., **6**, 4227 (2000).

21. Mahmoudkhani, A. H. and Langer, V., "Structural correlations in methylphosphonate and phosphite salts: Crystal structures of anilinium and ethylenediammonium methylphosphonates", *J. Mol. Struct*., **609**, 55 (2002).
22. Mahmoudkhani, A. H. and Langer, V., "Supramolecular isomerism and isomorphism in the structures of 1,4-butanebisphosphonic acid and its organic ammonium salts", *Cryst. Growth Des*., **2**, 21 (2002).
23. Bruckmann, J., Kruger, C., Lehmann, C. W., Leitner, W., Rust, J. and Six, C., "Ethylenebis(phosphonic acid)", *Acta Crystallogr., Sect. C: Cryst. Struct. Commun*., **C55**, 695 (1999).
24. Bowes, K. F., Ferguson, G., Lough, A. J., Zakaria, C. M. and Glidewell, C., "Phosphonoacetic acid as a building block in supramolecular chemistry: Salts with organic polyamines", *Acta Crystallogr, Sect. B: Struct. Sci*., **B59**, 87 (2003).
25. Bowes, K. F., Ferguson, G., Lough, A. J. and Glidewell, C., "4,4'-Trimethylenedipyridinium bis[carboxymethylphosphonate(1-)]: A three-dimensional framework structure built from O–H···O, N–H···O and C–H···O hydrogen bonds", *Acta Crystallogr., Sect. C: Cryst. Struct. Commun*., **C59**, 464 (2003).
26. Farrell, D. M. M., Ferguson, G., Lough, A. J. and Glidewell, C., "N,N'-Dimethylpiperazinium(2+) phosphonoacetate: Hydrogen-bonded anion sheets containing cation-templated R-6(6) (28) rings", *Acta Crystallogr., Sect. C: Cryst. Struct. Commun*., **C57**, 952 (2001).
27. Singh, U. P., Kashyap, S., Butcher, R. J., Singh, H. J. and Mishra, B. K., "Effect of electron donating substituents on supramolecular structure of salts having phenylphosphonic acid and pyrazoles", *Struct. Chem*., **22**, 931 (2011).
28. Plabst, M., Stock, N. and Bein, T., "Hydrogen-bonded networks of ammonium bis- and tetrakisphosphonates—Synthesis, high-throughput screening and structural trends", *Cryst. Growth Des*., **9**, 5049 (2009).
29. López, C., Claramunt, R. M., García, M. A., Pinilla, E., Torres, M. R., Alkorta, I. and Elguero, J., "Co-crystals of 3,5-dimethyl-1*H*-pyrazole and salicylic acid: Controlled formation of trimers via O–H···N hydrogen bonds", *Cryst. Growth Des*., **7**, 1176 (2007).

30. Basu, T., Sparkes, H. A. and Mondal, R., "Construction of extended molecular networks with heterosynthons in co-crystals of pyrazole and acids", *Cryst. Growth Des*., **9**, 5164 (2009).
31. Bureiko, S. F., Golubev, N. S., Denisov, G. S., Kucherov, S. Y. and Tolstoi, P. M., "3,5-Dimethylpyrazole complexes with strong carboxylic acids", *Russ. J. Gen. Chem*., **75**, 1821 (2005).
32. Ugono, O., Rath, N. P. and Beatty, A. M., "Exceptions to the rule: New hydrogen-bonded networks from an old reliable", *CrystEngComm*, **13**, 753 (2011).
33. Singh, U. P., Kashyap, S., Singh, H. J. and Butcher, R. J., "Anion directed supramolecular architecture of pyrazole based ionic salts", *CrystEngComm*, **13**, 4110 (2011).
34. Han, L. L., Li, Z.-H., Chen, J.-S., Wang, X. and Sun, D., "Solution and mechanochemical syntheses of two novel co-crystals: Ligand length modulated interpenetration of hydrogen-bonded 2D 6^3-hcb networks based on a robust trimeric heterosynthon", *Cryst. Growth Des*., **14**, 1221 (2014).
35. Mahmoudkhani, A. H. and Langer, V., "Phenyl phosphonic acid as a building block for two-dimensional hydrogen bonded supramolecular arrays", *J. Mol. Str*., **609**, 97 (2002).
36. Mahmoudkhani, A. H. and Langer, V., "Self-assemblies of extended hydrogen-bonded arrays using 1,4-butanebisphosphonic acid as a versatile building block", *Phosphorus, Sulfur Silicon Relat. Elem*., **177**, 2941 (2002).
37. Beckmann, J., Rüttinger, R. and Schwich, T., "1,3,5-Benzene-tri-*p*-phenylphosphonic acid. A new building block in supramolecular chemistry", *Cryst. Growth Des*., **8**, 3271 (2008).
38. Hix, G. B., Caignaert, V., Rueff, J.-M., Pluart, L. L., Warren, J. E. and Jaffrés, P.-A., "A supramolecular ladder like structure formed by the auto assembly of benzene-1,3,5-triphosphonic acid", *Cryst. Growth Des*., **7**, 208 (2007).
39. Vosko, S. H., Wilk, L. and Nusair, M., "Accurate spin-dependent electron liquid correlation energies for local spin density calculations: A critical analysis", *Can. J. Phys*., **58**, 1200 (1980).
40. Lee, C., Yang, W. and Parr, R. G., "Development of the Colle-Salvetti correlation-energy formula into a functional of the electron density", *Phys. Rev. B*, **37**, 785 (1988).

41. Stephens, P. J., Devlin, F. J., Chabalowski, C. F. and Frisch, M. J., "Ab initio calculation of vibrational absorption and circular dichroism spectra using density functional force fields", *J. Phys. Chem.*, **98**, 11623 (1994).
42. The simplified network was generated by the program "TOPOS-4.0", see http://www.topos.ssu.samara.ru. Blatov, V. A., *IUCr CompComm Newsletter*, **7**, 4 (2006).
43. Spek, A. L., PLATON99, A Multipurpose Crystallographic Tool; Utrecht University: Utrecht, The Netherlands (1999).
44. Flack, H. D., "On enantiomorph-polarity estimation", *Acta Cryst.*, **A39**, 876 (1983).
45. Bruker, 2010. *APEX2*, *SAINT*, *SADABS* and *XSHELL*. *Bruker AXS Inc.*, Madison, Wisconsin, USA.
46. Desiraju, G. R., "On the presence of multiple molecules in the crystal asymmetric unit (*Z'* > 1)", *CrystEngComm*, **9**, 91 (2007).
47. Anderson, K. M., Probert, M. R., Goeta, A. E. and Steed, J. W., "Size does matter—The contribution of molecular volume, shape and flexibility to the formation of co-crystals and structures with Z' > 1", *CrystEngComm*, **13**, 83 (2011).
48. Sun, Z., Liu, X., Wang, X., Li, L., Shi, X., Li, S., Ji, C., Luo, J. and Hong, M., "Engineering of acentric stilbazolium salts with large second-order optical nonlinearity and enhanced environmental stability", *Cryst. Growth Des.*, **12**, 6181 (2012).
49. *Gemini, v1.02, Autoindexing program for twinned crystals*, Bruker AXS, Inc., Madison, WI, 2000.
50. Baboul, A. G., Curtiss, L. A., Redfern, P. C. and Raghavachari, K., "Gaussian-3 theory using density functional geometries and zero-point energies", *J. Chem. Phys.*, **110**, 7650 (1999).
51. Kim, K. S., Tarakeshwar, P. and Lee, J. Y., "Molecular clusters of pi-systems: Theoretical studies of structures, spectra, and origin of interaction energies", *Chem. Rev.*, **100**, 4145 (2000).
52. Ikkala, O. and Brinke, G., "Functional materials based on self-assembly of polymeric supramolecules", *Science*, **295**, 2407 (2002).

Chapter 3

Solvent Induced Solid State Structures of Pyrazole and a New Anthracene Based Phosphonic Acid

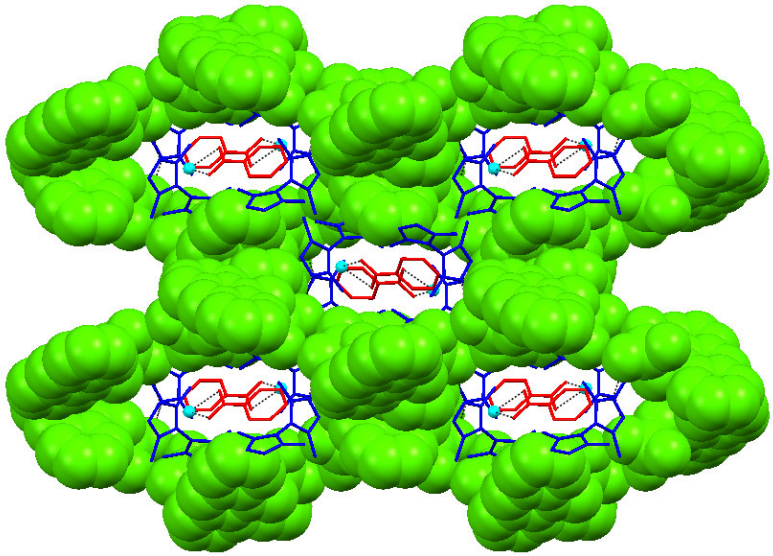

Solvated structure has received a great consideration attributable towards the diversity of interactions involved, resulting in the modified properties of the organic molecules in the solid state [1-2]. In fact, inclusion of guest molecules into the framework generally relies on their intermolecular interactions with the host assembly. Therefore, in order to amend the molecular arrangements of the molecules in the solid state, variety of crystalline forms has been assayed [3-5]. The various conventional hydrogen bonding such as O–H···O, N–H···O interactions etc., show their elementary significance in crystal engineering. However, the unconventional weak intermolecular interactions such as C–H···O, C–H···π, π···π also play an essential role in executing the crystal structure of particular conformation by influencing the interaction of guest molecules with the host [6-8]. Moreover, many reports in the last decade have exhibited that inclusion of solvent molecules materialize owing to the stabilization of lattice by intensifying the packing efficiency. Consequently, the host molecule has the ability to construct solvates with a number of solvent molecules leading to the formation of solid materials with numerous different properties [9-10].

The solvates are often isostructural but few show distinct structures due to change in conformation of the molecule caused by the solvent molecule. It generally depends upon the solvent molecule with distinct H–bonding moieties, which induces the intermolecular interactions with the host, thereafter; tune the alignment of the parent molecule in the host assembly. Therefore, researchers in last few decades have been attracted towards the field of pseudo-polymorphism (solvate formation), which provides the complete knowledge of the change in the conformation. Consequently, it resulted into the diversity of supramolecular framework with the inclusion of solvent molecule [11-13]. Considering the bispyrazole-phosphonic system, no report has been found to predict the effect of solvates on this system. Therefore, facilitating the comprehensive understanding of the effect of various solvent molecules on conformationally flexible bispyrazole and phosphonic system, various solvates of bispyrazole-phosphonic system were attempted successfully in this chapter. However, there are few reports on the solvates of pyrazole system in the literature [14-17], which have been discussed below including the solvates of other components.

Li et al. [14] reported a solvate of 3,4-dinitro-1H-pyrazole with benzene. Structural analysis revealed that the asymmetric unit was comprised of two independent dinitropyrazole

molecules and half a molecule of benzene (Fig. 3.1). They found that each pyrazole molecule is planar with the nitro groups rotated out of the plane.

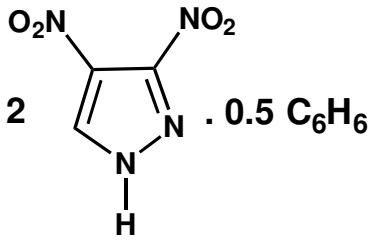

Fig. 3.1: Asymmetric unit in 3,4-dinitro-1H-pyrazole benzene 0.25-solvate

Elgemeie et al. [15] and Stumpf et al. [16] reported solvates of 5-amino-3-anilino-N-(chlorophenyl)-1H-pyrazole-4-carboxamide and 4-hydroxymethyl-3,5-dimethyl-1H-pyrazole respectively (Fig. 3.2). The former pyrazole analogue is solvated by an ethanol molecule and the authors found that the molecule is planar except the aniline group. They also observed that the solvate is stabilized by O–H···O and N–H···N interactions. However, the latter analogue is solvated with chloroform molecule and the solvate is stabilized through N–H···O, O–H···N and C–H···O hydrogen bonds.

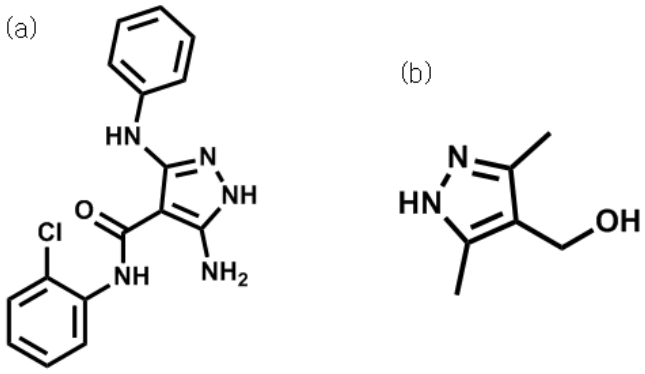

Fig. 3.2: Molecular structure of (a) 5-amino-3-anilino-N-(chlorophenyl)-1H-pyrazole-4-carboxamide and (b) 4-hydroxymethyl-3,5-dimethyl-1H-pyrazole

Boldog et al. [ref. [37] of chapter 1] reported isomorphous pseudopolymorphs of 3,3',5,5'-tetramethyl-4,4'-bipyrazolyl (4,4'-Me_4bpz) using solvents such as acetone, ethylacetate and THF along with its polymorphs. They found that the same 4,4'-Me_4bpz tecton is formed in isomorphous compounds with the tendency for helical self assembly as observed in its polymorph. They observed that the 3D structures of these isomorphous pseudopolymorphs can be clearly derived from the chiral (10,3)-c topology. Later, Boldog [ref. [38] of chapter 1] and his

co-workers reported the solvate of 4,4'-Me_4bpz with methanol and chloroform molecule. They concluded that with the incorporation of hydrogen bonded moieties, the trimeric synthon of 4,4'-Me_4bpz is expanded without changing the network connectivity.

Karpinska et al. [17] crystallized an anabolic steroid stanozolol (17β-hydroxy-17α-methylandrostano[3,2-c]pyrazole) in two polymorphs using sublimation method and they investigated that these polymorphs possess the voids with unused hydrogen bonding capacity. Moreover, they have also reported various solvates of stanozolol, which exhibited variety of hydrogen bonding networks formed by the maximal usage of hydrogen bonded moieties with no voids (Fig. 3.3).

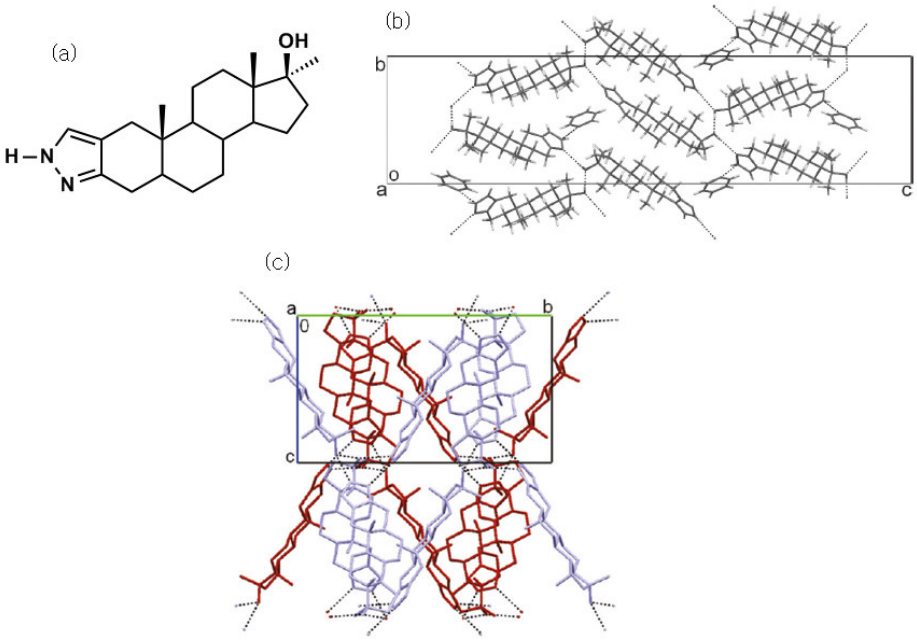

Fig. 3.3: (a) Chemical structure of stanozolol; (b) 3D hydrogen bonding network of stanozolol.solvate without any void and (c) representation of void formation in 3D hydrogen bonding network of one of its polymorph

Bingham et al. [18] reported hundred solvates of sulfadrug i.e., sulfathiazole (Fig. 3.4). After structural analysis, they found that its solvates showed more structural versatility than any other organic molecule.

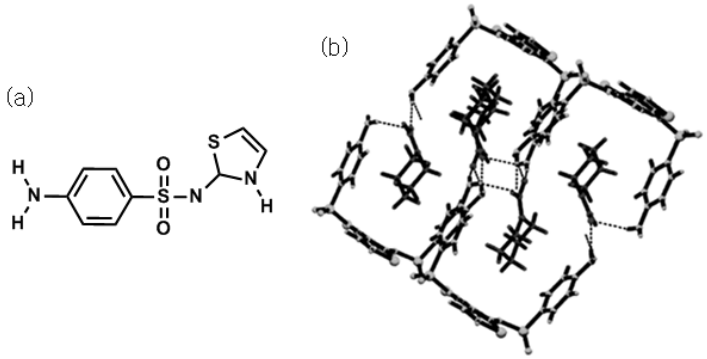

Fig. 3.4: (a) Chemical structure of sulfadrug, sulfathiazole and (b) the crystal structure of the 1:1 adduct sulfathiazole-*N*-formylpiperidinea–co-crystal

Tanaka et al. [19] reported a coordinatively saturated 2D net for solvates of two different hosts (9-(3,5-dihydroxy-1-phenyl)acridine) and (9-(3,5-dihydroxy-1-phenyl)-4-hydroxyacridine) differing in polar modification, with the addition of –OH group on the second host. They observed that both of the host moieties formed adducts with variety of polar and non-polar solvents. Though the cavities in both cases have been preserved but the latter showed the adduct formation with small polar guests due to the H-bonding formation with –OH group (Fig. 3.5). Hence, they concluded that (9-(3,5-dihydroxy-1-phenyl)-4-hydroxyacridine) acts as the polarity modifier of preserved cavities due to difference in substituents, therefore, various functional group might also be introduced as selectivity-controllers.

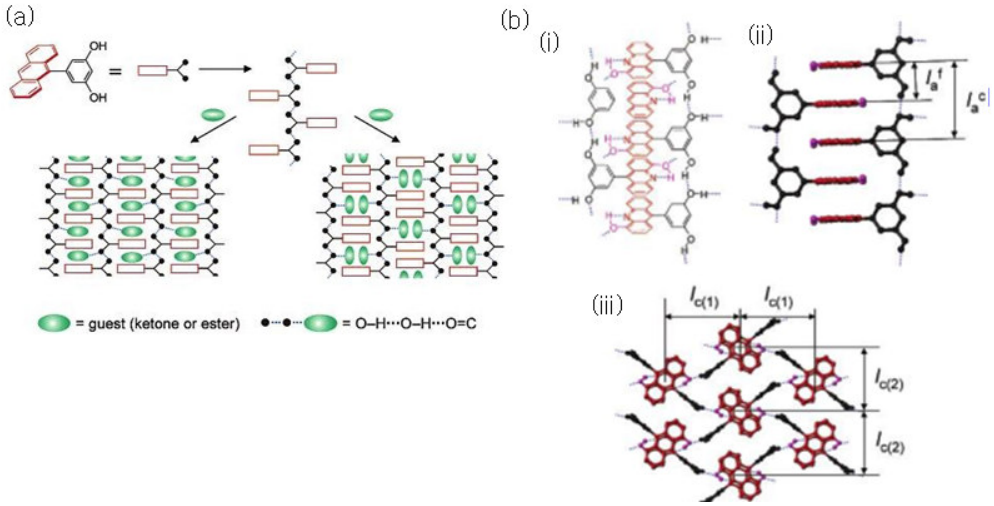

Fig. 3.5: 2D net in adducts (a) (9-(3,5-dihydroxy-1-phenyl)acridine).guest and (b) crystal structure of guest-free apohost (9-(3,5-dihydroxy-1-phenyl)-4-hydroxyacridine): side view of a stacked acridine column (i and ii) and top view of columns (iii)

Singh and Baruah [20] reported the importance of weak interactions of the solvent with the host molecules *viz*., 2-(3,4-dihydroxyphenethyl)isoindole-1,3-dione and 2,6-bis-[2-(3,4-dihydroxyphenyl)ethyl]pyrrolo[3,4-f]isoindole-1,3,5,7-tetraone in modifying the packing pattern (Fig. 3.6). They noticed that all weak interactions such as C–H···π, O–H···N caused by the solvent molecules with the host have led to the structural change. They have also studied the structural feature of the solvates by powder X-ray diffraction (PXRD), thermogravimetric analyses (TGA) and differential scanning calorimetric (DSC) measurements.

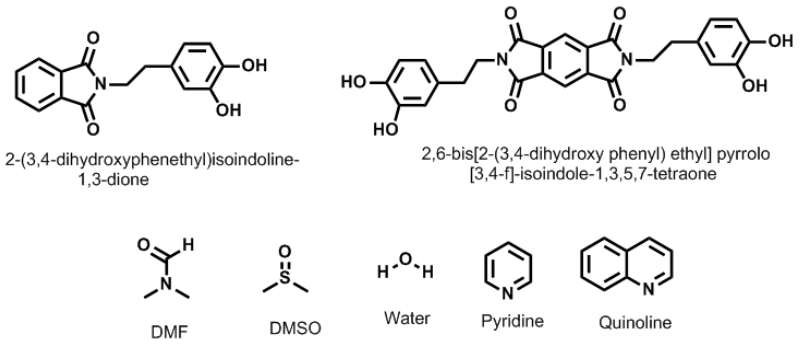

Fig. 3.6: Structure of cyclic imide derivatives and some solvent molecules used for preparation of their solvates

Mizobe et al. [21] reported the ternary system acquiring molecular arrangement of anthracene moieties in ammonium anthracene disulfonate and adducts such as dioxane, thioxane and benzene. On the basis of adducts chosen, they observed that the ternary system showed the modulation in solid-state emission. They have explained the transcribing of molecular information from adducts to the arrangement of the molecules, which was further

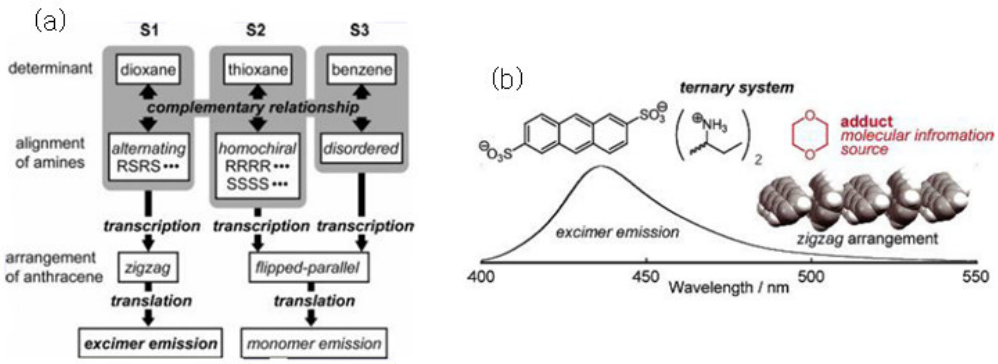

Fig. 3.7: (a) View of assembly processes of the components in ternary systems with dioxane, thioxane and benzene and (b) the solid-state emission spectral profile for dioxane

translated into the emission mode and correlated it with the central dogma (Fig. 3.7a). After analysis, they found that the ternary system with dioxane resulted in *zig-zag* arrangement which display emission maximum at 438 nm on solid-state emission spectral profile and led to the rare emission of anthracene excimer (Fig. 3.7b).

Nauha et al. [22] investigated the polymorphism and solvate formation of a fungicide i.e., thiophanate-ethyl and compared it with thiophanate-methyl. They observed that both of the fungicidal actives with same functional group resulted in variety of solvates and polymorphs but with the variation in hydrogen bond motifs and the conformation of the molecules (Fig. 3.8). Therefore, they demonstrated that these analogues with different packings provide the challenge in using supramolecular synthon approach. They have also endorsed the significance in searching methods to make use of packing effects and lipophilic interactions in crystal engineering.

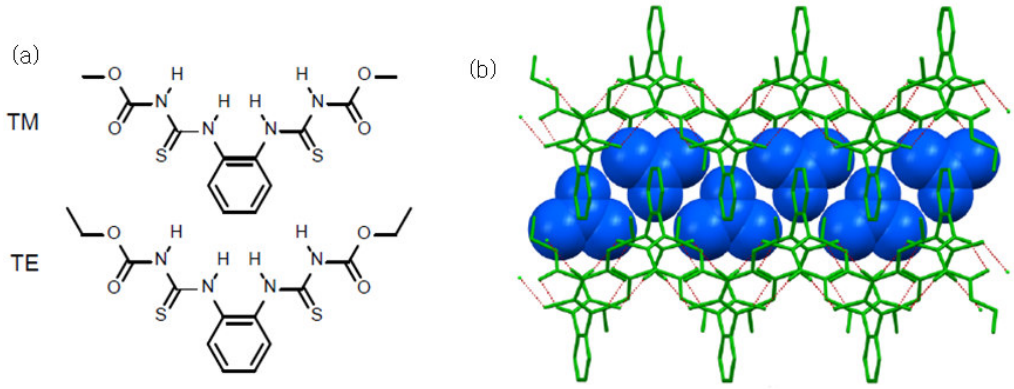

Fig. 3.8: (a) Molecular structures of thiophanate-methyl (TM) and thiophanate-ethyl (TE) and (b) hydrogen bonded chains of TE acetone solvate

Mondal and Howard [23] synthesized six different solvates of *trans*-1,4-bis(phenylethynyl)-cyclohexane-1,4-diol. On structural analysis, they reported the formation of 1:2 host-guest inclusion compound in presence of smaller guest molecules whereas with bigger guests it crystallized in 1:1 ratio. They observed that the strong hydrogen bond interactions such as O–H···O, N–H···O are the fundamental interactions for the formation of solid materials. Besides, weak interactions like C–H···O and C–H···π interactions also play an important role in stabilizing the network (Fig. 3.9). Apparently, they concluded that the particular type of upcoming guest remarkably influences the orientation of phenylethynyl group, which further directs the formation of C–H···O and C–H···π interactions.

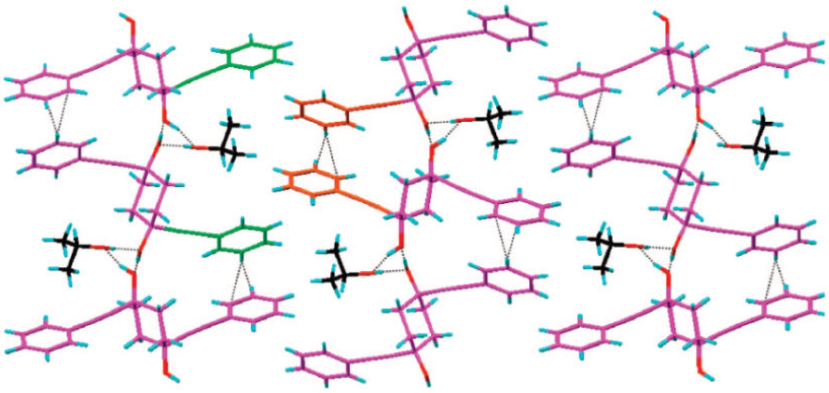

Fig. 3.9: Crystal packing of *trans*-1,4-bis(phenylethynyl)-cyclohexane-1,4-diol.isopropyl showing the interdigitation and orientation adopted by molecules in order to accommodate the solvent molecules

Feng et al. [24] synthesized a new pyrene analogue i.e., 1-acetyl-3-phenyl-5-(1-pyrenyl)-pyrazoline and reported its two polymorphs, two solvates with chloroform and acetic acid and, a co-crystal with phenol molecule (Fig. 3.10). They have discussed its stability and correlated their optical-physical properties. As a result, they observed that the different arrangement of fluorophores such as edge-to-face π–π stacking, monomer arrangement, and face-to-face π–π stacking was responsible for the tuning in optical physical properties as evident by single crystal X-ray analysis (Fig. 3.11).

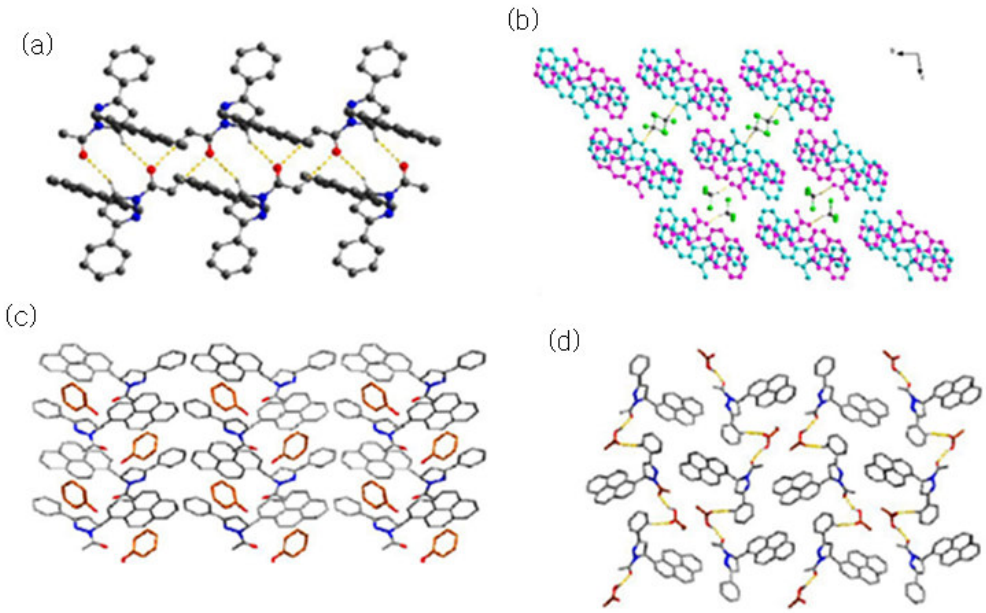

Fig. 3.10: Packing diagram of polymorph I (a); solvates, $CHCl_3$ (b); phenol (c) and acetic acid (d)

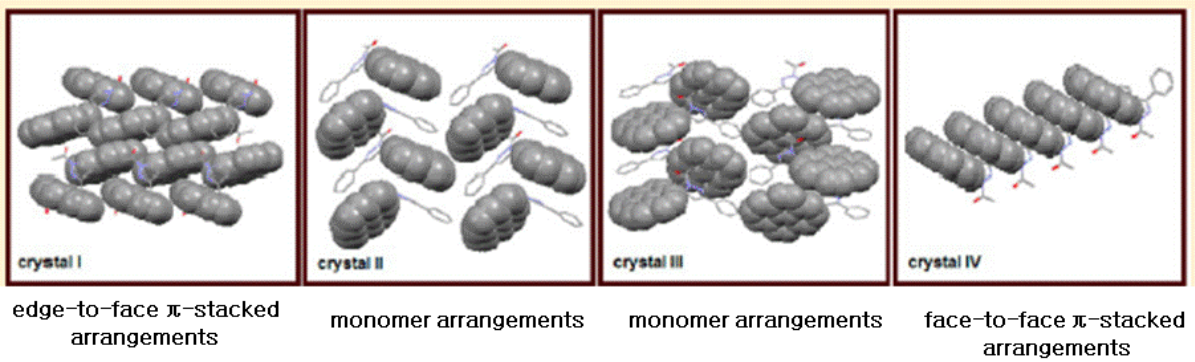

Fig. 3.11: Different arrangements of fluorophores in solvates and crystals

On analysis, they deduced that the system with π-stacking exhibits the larger red-shifted emissions. Therefore, they suggested that the strategy for fluorescence modulation on the grounds of solvates and co-crystals can also be applied to other fluorescent compounds.

Bhattacharya and Saha [25] reported the solvates of 2,4,6-triethyl-1,3,5-tris(phenoxymethyl)-benzene and exhibited three different forms on desolvation of some solvates (Fig. 3.12).

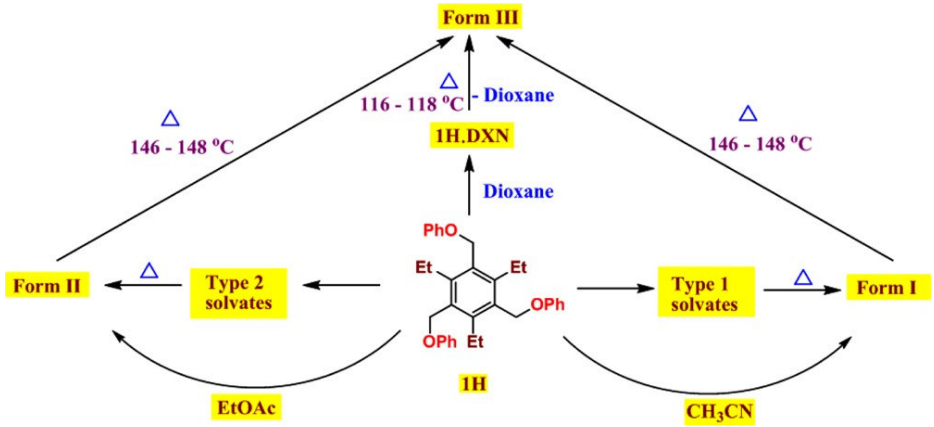

Fig. 3.12: Schematic representation of different forms of solvates observed on desolution

On structural analysis, they found that the host yielded two sets of concomitant solvates with the variation in host to guest ratio. Hence, different types of solvates yielded distinct structures, which might be owing to the flexibility in the host molecule as it tends to orient itself according to the size of the incoming guest molecule (Fig. 3.13). Interestingly, a rare case of concomitantly crystallizing a native host with the solvate was also observed with this flexible host molecule.

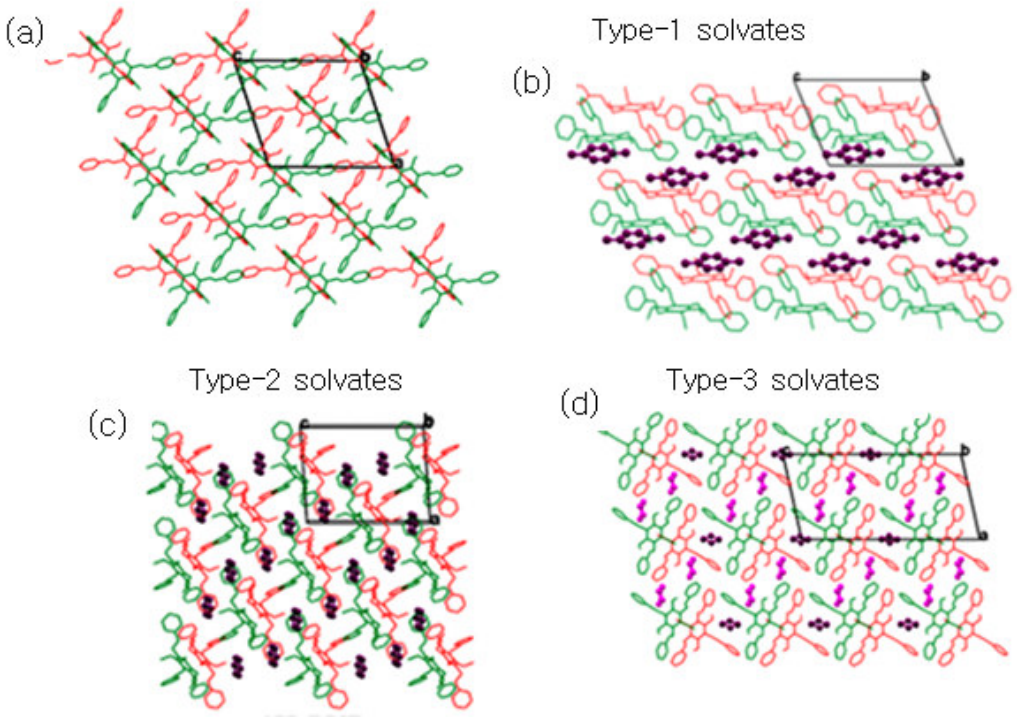

Fig. 3.13: (a) 3D packing diagrams of the guest-free form I; different forms of solvates observed (b) Form I; (c) Form II and (d) Form III

Besides these solvates and polymorphism, there is another challenging task to synthesize the multicomponent systems such as ternary, quaternary etc. It has been observed that with subtle change in basicity of the nitrogen and the difference in conformational flexibility of the host molecule that may give rise to the multicomponent systems [26]. Moreover, there are very few reports on the inclusion of solid component in the host-assembly of binary motifs, which led to the formation of ternary co-crystals [27-28]. Therefore, in order to design ternary supramolecule, it is central to know the synthetic strategies and supramolecular reactions that will result in multi-component supramolecular design. Some of the relevant literatures regarding ternary system have been discussed below.

Bhogala et al. [29] synthesized the ternary co-crystal [H_3CTA.bipy-eta(*gauche*).(bipy-bu)$_{0.5}$] from 1,3,5-cyclohexanetricarboxylic acid (H_3CTA) with 4,4'-bipyridine based bases of different CH_2 chain lengths. They compared the influence of flexible bipyridyl base on structural feature of the ternary co-crystal. Besides, they have also reported a quaternary co-crystal, which was attained by the inclusion of *p*-dichlorobenzene in the hydrogen bonded cavities of the ternary system (Fig. 3.14).

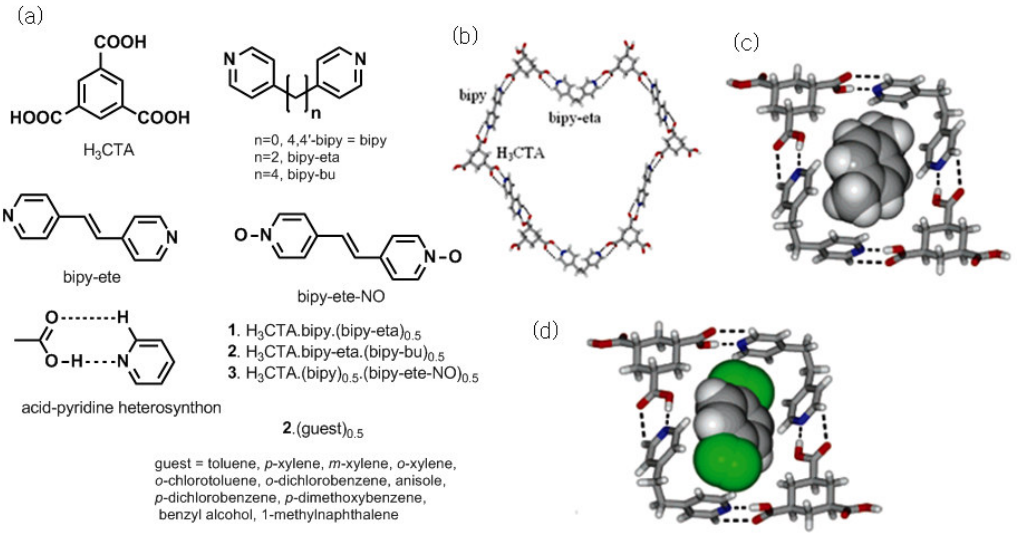

Fig. 3.14: (a) Chemical components for assembly of ternary co-crystals; (b) view of heterosynthons aggregating in hydrogen bonded ring with molecular necklace void; inclusion of (c) *p*-xylene and (d) *p*-dichlorobenzene in $H_3CTA.bipy.(bipy\text{-}eta)_{0.5}$ system

Tothadi and Desiraju [30] endeavored many experiments for the formation of ternary system based on the strategy of involving hydrogen and halogen bonds. On the basis of their observation, a strategy was proposed for the construction of ternary compounds by incorporating the halo compounds to the strong binary systems of the components (Fig. 3.15). Hence, authors used variety of halo compounds in order to raise halogen-hydrogen bonding. They have also suggested that the binary system should not be very strong or insol-

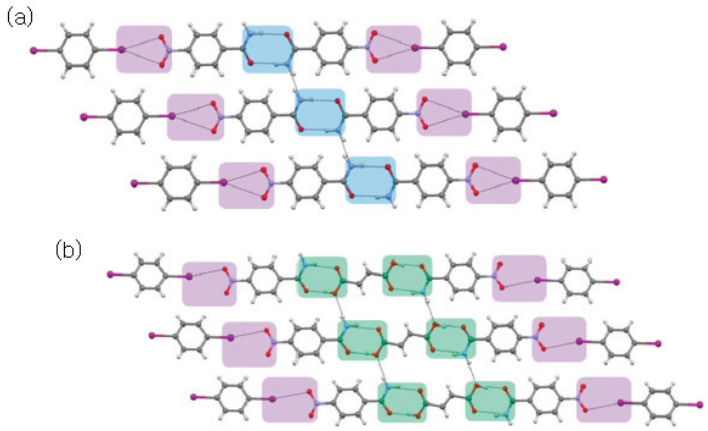

Fig. 3.15: (a) Binary 2:1 co-crystal of 4-nitrobenzamide and 1,4-diiodobenzene and (b) 2:1:1 ternary co-crystal of 4-nitrobenzamide:fumaric acid:1,4-diiodobenzene. Note: the amide···amide homosynthons (blue) and the symmetrical I···O_2N halogen bonded synthon (pink)

uble as it would end in the formation of binary system itself. Hence, the control of the interactions and the solubility of the system would lead to the formation of ternary co-crystals.

Last few decades have witnessed that the subject of metal organophosphonates has been an active area of research by virtue of their variety in structural aspect and its potential application in sorption, catalysis, non-linear materials and magnetic materials etc [31-34]. It is well established that the metal organophosphonate exhibit diverse coordination networks such as mononuclear, linear 1D complex and layered structures [35-38]. Although the organophosphonate show multidenticity but the difficulty in crystallizing the metal phosphonate still persist. Nonetheless, many researchers have reported the synthesis of metal phosphonates in the literature using different strategies which have been discussed below.

Chandrasekhar et al. [39] synthesized two multi-metal molecular systems of phosphonic acid and 3,5-dimethylpyrazole with Zn(II) in the presence of triethylamine affording trinuclear Zn cluster $[Zn_3Cl_2(3,5\text{-}Me_2Pz)_4(t\text{-}BuPO_3)_2]$ using sterically hindered *tert*-butylphosphonic acid and hexanuclear assembly $[Zn_6Cl_4(3,5\text{-}Me_2PzH)_8(PhPO_3)_4]$ using phenylphosphonic acid (Fig. 3.16). Hence, the authors determined that more cluster assembly can be synthesized by using the same synthetic strategy.

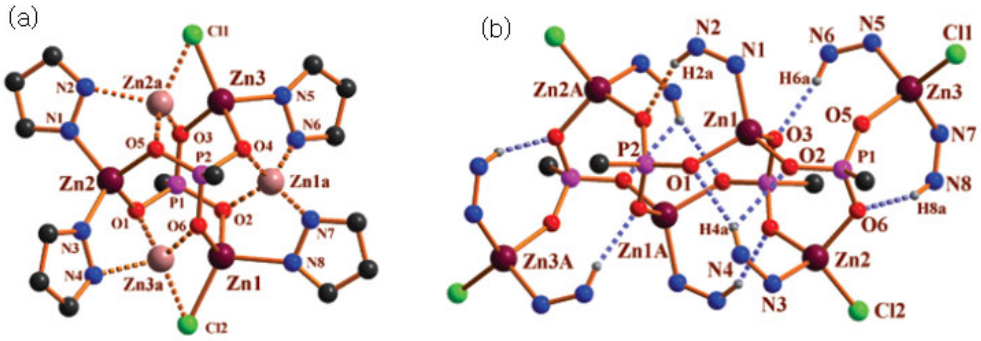

Fig. 3.16: View of the (a) trinuclear cluster $[Zn_3Cl_2(3,5\text{-}Me_2Pz)_4(t\text{-}BuPO_3)_2]$ showing the positionally disordered zinc atoms and (b) hexanuclear assembly $[Zn_6Cl_4(3,5\text{-}Me_2PzH)_8(PhPO_3)_4]$

Chandrasekhar et al. [40] also reported multimetallic phosphonates $[Cu_4(\mu_3\text{-}OH)_2\{ArPO_2(OH)\}_2(CH_3CO_2)_2(DMPZH)_4]\text{-}[CH_3COO]_2.CH_2Cl_2$ and $[Zn_4\{ArPO_3\}_2\{ArPO_2(OH)\}_2\{DMPZH\}_4(DMPZ)_2].5MeOH$ by using sterically hindered lipophilic 2,4,6-isopropylphenylphosphonic acid $(ArP(O)(OH)_2)$ with 3,5-dimethylpyrazole

(DMPZH) (Fig. 3.17). They demonstrated the importance of hindered lipophilic phosphonic acid and the pyrazole ligand, which provided the certainty for obtaining the crystals as a result of dissolving the molecular complex. They have also carried out the magnetic study of the synthesized complexes and concluded that multinuclear Cu(II) molecular complex displays the antiferromagnetic behavior.

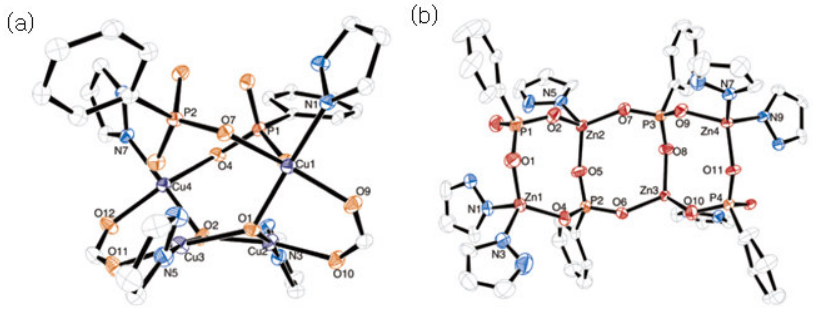

Fig. 3.17: ORTEP diagram of (a) $[Cu_4(\mu_3\text{-}OH)_2\{ArPO_2(OH)\}_2(CH_3CO_2)_2(DMPZH)_4]$-$[CH_3COO]_2.CH_2Cl_2$ and (b) $[Zn_4\{ArPO_3\}_2\{ArPO_2(OH)\}_2\{DMPZH\}_4(DMPZ)_2].5MeOH$

Chandrasekhar et al. [41] again reported the synthesis of multimetallic phosphonates i.e. decanuclear soluble molecular copper(II) phosphonates involving sterically

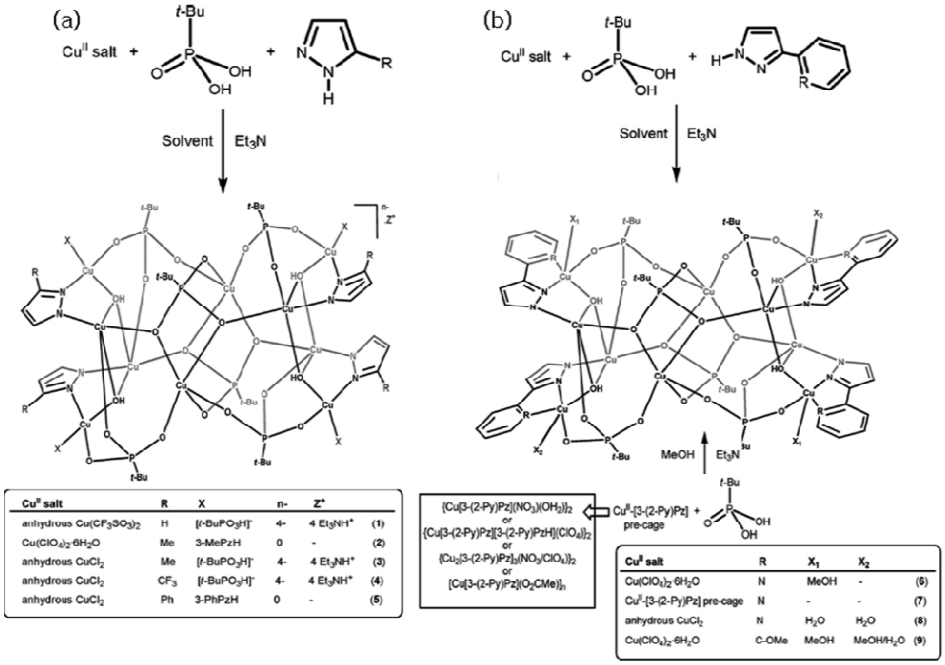

Fig. 3.18: Synthesis of decanuclear soluble molecular copper(II) phosphonates

hindered phosphonic acid, *tert*-butylphosphonic acid with variety of pyrazole analogues starting from simple pyrazole to sterically hindered pyrazole, 3-R-PzH, where R = H, Me, CF_3, Ph, 2-pyridyl (2-Py), and 2-methoxyphenyl (2-MeO-C_6H_4) (Fig. 3.18). Structural analysis displayed the formation of a butterfly shaped core. They found that some of the molecular complexes possessed tetra-anionic core depending upon the type of pyrazolate used, where some complexes possess more phosphonate group than pyrazole ligands and vice-versa.

The above literature revealed that no study has been done to study the solvent effect on the pyrazole-phosphonic acid and no ternary compounds have been reported earlier. Chandrasekhar with his co-workers has reported various metal phosphonate with the implementation of some strategies. Following those strategies, the synthesis of metal phosphonate was also carried out using a phosphonomonoester. Till now no such metal complex of phosphonomonoester has been reported.

This chapter has dealt with formation of new anthracene based phosphonic acid and studied its propensity to form several psuedopolymorphs with 3,3',5,5'-tetramethyl-1H,1'H-4,4'-bipyrazole (BPz) in order to attain the better understanding of the phosphonic-pyrazole system. Some of the ternary systems were also endeavored. Moreover, zero dimensional Cu(II) molecular systems were also attained from newly synthesized anthracene based phosphonomonoester involving solid state transformation.

Result and discussion:

A series of solvates was afforded by the crystallization of newly synthesized (anthracen-9-ylmethyl)phosphonic acid (H_2APa) and 3,3',5,5'-tetramethyl-1H,1'H-4,4'-bipyrazole (BPz) system (APaBPz) together with numerous solvents. The APaBPz system may be considered as a promising candidate as these supple components produce a framework that has the capability to accommodate any guest molecule. Hence, the propensities of the APaBPz system to produce remarkable variety of solvates whether it may be aromatic or any common solvent, which has established an insight into the nature of their solvates and ternary co-crystals. In this context, the formation of distinct solvates of this system *viz*., [($HAPa^-$).($HBPz^+$).THF] (**3a**), [($HAPa^-$).($HBPz^+$).dioxane] (**3b**), [($HAPa^-$).($HBPz^+$).benzene] (**3c**), [($HAPa^-$).($HBPz^+$).thiophene] (**3d**), [($HAPa^-$).($HBPz^+$).nitromethane] (**3e**), [($HAPa^-$)$_2$.($HBPz^+$)$_2$.nitrobenz.H_2O] (**3f**), [($HAPa^-$)$_2$.($HBPz^+$)$_2$.thiophenol] (**3g**), [($HAPa^-$)$_2$.($HBPz^+$)$_2$.toluene] (**3h**), [($HAPa^-$)$_2$.($HBPz^+$)$_2$.*p*-cresol.H_2O] (**3i**), [($HAPa^-$).(H_2BPz^{2+})$_{0.5}$.phenol] (**3j**), [($HAPa^-$)$_2$.H_2BPz^{2+}.2-NP.*n*-butanol] (**3k**), [($HAPa^-$)$_2$.H_2BPz^{2+}.4-NP.S] (**3l**), [($HAPa^-$)$_2$.($HBPz^+$)$_2$.(H_2APa)$_2$.H_2O] (**3m**) (Scheme 3.1) have been attempted. Although, all solvates successfully represented the host-guest assembly but some showed diverse structural attributes, which have been categorized into three forms based on the size and the accessibility of the hydrogen bonded moieties on the solvent molecule [42]. These three categories manifest three distinct hydrogen bonded sheets (Fig. 3.68): **type I** (solvates **3a**-**3e**); **type II** (solvates **3f**-**3i**); **type III** (ternary compounds **3j**-**3l**).

Type I includes THF (**3a**), dioxane (**3b**), benzene (**3c**), thiophene (**3d**) and nitromethane (**3e**); nitrobenzene (**3f**), thiophenol (**3g**), toluene (**3h**) and *p*-cresol (**3i**) are associated with **type II**. **Type III** comprises of phenol (**3j**), 2-nitrophenol (2-NP) (**3k**) and 4-nitrophenol (4-NP) (**3l**).

During investigation of various solvates of APaBPz system, it was found that flexible H_2APa can change its conformation accordingly depending upon the approaching guest molecule in the system.

After the structure analysis of all the solvates, it was found that the APaBPz system has the capability to allow all approaching solvates to be accommodated. Hence, it was anticipated that it might produce ternary co-crystals, which have fewer reports in the literature as compare to

binary. Therefore, the ternary co-crystals were produced using *p*-cresol (**3i**), phenol (**3j**), 2-nitrophenol (2-NP) (**3k**) and 4-nitrophenol (4-NP) (**3l**) with APaBPz system which generated **type II-III** framework.

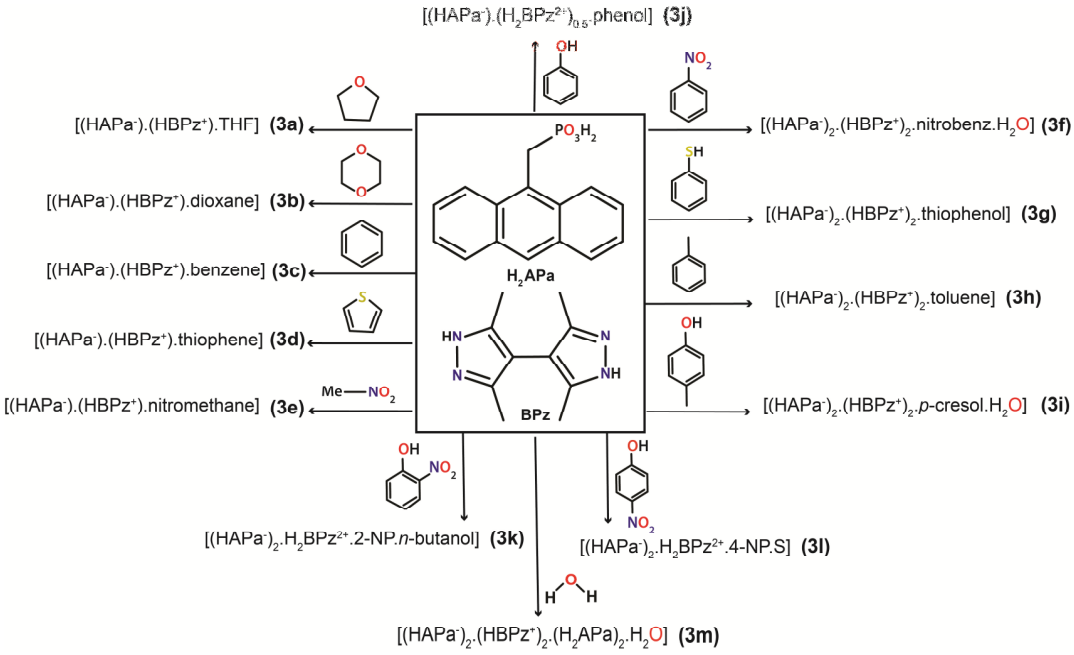

Scheme 3.1: Synthetic schematic representation of solvates **3a**-**3h**, ternary co-crystals **3i**-**3l** and hydrated ABaBPz **3m**

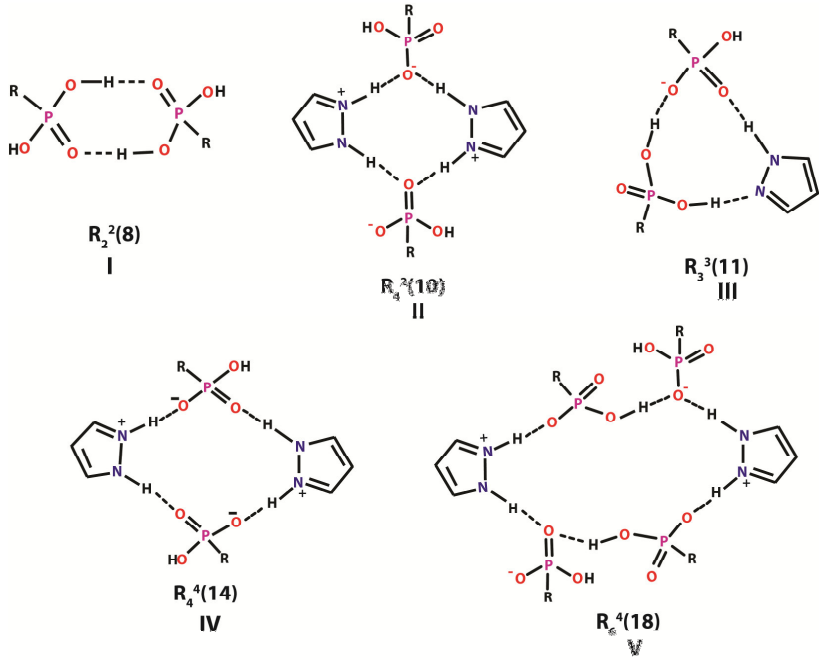

Scheme 3.2: Various synthons observed in solvates and ternary systems of APaBPz

It may be noted that some new synthons have also been found in case of (anthracen-9-ylmethyl)phosphonic acid (H_2APa) and 3,3',5,5'-tetramethyl-1H,1'H-4,4'-bipyrazole (BPz) system as compare to the system discussed earlier in chapter 2. The presence of flexible $-CH_2-$ moiety between the bulky aromatic organic component and the phosphonic group helps in providing distinct conformations in the system (Scheme 3.2). The crystallographic data for solvates **3a**-**3h**, **3m** and for ternary co-crystals **3i**-**3l** have been tabulated in Table 3.1-3.8; 3.13 and 3.9-3.12 respectively. Selected bond lengths of all the solvates **3a**-**3h**, **3m** and for ternary co-crystals **3i**-**3l** are given in Table 3.17.

Crystal structure of type I (3a-3e):

All solvates lying in this category are isostructural. **Type I** is a 1:1 APa:BPz system crystallized in *C2/c* space group with one molecule each of bispyrazole cation, phosphonate anion and a guest molecule in its asymmetric unit as shown in particular solvate such as THF (Fig. 3.19), dioxane (Fig. 3.23), benzene (Fig. 3.26), thiophene (Fig. 3.29) and nitromethane (Fig. 3.32).

The framework is sustained by the two synthons i.e., an ubiquitous homodimer, **I** ($R_2^2(8)$) and a new synthon was observed different from that reported in chapter 2, i.e., tetramer motif, **II** ($R_4^2(10)$) synthon (Scheme 3.2) with inverted symmetry using N–H···O interaction (Fig. 3.20), which finally yields a 2D **type I** supramolecular hydrogen bonded sheet (Fig. 3.21). On probing the structural data, it was observed that BPz plays an important role in linking the two adjacent homodimer and is also responsible for extending the framework to generate 3D supramolecular construct.

Furthermore, the framework was also stabilized by some C–H···π($HBPz^+$), C–H···O interactions and by edge π···π interactions as well, between two anthracene moieties of the phosphonic acids. Subsequently, these interactions resulted in the generation of a channel along *c*-axis, accommodated by the solvent molecule, which further interacts to the host through weak intermolecular interactions in solvates **3a**-**3e** (Fig. 3.22, 3.25, 3.28, 3.31 and 3.34). Therefore, the **type I** framework resulted in the hydrogen bonded cavities, which have been occupied by the guest molecules. The various intermolecular interactions involved in solvate **3a** are the dimer formation (O1–H1E···O3, 1.849 Å); tetramer motif through N–H···O interactions (N3–H3D···O2, 1.822 Å; N4–H4D···O2, 1.909 Å) whereas the secondary weak interactions

involved are C–H···π(HBPz$^+$), 2.746 Å; C–H(HBPz$^+$)···O(–P(OH)), 2.623 Å and edge π···π, 2.232 Å (Fig. 3.22).

Similarly in solvate **3b**, dioxane showed weak interaction with HBPz$^+$ molecule and moreover it forms weak interaction with another dioxane molecule. On the other hand, the oxygen of the dioxane, in contrast to THF, participates in the hydrogen bonding formation with anthracene molecule (C–H(anthra)···O(dioxane), 2.660 Å). The various intermolecular interactions involved in solvate **3b** are the dimer formation (O1–H1E···O3, 1.824 Å); tetramer motif using N–H···O interaction (N4–H4D···O2, 1.807 Å; N3–H3D···O2, 1.915 Å) (Fig. 3.24). The secondary weak interactions involved are C–H···π(BPz), 2.711 Å and edge π···π interaction, 2.301; 2.336 Å (Fig. 3.25).

In case of solvate **3c**, benzene showed three distinct C–H···π interactions (2.535, 2.664, 2.791 Å) with the π-electron cloud of anthracene and HBPz$^+$ molecule and, the adjacent benzene molecules are linked to each other through edge π···π interactions. The various intermolecular interactions involved in solvate **3c** are the dimer formation (O1–H1E···O2, 1.840 Å); tetramer motif via N–H···O interactions (N4–H4D···O3, 1.897 Å; N3–H3D···O3, 1.806 Å) (Fig. 3.27). The secondary weak interactions involved are C–H···π(HBPz$^+$), 2.744 Å and edge π···π interactions, 2.082, 2.351 Å, which further stabilize the host-guest assembly (Fig. 3.28).

The solvate **3d** was composed of thiophene also displayed three distinct C–H···π interactions (2.606, 2.707, 2.664 Å) involving the π-electron density of anthracene and HBPz$^+$ molecule. The various intermolecular interactions involved in solvate **3d** are the dimer formation (O3–H3E···O2, 1.800 Å); tetramer motif using N–H···O interaction (N2–H2D···O1, 1.854 Å; N1–H1D···O1, 1.794 Å) (Fig. 3.30). The secondary weak interactions involved are C–H···π(HBPz$^+$), 2.386 Å and edge π···π interactions, 2.023, 2.339 Å further stabilizes the host-guest assembly (Fig. 3.31).

The solvent nitromethane in solvate **3e** represented two distinctive C–H···π interactions 2.180 Å; 2.443 Å with anthracene group and HBPz$^+$ molecule respectively. Notably, the –NO_2 group of nitromethane in **3f** does not participate and remains free from any intermolecular hydrogen bonding. The various intermolecular interactions involved in solvate **3e** are the dimer formation (O3–H3E···O2, 1.771 Å); tetramer motif via N–H···O interactions (N1–H1D···O1, 1.835 Å; N2–H2D···O1, 1.896 Å) (Fig. 3.33). The secondary weak interactions involved are

C–H···π(HBPz$^+$), 2.833 Å; edge π···π, 2.393 Å and additionally, face to face π···π interaction, 3.538 Å further stabilize the host-guest assembly (Fig. 3.34).

Crystal structure of type II (3f-3i):

The solvates under this category were crystallized in $P2_1/n$ (~ $P2_1/c$) space group and comprised of two molecules each of monocation and monoanion along with one molecule of guest in the asymmetric unit, in case of nitrobenzene (Fig. 3.35), thiophenol (Fig. 3.39), toluene (Fig. 3.42) and *p*-cresol (Fig. 3.45).

The framework held the dimer and the synthon **II** similar to the above described network. The adjacent phosphonic homodimers were interlinked by the linker, HBPz$^+$ molecule, generated the 1D tape along *ab*-plane (Fig. 3.36). Furthermore, the 1D tape is extended to 2D **type II** hydrogen bonded sheet using various C–H···π interactions formed between two anthracene moieties (Fig. 3.37). Structural analysis revealed that the interaction of adjacent 2D neighbor sheets via synthon **II** formation using linker, HBPz$^+$ and C–H···π interactions between two anthracene moieties from two different sheets raises the dimensionality of the network from 2D to 3D supramolecular framework. Consequently, the host-guest assembly is generated with the guest molecules residing the channel along *c*-axis in 3D (Fig. 3.38, 3.41, 3.44 and 3.47).

The various intermolecular interactions involved in solvate **3f** are the dimer formation (O2–H2E···O5, 1.792 Å; O4–H4E···O3, 1.797 Å), tetramer motif via N–H···O interactions (N1–H1D···O6, 1.834 Å; N2–H2D···O1, 1.805 Å, N5–H5D···O6, 1.797 Å; N6–H6D···O1, 1.948 Å) as displayed in Fig. 3.36. The various secondary weak interactions involved are C–H···π(anthra), 3.387 Å; C50–H50···O4, 2.696 Å and C41–H41A···O4, 2.584 Å. On the other hand, the nitrobenzene in **3f** forms C–H···π(HBPz$^+$), 2.721 Å and C–H···π(anthra), 2.799 Å.

In case of thiophenol, **3g** displays various intermolecular interactions involved in framework such as dimer formation (O1–H1E···O5, 1.801 Å; O6–H6E···O2, 1.798 Å), tetramer motif via N–H···O interactions (N3–H3D···O3, 1.817 Å; N4–H4D···O4, 1.855 Å, N6–H6D···O3, 1.943 Å; N5–H5D···O4, 1.795 Å) (Fig. 3.40). The secondary weak interaction involved is C–H···π(anthra), 2.870 Å. However, thiophenol molecule form C–H···π(anthra), 2.854 Å; C–H···π(HBPz$^+$), 2.682 Å, 2.637 Å, while the thiol group –SH interact with the π electron density of the anthracene molecule (S1–H1Z···π, 2.991 Å) as shown in Fig. 3.41.

The solvate **3h** involves O1–H1E···O5, 1.842 Å; O6–H6E···O2, 1.820 Å associated with the dimer and, tetramer motif involves N–H···O interactions such as N2–H2D···O3, 1.809 Å; N5–H5D···O3, 1.933 Å, N6–H6D···O4, 1.788 Å; N1–H1D···O4, 1.828 Å (Fig. 3.43). The other secondary intermolecular interactions engaged in further stabilizing the network are C–H(HBPz$^+$)···π(anthra), 2.867 Å; C–H(HBPz$^+$)···O(–P=O), 2.486 Å and C–H(anthra)···π(anthra), 2.385 Å. On the other hand, toluene forms C–H···π(HBPz$^+$) interaction, 2.711 Å (Fig. 3.44).

After analyzing the results, it was assumed that the flexible feature of H_2APa in solvates endows the system to adapt any guest molecule. Hence, a challenging task was carried out with the conception of producing ternary co-crystals by the inclusion of solid components into the system [43].

The solid entity, *p*-cresol exhibited the same 2D hydrogen bonded sheet as observed in **type II**, which led to a three component system with APaBPz along with one water molecule (Fig. 3.45). In **3i**, the dimer entails O–H···O interactions (O1–H1E···O5, 1.786 Å; O4–H4E···O2, 1.790 Å) and tetramer motif involving various N–H···O interactions (N4–H4D···O6, 1.840 Å; N6–H6D···O6, 1.809 Å, N3–H3D···O3, 1.807 Å; N5–H5D···O3, 1.921 Å) (Fig. 3.46). Diverse other weak interactions involved are C–H(anthra)···π(anthra), 2.879 Å; C–H(HBPz$^+$)···O(–P=O), 2.632 Å. At the other end, *p*-cresol engages into various secondary interactions such as C–H···π(HBPz$^+$), 2.774 Å; O–H···π(HBPz$^+$), 2.361 Å and C–H(anthra)···O(OH–*p*-cresol) , 2.710 Å (Fig. 3.47).

Notably, the phenol from **type III**, exhibited the same space group as found in **type I**. Also, the guest molecules 2-nitrophenol (2-NP) and 4-nitrophenol (4-NP) from **type III** evidenced the same space group similar to the solvates of **type II** but probably the presence of –OH group (hydrogen bond donor) results in different supramolecular construct.

Crystal structure of type III (3j-3l):

Crystallization of phosphonic acid with the bifunctional pyrazole in the presence of phenol and *n*-butanol yields **3j** with half the molecule of cation and one molecule each of anion and phenol molecule in the asymmetric unit (Fig. 3. 48).

The bifunctional cation being a good base with the capability of forming strong H-bond, links the phosphonic dimer (O1–H1E···O2, 1.817Å) in all its four direction (Fig. 3.49). The dimer motif being bridged by $HBPz^+$ molecules with the help of N–H···O interactions (N1–H1D···O3, 1.743 Å; N2–H2D···O2, 1.827 Å) forms a centrosymmetric tetramer motif **IV**, $R_4^4(14)$, which later derived a 2D sheet in *ab*-plane (Fig. 3.51). Notably, phenol with hydrogen bonded moiety facilitates the formation of O4–H4Z···O3 (1.930 Å) interaction with phosphonic acid. Hence, the phenol molecule is embedded into the 2D sheet formed by the cation and anion linked together by O–H···O and C–H···π interactions involving the π-electrons of $HBPz^+$ (Fig. 3.50).

A closer inspection of the network in **3j** revealed that the dimensionality of the framework is extended from 2D to 3D network through π···π interactions (Fig. 3.52). As a result, the 3D supramolecular framework displays the host-guest assembly, which resides the phenol molecule inside the cavity. However, the –OH group of phenol is involved in the intermolecular interaction with the host forming O–H···O interaction and the framework is further stabilized by π···π interaction formed between the phenol molecule and the host (Fig. 3.53).

Crystal structure of [$(HAPa^-)_2$.H_2BPz^{2+}.2-NP.*n*-butanol] (3k) and [$(HAPa^-)_2$.H_2BPz^{2+}.4-NP.S] (3l)

It is a 2:1:1 ternary system of the H_2APa and BPz and one solid guest molecule, crystallized in $P2_1/n$ space group. The asymmetric unit of **3k** and **3l** was composed of two molecules of monodeprotonated anion and a diprotonated BPz with one molecule of guest i.e. 2-nitrophenol (2-NP) (Fig. 3.54) and 4-nitrophenol (4-NP) (Fig. 3.59), respectively.

This category was constituted of two positional isomers as the guest molecule i.e. 2-NP and 4-NP. On probing, it was found that the extension of the network occurs similarly as found in case of compound **3j** (Fig. 3.56). Hence, a 2D supramolecular sheet increases its dimensionality 3D with the help of C–H···π interaction between two organic moieties of the phosphonic acids from two adjacent 2D sheets (2.690 Å) and also within the same sheet (2.872 Å) (Fig. 3.57). Subsequently, the host-guest assembly of APaBPz system was attained with the guest molecules residing the channel generated along *a*-axis with the formation of synthon **I** (O6–H6E···O2, 1.838 Å; O1–H1E···O5, 1.764 Å) and **IV** (N3–H3D···O5, 1.866 Å; N1–H1D···O4, 1.738 Å; N2–H2D···O2, 1.846 Å; N4–H4D···O3, 1.679 Å) (Fig. 3.55).

In contrast to the phenol in **3j**, the –OH group of 2-nitrophenol in **3k** does not interact with framework due to presence of additional NO_2 group at *o*-position on the guest molecule. The –OH group in 2-NP is engaged in forming intermolecular interaction with the adjacent 2-NP (O7–H7Z···O9, 2.682 Å). On the other hand, some weak C–H···O interactions (C42–H42···O1, 2.670 Å; C43–H43···O3, 2.680 Å) between 2-NP and anthracene moieties in the framework stabilizes the host-guest assembly to some extent (Fig. 3.57). Moreover, **3k** also contains *n*-butanol molecule aided in crystallization of APaBPz system in 2NP solvent further stabilizing the framework via C–H···O interactions (2.426 Å, 2.599 Å). Subsequently, it led to the formation of distinct host-guest assembly (Fig. 3.58) as found in earlier cases.

Likely in **3k**, the same framework is produced in **3l**. The 2D framework sustained the same dimer **I** involving O–H···O interactions (O3–H3E···O6, 1.814 Å; O4–H4E···O2, 1.756 Å) and synthon **IV** associated by N–H···O interactions (N1–H1D···O2, 1.862 Å; N3–H3D···O1, 1.734 Å; N4–H4D···O6, 1.838 Å) (Fig. 3.60). Furthermore, the extended 3D framework is generated via C–H···π interactions (2.779 Å). In contrast to **3k**, here the guest molecule stabilizes the network more than 2-NP due to the formation of weak C–H···O interaction with the framework by –OH and $–NO_2$ group of 4-NP at *para*-position (Fig. 3.61). However, the –OH group of 4-NP interacts with the π ring of the anthracene moiety, which finally led to the formation of host-guest assembly filled with 4-NP inside the channel along *a*-axis (Fig. 3.62).

Notably, some of the electron density of guest molecules was diffused as it was difficult to achieve a better model for the same. Hence, this disordered solvent molecule was removed by using PLATON/SQUEEZE program with the potential disordered solvent void of 169.0 $Å^3$ containing 54 electrons/asymmetric unit as determined by the PLATON, which can tentatively be assigned to one *n*-butanol molecule present in the asymmetric unit according to the TGA and squeezed data. During analysis, it was found that $–NO_2$ group of 4-NP showed the static disorder.

In addition to these solvents, water, the easily accessible solvent and has the potential to attain strong H-bonding in the framework influences the supramolecular organization (**3m**) significantly as obtained with other solvents. Therefore, it can be said that the solvates of APaBPz are solvent mediated construction as the choice of the solvent stimulates the formation of particular solvate.

Crystal structure of hydrated APaBPz system (3m):

The hydrate of APaBPz was also achieved with the easy accessible solvent, water molecule which has the higher propensity for hydrogen bonding. The solvate APaBPz.water is crystallized in *P*-1 space group with two molecules each of monoanion ($HAPa^-$), monocation ($HBPz^+$) and neutral H_2APa along with one water molecule (Fig. 3.63).

Similar to aforementioned solvates, the adjacent homodimers **I** (O3–H3E···O10, 1.752 Å; O11–H11E···O2, 1.742 Å) were interlinked through the linker, $HBPz^+$. In addition to the dimer, the framework also sustained the formation of trimer **III** $R_3^3(11)$, hexamer **V** $R_6^4(18)$ and octameric (in chair form) supramolecular motif **VI** $R_8^5(22)$ involving distinct O–H···O and N–H···O interactions due to presence of number of donors and acceptors in the system (Fig. 3.63). Hence, the 2D sheet is associated with an array of dimers, trimers, hexamer and octamer motifs (Fig. 3.65). It is important to point out that hexameric and octameric (in chair form) moieties repeat themselves alternatively to each other in a 2D sheet. Thereafter in 3D, these 2D adjacent sheets are further interlinked through π···π interactions between four organic moieties of the phosphonic acids (Fig. 3.66). Hence, in this case no such host-guest assembly is observed rather the water molecule itself is involved in the formation of the network. The various intermolecular interactions involved are C–H···π(anthra), 2.395 Å; C–H···O, 2.719 Å; C–H($HBPz^+$)···π(anthra), 2.860; N–H($HBPz^+$)···O(water), 1.847 Å and P(O–H)···O(water), 1.750 Å further stabilizes the hydrate of APaBPz system (Fig. 3.67).

Recently, researchers have come across the subject of porous soft material, which exhibits the dynamic behaviour with the stimuli response. It is of particular interest to study the structural dynamism resulting from change in chemical environment available to the framework [44-46].

It is well known that the metal organophosphonate has the strong feasibility to exhibit voluminous coordination chemistry including mononuclear, layered complex and 3D structures [47-49]. The propensity of organophosphonate to show multidenticity is often confronted obstacle for crystallizing the phosphonate as the formation of insoluble compound take place. In this context, various strategies have been attempted in order to overcome this solubility issue to tailor the molecular metal phosphonate such as 1) use of sterically hindered phosphonic acid; 2) use of chelating ligand, which limits the coordination site available on metal, thereby, resulting

in the confinement of reactive site on metal and 3) controlled degree of protonation i.e., the exploitation of phosphonic acid as the source of monoanionic in bidentate chelation mode. At this end, the molecular metal phosphonate has been produced from newly synthesized anthracene based phosphonomonoester and a chelating ligand i.e., 2,2'-bipyridine, which fulfills the aforementioned strategies by making the use of bulky phosphonic acid and chelating ligand. It may be noted that there is no report on molecular complex using monoester of phosphonic acid, which subsequently limits the possibility of coordinating to the metal ion. Hence, it increases the solubility of the compound, hence further increasing the chances of getting it crystallize.

Additionally, low-dimensional metal phosphonates based on fluorescent phosphonic acid have been rarely reported. Herein to gain the information of interest here, the dinuclear molecular system has been accomplished by employing Cu(II) ion with novel flexible phosphonomonoester, ethyl hydrogen (anthracen-9-ylmethyl)phosphonate (**3n**) and the auxillary basic ligand i.e., 2,2'-bipyridine ($^{2,2'}$BPy) and resulted in the formation of the porous supramolecular network (Scheme 3.3). One thing that was worth noting is the presence of $-CH_2-$ group between π-aromatic ring and the phosphonate group, which allows the rotation about the single bond. Hence, it is capable of adjusting themselves as such that its organic moiety and the auxiliary ligand stacks over one another, owing to the flexibility of monoester, henceforth, resulted in the structural dynamism of the framework.

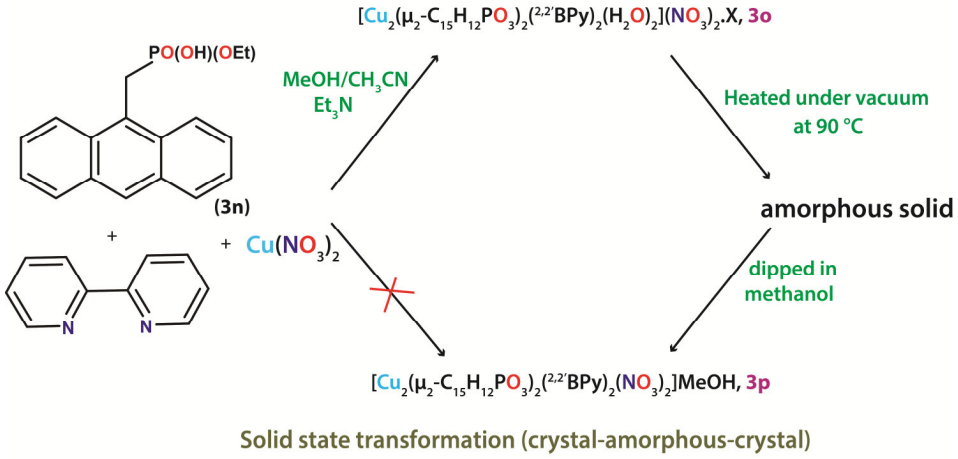

Scheme 3.3: Schematic synthesis of metal complexes **3o** and **3p**

Crystal structure of 3n:

Compound **3n** crystallizes in monoclinic space group, *C*2/*c* and contains one molecule of the phosphonomonoester in the asymmetric unit. Unlikely in other phosphonic system, no phosphonic homodimer was observed in this case. One of the P–OH unit in one molecule acts as a donor and is hydrogen bonded to the P=O group of other molecule which acts as an acceptor (Fig. 3.69). Out of three oxygen of the phosphonate molecule, two of them are involved in intermolecular hydrogen bonded. Thereby, this has led to the formation of ladder like structure in 1D. The intermolecular interaction O···O involved lies in the range of 2.439-2.441 Å. The crystallographic data of **3n** is given in Table 3.14.

Crystal structure of 3o:

Single crystal X-ray diffraction analysis revealed that $[Cu_2(\mu_2\text{-}C_{15}H_{12}PO_3)_2(^{2,2'}BPy)_2(H_2O)_2]((NO_3)_2.X)$ (**3o**), is crystallized in the triclinic space group, *P*-1. The asymmetric unit contained one crystallographically Cu(II) ion, one molecule each of monoester, an auxiliary ligand: 2,2'-bipyridine ($^{2,2'}$BPy), one coordinated water molecule and an uncoordinated distorted nitrate anion lying on a symmetrical axis along with squeezed solvent molecule, X (Fig. 3.70). It may be noted that the nitrate anion lie on the special position and the five-coordinated copper ion lies on a crystallographic two-fold axis and hence, led to the formation of the dinuclear assembly. This dimer assembly is represented as a composite building unit for the resulting supramolecular network. The coordination environment around the Cu(II) atom is displayed in Fig. 3.71 along with the atom numbering scheme, which clearly represent that the Cu(II) exhibited a distorted square pyramidal coordination with N_2O_3 donor set. The equatorial plane endured two nitrogen-coordinating sites from same bidendate ligand and two oxygen of the monoester whereas the fifth site is engaged by the oxygen of the water molecule, which is nearly perpendicular to the plane. The Cu(II)–N1, Cu(II)–N2, Cu(II)–O1, Cu(II)–O3 and Cu(II)–O4(water) distances were in agreement with those reported for other Cu(II) phosphonate compounds such as 2.008, 2.018, 1.944, 1.932 and 2.247 Å respectively [50]. Each of two bipyridine moieties and monoester altogether held the dinuclear assembly, where the latter is bridged isobidentatly to the metal atom resulting in the formation of a chair shaped single eight membered ring ($Cu_2O_4P_2$). The average bond distance Cu(II)–O involved in the ring is 1.947Å, that is found to be in good agreement with the previous studies [40]. Its resemblance to the S8R building unit of zeolites is the remarkable feature of this molecule [51]. The

crystallographic data for **3o** is given in Table 3.15, and selected bond distances and angles are listed in Table 3.18.

To the best of our knowledge, the porous network from the same copper dinuclear complex using phosphonomonoester has been rarely reported. On scrutiny, it was observed that the 1D chain of the composite unit and the uncoordinated nitrate ion runs along *bc*-plane, connected via hydrogen bond between the coordinated water molecule and uncoordinated nitrate ion (O4–H4D···O5, 1.924 Å). These 1D chains run parallel to each other, which were further glued together through C–H···O and C–H···N interactions in *ac*-plane resulting in interdigitated structure (Fig. 3.72). The different interlayer non-conventional interactions involved between two 1D chains are C9–H9···O6, 2.698; C21–H21···N3, 2.581; C21–H21···O5, 2.505 Å. Further, these discrete 2D sheets stacked over one another along *b*-axis, thereby resulted in a porous supramolecular framework ending in 1D channel along *a*-axis, accommodated by disordered nitrate and disordered solvent molecules (Fig. 3.73). The strength of the framework is based on an array of π-π stacking between the π electron cloud of the anthryl group and the $^{2,2'}$BPy. Subsequently, the composite building unit, assembled through π-π stacking, is mainly responsible for generation of 3D supramolecular network.

Besides, a disordered nitrate anion, the presence of residual electron density was indicated by X-ray crystallography in the crystal lattice confirms the presence of solvent molecules, X. However, the solvent molecule present in the cavity of complex **3o** cannot be modeled due to severe disorder. Hence, the residual electron density was removed by PLATON\SQUEEZE program. In addition, there is a potential disordered solvent void of 183.6 $Å^3$ containing 65 electrons/unit cell as determined by the Platon, which might be consigned two methanol molecules present in the asymmetric unit.

Crystal structure of 3p:

The neutral complex, $[Cu_2(\mu_2\text{-}C_{15}H_{12}PO_3)_2(^{2,2'}BPy)_2(NO_3)_2]$.MeOH (**3p**) is formed from cationic complex, **3o** via solid state transformation (crystal-amorphous-crystal). The coordination environment around Cu(II) remain unchanged with a same N_2O_3 donor set in both complexes but differs in the crystal system, the unit cell parameters and the space group, which changed from triclinic (*P*-1) to monoclinic ($P2_1/c$). Structurally, the coordinated water molecule in **3o** is substituted by nitrate ion in complex **3p**, thereafter, changing the cationic framework to neutral

framework. The bond lengths and angles around Cu(II) were observed close to the bond lengths found in complex **3o**. The asymmetric unit consisted of the neutral composite unit along with the extra-framework solvent molecule, methanol (Fig. 3.74a). The formation of S8R ring (Fig. 3.74b) with the extension to 2D framework, assembled further to generate 3D network, remain unchanged. These intermolecular non-covalent interactions such as π-π stacking are responsible for increasing the dimensionality of the framework from zero dimensional structure to three dimensional network.

Structural study showed that the composite unit of compound **3p** forms 1D chain along *b*-axis which are further stitched together by π-π stacking between $^{2,2'}$BPy and anthracene ring of the two different composite units. This 1D chain is extended to 2D via C12–H12···O6 interaction between anthranyl C–H to nitrate anion of another layer along *a*-axis, thereby leading to the formation of a sheet (Fig. 3.75). Moreover, the 2D sheets are further assembled into 3D supramolecular polymer through π-π interactions in *ac*-plane (Fig. 3.77). The offset π-π (centroid-centroid) distance in interlayer and intralayer are 3.358 and 3.735Å respectively and, the π-rings are displaced by 1.253 Å in interlayer and 1.375 Å in intralayer (Fig. 3.76) as calculated by Olex2 (version 1.2.2). The different non-covalent interactions between the aromatic C–H and the nitrate involved in interlayer sheets are C21–H21···O4, 2.337 Å; C5–H5···O6, 2.657 Å and C24–H24···O5, 2.477 Å. The crystallographic data and selected bond distances of **3p** are given in Table 3.16 and 3.19 respectively.

Solid state transformation (crystal-amorphous-crystal):

The combination of $Cu(NO_3)_2$, **3n** and 2,2'-bipyridine ($^{2,2'}$BPy) as an auxillary ligand in methanol-acetonitrile solvent system in presence of triethylamine resulted in the formation of molecular metal complex **3o**. Single crystal analysis of compound **3o** revealed the formation of 1D chain, further H-bonded to other chains through uncoordinated anions and solvent molecules resulting in the supramolecular network with 1D channel.

A remarkable effect was observed when crystals of **3p** were removed from the mother liquor and the crystals were allowed to evacuate for one day. As a result, the crystals started losing its transparency and eventually led to the formation of amorphous solid (crystal to amorphous) as confirmed by PXRD (Fig. 3.83). Thereafter, the resulted solid was later kept in methanol solvent where the amorphous solid changes to crystal (amorphous to crystal) and

hence, ended up in a different complex, **3p** as evident by single crystal XRD. It showed change in unit cell parameters from **3o** and structural analysis revealed that a new compound (**3p**) was formed by replacing the coordinated water molecule per Cu(II) by the extra framework nitrate anion (Scheme 3.4).

Hence, new non-porous supramolecular polymer was established from porous supramolecular polymer although, the geometry of the metal centre remain unchanged. Consequently, the overall structural change supports the dynamic behavior for compound **3o**.

Infra-red spectral and thermal study

Both complexes were characterized by IR spectral studies, elemental analysis, thermal analysis, powder XRD (PXRD) as well as single crystal XRD. Hence, the solvates of APaBPz are stable at room temperature and found to be stable upto 240-250 ºC as manifested by thermogravimetric analysis (TGA). According to TG curve, solvates **3a**-**3e** were found to be stable upto 260 ºC (Fig. 3.80). The primarily loss in solvates **3a**-**3e** corresponds to the loss of their crystallized solvent with the mass loss of 15.0 % at 98 ºC, 17.0 % at 169 ºC, 15.6 % at 120 ºC, 16.3 % at 105 ºC and 12.3 % at 140 ºC respectively. In case of **3f**-**3i**, the first three solvates show the similar two step decomposition with the first curve attributes to the loss of the solvent molecule with the mass loss of 12.8 % at 145 ºC for **3f**, 12.2 % loss at 140 ºC for **3g** and 10.2 % loss at 130 ºC for **3h**. From the thermal profile, it was clear that the second mass loss starts around 200 ºC, which may be associated with the loss of the organic component. On the other hand, **3j** showed two sharp curves, which illustrated the loss of the solvent molecule (mass loss 21.0 %) first around 150 ºC then the loss of the organic part of the phosphonic acid near 255 ºC. Later, the hydrate of APaBPz system (**3m**) showed the higher stability as it decomposes around 300 ºC probably due to involvement of water molecule in strong intermolecular hydrogen bonding involved in the framework (Fig. 3.81).

The thermal study of compounds **3o** and **3p** followed almost the same decomposition pattern. Both compounds showed two mass loss steps. In case of **3o**, the loss of uncoordinated methanol molecule and coordinated water occurs at 90 ºC and 130 ºC whereas the mass loss at 85 ºC for **3p** corresponds to the loss of non-coordinated methanol molecule present in the lattice. On the other hand, the second mass loss attributes to the decomposition of the system at 260 ºC for compound **3o** and 250 ºC for compound **3p** (Fig. 3.82).

The characteristic infra-red (IR) absorption band in complex **3o** with medium intensity of M−OH appeared at 3765 cm^{-1} and that of N−O at 1370 cm^{-1} corresponding to the coordinated water molecule to the metal and free nitrate anion respectively (Fig. 3.83). Moreover in complex **3p**, the broad absorption band at 3200 cm^{-1} exemplified the presence of hydrogen bonded O−H present in methanol molecule and the corresponding absorption band for coordinated N−O from nitrate ion was displayed at 1320 cm^{-1}. The PXRD measurement for **3o** and **3p** ascertained that the PXRD pattern of as-synthesized compounds was found to be in agreement with the simulated one (Fig. 3.84).

Theoretical studies:

To ascertain the ideal geometries of salts **3a**-**3m**, the hydrogen bond interaction energy was calculated at DFT level using (B3LYP)/6-31G(d,p) basis set on Gaussian 03 suite of program. The various factors responsible for the higher stability have already been discussed in chapter 2. The hydrate, **3m** showed the highest stability as compare to others, apparently due to presence of more interactions involved in the supramolecular network, followed by *p*-cresol in solvate **3j** (Table 3.21). Among **3g**-**3l**, **3i** showed the higher stability due to presence of two +I group and involvement of $–CH_3$ and –OH group in intermolecular interactions followed by **3j** and **3g**-**3h** possessing one +I group. In case of **3k** and **3l**, the latter showed the higher stability than the former as the $–NO_2$ and −OH group at *ortho*-position induces the steric hindrance and further reduces the availability of the electron density for interaction. However, **3c** does not have any such group but still show higher stability than **3f** as the latter consists of –I group i.e., $–NO_2$ group, which decreases the electron density of the system. Notably, the stability is higher for **3a** having THF molecule followed by the solvate **3b**, dioxane that can be assumed as in latter the two oxygen atoms are non-planar and causes steric as compare to the solvate **3a**.

Solid-state luminescence properties

The solid-state luminescence property of the (anthracen-9-ylmethyl)phosphonic acid exhibited strong emission at 425 nm on excitation at 212 nm. Moreover, the effect of the guest molecules on the emission of the ligand was also investigated at room temperature as shown in Fig. 3.79. From the emission profile of the compounds **3e**-**3g** and **3i**-**3l**, it was found that 4-NP exhibited higher fluorescence quenching response towards the emission of the ligand probably due to the electrostatic interactions. On analyzing the results, it was observed that the guest

molecule with −OH group showed the higher quenching [52] owing to the presence of hydrogen bonded moiety, which interact with the system and hence, may be responsible for quenching the fluorescence emission.

Summary:

In total, nine solvates and four ternary systems of APaBPz were constructed. Mainly, the four forms of the solvates were categorized according to the acid:base ratio at which these are crystallized in the asymmetric unit. Notably, all four forms of the solvates sustained acid-acid dimer in all cases even in the presence of various functional groups present on the solvent molecule. These results clearly confirmed that synthon **I** is considered to be a robust synthon for the formation of the host-guest assembly with the channel resided by the guest molecules. Variety of new synthons from phosphonic acid and pyrazole were observed in the generation of these supramolecular frameworks. On the other hand, some of the solvates showed synthon polymorphism, which has provided the opportunity to understand the relativity in stability of the solvates on the basis of intermolecular interactions. The presence of bulky and aromatic moiety on the phosphonic acid was also responsible for the change in framework with the upcoming guest molecule. Hence, the network was stabilized via distinct π···π and C–H···π interactions with the successful attempt of producing various solvates, further suggesting the system to be supple that it can accommodate any solvent. Moreover, the flexible feature of APaBPz system has also led to the formation of some ternary co-crystals with *p*-cresol, phenol, 2-NP and 4-NP. The hydrated APaBPz system found to display variety of bigger synthons involving more intermolecular interactions and the solvent molecule itself is responsible for the formation of the framework. Therefore, among all the solvates, it is more stable solvate as deduced by the thermal study. All these solvates display fluorescence quench response towards the emission of the ligand with respect to the guest used due to the electronic interaction of the guest moiety.

Furthermore, two metal organophosphonate were also formed involving solid state transformation. The molecular cationic zero dimensional phosphonomonoester, (ethyl hydrogen (anthracen-9-ylmethyl)phosphonate) based Cu(II) complex, **3o** in the presence of auxillary ligand bidendate pyridyl ($^{2,2'}$BPy). Structurally characterized, it led to the formation of supramolecular porous network with 1D channel. Remarkably, complex **3o** resulted in the formation of complex **3p** via solid state transformation (crystal-amorphous-crystal

transformation), involving the formation of neutral coordination complex from cationic coordination complex on external stimuli. The structural change from porous to non-porous has been evidenced by single-crystal XRD. It is hypothesized that the compound showed the mobility of uncoordinated nitrate ion from the lattice to the metal, hence, resulting in the transformation of cationic metal complex to neutral metal complex and thereby, it may show tunable luminescent behavior.

Table 3.1: Crystal Data and Collection Details of [($HAPa^-$).($HBPz^+$).THF] (3a)

Emprical formula	$C_{29}H_{35}N_4O_4P$
Formula weight	534.58
Crystal system	Monoclinic
Space group	*C2/c*
a/ Å	20.340(3)
b/ Å	14.941(2)
c/ Å	19.649(3)
α/ ^{o}	90
β/ ^{o}	113.02(8)
γ/ ^{o}	90
V / Å^3	5495.7(14)
Z	8
D_{calc} (g cm^{-3})	1.292
μ/mm^{-3}	0.142
θ range/ ^{o}	1.74 - 26.57
Reflections collected	5656
Independent reflections	3176
Parameters/ Restraints	348/0
GOF (F^2)	1.151
R_1; wR_2 [I>2σ(I)]	0.0636; 0.1698
R_1; wR_2 (all data)	0.1281; 0.2082
$\Delta\rho_{max}$; $\Delta\rho_{min}$	0.494; -0.445

Table 3.2: Crystal Data and Collection Details of [($HAPa^-$).($HBPz^+$).dioxane] (3b)

Emprical formula	$C_{29}H_{35}N_4O_5P$
Formula weight	550.58
Crystal system	Monoclinic
Space group	*C2/c*
a/ Å	20.088(13)
b/ Å	15.049(10)
c/ Å	20.142(14)
α/ ^{o}	90
β/ ^{o}	112.84(4)
γ/ ^{o}	90
V / Å^3	5611.9(7)
Z	8
D_{calc} (g cm^{-3})	1.303
μ/mm^{-3}	0.143
θ range/ ^{o}	1.74 - 26.46
Reflections collected	5768
Independent reflections	2490
Parameters/ Restraints	357/4
GOF (F^2)	1.123
R_1; wR_2 [I>2σ(I)]	0.0788; 0.1864
R_1; wR_2 (all data)	0.2009; 0.2426
$\Delta\rho_{max}$; $\Delta\rho_{min}$	0.605; -0.338

Table 3.3: Crystal Data and Collection Details of [($HAPa^-$).($HBPz^+$).benzene] (3c)

Emprical formula	$C_{31}H_{33}N_4O_3P$
Formula weight	540.58
Crystal system	Monoclinic
Space group	*C2/c*
a/ Å	20.046(10)
b/ Å	15.292(8)
c/ Å	19.941(11)
α/ ^{o}	90
β/ ^{o}	112.45(3)
γ/ ^{o}	90
V / Å^3	5649.8(5)
Z	8
D_{calc} (g cm^{-3})	1.271
μ/mm^{-3}	0.136
θ range/ ^{o}	2.20 - 26.57
Reflections collected	5752
Independent reflections	2686
Parameters/ Restraints	316/0
GOF (F^2)	1.063
R_1; wR_2 [I>2σ(I)]	0.0847; 0.2317
R_1; wR_2 (all data)	0.1750; 0.2893
$\Delta\rho_{max}$; $\Delta\rho_{min}$	0.521; -0.357

Table 3.4: Crystal Data and Collection Details of [($HAPa^-$).($HBPz^+$).thiophene] (3d)

Emprical formula	$C_{29}H_{31}N_4O_3PS$
Formula weight	546.62
Crystal system	Monoclinic
Space group	*C2/c*
a/ Å	20.214(17)
b/ Å	14.891(14)
c/ Å	19.186(17)
α/ ^{o}	90
β/ ^{o}	113.47(4)
γ/ ^{o}	90
V / Å^3	5297.7(8)
Z	8
D_{calc} (g cm^{-3})	1.371
μ/mm^{-3}	0.222
θ range/ ^{o}	2.20 - 26.48
Reflections collected	5442
Independent reflections	3240
Parameters/ Restraints	340/30
GOF (F^2)	0.971
R_1; wR_2 [I>2σ(I)]	0.1019; 0.2533
R_1; wR_2 (all data)	0.1635; 0.3010
$\Delta\rho_{max}$; $\Delta\rho_{min}$	0.849; -0.698

Table 3.5: Crystal Data and Collection Details of [($HAPa^-$).($HBPz^+$).nitromethane] (3e)

Emprical formula	$C_{26}H_{30}N_5O_5P$
Formula weight	523.52
Crystal system	Monoclinic
Space group	*C2/c*
a/ Å	20.456(17)
b/ Å	14.476(13)
c/ Å	19.163(3)
α/ ^{o}	90
β/ ^{o}	114.35(3)
γ/ ^{o}	90
V / Å^3	5169.6(10)
Z	8
D_{calc} (g cm^{-3})	1.345
μ/mm^{-3}	0.153
θ range/ ^{o}	1.78 - 28.32
Reflections collected	6435
Independent reflections	5093
Parameters/ Restraints	340/0
GOF (F^2)	1.663
R_1; wR_2 [I>2σ(I)]	0.0652; 0.2104
R_1; wR_2 (all data)	0.0849; 0.2260
$\Delta\rho_{max}$; $\Delta\rho_{min}$	1.434; -0.831

Table 3.6: Crystal Data and Collection Details of [$(HAPa^-)_2$.$(HBPz^+)_2$.nitrobenz.H_2O] (3f)

Emprical formula	$C_{56}H_{59}N_9O_9P_2$
Formula weight	1064.06
Crystal system	Monoclinic
Space group	$P2_1/n$
a/ Å	19.287(18)
b/ Å	14.790(14)
c/ Å	21.692(18)
α/ ^{o}	90
β/ ^{o}	121.17(6)
γ/ ^{o}	90
V / Å^3	5294.9(9)
Z	4
D_{calc} (g cm^{-3})	1.335
μ/mm^{-3}	0.149
θ range/ ^{o}	1.23 - 28.43
Reflections collected	13191
Independent reflections	8183
Parameters/ Restraints	681/6
GOF (F^2)	1.020
R_1; wR_2 [I>2σ(I)]	0.0675; 0.1838
R_1; wR_2 (all data)	0.1163; 0.2285
$\Delta\rho_{max}$; $\Delta\rho_{min}$	1.416; -0.662

Table 3.7: Crystal Data and Collection Details of [$(HAPa^-)_2.(HBPz^+)_2$.thiophenol] (3g)

Emprical formula	$C_{56}H_{60}N_8O_6P_2S$
Formula weight	1035.13
Crystal system	Monoclinic
Space group	$P2_1/n$
a/ Å	19.253(9)
b/ Å	14.886(6)
c/ Å	20.281(9)
α/ ^{o}	90
β/ ^{o}	113.63(14)
γ/ ^{o}	90
V / Å^3	5325.0(4)
Z	4
D_{calc} (g cm^{-3})	1.291
μ/mm^{-3}	0.179
θ range/ ^{o}	1.75 - 28.28
Reflections collected	13150
Independent reflections	8971
Parameters/ Restraints	627/0
GOF (F^2)	1.018
R_1; wR_2 [I>2σ(I)]	0.0808; 0.2255
R_1; wR_2 (all data)	0.1171; 0.2622
$\Delta\rho_{max}$; $\Delta\rho_{min}$	1.098; -0.516

Table 3.8: Crystal Data and Collection Details of [$(HAPa^-)_2$.$(HBPz^+)_2$.toluene] (3h)

Emprical formula	$C_{57}H_{62}N_8O_6P_2$
Formula weight	1017.09
Crystal system	Monoclinic
Space group	$P2_1/n$
a/ Å	19.364(5)
b/ Å	15.147(4)
c/ Å	20.207(5)
α/ ^{o}	90
β/ ^{o}	113.00(1)
γ/ ^{o}	90
V / Å^3	5455.9(2)
Z	4
D_{calc} (g cm^{-3})	1.238
μ/mm^{-3}	0.137
θ range/ ^{o}	1.24 - 26.55
Reflections collected	11322
Independent reflections	7383
Parameters/ Restraints	622/0
GOF (F^2)	1.048
R_1; wR_2 [I>2σ(I)]	0.0648; 0.1953
R_1; wR_2 (all data)	0.1052; 0.2352
$\Delta\rho_{max}$; $\Delta\rho_{min}$	0.681; -0.652

Table 3.9: Crystal Data and Collection Details of [$(HAPa^-)_2.(HBPz^+)_2$,*p*-cresol.H_2O] (3i)

Emprical formula	$C_{57}H_{62}N_8O_8P_2$
Formula weight	1049.09
Crystal system	Monoclinic
Space group	$P2_1/c$
a/ Å	19.219(3)
b/ Å	14.730(2)
c/ Å	21.630(3)
α/ ^{o}	90
β/ ^{o}	120.47(10)
γ/ ^{o}	90
V / Å^3	5277.5(14)
Z	4
D_{calc} (g cm^{-3})	1.320
μ/mm^{-3}	0.146
θ range/ ^{o}	1.23 - 28.37
Reflections collected	13138
Independent reflections	9739
Parameters/ Restraints	676/0
GOF (F^2)	0.918
R_1; wR_2 [I>2σ(I)]	0.0756; 0.2091
R_1; wR_2 (all data)	0.1025; 0.2446
$\Delta\rho_{max}$; $\Delta\rho_{min}$	1.472; -1.323

Table 3.10: Crystal Data and Collection Details of [$(HAPa^{-}).(H_2BPz^{2+})_{0.5}$.phenol] (3j)

Emprical formula	$C_{26}H_{26}N_2O_4P$
Formula weight	461.46
Crystal system	Monoclinic
Space group	*C2/c*
a/ Å	25.059(9)
b/ Å	8.046(3)
c/ Å	22.871(8)
α/ ^{o}	90
β/ ^{o}	94.48(2)
γ/ ^{o}	90
V / Å^3	4597.7(3)
Z	8
D_{calc} (g cm^{-3})	1.333
μ/mm^{-3}	0.156
θ range/ ^{o}	1.63 - 26.48
Reflections collected	4746
Independent reflections	3398
Parameters/ Restraints	302/0
GOF (F^2)	1.094
R_1; wR_2 [I>2σ(I)]	0.0451; 0.1328
R_1; wR_2 (all data)	0.0745; 0.1614
$\Delta\rho_{max}$; $\Delta\rho_{min}$	0.418; -0.522

Table 3.11: Crystal Data and Collection Details of [$(HAPa^-)_2.H_2BPz^{2+}$.2-NP.*n*-butanol] (3k)

Emprical formula	$C_{50}H_{55}N_5O_{10}P_2$
Formula weight	947.93
Crystal system	Monoclinic
Space group	$P2_1/n$
a/ Å	13.499(3)
b/ Å	23.846(5)
c/ Å	15.894(3)
α/ ^{o}	90
β/ ^{o}	109.55(1)
γ/ ^{o}	90
V / Å^3	4821.2(18)
Z	4
D_{calc} (g cm^{-3})	1.306
μ/mm^{-3}	0.154
θ range/ ^{o}	1.61 - 28.31
Reflections collected	11976
Independent reflections	6277
Parameters/ Restraints	605/1
GOF (F^2)	1.286
R_1; wR_2 [I>2σ(I)]	0.0734; 0.2007
R_1; wR_2 (all data)	0.1529; 0.2356
$\Delta\rho_{max}$; $\Delta\rho_{min}$	0.634; -0.676

Table 3.12: Crystal Data and Collection Details of [$(HAPa^-)_2.H_2BPz^{2+}$.4-NP.S], (squeezed) (3l)

Emprical formula	$C_{50}H_{55}N_5O_{10}P_2$
Formula weight	947.95
Crystal system	Monoclinic
Space group	$P2_1/c$
a/ Å	13.572(3)
b/ Å	23.537(6)
c/ Å	17.178(4)
α/ ^{o}	90
β/ ^{o}	118.96(16)
γ/ ^{o}	90
V / Å^3	4801.0(2)
Z	4
D_{calc} (g cm^{-3})	1.209
μ/mm^{-3}	0.147
θ range/ ^{o}	1.61 - 19.32
Reflections collected	38128
Independent reflections	4039
Parameters/ Restraints	551/0
GOF (F^2)	1.144
R_1; wR_2 [I>2σ(I)]	0.0682; 0.1903
R_1; wR_2 (all data)	0.0805; 0.2007
$\Delta\rho_{max}$; $\Delta\rho_{min}$	0.583; -0.327

Table 3.13: Crystal Data and Collection Details of $[(HAPa^-)_2.(HBPz^+)_2.(H_2APa)_2.H_2O]$ (3m)

Emprical formula	$C_{80}H_{80}N_8O_{13}P_4$
Formula weight	1485.40
Crystal system	Triclinic
Space group	*P*-1
a/ Å	12.826(15)
b/ Å	15.732(18)
c/ Å	21.183(3)
α/ ^{o}	71.81(5)
β/ ^{o}	80.10(5)
γ/ ^{o}	67.03(5)
V / Å^3	3733.1(8)
Z	2
D_{calc} (g cm^{-3})	1.321
μ/mm^{-3}	0.171
θ range/ ^{o}	1.01 - 25.00
Reflections collected	12984
Independent reflections	8557
Parameters/ Restraints	960/0
GOF (F^2)	1.104
R_1; wR_2 [I>2σ(I)]	0.0555; 0.1520
R_1; wR_2 (all data)	0.0933; 0.1841
$\Delta\rho_{max}$; $\Delta\rho_{min}$	0.545; -0.480

Table 3.14: Crystal Data and Collection Details of ethyl hydrogen (anthracen-9-ylmethyl)phosphonate, (3n)

Emprical formula	$C_{17}H_{16}O_3P$
Formula weight	299.27
Crystal system	Monoclinic
Space group	*C2/c*
a/ Å	31.668(16)
b/ Å	8.637(4)
c/ Å	11.442(6)
α/ ^{o}	90
β/ ^{o}	102.52(3)
γ/ ^{o}	90
V / Å^3	3055.0(3)
Z	8
D_{calc} (g cm^{-3})	1.301
μ/mm^{-3}	0.187
θ range/ ^{o}	1.32 - 30.30
Reflections collected	3906
Independent reflections	1647
Parameters/ Restraints	191/0
GOF (F^2)	1.013
R_1; wR_2 [I>2σ(I)]	0.0684; 0.1782
R_1; wR_2 (all data)	0.1860; 0.2355
$\Delta\rho_{max}$; $\Delta\rho_{min}$	0.366; -0.387

Table 3.15: Crystal Data and Collection Details of $[Cu_2(\mu_2\text{-}C_{15}H_{12}PO_3)_2(^{2,2'}BPy)_2(H_2O)_2]((NO_3)_2.X)$, (3o) (squeezed)

Emprical formula	$C_{56}H_{60}Cu_2N_6O_{14}P_2$
Formula weight	1230.15
Crystal system	Triclinic
Space group	*P*-1
a/ Å	11.543(2)
b/ Å	11.603(2)
c/ Å	12.615(2)
α/ ^{o}	69.35(10)
β/ ^{o}	63.37(1)
γ/ ^{o}	78.51(12)
V / Å^3	1411.6(5)
Z	1
D_{calc} (g cm^{-3})	1.354
μ/mm^{-3}	0.873
θ range/ ^{o}	2.23 - 26.44
Reflections collected	5705
Independent reflections	3812
Parameters/ Restraints	352/10
GOF (F^2)	0.990
R_1; wR_2 [I>2σ(I)]	0.0470; 0.1100
R_1; wR_2 (all data)	0.0786; 0.1189
$\Delta\rho_{max}$; $\Delta\rho_{min}$	0.295; -0.406

Table 3.16: Crystal Data and Collection Details of [$Cu_2(\mu_2$-$C_{15}H_{12}PO_3)_2(^{2,2'}BPy)_2(NO_3)_2$].MeOH, (3p)

Emprical formula	$C_{56}H_{56}Cu_2N_6O_{14}P_2$
Formula weight	1226.11
Crystal system	Monoclinic
Space group	$P2_1/c$
a/ Å	11.129(3)
b/ Å	14.638(4)
c/ Å	16.334(4)
α/ ^{o}	90
β/ ^{o}	90.25(10)
γ/ ^{o}	90
V / Å^3	2660.9(12)
Z	2
D_{calc} (g cm^{-3})	1.530
μ/mm^{-3}	0.934
θ range/ ^{o}	2.30 - 28.62
Reflections collected	6702
Independent reflections	4775
Parameters/ Restraints	374/0
GOF (F^2)	0.834
R_1; wR_2 [I>2σ(I)]	0.0389; 0.1070
R_1; wR_2 (all data)	0.0702; 0.1312
$\Delta\rho_{max}$; $\Delta\rho_{min}$	0.594; -0.877

Table 3.17: Non-covalent interactions for 3a-3m (Å and ^{o})

D-H···A	d(D-H)	d(H-A)	d(D-A)	<(DHA)>	Symmetery codes
[(HAPa^{-}).(HBPz^{+}).THF] (3a)					
N2–H2D···O3	0.860(3)	1.957(2)	2.817(4)	179.0	x+1/2,+y+1/2,+z
N3–H3D···O2	0.859(3)	1.822(3)	2.673(5)	170.6	-
N4–H4D···O2	0.861(3)	1.909(3)	2.719(4)	156.2	-x+1,+y,-z+1/2
O1–H1E···O3	0.819(4)	1.849(9)	2.649(13)	164.6	-x+1/2,-y+1/2,-z
[(HAPa^{-}).(HBPz^{+}).dioxane] (3b)					
N1–H1D···O3	0.860(5)	1.944(3)	2.802(6)	176.5	x,-y+2,+z+1/2
N3–H3D···O2	0.860(4)	1.915(3)	2.724(6)	156.1	-x+1/2,-y+1/2+1,-z+1
N4–H4D···O2	0.861(4)	1.807(3)	2.664(5)	173.1	x+1/2,-y+1/2+1,+z+1/2
O1–H1E···O3	0.819(3)	1.824(5)	2.628(7)	166.4	-x+1/2,-y+1/2+1,-z+1
[(HAPa^{-}).(HBPz^{+}).benzene] (3c)					
N1–H1D···O2	0.861(6)	1.960(3)	2.821(7)	177.9	x+1/2,+y+1/2,+z
N3–H3D···O3	0.859(4)	1.806(3)	2.662(5)	174.0	-
N4–H4D···O3	0.862(4)	1.897(3)	2.723(5)	160.1	-x+1,+y,-z+1/2
O1–H1E···O2	0.821(3)	1.840(4)	2.637(6)	163.4	-x+1/2,-y+1/2+1,-z
[(HAPa^{-}).(HBPz^{+}).thiophene] (3d)					
N1–H1D···O1	0.859(4)	1.794(3)	2.641(6)	168.2	-x+1,+y,-z+1/2
N2–H2D···O1	0.860(6)	1.854(4)	2.670(7)	151.0	-

N3–H3D···O2	0.860(6)	1.947(3)	2.804(7)	173.7	-x+1/2,+y-1/2,-z+1/2
O3–H3E···O2	0.820(3)	1.800(5)	2.605(7)	167.0	-x+1/2,-y+1/2+1,-z
[($HAPa^-$).($HBPz^+$).nitromethane] (3e)					
N1–H1D···O1	0.860(2)	1.835(2)	2.675(3)	165.3	-x+1,+y,-z+1/2
N2–H2D···O1	0.861(2)	1.896(2)	2.676(3)	149.8	-
N4–H4D···O2	0.861(2)	1.946(2)	2.798(3)	169.9	x,+y+1,+z
O3–H3E···O2	0.819(2)	1.771(3)	2.578(5)	168.2	-x+1/2,+y+1/2,-z+1/2
[($HAPa^-$)$_2$.($HBPz^+$)$_2$.nitrobenz.H_2O] (3f)					
N1–H1D···O6	0.859(3)	1.834(2)	2.672(4)	164.7	x+1,+y,+z
N2–H2D···O1	0.860(4)	1.805(7)	2.650(11)	167.0	x+1,-y+1/2+1,+z+1/2
N3–H3D···O5	0.859(3)	1.910(3)	2.767(4)	175.3	-x+1,+y+1/2,-z+1/2+1
N5–H5D···O6	0.860(4)	1.797(8)	2.644(12)	142.0	x,+y,+z-1
N6–H6D···O1	0.859(3)	1.948(3)	2.678(4)	168.2	x,-y+1/2+1,+z-1/2
N7–H7D···O3	0.860(3)	1.940(2)	2.794(4)	171.2	x,-y+1/2+1,+z-1/2
O2–H2E···O5	0.820(3)	1.792(4)	2.601(6)	168.5	-
O4–H4E···O3	0.819(3)	1.797(4)	2.606(6)	168.9	-
[($HAPa^-$)$_2$.($HBPz^+$)$_2$.thiophenol] (3g)					
O1–H1E···O5	0.821(5)	1.801(15)	2.607(20)	167.0	-
O6–H6E···O2	0.821(6)	1.798(15)	2.604(21)	166.6	-
N2–H2D···O5	0.860(3)	1.939(3)	2.795(5)	173.0	-x+1,-y+1,-z+1
N3–H3D···O3	0.861(4)	1.817(3)	2.660(6)	165.8	-

N4–H4D···O4	0.860(3)	1.855(3)	2.687(5)	162.0	x+1/2,-y+1/2,+z+1/2
N5–H5D···O4	0.860(3)	1.795(4)	2.646(7)	170.0	x,+y,+z+1
N6–H6D···O3	0.860(3)	1.943(4)	2.671(6)	141.6	x-1/2,-y+1/2,+z+1/2
N7–H7D···O2	0.860(3)	1.945(2)	2.799(4)	171.9	-x+1,-y,-z+1
[$(HAPa^-)_2$.$(HBPz^+)_2$.toluene] (3h)					
N1–H1D···O4	0.859(3)	1.828(2)	2.684(4)	174.7	-x+1/2,+y+1/2,-z+1/2+1
N2–H2D···O3	0.861(2)	1.809(2)	2.662(3)	170.7	x,+y,+z+1
N3–H3D···O5	0.860(3)	1.956(2)	2.811(4)	172.3	x,+y+1,+z
N5–H5D···O3	0.859(3)	1.933(2)	2.693(4)	146.9	x,+y,+z+1
N6–H6D···O4	0.861(2)	1.788(2)	2.645(3)	172.7	-
N8–H8D···O2	0.861(3)	1.954(2)	2.812(4)	174.4	-
O1–H1E···O5	0.820(2)	1.842(2)	2.631(3)	161.1	-x+1,-y+1,-z+1
O6–H6E···O2	0.820(2)	1.820(2)	2.623(3)	166.0	-x+1,-y+1,-z+1
[$(HAPa^-)_2$.$(HBPz^+)_2$.*p*-cresol.H_2O] (3i)					
N2–H2D···O5	0.859(3)	1.918(4)	2.770(5)	170.7	-x,-y+2,-z+1
N3–H3D···O3	0.861(6)	1.807(11)	2.650(18)	166.2	x,-y+1/2+1,+z+1/2
N4–H4D···O6	0.860(3)	1.840(3)	2.673(4)	162.4	x+1,-y+1/2+1,+z+1/2
N5–H5D···O3	0.859(3)	1.921(4)	2.668(5)	144.6	x-1,+y,+z
N6–H6D···O6	0.860(7)	1.809(13)	2.657(19)	168.6	-
N7–H7D···O2	0.860(3)	1.944(3)	2.797(4)	171.8	-x+1,+y-1/2,-z+1/2+1
O1–H1E···O5	0.821(4)	1.786(6)	2.595(10)	168.2	x+1,-y+1/2+1,+z+1/2

O4–H4E···O2	0.821(4)	1.790(6)	2.598(9)	167.6	x-1,-y+1/2+1,+z-1/2
O8–H8Z···N1	0.821(5)	2.168(6)	2.965(9)	163.6	x,-y+1/2+1,+z-1/2
[($HAPa^-$).(H_2BPz^{2+})$_{0.5}$.phenol] (3j)					
N1–H1D···O3	0.860(2)	1.743(2)	2.591(3)	168.1	-
N2–H2D···O2	0.860(2)	1.827(2)	2.672(2)	166.9	-x+1,-y+1,-z
O1–H1E···O2	0.820(2)	1.817(1)	2.621(2)	166.2	-x+1,-y,-z
O4–H4Z···O3	0.819(2)	1.930(1)	2.732(2)	169.8	-x+1/2,-y+1/2+1,-z
[($HAPa^-$)$_2$.H_2BPz^{2+}.2-NP.*n*-butanol] (3k)					
N1–H1D···O4	0.835(37)	1.738(37)	2.566(4)	170.9	x+1/2,-y+1/2,+z+1/2
N2–H2D···O2	0.860(3)	1.846(2)	2.670(3)	160.0	-
N3–H3D···O5	0.861(3)	1.866(2)	2.716(3)	169.3	x+1,+y,+z
N4–H4D···O3	0.860(3)	1.679(2)	2.537(4)	175.4	x+1/2,-y+1/2,+z-1/2
O1–H1E···O5	0.820(2)	1.764(2)	2.561(3)	163.9	-
O6–H6E···O2	0.819(2)	1.838(2)	2.610(3)	156.6	-
O7–H7Z···O9	0.820(10)	2.682(2)	3.358(11)	140.9	-x,-y,-z+2
[($HAPa^-$)$_2$.H_2BPz^{2+}.4-NP.S] (3l)					
N4–H4D···O6	0.859(6)	1.838(5)	2.675(8)	164.5	x-1,+y,+z
N3–H3D···O1	0.860(11)	1.734(23)	2.580(33)	167.2	x,-y+1/2,+z-1/2
O3–H3E···O6	0.818(7)	1.814(8)	2.612(15)	164.5	x-1,+y,+z
N2–H2D···O5	0.859(12)	1.720(23)	2.578(34)	175.6	x,-y+1/2,+z+1/2
O4–H4E···O2	0.818(7)	1.756(15)	2.554(15)	164.6	x+1,+y,+z

N1–H1D···O2	0.859(6)	1.862(9)	2.714(7)	171.2	x+1,+y,+z
$[(HAPa^-)_2.(HBPz^+)_2.(H_2APa)_2.H_2O]$ (3m)					
N2–H2D···O10	0.861(3)	2.077(5)	2.892(5)	157.8	x+1,+y,+z
N3–H3D···O13	0.860(3)	1.847(4)	2.657(6)	156.2	-
N4–H4D···O12	0.860(3)	1.738(3)	2.577(5)	164.3	-
N5–H5D···O1	0.860(3)	1.758(4)	2.612(6)	172.1	-
N6–H6D···O6	0.861(4)	1.837(4)	2.658(6)	158.9	-x+1,-y+1,-z+1
N8–H8D···O2	0.861(3)	2.002(4)	2.840(7)	164.3	x-1,+y,+z
O3–H3E···O10	0.820(3)	1.752(4)	2.556(5)	165.8	-
O5–H5E···O1	0.820(4)	1.741(5)	2.540(5)	164.5	-
O8–H8E···N1	0.819(3)	1.797(5)	2.576(6)	157.9	x-1,+y-1,+z
O9–H9E···O12	0.820(4)	1.745(7)	2.564(11)	178.2	x,+y-1,+z
O11–H11E···O2	0.820(3)	1.724(4)	2.550(6)	168.0	-

Table 3.18: Bond distances and angles for complex 3o (Å and °)

$[Cu_2(\mu_2\text{-}C_{15}H_{12}PO_3)_2(^{2,2'}BPy)_2(H_2O)_2]((NO_3)_2.X)$ (3o)			
Bond Distances			
Cu(II)–O3	1.932(14)	Cu(II)–$O1^{\#1}$	1.944(12)
Cu(II)–N1	2.008(15)	Cu(II)–N2	2.018(9)
Cu(II)–O4	2.247(13)		
Bond Angles			
O3–Cu(II)–N2	90.43(13)	N2–Cu(II)–O4	99.46(15)
O3–Cu(II)–O4	93.82(13)	$O1^{\#1}$–Cu(II)–N1	93.42(12)
N1–Cu(II)–N2	80.31(14)	$O1^{\#1}$–Cu(II)–O4	93.75(13)
N1–Cu(II)–O4	94.07(15)	O3–Cu(II)–$O1^{\#1}$	94.11(10)
O3–Cu(II)–N1	168.71(13)	$O1^{\#1}$–Cu(II)–N2	165.72(11)

Symmetry codes for Complex 3o: 1-x, -y, 1-z (#1)

Table 3.19: Bond distances and angles for complex 3p (Å and °)

$[Cu_2(\mu_2\text{-}C_{15}H_{12}PO_3)_2(^{2,2'}BPy)_2(NO_3)_2]$.MeOH (3p)			
Bond Distances			
Cu(II)–O1	1.957(3)	Cu(II)–O3	1.934(9)
Cu(II)–O4	2.283(8)	Cu(II)–N1	1.993(2)
Cu(II)–N2	1.989(9)		
Bond Angles			
O1–Cu(II)–N2	93.74(8)	O1–Cu(II)–O4	88.75(7)
O3–Cu(II)–O1	93.43(7)	O3–Cu(II)–N1	90.87(8)
O3–Cu(II)–O4	91.66(7)	N2–Cu(II)–N1	81.24(8)
O3–Cu(II)–N2	171.70(8)	N2–Cu(II)–O4	92.67(15)
N1–Cu(II)–O4	103.45(7)	O1–Cu(II)–N1	166.95(8)

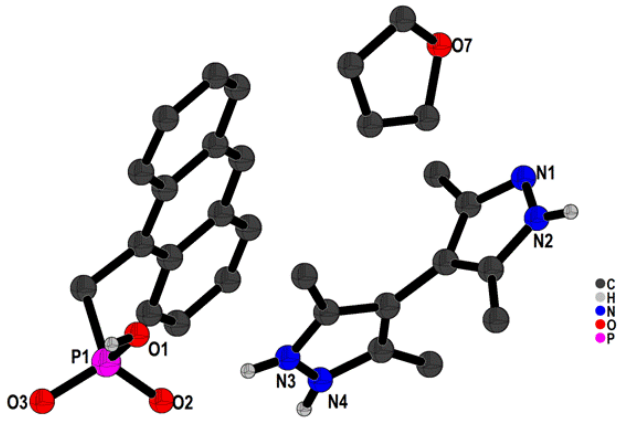

Fig. 3.19: Crystal structure of [($HAPa^-$).($HBPz^+$).THF] (**3a**). (C–H bonds are not shown for clarity)

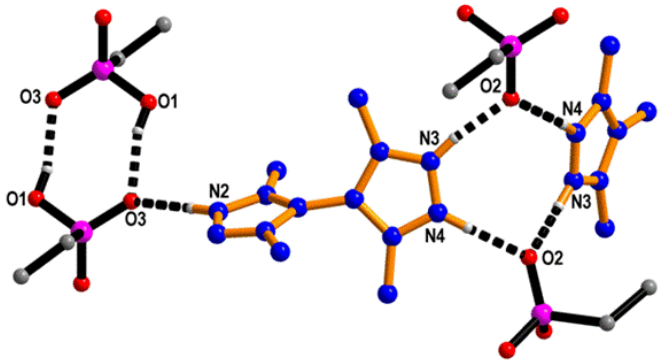

Fig. 3.20: Intermolecular non-covalent interaction in solvate **3a** sustaining synthons **I** and **II**

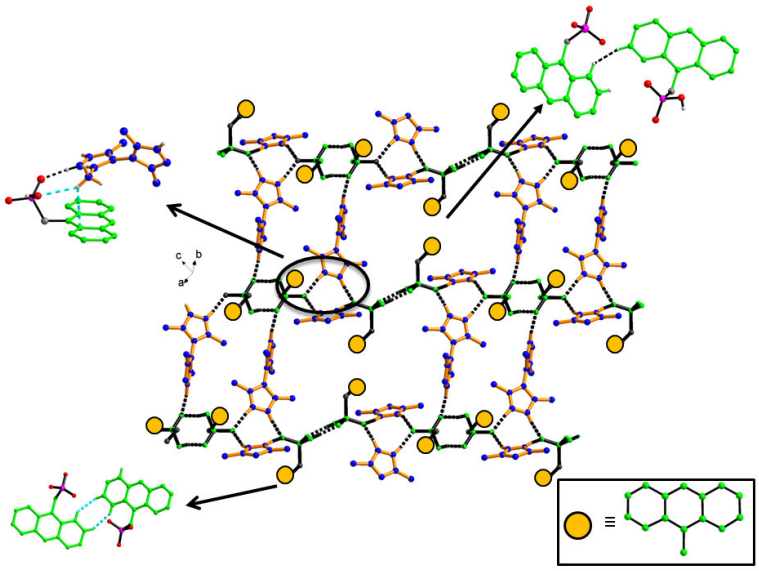

Fig. 3.21: View of 2D sheet displaying synthons **I** and **II**; showing interaction between $HAPa^-$ and $HBPz^+$ in **3a** and representing **type I** hydrogen bonded sheet. (Note: anthracene moiety of the phosphonic acid has been shown by a yellow circle for clarity)

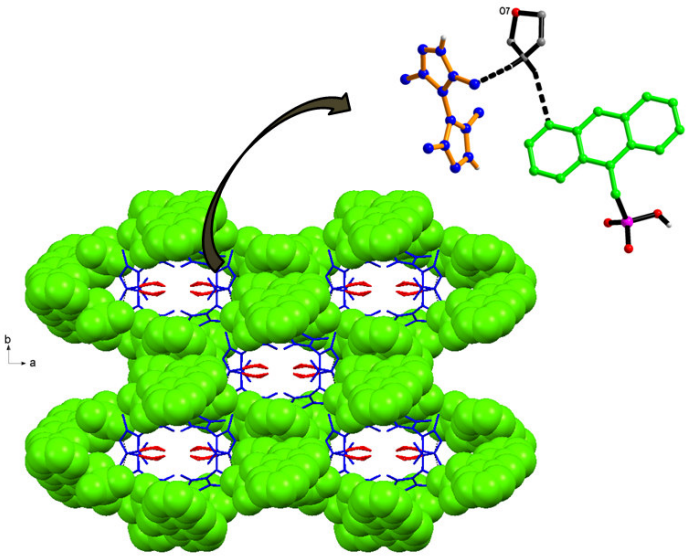

Fig. 3.22: Representation of 3D supramolecular hydrogen bonded porous framework of $HAPa^-$ (green color) and $HBPz^+$ (blue color) with THF molecules (red color) residing inside the cavity in **3a**

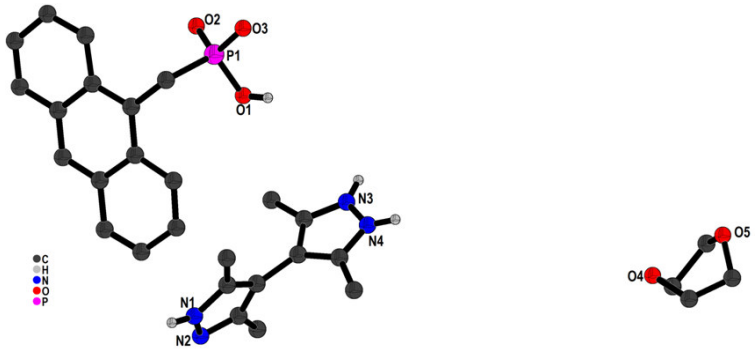

Fig. 3.23: Crystal structure of [($HAPa^-$).($HBPz^+$).dioxane] (**3b**). (C–H bonds are not shown for clarity)

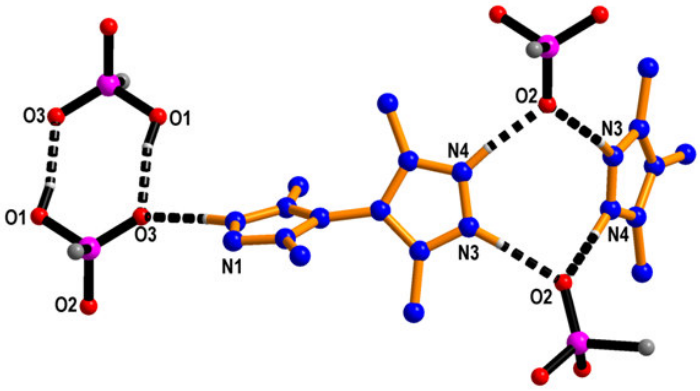

Fig. 3.24: Intermolecular non-covalent interaction in solvate **3b** sustaining synthons **I** and **II**

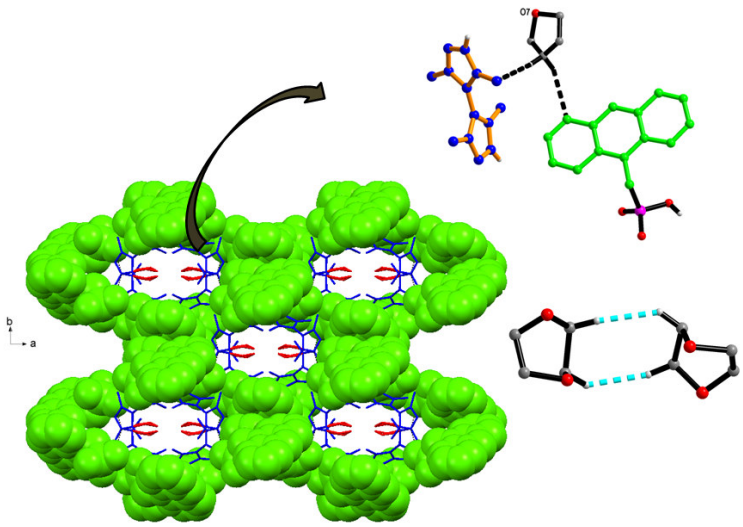

Fig. 3.25: Representation of 3D supramolecular hydrogen bonded porous framework of $HAPa^-$ (green color) and $HBPz^+$ (blue color) with dioxane molecules (red color) residing inside the cavity in **3b**

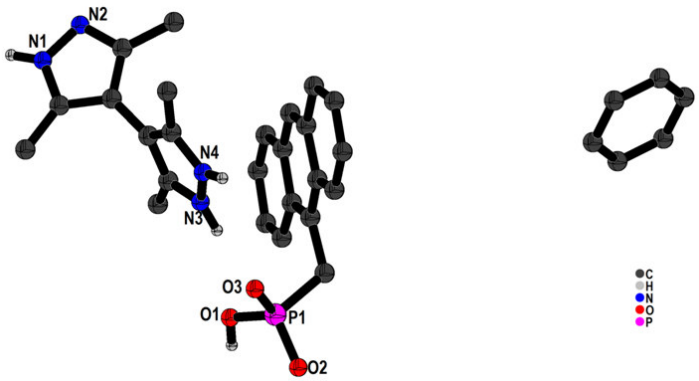

Fig. 3.26: Crystal structure of [($HAPa^-$).($HBPz^+$).benzene] (**3c**). (C–H bonds are not shown for clarity)

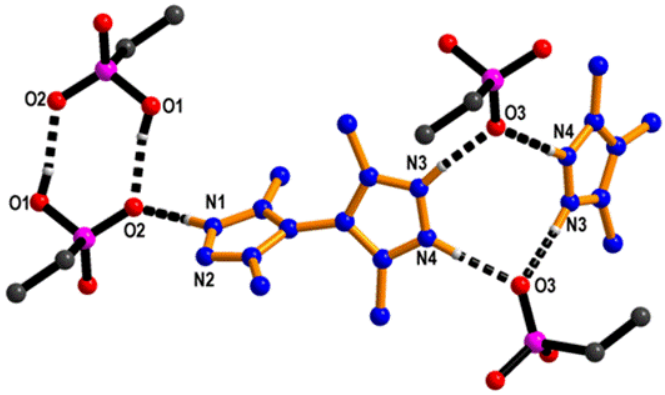

Fig. 3.27: Intermolecular non-covalent interaction in solvate **3c** sustaining synthons **I** and **II**

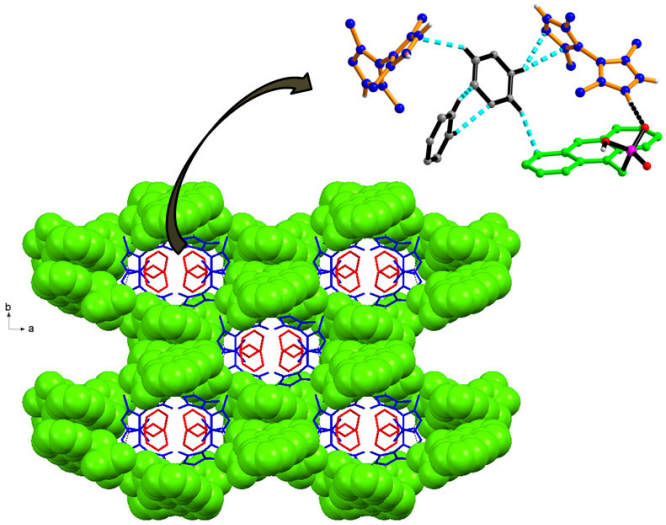

Fig. 3.28: Representation of 3D supramolecular hydrogen bonded porous framework of $HAPa^-$ (green color) and $HBPz^+$ (blue color) with benzene molecules (red color) residing inside the cavity in **3c**

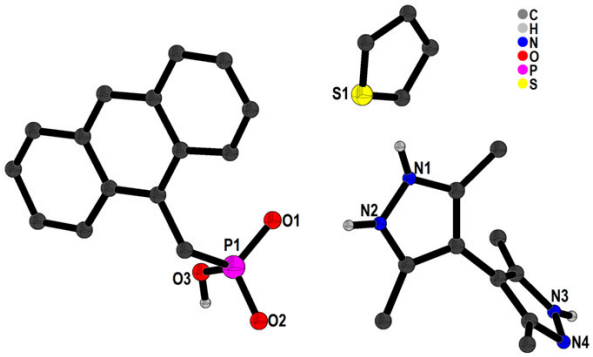

Fig. 3.29: Crystal structure of [($HAPa^-$).($HBPz^+$).thiophene] (**3d**). (C-H bonds are not shown for clarity)

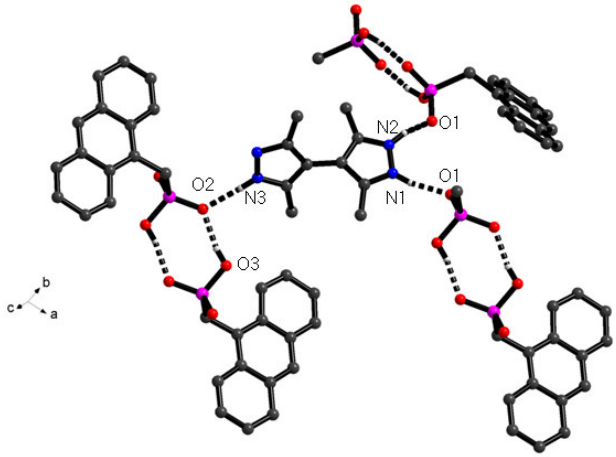

Fig. 3.30: Intermolecular non-covalent interaction in solvate **3d**

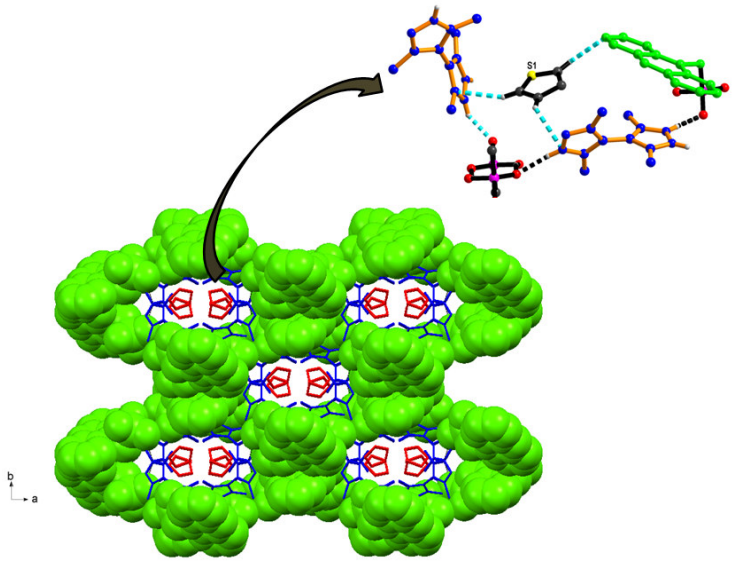

Fig. 3.31: Representation of 3D supramolecular hydrogen bonded porous framework of $HAPa^-$ (green color) and $HBPz^+$ (blue color) with thiophene molecules (red color) residing inside the cavity in **3d**

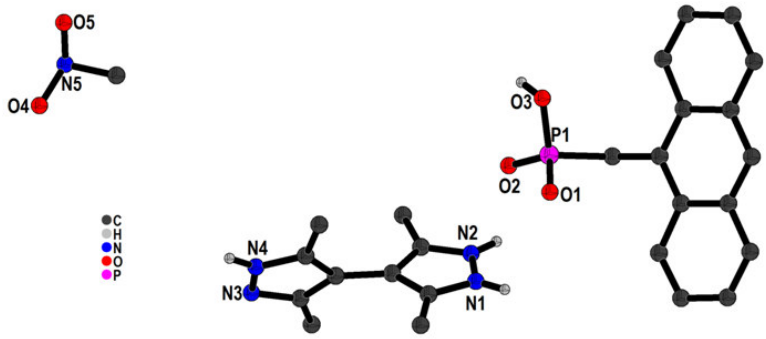

Fig. 3.32: Crystal structure of [($HAPa^-$).($HBPz^+$).nitromethane] (**3e**). (C–H bonds are not shown for clarity)

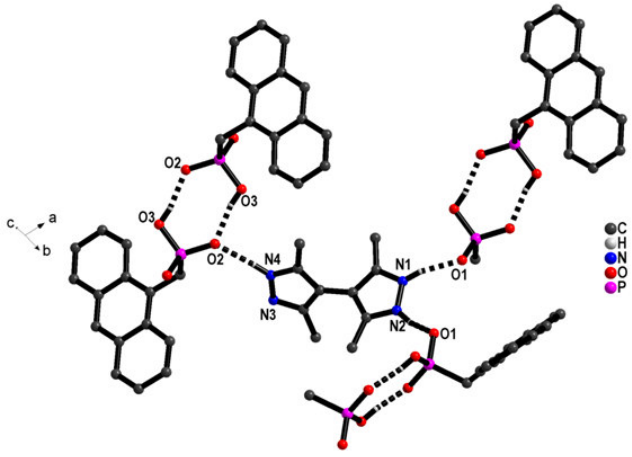

Fig. 3.33: Intermolecular non-covalent interaction in solvate **3f**

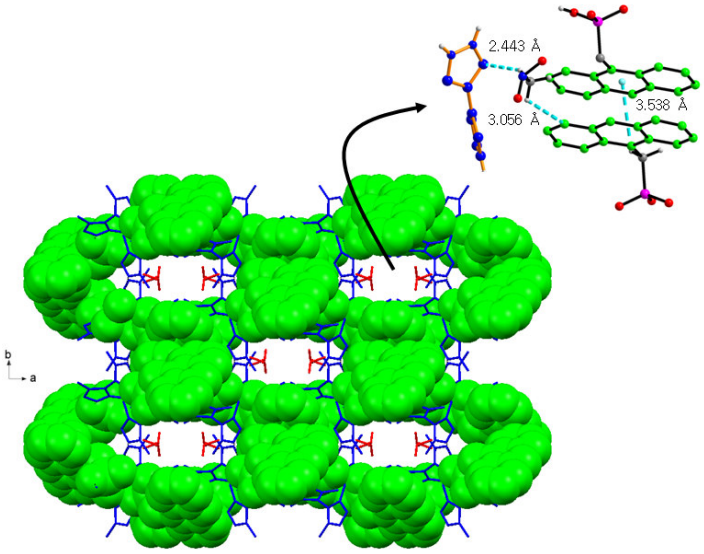

Fig. 3.34: Representation of 3D supramolecular hydrogen bonded porous framework of $HAPa^-$ (green color) and $HBPz^+$ (blue color) with nitromethane molecules (red color) residing inside the cavity in **3e**

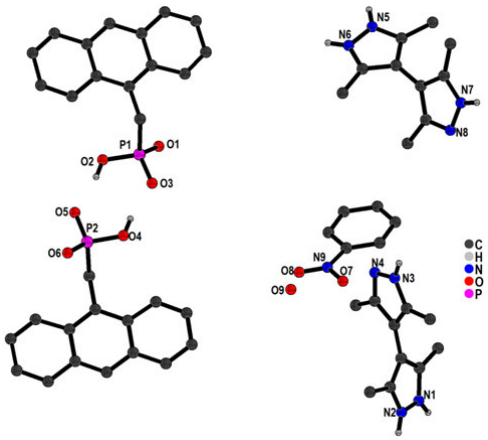

Fig. 3.35: Crystal structure of $[(HAPa^-)_2.(HBPz^+)_2.nitrobenz.H_2O]$ (**3**f). (C–H bonds are not shown for clarity)

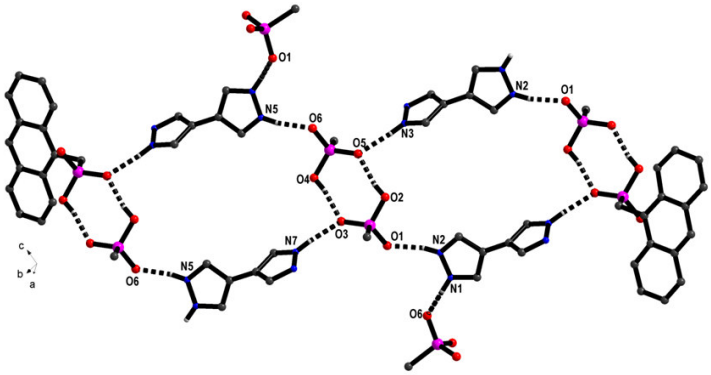

Fig. 3.36: View of 1D tape in *ab*-plane displaying $HBPz^+$ bridging the adjacent dimer **I** and synthon **II** in **3f**

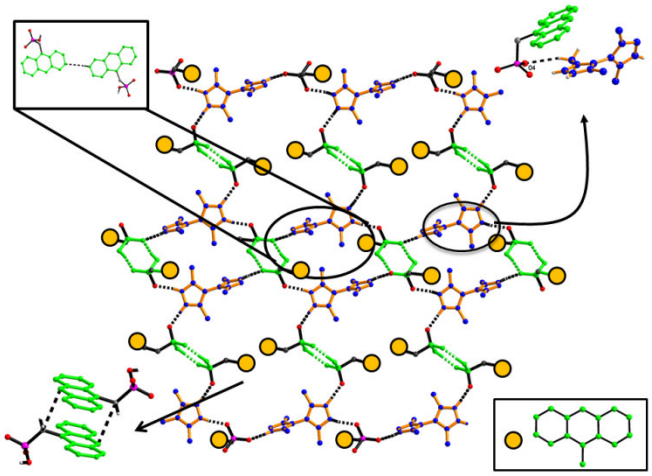

Fig. 3.37: View of 2D sheet displaying synthon **I** and various secondary intermolecular interactions such as C–H···O, N–H···O and C–H···π interaction in **3f** and representing **type II** hydrogen bonded sheet

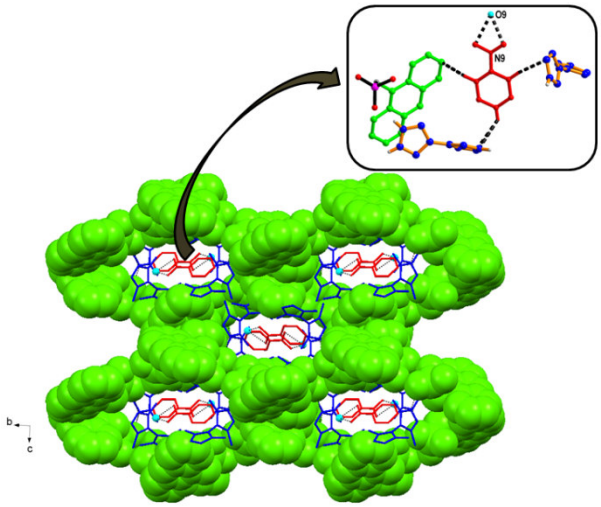

Fig. 3.38: Representation of 3D supramolecular hydrogen bonded porous framework of $HAPa^-$ (green color) and $HBPz^+$ (blue color), nitrobenzene molecules (red color) residing inside the cavity in **3f**

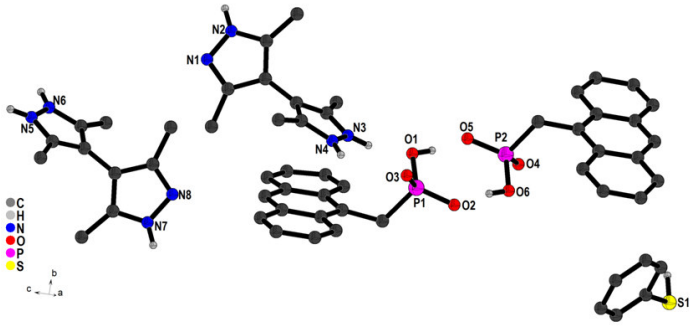

Fig. 3.39: Crystal structure of [$(HAPa^-)_2$.$(HBPz^+)_2$.thiophenol] (**3g**). (C–H bonds are not shown for clarity)

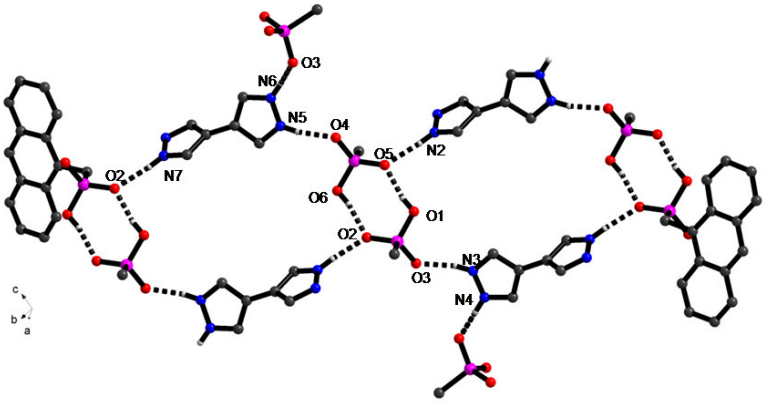

Fig. 3.40: View of 1D tape in *ab*-plane displaying $HBPz^+$ bridging the adjacent dimer **I** in **3g**

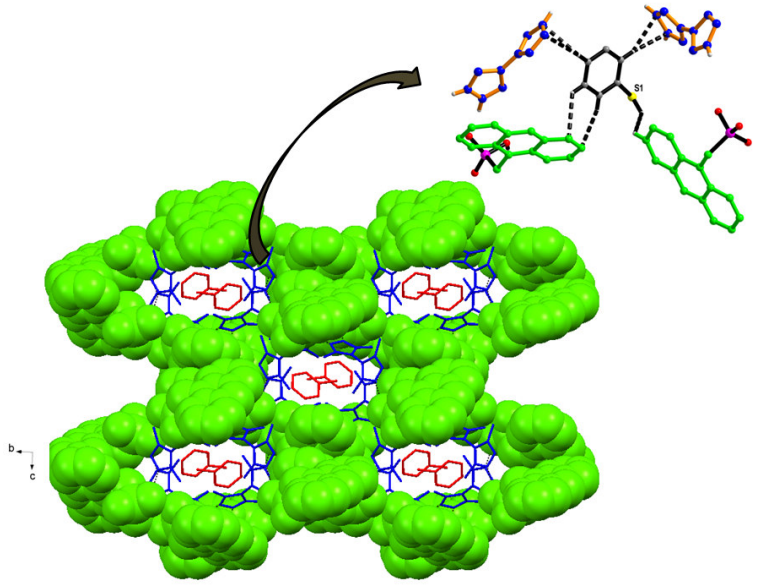

Fig. 3.41: Representation of 3D supramolecular hydrogen bonded porous framework of $HAPa^-$ (green color) and $HBPz^+$ (blue color) with thiophenol molecules (red color) residing inside the cavity in **3g**

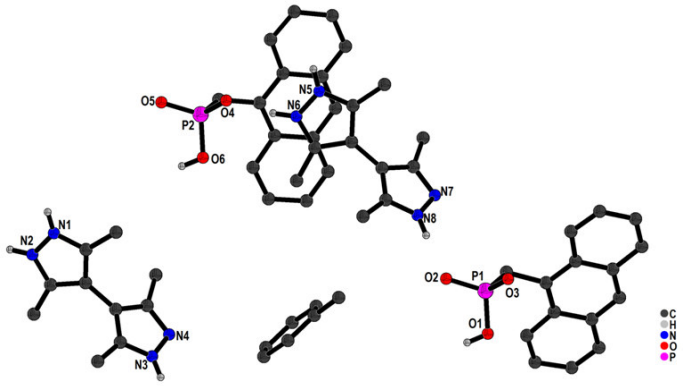

Fig. 3.42: Crystal structure of $[(HAPa^-)_2.(HBPz^+)_2.toluene]$ (**3h**). (C–H bonds are not shown for clarity)

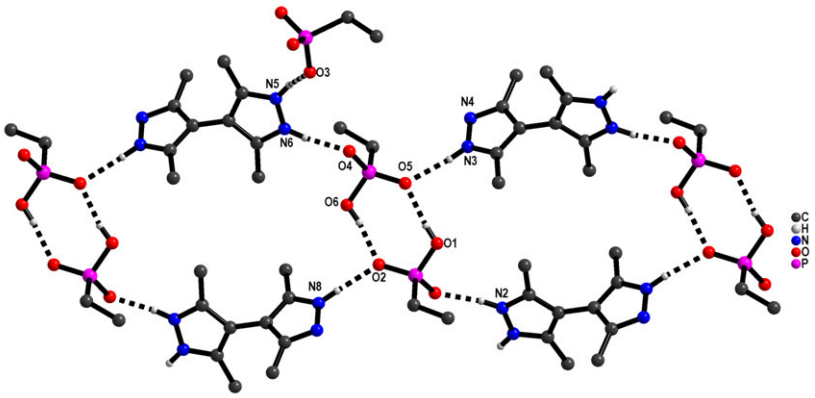

Fig. 3.43: View of 1D tape in *ab*-plane displaying $HBPz^+$ bridging the adjacent dimer **I** in **3h** (Note: anthracene group has not been shown due to clarity)

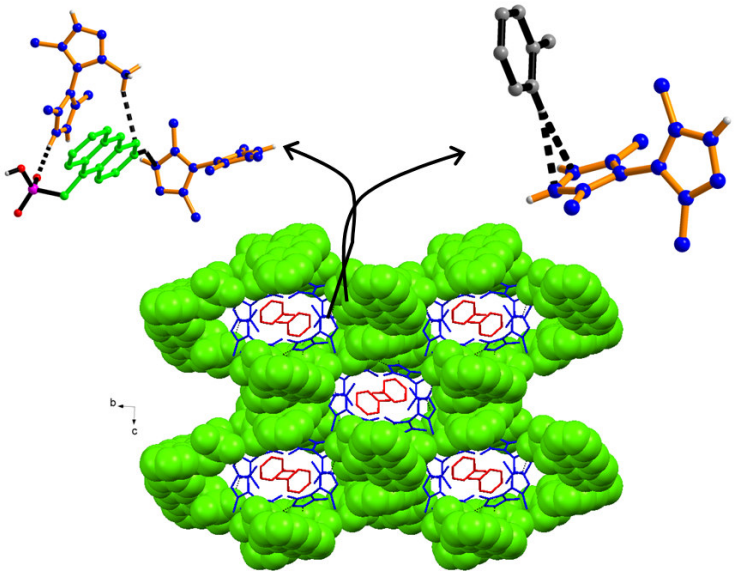

Fig. 3.44: Representation of 3D supramolecular hydrogen bonded porous framework of $HAPa^-$ (green color) and $HBPz^+$ (blue color) with toluene molecules (red color) residing inside the cavity in **3h**

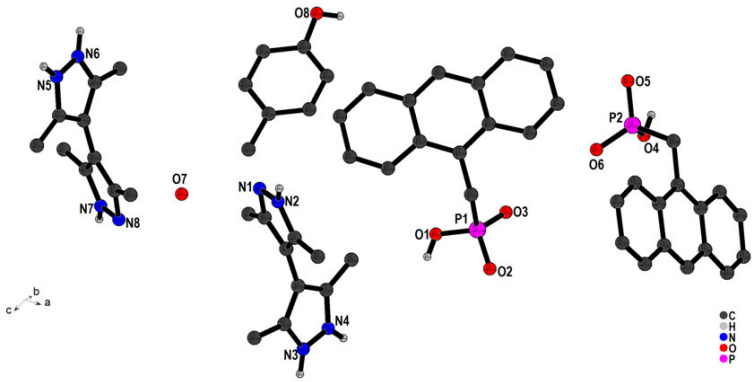

Fig. 3.45: Crystal structure of $[(HAPa^-)_2.(HBPz^+)_2.p\text{-cresol}.H_2O]$ (**3i**). (C–H bonds are not shown for clarity)

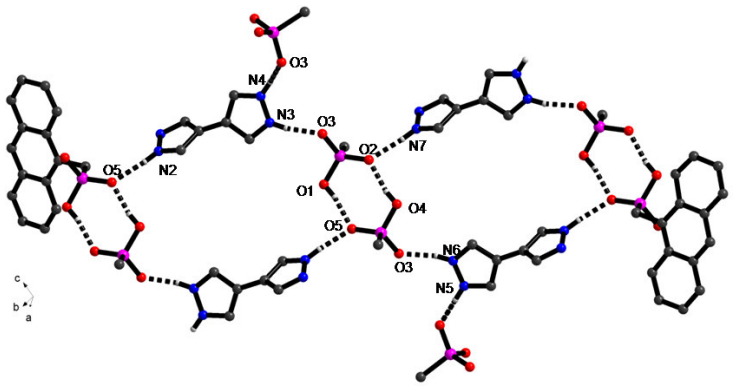

Fig. 3.46: View of 1D tape in *ab*-plane displaying $HBPz^{+}$ bridging the adjacent dimer **I** in **3i**

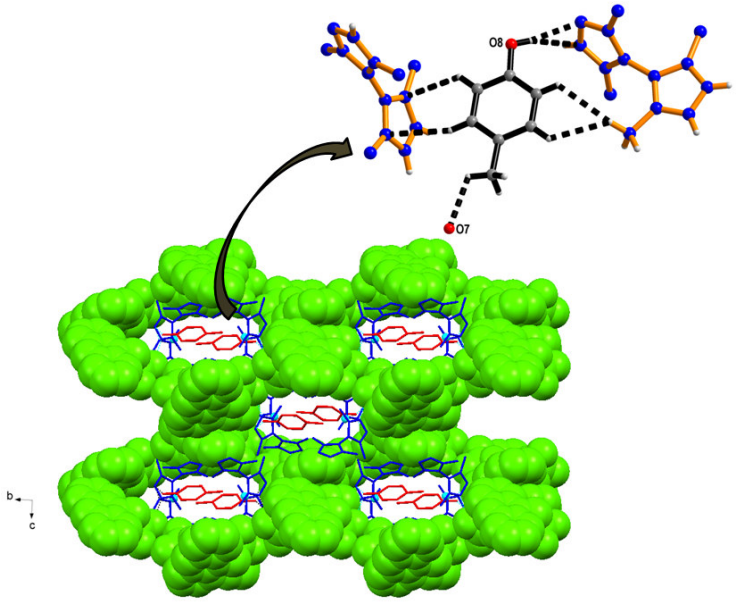

Fig. 3.47: Representation of 3D supramolecular hydrogen bonded porous framework of $HAPa^{-}$ (green color) and $HBPz^{+}$ (blue color) with *p*-cresol molecules (red color) residing inside the cavity in **3i**

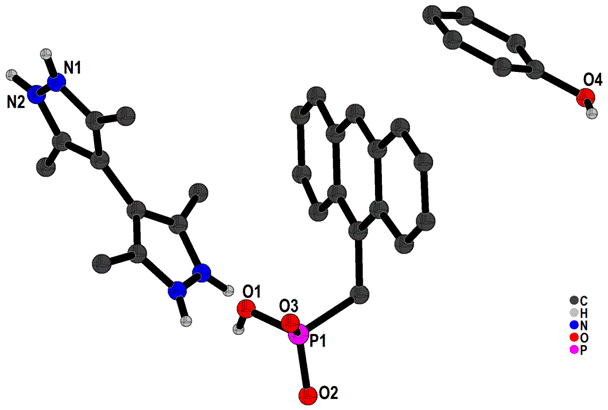

Fig. 3.48: Crystal structure of [$(HAPa^{-})$.$(H_2BPz^{2+})_{0.5}$.phenol] (**3j**). (C–H bonds are not shown for clarity)

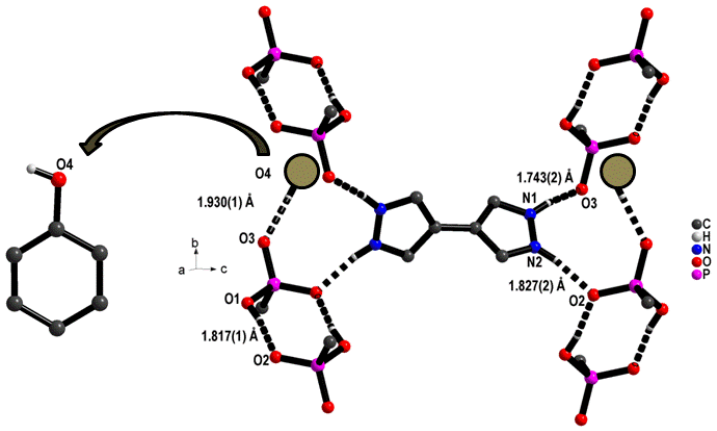

Fig. 3.49: Intermolecular non-covalent interaction in solvate **3j** representing interaction of phenol in the framework

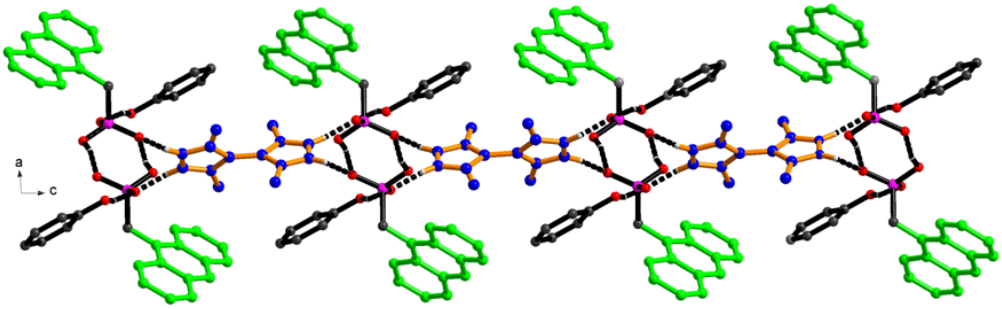

Fig. 3.50: View of 1D tape in *ac*-plane displaying $HBPz^{+}$ bridging the adjacent dimer **I** in **3j**

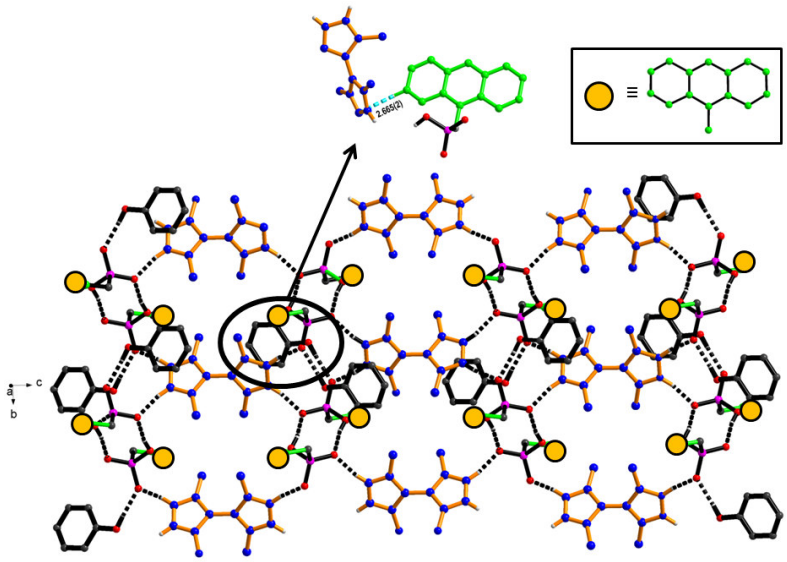

Fig. 3.51: Representation of 2D sheet in *bc*-plane with phenol molecules interacting above and below the sheet via O–H···O interaction in **3j** and representing **type III** hydrogen bonded sheet

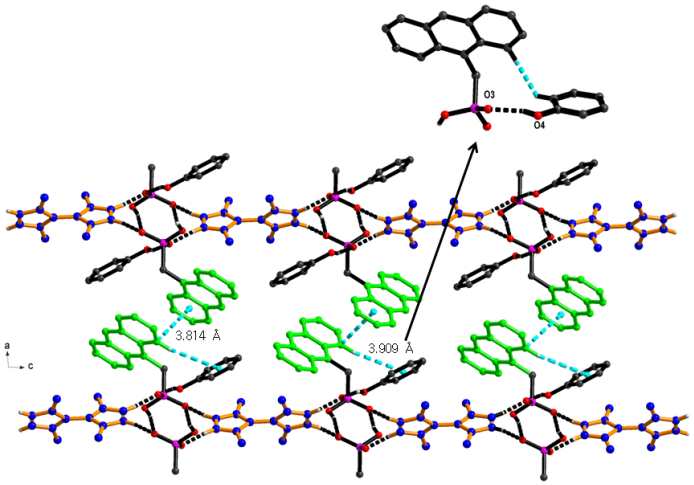

Fig. 3.52: Extension of 2D sheet to 3D supramolecular framework via π···π interaction in **3j**

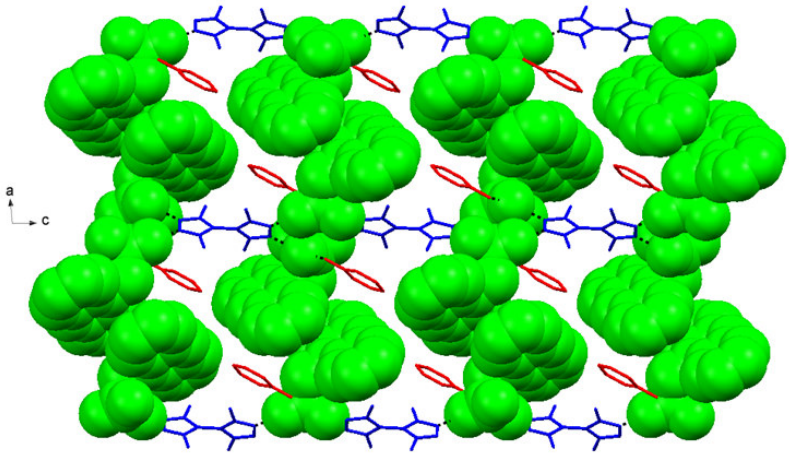

Fig. 3.53: Representation of 3D supramolecular hydrogen bonded porous framework of $HAPa^-$ (green color) and $HBPz^+$ (blue color) with phenol molecules (red color) residing inside the cavity in **3j**

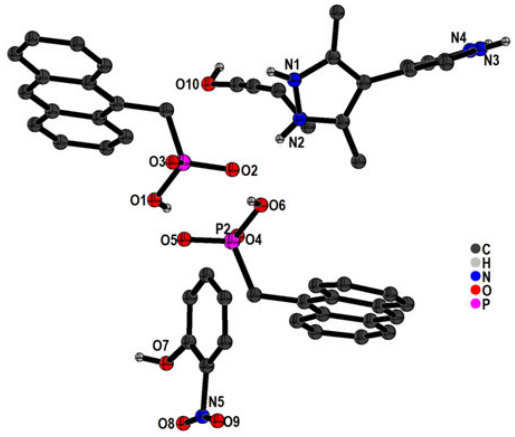

Fig. 3.54: Crystal structure of $[(HAPa^-)_2.H_2BPz^{2+}.2\text{-NP}.n\text{-butanol}]$ (**3k**). (C–H bonds are not shown for clarity)

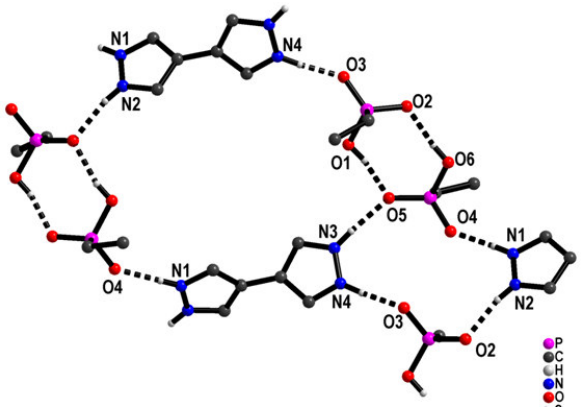

Fig. 3.55: Intermolecular non-covalent interaction in ternary complex **3k** showing synthons **I** and **IV**

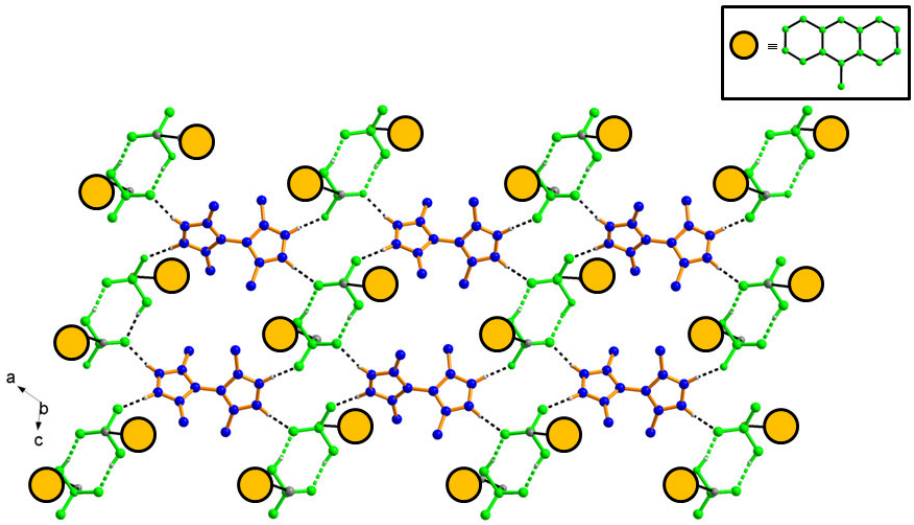

Fig. 3.56: View of 2D sheet in *ac*-plane displaying synthon **I** and **IV** in **3k** and **3l**; representing **type III** hydrogen bonded sheet

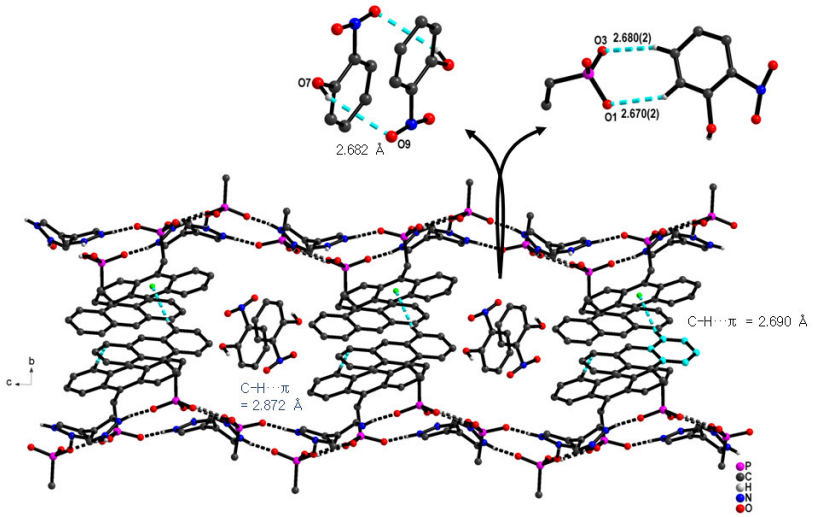

Fig. 3.57: Interlinking of two adjacent 2D sheets in *bc*-plane by C–H···π interaction in **3k**

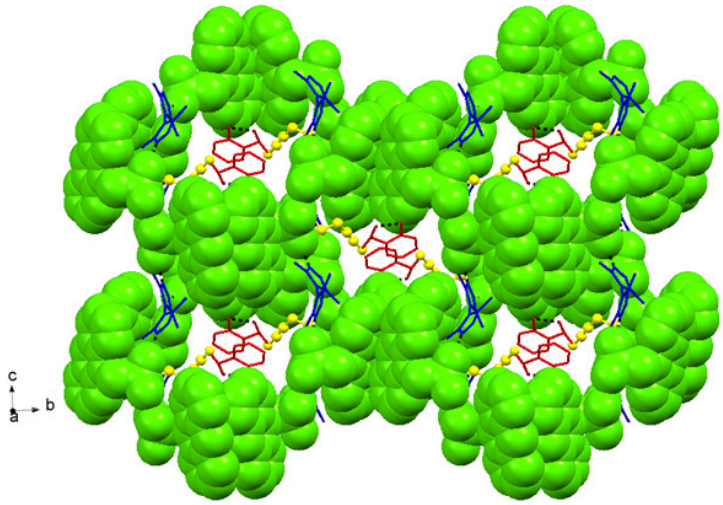

Fig. 3.58: Representation of 3D supramolecular hydrogen bonded porous framework of $HAPa^-$ (green color) and $HBPz^+$ (blue color) with 2-NP molecules (red color) and *n*-butanol (represented in yellow ball and stick model) residing inside the cavity in **3k**

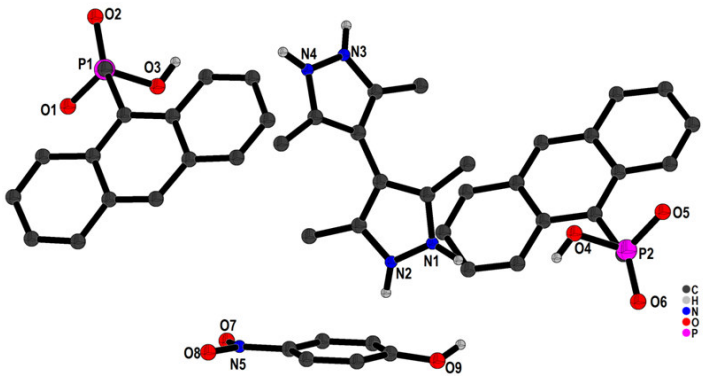

Fig. 3.59: Crystal structure of $[(HAPa^-)_2.H_2BPz^{2+}.4\text{-NP.S}]$ (**3l**). (C–H bonds are not shown for clarity)

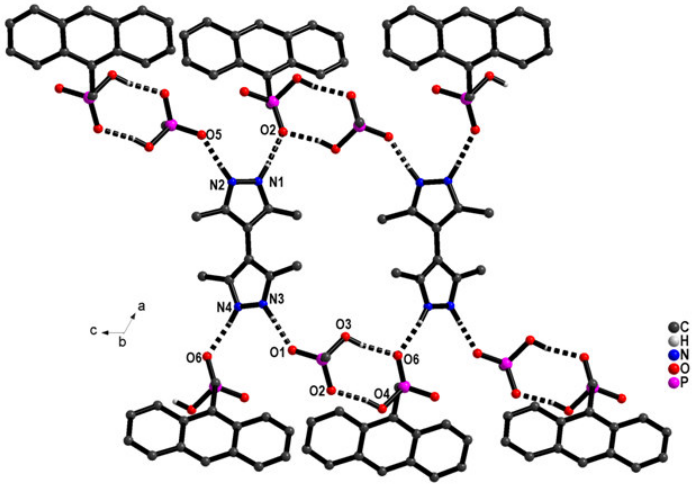

Fig. 3.60: Intermolecular non-covalent interaction in solvate **3l**

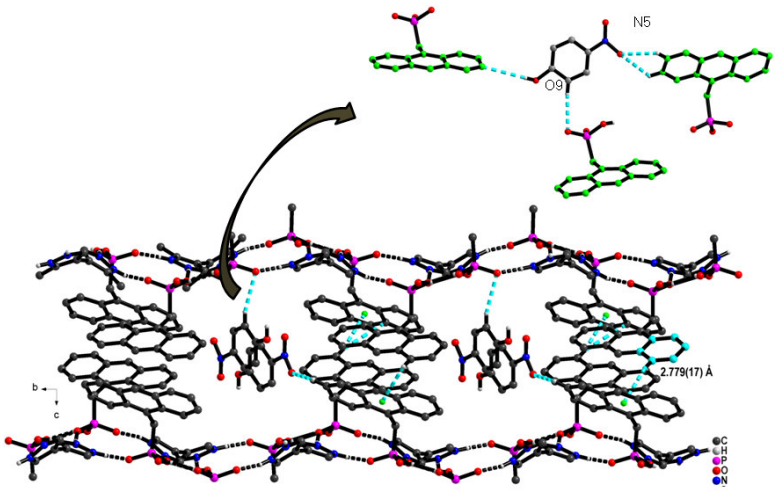

Fig. 3.61: Interlinking of two adjacent 2D sheets in *bc*-plane by C–H···π interaction in **3l**

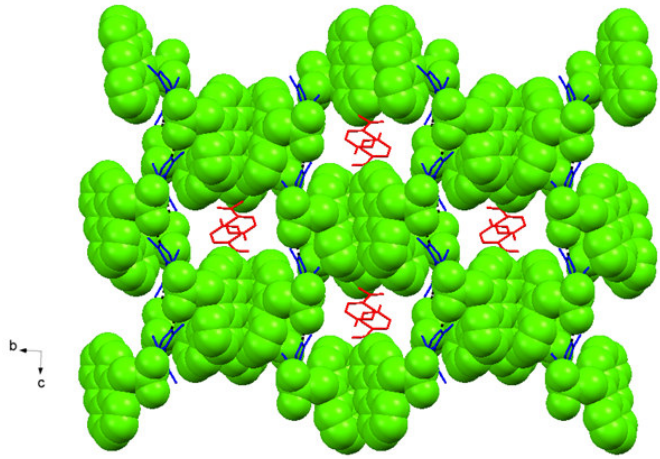

Fig. 3.62: Representation of 3D supramolecular hydrogen bonded porous framework of $HAPa^-$ (green color) and $HBPz^+$ (blue color) with 4-NP molecules (red color) residing inside the cavity in **3l**

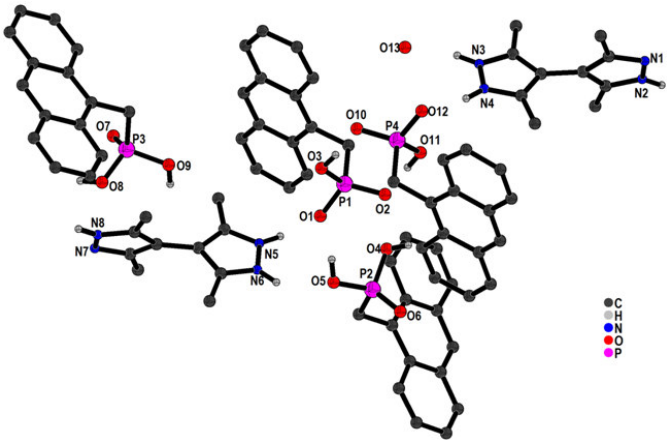

Fig. 3.63: Crystal structure of $[(HAPa^-)_2.(HBPz^+)_2.(H_2APa)_2.H_2O]$ (**3m**). (C–H bonds are not shown for clarity)

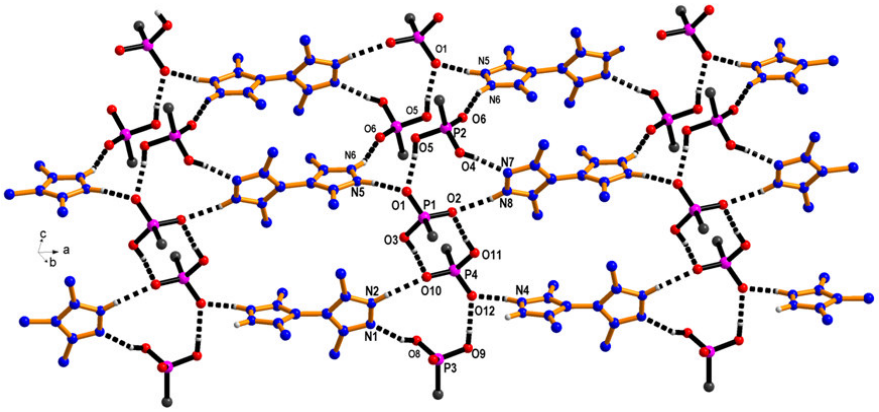

Fig.3.64: View of 2D sheet in *bc*-plane representing dimeric, trimeric and hexameric synthons in **3m**

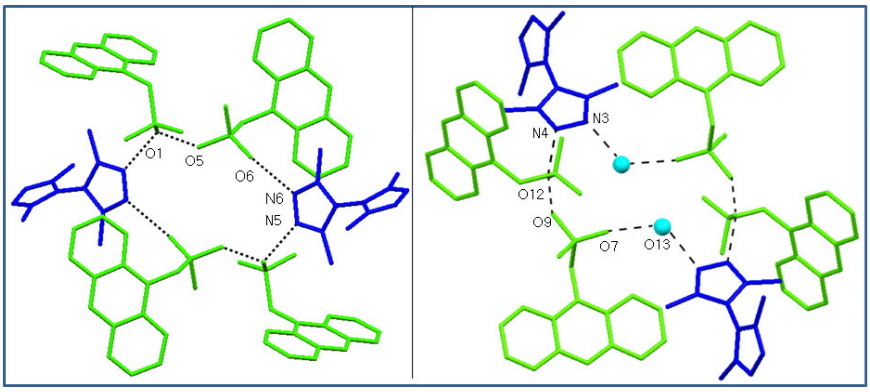

Fig. 3.65: Representation of hexameric,**V** $R_6^4(18)$ and octameric motif, **VI** $R_8^5(22)$ (in chair form) observed in hydrate of APaBPz system in **3m**

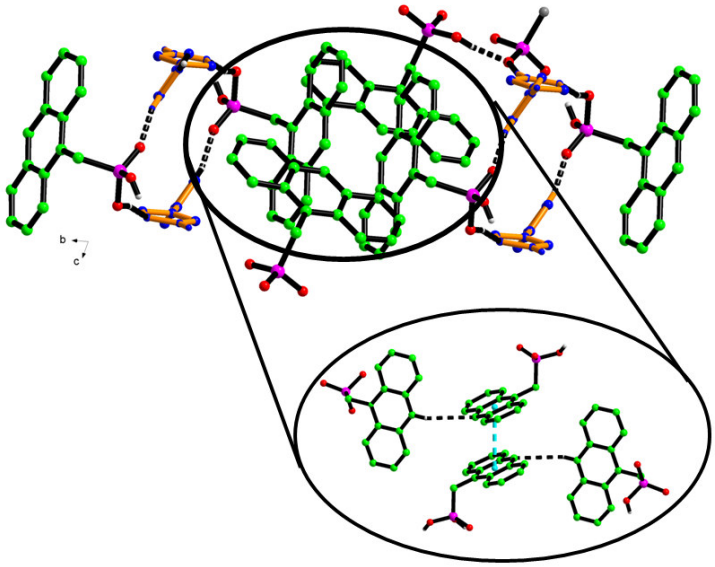

Fig. 3.66: Displaying C–H···π and π···π interaction between four moieties of anthracene responsible for extending 2D to 3D framework in **3m**

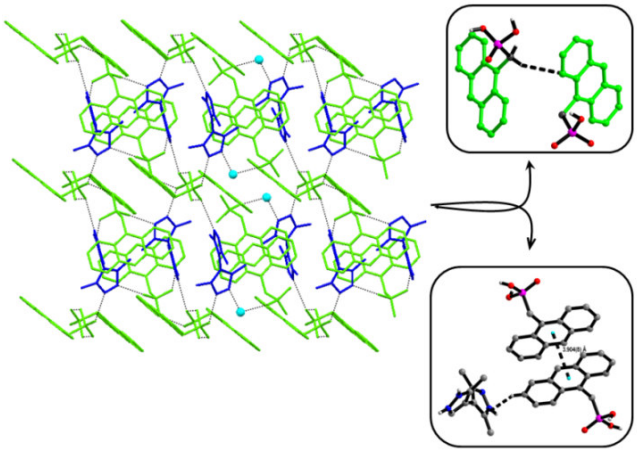

Fig. 3.67: View of 3D supramolecular framework in **3m**

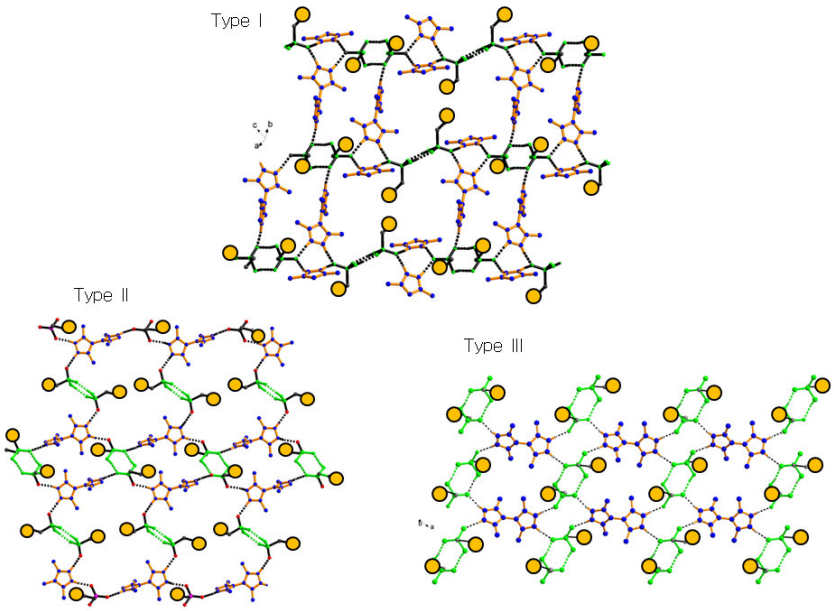

Fig. 3.68: Distinct types (type **I-III** hydrogen bonded sheet) of 2D framework observed **type I** (solvates **3a**-**3e**); **type II** (solvates **3f**-**3i**); **type III** (ternary compounds **3j**-**3l**)

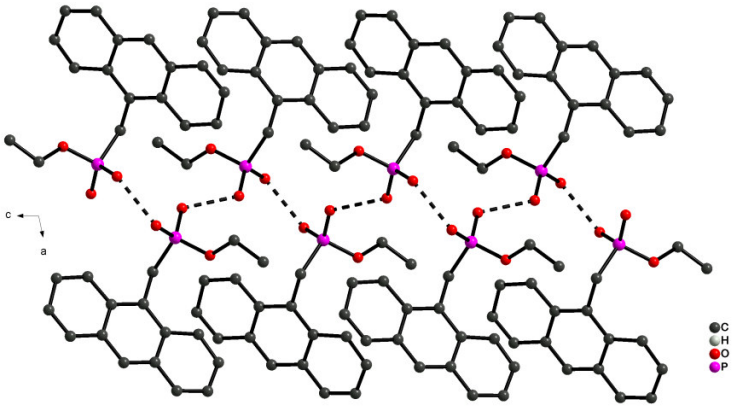

Fig. 3.69: View of 1D chain along *ac*-plane in **3n**

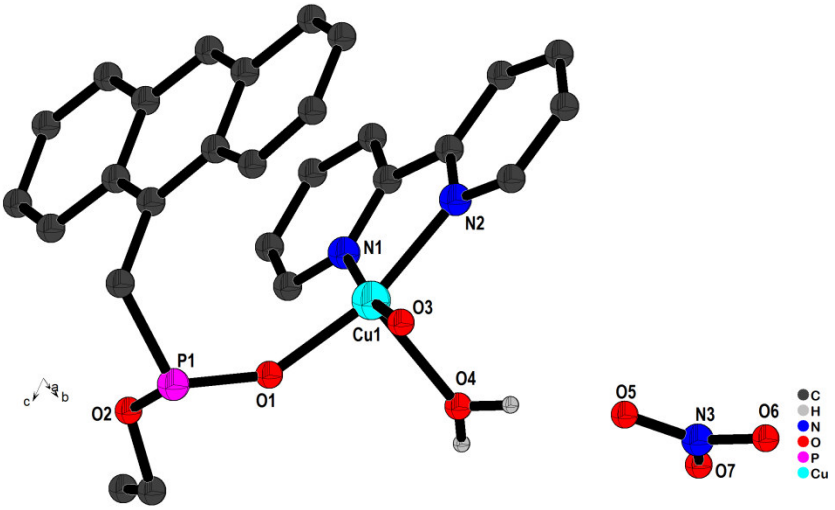

Fig. 3.70: Crystal structure of $[Cu_2(\mu_2\text{-}C_{15}H_{12}PO_3)_2(^{2,2'}BPy)_2(H_2O)_2](NO_3)_2.X$) (**3o**). (C–H bonds are not shown for clarity)

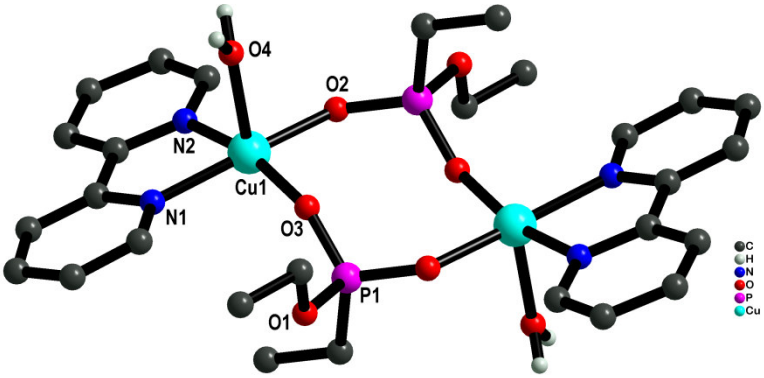

Fig. 3.71: Coordination environment around Cu(II) center with N_2O_3 donor set in **3o**

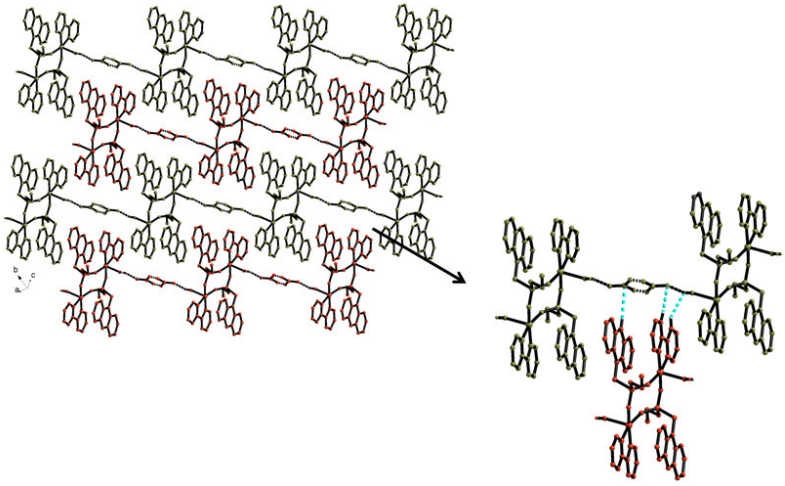

Fig. 3.72: View of interdigitated parallel 1D chains of composite unit and nitrate anion in *ac*-plane interacting through C–H···O and N–H···O interaction in **3o**

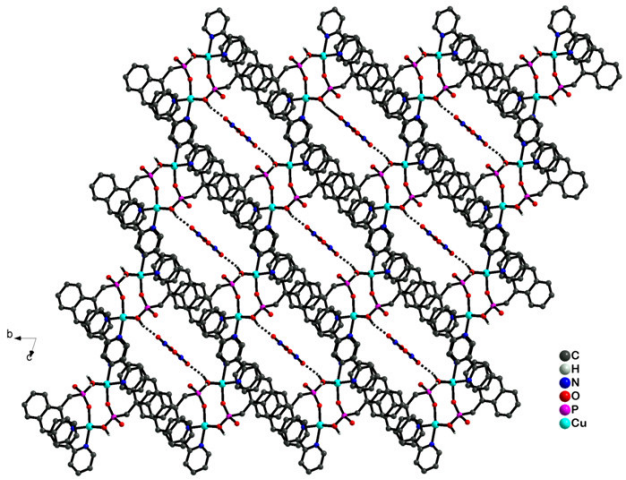

Fig. 3.73: 3D extended framework in *bc*-plane displaying the porous framework with uncoordinated nitrate anion inside the pores in **3o**

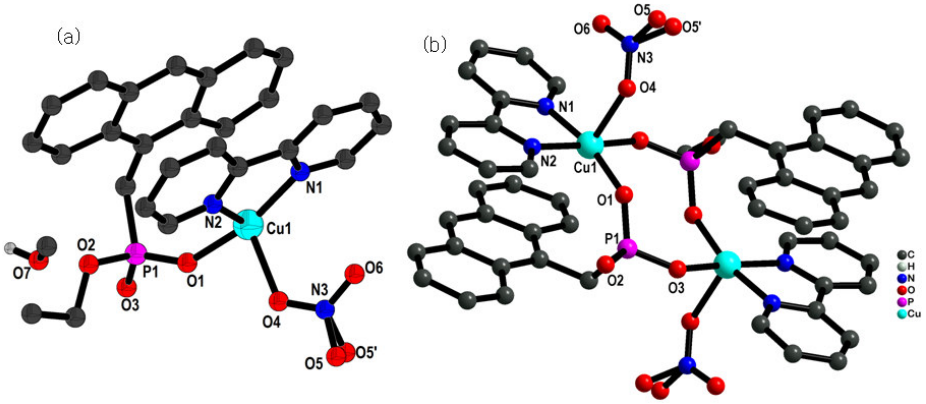

Fig. 3.74: (a) Crystal structure of $[Cu_2(\mu_2\text{-}C_{15}H_{12}PO_3)_2(^{2,2'}BPy)_2(NO_3)_2]$.MeOH (**3p**) and (b) Coordination environment around Cu(II) center in **3p**

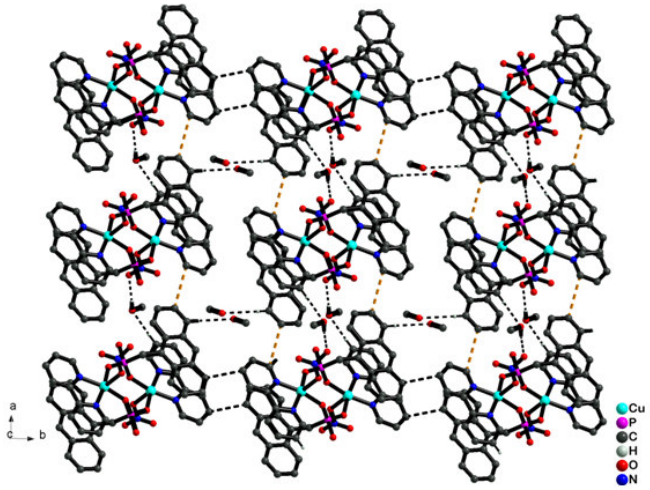

Fig. 3.75: View of 2D sheet representing the interaction of methanol molecule with the framework along *c*-axis in **3p**

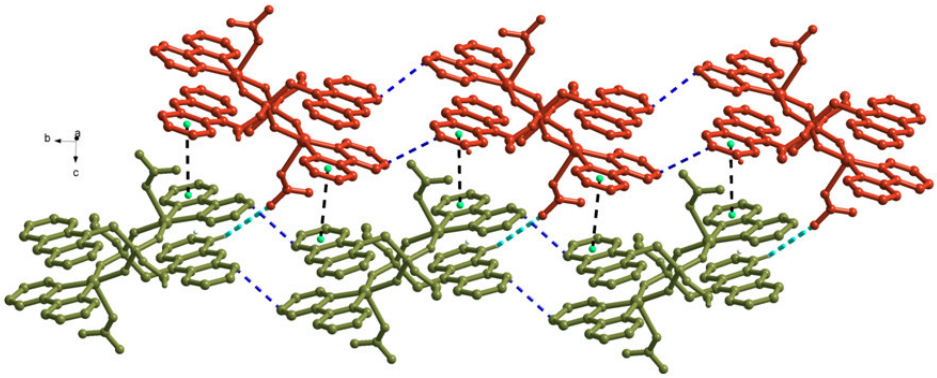

Fig. 3.76: Parallel stacking of 2D sheets interlinked by various secondary intermolecular interactions such as C–H···O, C–H···π and π···π along *a*-axis in **3p**

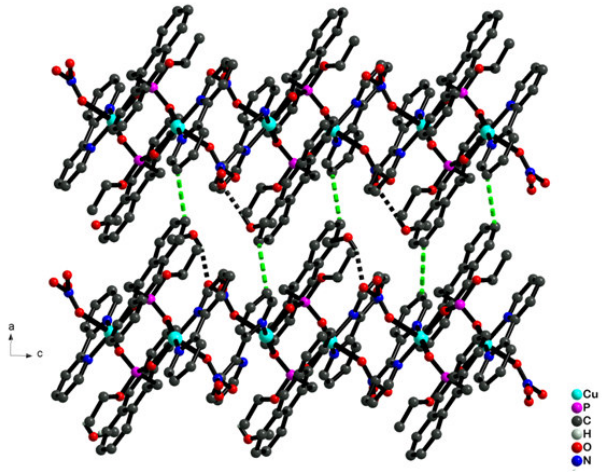

Fig. 3.77: 3D representation of **3p** in *ac*-plane displaying the π···π interaction between the anthracene moiety and 2,2'-BPy units of neighboring 2D sheets in **3p**

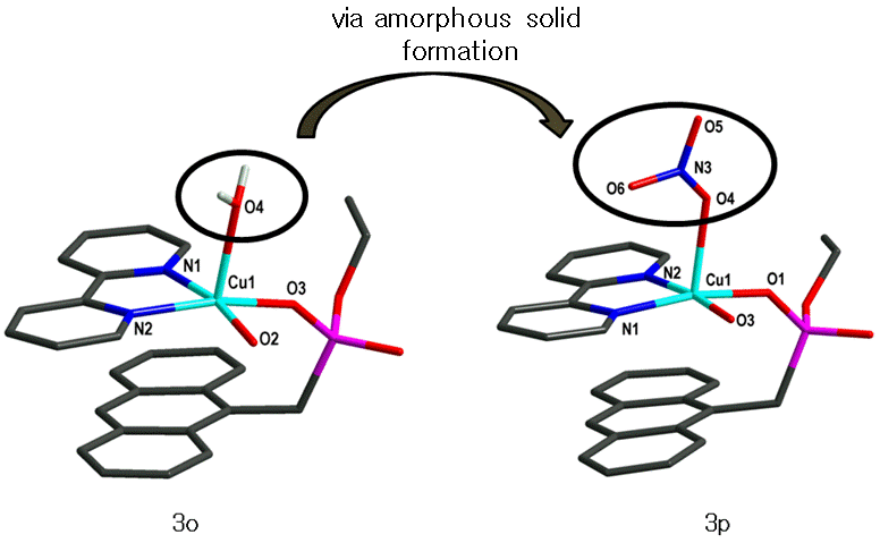

Scheme 3.4: Schematic representation of change of coordination environment of Cu(II) in **3o** and **3p** through solid state transformation

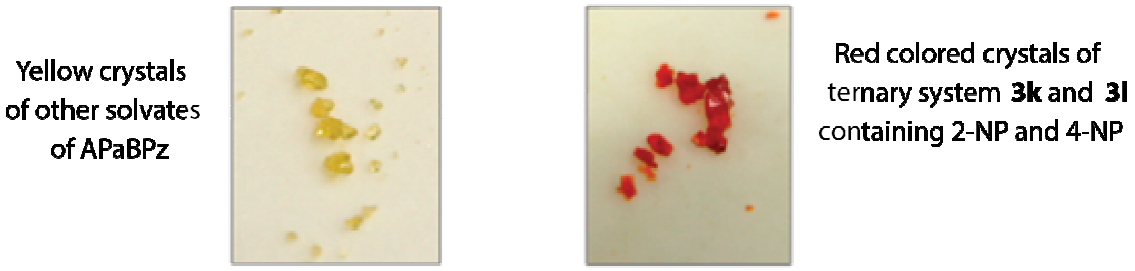

Fig. 3.78: Yellow crystals of the solvates of APaBPz system and the red crystals in case of 2-NP (**3k**) and 4-NP (**3l**)

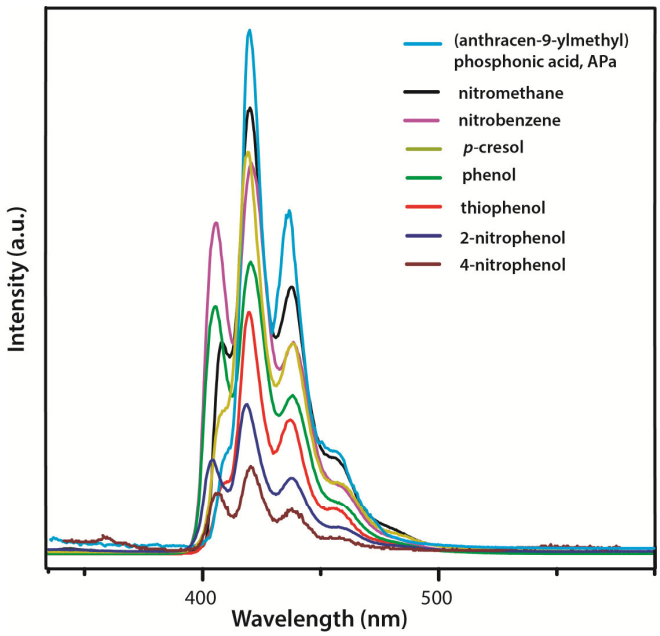

Fig. 3.79: Solid state emission spectra of the ligand and complexes **3e**-**3g** and **3i**-**3l**

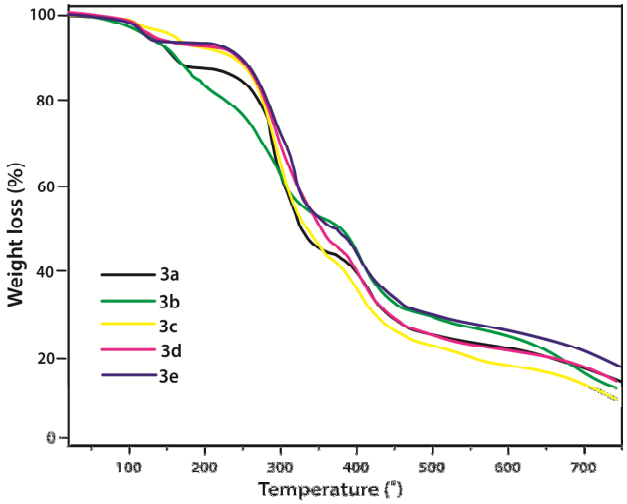

Fig. 3.80: Thermogravimetric curve for solvates **3a**-**3e**

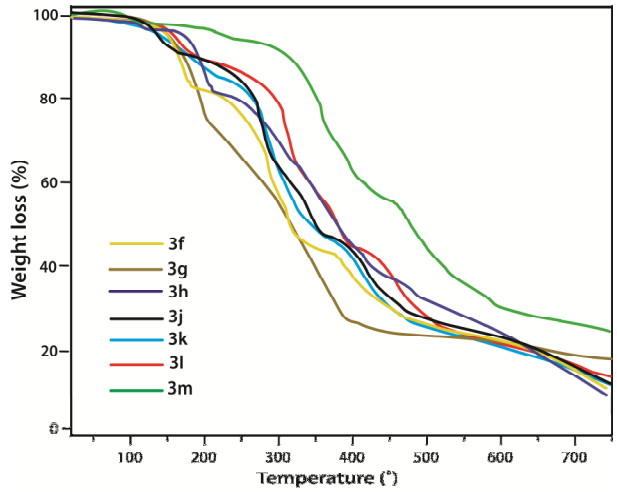

Fig. 3.81: Thermogravimetric curve for solvates 3f-3m

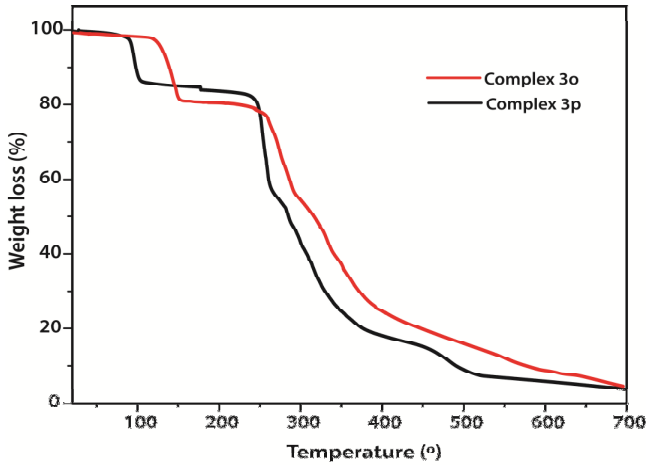

Fig. 3.82: Thermogravimetric curve for complexes **3o-3p**

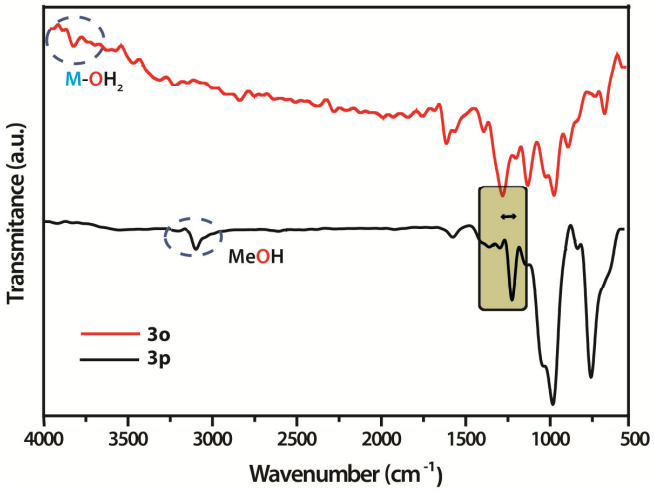

Fig. 3.83: IR spectra for compound **3o-3p**

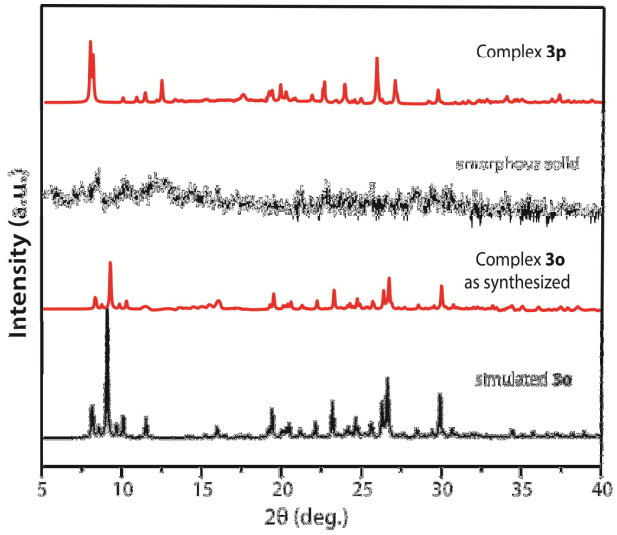

Fig. 3.84: PXRD pattern of complexes **3o**-**3p**

Table 3.20: Summary of solvates/ternary co-crystals:

	Solvates		**Ternary co-crystals**	
Different forms of structures	**Form I**	**Form II**	**Form III**	**Form III**
Acid : base ratio in the asymmetric unit	1:1 (*C*2/*c*)	2:2 ($P2_1/n$ or $P2_1/c$)	1:0.5 (*C*2/*c*)	2:1 ($P2_1/n$)
	3a	**3f**	**3j**	**3k**
	3b	**3g**		**3l**
	3c	**3h**		
	3d	**3i**		
	3e			

Table 3.21: Hydrogen Bond interaction energy in solvates (3a-3h, 3m) and ternary systems (3i-3l) (Kcal/mol)

Solvate	Solvent	Hydrogen Bond interaction energy (Kcal/mol)
3a	THF	-26.1043
3b	dioxane	-22.1255
3c	benzene	-19.4527
3d	thiophene	-11.6578
3e	nitromethane	-6.2939
3f	nitrobenzene	-10.7931
3g	thiophenol	-25.1229
3h	toluene	-23.2903
3i	*p*-cresol	-27.5339
3j	phenol	-26.3594
3k	2-nitrophenol	-22.4536
3l	4-nitrophenol	-23.1777
3m	water	-28.0308

References:

1. Nassimbeni, L. R., "*In Crystal Engineering. From Molecules and Crystals to Materials*", Braga, D., Grepioni, F., Orpen, A. G., Kluwer Academic Publishers, Dordrecht, The Netherlands, 163 (1999).
2. Rekharsky, M. and Inoue, Y., "*Supramolecular Chemistry: From Molecules to Nanomaterials*, John Wiley & Sons, Inc., (2012).
3. Yan, D., Fan, G., Guan, Y., Meng, Q., Li, C. and Wang, J., "Tuning solid-state blue and red luminescence by the formation of solvate crystals", *Phys. Chem. Chem. Phys*., **15**, 19845 (2013).
4. Yamamoto, H. M., Yamaura, J.-I. and Kato, R., "Multicomponent molecular conductors with supramolecular assembly: Iodine-containing neutral molecules as building blocks", *J. Am. Chem. Soc.*, **120**, 5905 (1998).
5. Natarajan, P., Bajpai, A., Venugopalan, P. and Moorthy, J. N., "Pseudopolymorphism of a highly adaptable tetraarylpyrene host that exhibits abundant solid-state guest inclusion", *Cryst. Growth Des*., **12**, 6134 (2012).
6. Sokolov, A. N., Friščić, T., Blais, S., Ripmeester, J. A. and MacGillivray, L. R., "Persistent one-dimensional face-to-face π-stacks within organic co-crystals", *Cryst. Growth Des.*, **6**, 2427 (2006).
7. Desiraju, G. R. and Steiner, T., "*The Weak Hydrogen Bond in Structural Chemistry and Biology*; Oxford University Press: Oxford, U.K., (1999).
8. Planas, J. G., Masalles, C., Sillanpää, R., Kivekäs, R., Teixidor, F. and Viñas, C., "Synthesis and solid state structure for a series of poly(1-pyrrolylmethyl)benzene derivatives. Control of the interplaying π–π and C–H···π interactions?", *CrystEngComm*, **8**, 75 (2006).
9. Herbstein, F. H., "Diversity amidst similarity: A multidisciplinary approach to phase relationships, solvates, and polymorphs", *Cryst. Growth Des.*, **4**, 1419 (2004).
10. Thakuria, R. and Nangia, A., "Olanzapinium salts, isostructural solvates, and their physicochemical properties", *Cryst. Growth Des.*, **13**, 3672 (2013).
11. Nangia, A. and Desiraju, G. R., "Pseudopolymorphism: Occurrences of hydrogen bonding organic solvents in molecular crystals", *Chem. Commun*., 605 (1999).

12. Thaimattam, R., Xue, F., Sarma, J. A. R. P., Mak, T. C. W. and Desiraju, G. R., "Inclusion compounds of tetrakis(4-nitrophenyl)methane: C–H···O networks, pseudopolymorphism, and structural transformations", *J. Am. Chem. Soc.*, **123**, 4432 (2001).
13. Mukherjee, A. and Desiraju, G. R., "Synthon polymorphism and pseudopolymorphism in co-crystals. The 4,4'-bipyridine-4-hydroxybenzoic acid structural landscape", *Chem. Commun.*, **47**, 4090 (2011).
14. Li, Y.-X., Du, S. and Wang, J.-L., "3,4-Dinitro-1H-pyrazole benzene 0.25-solvate", *Acta Cryst.,* **E67**, o1369 (2011).
15. Elgemeie, G. H. and Jones, P. G., "5-Amino-3-anilino-N-(chlorophenyl)-1H-pyrazole-4-carboxamide ethanol solvate", *Acta Cryst., **E60**, o1616 (2004).*
16. Stumpf, S., Wagner, M. and Bolte, M., "4-Hydroxymethyl-3,5-dimethyl-1H-pyrazole chloroform solvate", *Acta Cryst., **E60**, o1754 (2004).*
17. Karpinska, J., Erxleben, A. and McArdle, P., "17β-Hydroxy-17r-methylandrostano[3,2-c]pyrazole, stanozolol: The crystal structures of polymorphs 1 and 2 and 10 solvates", *Cryst. Growth Des., **11**, 2829 (2011).*
18. Bingham, A. L., Hughes, D. S., Hursthouse, M. B., Lancaster, R. W., Tavener, S. and Threlfall, T. L., "Over one hundred solvates of sulfathiazole", *Chem. Commun.*, 603 (2001).
19. Tanaka, T., Tasaki, T. and Aoyama, Y., "Acridinylresorcinol as a self-complementary building block of robust hydrogen-bonded 2D nets with coordinative saturation. Preservation of crystal structures upon guest alteration, guest removal, and host modification", *J. Am. Chem. Soc.*, **124**, 12453 (2002).
20. Singh, D. and Baruah, J. B., "Structural study on solvates of dopamine-based cyclic imide derivatives", *Cryst. Growth Des.*, **11**, 768 (2011).
21. Mizobe, Y., Miyata, M., Hisaki, I., Hasegawa, Y. and Tohnai, N., "Anomalous anthracene arrangement and rare excimer emission in the solid state: Transcription and translation of molecular information", *Org. Lett*., **8**, 4295 (2006).
22. Nauha, E., Ojala, A., Nissinen, M. and Saxell, H., "Comparison of the polymorphs and solvates of two analogous fungicides − A case study of the applicability of a

supramolecular synthon approach in crystal engineering", *CrystEngComm*, **13**, 4956 (2011).

23. Mondal, R. and Howard, J. A. K., "A structural investigation of six solvates of *trans*-1,4-bis(phenylethynyl)-cyclohexane-1,4-diol", *Cryst. Growth Des.*, **8**, 4359 (2008).
24. Feng, Q., Wang, M., Dong, B., He, J. and Xu, C., "Regulation of arrangements of pyrene fluorophores via solvates and co-crystals for fluorescence modulation", *Cryst. Growth Des.*, **13**, 4418 (2013).
25. Bhattacharya, S. and Saha, B. K., "Polymorphism through desolvation of the solvates of a van der waals host", *Cryst. Growth Des*., **13**, 606 (2013).
26. Aakeröy, C. B., Desper, J. and Urbina, J. F., "Supramolecular reagents: Versatile tools for non-covalent synthesis", *Chem. Commun*., 2820 (2005).
27. Friščić, T., Trask, A. V., Jones, W. and Motherwell, W. D. S., "Screening for inclusion compounds and systematic construction of three-component solids by liquid-assisted grinding", *Angew. Chem., Int. Ed.*, **118**, 7708 (2006).
28. Aakeröy, C. B., Beatty, A. M. and Helfrich, B. A., "'Total Synthesis' supramolecular style: Design and hydrogen-bond directed assembly of ternary supermolecules", *Angew. Chem., Int. Ed.*, **40**, 3240 (2001).
29. Bhogala, B. R., Basavoju, S. and Nangia, A., "Three-component carboxylic acid-bipyridine lattice inclusion host. Supramolecular synthesis of ternary co-crystals", *Cryst. Growth Des.*, **5**, 1683 (2005).
30. Tothadi, S. and Desiraju, G. R., "Designing ternary co-crystals with hydrogen bonds and halogen bonds", *Chem. Commun.*, **49**, 7791 (2013).
31. Chandrasekhar, V., Sahoo, D., Narayanan, R. S., Butcher, R. J., Lloret, F. and Pardo, E., "A hexaicosametallic copper(II) phosphonate", *Dalton Trans.*, **42**, 8192 (2013).
32. Chandrasekhar, V., Senapati, T. and Sañudo, E. C., "Synthesis, structure, and magnetism of hexanuclear copper(II) phosphonates", *Inorg. Chem*., **47**, 9553 (2008).
33. Wu, J., Hou, H., Han, H. and Fan, Y., "Highly selective ferric ion sorption and exchange by crystalline metal phosphonates constructed from tetraphosphonic acids", *Inorg. Chem*., **46**, 7960 (2007).

34. Rocha, G. M. S. R. O., Domingues, R. M. A., Simões, M. M. Q. and Silva, A. M. S., "Catalytic activity of tetravalent metal phosphates and phosphonates on the oxidation of (+)-3-carene", *Appl. Catal. A: Gen.*, **353**, 236 (2009).
35. Yang, X.-J., Bao, S.-S., Ren, M., Hoshino, N., Akutagawa, T. and Zheng, L.-M., "Polar metal phosphonate containing unusual μ_4-OH bridged double chains showing canted antiferromagnetism with large coercivity", *Chem. Commun.*, **50**, 3979 (2014).
36. Mateescu, A., Raptopoulou, C. P., Terzis, A., Tangoulis, V. and Salifoglou, A., "pH-specific synthesis and structural and spectroscopic characterization of a complex between Co^{II} and *N*,*N*-Bis(phosphonomethyl)glycine: Cobalt–phosphonate interactions in the solid state and in solution", *Eur. J. Inorg. Chem*., 1945 (2006).
37. Cao, G., Hong, H.-G. and Mallou, T. E., "Layered metal phosphates and phosphonates: From crystals to monolayers", *Acc. Chem. Res.*, **25**, 427 (1992).
38. Shi, F.-N., Paz, F. A. A., Girginova, P., Rocha, J., Amaral, V. S., Klinowski, J. and Trindade, T., "One-dimensional coordination polymer of *N*-(phosphonomethyl)iminodiacetic acid with iron(II)", *J. Mol. Struct*., **789**, 200 (2006).
39. Chandrasekhar, V., Kingsley, S., Rhatigan, B., Lam, M. K. and Rheingold, A. L., "New structural forms in molecular metal phosphonates: Novel tri- and hexanuclear zinc(II) cages containing phosphonate and pyrazole ligands", *Inorg. Chem*., **41**, 1030 (2002).
40. Chandrasekhar, V., Sasikumar, P., Boomishankar, R. and Anantharaman, G., "Assembly of lipophilic tetranuclear (Cu_4 and Zn_4) molecular metallophosphonates from 2,4,6-triisopropylphenylphosponic acid and pyrazole ligands", *Inorg. Chem*., **45**, 3344 (2006).
41. Chandrasekhar, V., Nagarajan, L., Hossain, S., Gopal, K., Ghosh, S. and Verma, S., "Multicomponent assembly of anionic and neutral decanuclear copper(II) phosphonate cages", *Inorg. Chem*., **51**, 5605 (2012).
42. Costa, F. S., "On the interpretation of the enthalpy of solvation of hydroxyl cyclohexane derivatives in different solvents", *J. Chem. Thermodyn.*, **32**, 311 (2000).
43. Bhogala, B. R. and Nangia, A., "Ternary and quaternary co-crystals of 1,3-cis,5-ciscyclohexanetricarboxylic acid and 4,4'-bipyridines", *New J. Chem*., **32**, 800 (2008).
44. Yanai, N., Kitayama, K., Hijikata, Y., Sato, H., Matsuda, R., Kubota, Y., Takata, M., Mizuno, M., Uemura, T. and Kitagawa, S., "Gas detection by structural variations of

fluorescent guest molecules in a flexible porous coordination polymer", *Nat. Mater*., **10**, 787 (2011).

45. Zhang, J.-P. and Chen, X.-M., "Exceptional framework flexibility and sorption behavior of a multifunctional cuprous triazolate framework", *J. Am. Chem. Soc*., **130**, 6010 (2008).
46. Yanai, N., Uemura, T., Inoue, M., Matsuda, R., Fukushima, T., Tsujimoto, M., Isoda, S. and Kitagawa, S., "Guest-to-host transmission of structural changes for stimuli-responsive adsorption property", *J. Am. Chem. Soc*., **134**, 4501 (2012).
47. Chandrasekhar, V. and Kingsley, S., "A dodecanuclear copper(II) cage containing phosphonate and pyrazole ligands", *Angew. Chem., Int. Ed.*, **39**, 2320 (2000).
48. Demadis, K. D., Barouda, E., Stavgianoudaki, N. and Zhao, H., "Inorganic-organic hybrid molecular ribbons based on chelating/bridging, "Pincer" tetraphosphonates, and alkaline-earth metals", *Cryst. Growth Des.*, **9**, 1250 (2009).
49. Liu, L., Sun, Z.-G., Zhang, N., Zhu, Y.-Y., Zhao, Y., Lu, X., Tong, F., Wang, W.-N. and Huang, C.-Y., "Syntheses, crystal structures, and luminescence properties of a series of novel lanthanide oxalatophosphonates with two types of 3D framework structures", *Cryst. Growth Des.*, **10**, 406 (2010).
50. Chandrasekhar, V., Senapati, T., Sañudo, E. C. and Clérac, R., "Tri-, tetra-, and hexanuclear copper(II) phosphonates containing N-donor chelating ligands: Synthesis, structure, magnetic properties, and nuclease activity", *Inorg. Chem*., **48**, 6192 (2009).
51. Yoshida, K., Toyoura, K., Matsunaga, K., Nakahira, A., Kurata, H., Ikuhara, Y. H. and Sasaki, Y., "Atomic sites and stability of Cs^+ captured within zeolitic nanocavities", *Scientific Reports*, **3**, article number: 2457, (2013).
52. Nagarkar, S. S., Joarder, B., Chaudhari, A. K., Mukherjee, S. and Ghosh, S. K., "Highly selective detection of nitro explosives by a luminescent metal–organic framework", *Angew. Chem., Int. Ed*., **52**, 2881 (2013).

Chapter 4

Synthesis and Structural Studies of Supramolecular Organic Frameworks (SOFs) using Ditopic Pyridyl Ligand

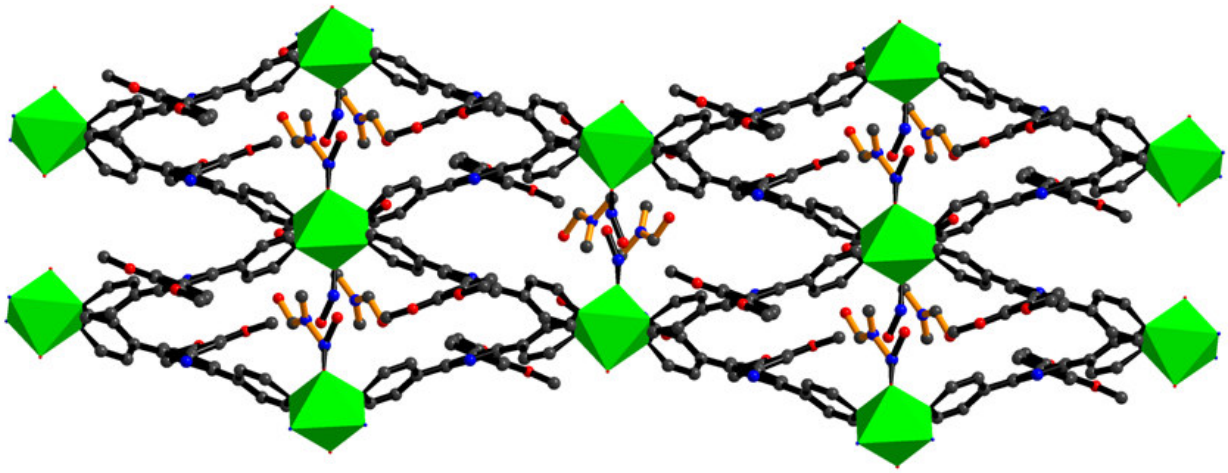

Rapid development in the field of crystal engineering involving pyridyl analogues has attracted the researchers in solid and material science [1-3]. Various pyridyl based ligand with potential functional groups have been employed. On the other hand, many reports were also found on the use of potential organic components with the pyridyl analogues in order to design new materials via supramolecular based concept [4-5]. These new materials with structure related applications can further be implemented as magnetic materials [6-8], sensors [9-10], catalyst [11] etc.

Various H-bonding supramolecular networks of pyridyls have been widely investigated, which mainly involve carboxylic acids [12-14], amides [15], urea [16] etc for the generation of supramolecular arrangement. Here, the subject of interest is to generate supramolecular architectures using phosphonic acids and pyridyl analogues, considered to be worth investigating as it may lead to intricate molecular complexes. Additionally, phosphonic acid also shows cooperative hydrogen bonding [17] in contrast to the complementary H-bonding of the carboxylic acids (Fig. 4.1).

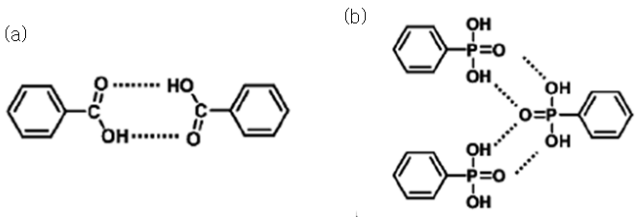

Fig. 4.1: Schematic illustration of the hydrogen bonding in a) phenylcarboxylic acid and b) phenylphosphonic acid

The system possessing functional moiety with rigid binding trait such as carboxylic, phosphonic group has been more exploited to construct rigid supramolecular framework. Concerning about the conformational flexibility in phosphonic acid, the flexible ((2,4,6-trimethylbenzene-1,3,5-triyl)tris(methylene))triphosphonic acid was employed with pyridyl ditopic ligands. It is, however, assumed that the insertion of methylene group into the phosphonic ligand may allow the flexible phosphonic acid to show polymorphism. Thereby, the flexible phosphonic acid with its flexible arm in the presence of any organic base such as ditopic, tritopic ligands may lead to the generation of variation in supramolecular architectures.

An another aspect of crystal engineering i.e., solid state transition triggered by external stimuli such as temperature, light etc. has received growing interest as these materials may serve

as the next generation of porous materials and might involve structural change via single crystal-to single-crystal transformation [18-19] (SC-SC transformation).

Pyridine based analogues are Lewis base possessing lone pair on the nitrogen, which is easily available for the hydrogen bonding for the construction of supramolecular networks. Many researchers have reported the networks by using pyridine based ditopic ligands as the coformer such as 2,2'-bipyridine, 4,4'-bipyridine etc. Some of the relevant literatures based on pyridyl analogues and phosphonic acids have been discussed below.

Sharma and Clearfield [20] reported that nitrilotri(methylphosphonic acid), exist in zwitter-ion form, revealed a complex of three-dimensional structure with no predictable structural patterns. When it was allowed to react with pyridine analogues in a 1:1 molar ratio, monodeprotonation of triphosphonic acid led to the formation of a prototypal self-complementary 3D hexagonal architecture (Fig. 4.2). The crystal structure study of all salts signified the importance of the ionic hydrogen bond donor:acceptor ratio in shaping 3D hexagonal network formation. They were first to implement the phosphonic group synthons for crystal engineering purposes.

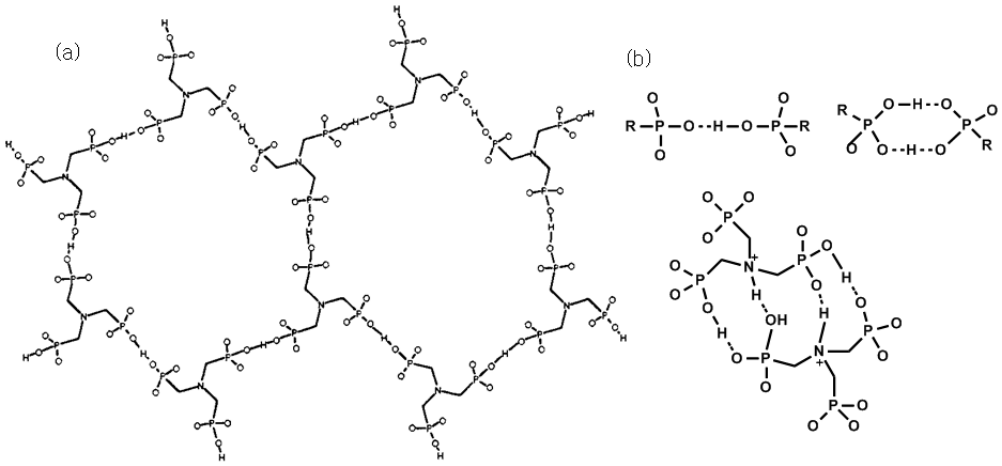

Fig. 4.2: (a) A hexagonal structure formed by very strong symmetrical ionic hydrogen bonds of nitrilotri(methylphosphonate) and (b) various synthons observed in salts

Kong et al. [21] reported the self assembly of a zwitter-ion, iminobis(methylene phosphonic acid) (NDP) and its 2D or 3D supramolecular hydrogen bonding architectures with pyridine based organic bases including a hexaazamacrocyclic crown ether ligand (KTM1). They observed that the phosphonic acid provides an array of synthons to construct robust architectures.

However, phosphonic acid resulted into the 2D layered structure via robust ionic hydrogen bond formation with pyridine molecules interconnecting the layers as pillars (Fig. 4.3). On the other hand, three-dimensional supramolecular hydrogen bonding has been achieved with the azacrown ether.

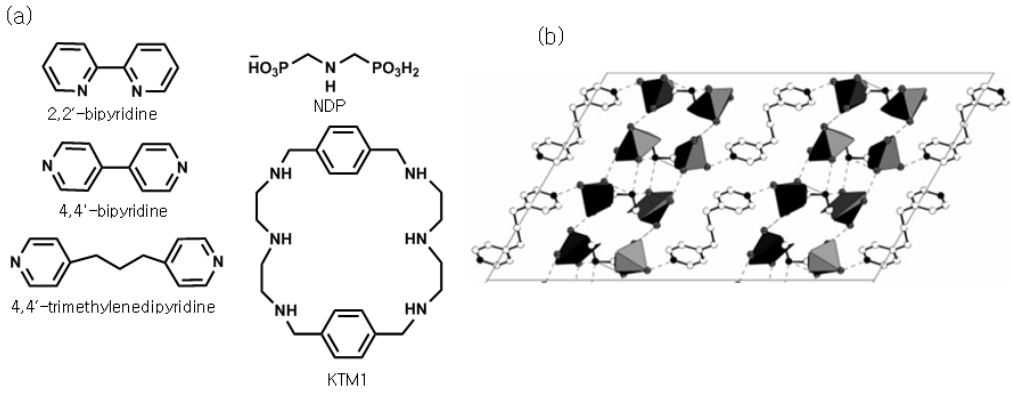

Fig. 4.3: (a) Building blocks used in supramolecular assemblies and (b) 2D hydrogen bonding in salt formed by NDP.4,4'-trimethylenepyridine

Kong et al. [22] further reported three hydrogen-bonded structures formed from 1,3,5-benzene-triphosphonic acid (BTP) and adamantane with the isolation of 2:1, 4:1, and 6:1 (amine to BTP ratios). They tried different ratios of phosphonic acid with fixed ratio of adamantane amine starting from 2:1 to 8:1. The structure analysis showed that all the amino

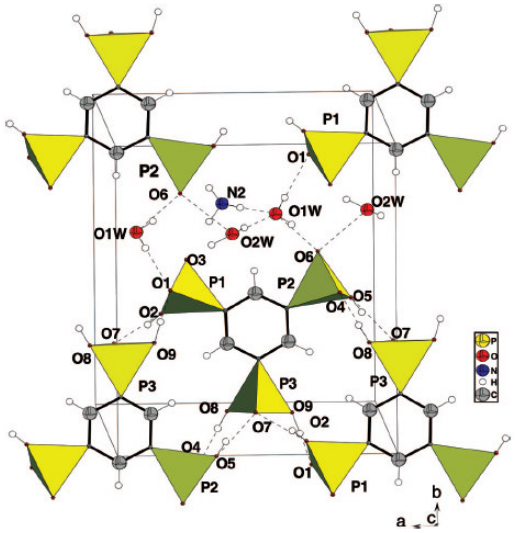

Fig. 4.4: A view of the BTP molecules in compound 2:1 (acid:adamantane) in *ab*-plane

groups were protonated and participated in the hydrogen bond by utilizing all three of their protons as donors. They explained the behavior of BTP is more intricate as compare to benezene

tricarboxylic acid (BTC) due to non-planarity of the phosphonic acid groups and their different orientations relative to the phenyl ring (Fig. 4.4). Moreover, they also evaluated the *pK*a values of the BTP protons by the analysis of potentiometric titration of BTP.

Beckmann et al. [23] synthesized a new potential building block of benzene-1,3,5-tri-*p*-phenylphosphonic acid via [$Pd(PPh_3)_4$]-catalyzed Arbuzov reaction. They tried to produce the single crystal for the same but it produced a single-crystalline salt with *p*-dimethylaminopyridine (DMAP) in 2:3 ratio (Fig. 4.5). They demonstrated that organic domains of the phosphonic acid are interlinked by P–O–H···O–P hydrogen bonds and π-stacking in the crystal structure. However, the protonated DMAP molecules further stabilized the network via participating in N–H···O–P hydrogen bonds and filled the voids formed by the phosphonic acid.

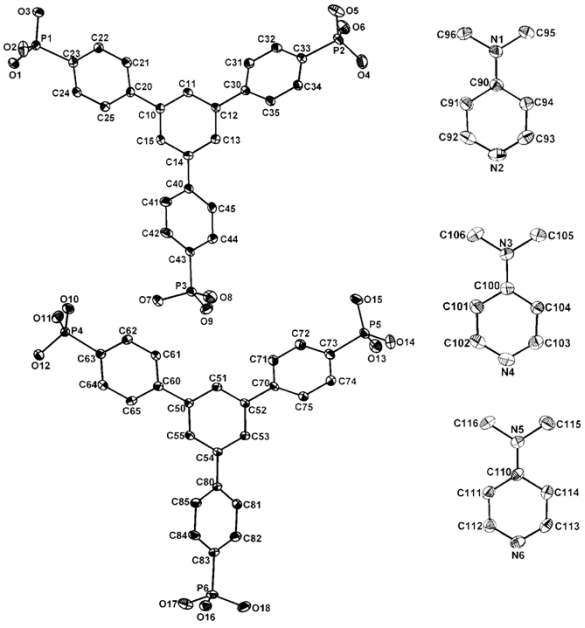

Fig. 4.5: Molecular structure of the two independent molecules of party deprotonated phosphonic acid and the three independent molecules of protonated DMAP

Kong and Clearfield [24] reported two salts of 1,3,5-benzenetri(phosphonic acid) (BTP) with 2,2'-bipyridine and 4,4'-bipyridine. They demonstrated via single crystal X-ray analysis that the deprotonation of BTP by 2,2'-bipyridine gave rise to layered structures of BTP with bipyridine molecules connecting the layers, acting as pillars, hence, led to the formation of 3D framework. In the latter salt, the network contained hexagonal channels, occupied by 4,4'-bipyridinium cations (Fig. 4.6). Furthermore, they have also discussed the deprotonation

tendency of BTP molecule by potentiometeric titration. They concluded that the first three H of BTP can be easily deprotonated but further the decrease in log K has been reported, which can be rationalized in terms of minimization of the electrostatic repulsion between positive charges in the protonated species.

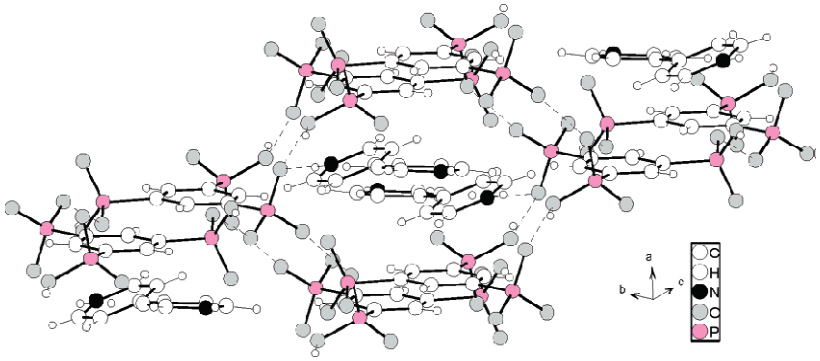

Fig. 4.6: Hydrogen bonding in the compound BTP.4,4'-bipyridine showing the pseudo-hexagonal channel

Mehring [25] reported two hydrogen bonded adducts using 3,5-bis(phosphonophenyl) phosphonic acid and 1,3,5-benzenetri(phosphonic acid) (BTP) with 4-(dimethylamino)pyridine from methanol and water. On structural analysis, they found that these structures are sustained by different hydrogen bonded motifs. In the latter case, the 3D

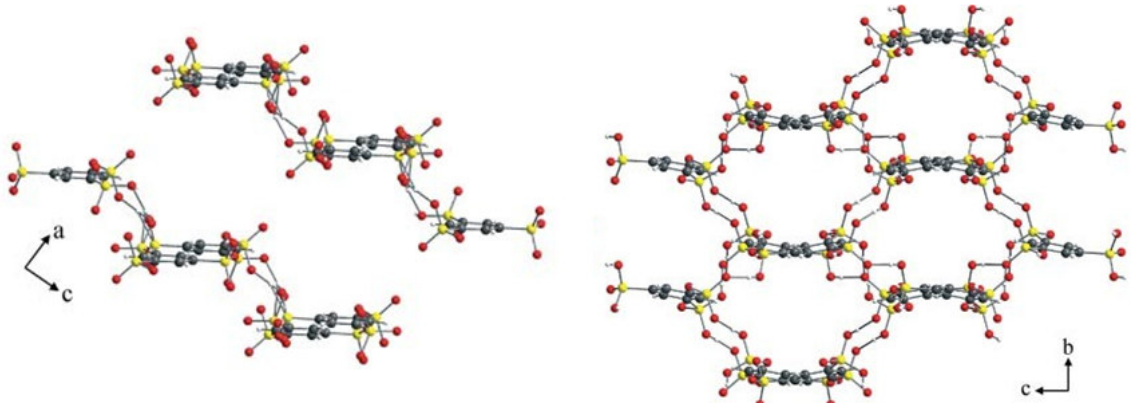

Fig. 4.7: View of the 2D structure and the 3D structure hydrogen bonded adducts (the cations $[4\text{-}(Me_2N)C_5H_4NH]^+$ are omitted for clarity)

structure was obtained through interlinking the adjacent layers by benzene, with $[4\text{-}(Me_2N)C_5H_4NH]^+$ cations occupying the channels. However, 2D hydrogen-bonded network was resulted in former case (Fig. 4.7).

Białek et al. [26] synthesized and characterized two naphthalene based phosphonic acids i.e., naphthalene-1,5-diphosphonic acid (H_4NDP(1,5)) and naphthalene-1,5-bis(methylphosphonic) acid (H_4NDP(1C,5C)). They also reported two distinct pseudopolymorphs, for each of these phosphonic acids, each with or without DMSO molecules.

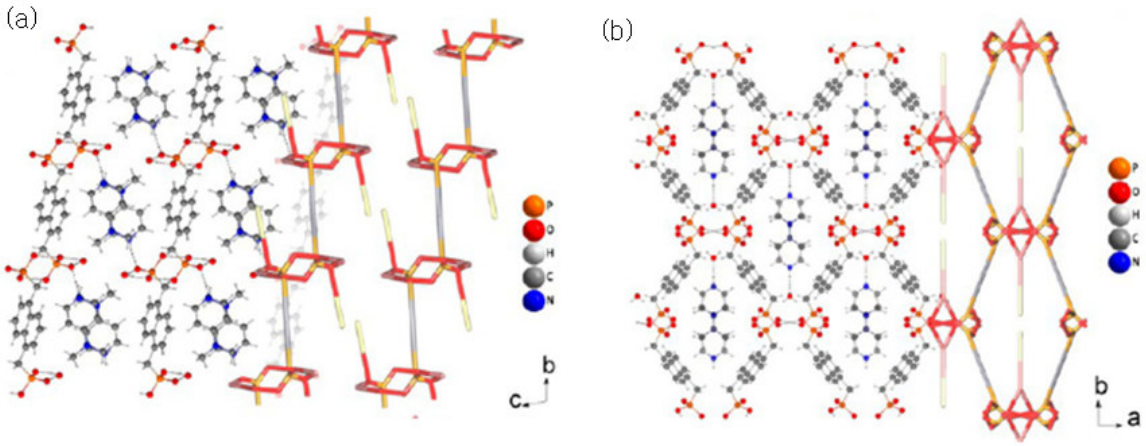

Fig. 4.8: Projections of crystal structure of adduct H_4NDP(1C,5C):DMAP in 1:1 (a) and 1:2 (b) ratio together with topological simplifications of the HB networks

They have also used these phosphonic acids to construct supramolecular assemblies, which showed conformational polymorphism with 4-(N,N-dimethylamino)pyridine (DMAP) by just changing the ratio of acid:base (1:1 and 1:2). Hence, four adducts have been obtained two each of the phosphonic acid (Fig. 4.8). Moreover, they reported two more adducts formed by using the same two phosphonic acids in the presence of morpholine in 1:2 ratio and compare the effect of phosphonic tectons with varying conformational flexibility on the resulted supramolecular adduct structure (Fig. 4.9). After analyzing the crystal structure, they found that the more flexible building block, H_4NDP(1C,5C), due to the possibility of rotation along bonds with the sp^3 carbon atom, is pivotal from the coordination application point of view as it showed better adjustment in the resulted systems.

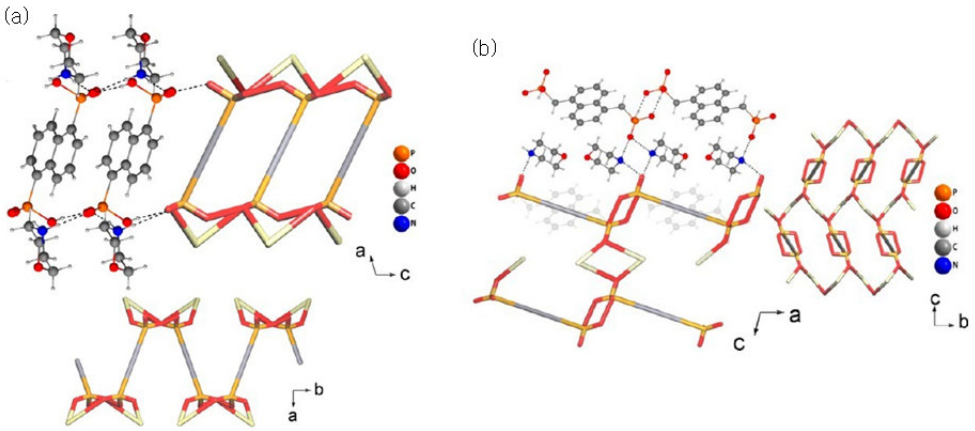

Fig. 4.9: Crystal structure projections of (a) H_4NDP(1,5):morpholine and (b) H_4NDP(1C,5C):morpholine in 1:2 along the *b*-axis together with topological simplifications of the HB networks

Functional metal organic frameworks (MOFs) are propitious materials because of their high intriguing architectures and their advanced material properties, like chemical separation, gas storage, catalysis, sensing etc. [27-29]. The usages of MOFs for gas storage (H_2, CO_2, CH_4, C_2H_2, etc.) and solvent adsorption/separations [30] are well documented in the literature. In order to improve the storage and separations abilities of these MOFs functionalization of organic linkers with various functional groups were attempted vastly [31]. The improved adsorption enthalpies during gas adsorption and elevated separation factor for the gas separation has been successfully achieved in MOFs due to the pore functionalization via organic ligands.

The utilization of multipyridyl ligands has received considerable attention and extensive work has been carried out using these rigid bridging ligands owing to the variety of coordination modes and structural features [32-33]. Strong coordination bonding between metal centers and nitrogen atoms from ligands results in the formation of MOFs with a greater level of complexity in their pore composition and structure, thus impacting the selectivity and multifunctionality of the pores. Analogous to the eminent 4,4'-bipyridine, the trigonal 3-connector such as 2,4,6-tris(4-pyridyl)-1,3,5-triazine and 2,4,6-tris(4-pyridyl)pyridine have been employed largely affording a number of MOFs and discrete supramolecular systems like squares, helices, cages, or rectangles [34]. Although, several MOFs bearing various degree of porosity have been synthesized, the functionalization of MOFs with multipyridyl ligands [35] is rare in the literature possibly due to the limitations for the functionalization of these ligands. Hence, in order to achieve the functionalization in MOFs using multipyridyl ligands, several synthetic and

post-synthetic modifications have been performed. Some related literatures have been discussed below.

Ikemoto et al. [36] showed the post-modification of the resulted coordination network formed from ZnI_2 and 1,3,5-tris(4-pyridyl)triazine ligand by carrying out Diel-Alder reaction within the porous network via heating. Similarly, Kawamichi et al. [37] demonstrated the use of porous coordination network as a molecular flask by diffusing the reagents into the pores and displayed that the reactivity of the reagents are similar as found in solution state with the advantage in the former as the reaction can be analyzed by crystallography (Fig. 4.10).

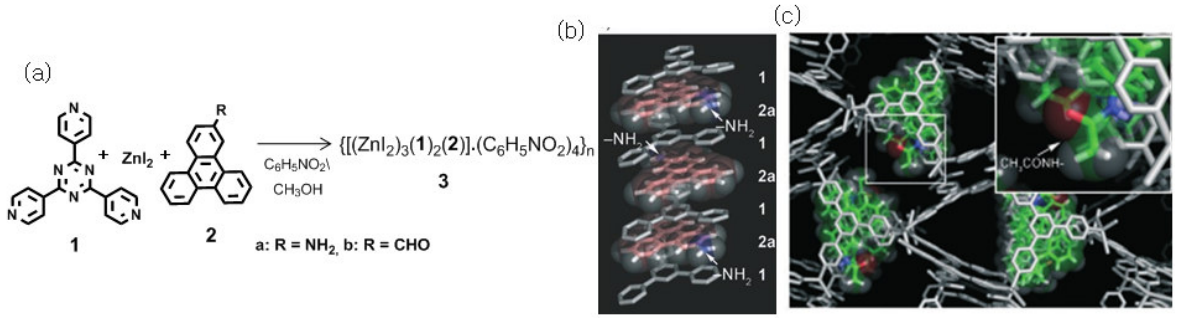

Fig. 4.10: (a) Schematic representation of the preparation of 3D porous networks; (b) perpendicular view to direction of pores, showing the columnar stacking of 1 and 2a in the network and (c) crystal structure of post-modified network

Wen et al. [38] reported the solvothermal synthesis of two microporous cadmium(II) metal organic frameworks (MMOFs), $[Cd(cptpy)(Ac)(H_2O)\cdot(DMA)(H_2O)]_n$ and $[Cd(cptpy)_2\cdot(DMF)_2]_n$ using 4-(4-carboxyphenyl)-2,2':4',4''-terpyridine (Hcptpy). They

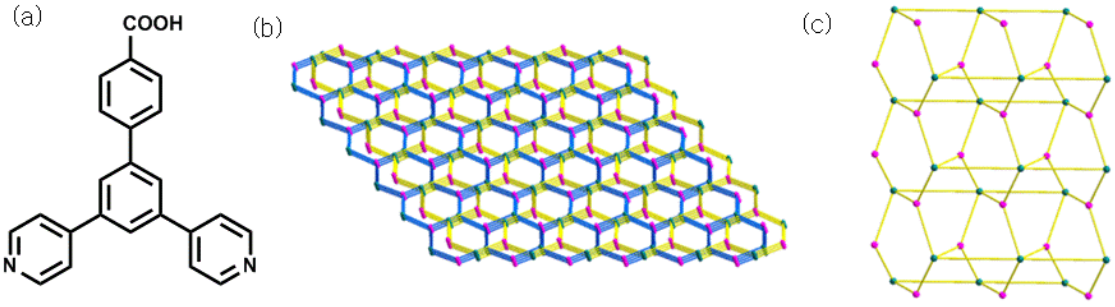

Fig. 4.11: (a) Chemical structure of ligand, Hcptpy; (b) schematic representation of the 'ths' network structure of $[Cd(cptpy)(Ac)(H_2O)\cdot(DMA)(H_2O)]_n$ and (c) schematic representation of binodal (3,5)-connected network of $[Cd(cptpy)_2\cdot(DMF)_2]_n$

found that the complex exhibited double-interpenetrating 3D network with 'ths' topology in DMA-H_2O reaction mixture, while non-interpenetrating (3,5)-connected 2D framework is obtained in presence of DMF-H_2O (Fig. 4.11). Furthermore, the two MMOFs showed selective adsorption of CO_2 over N_2 and H_2O over CH_3OH. They reported that the second MMOF displayed higher adsorptive property for CO_2 than the former one.

Constable et al. [39] reported 2D coordination assembly of 4'-phenyl-4,2':6',4''-terpyridine with Cd^{2+} in methanol and chloroform mixture. The structural study revealed that the undulating chains of *trans*-coordinated ligand with metal resulted in two-dimensional sheets, which are further interdigitated to each other via efficient π-stacking involving the phenyl substituents (Fig. 4.12).

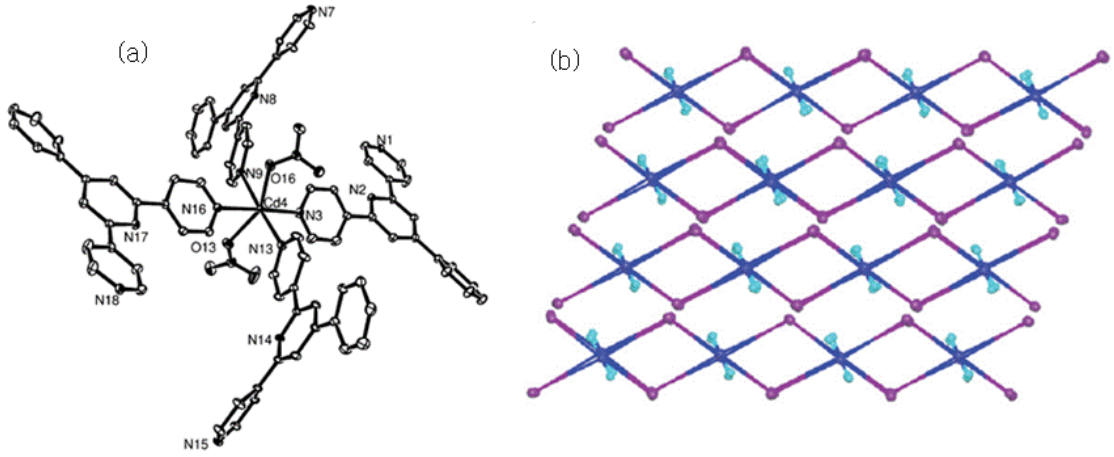

Fig. 4.12: (a) Coordination environment around one of the four independent cadmium atoms in [Cd(4'-phenyl-4,2':6',4''-terpyridine)$_2$(ONO_2)$_2$.MeOH.$CHCl_3$]$_n$ and (b) parallel arrangement of the nets

Martí-Rujas et al. [40] studied the three isostructural porous networks, [(ZnX_2)$_3$(TPT)$_2$]$_n$.solvent, where TPT = tris(4-pyridyl)triazine and X = I^-, Br^-, Cl^-, exhibiting crystalline-to-amorphous-to-crystalline (CAC) phase transformations to three new networks, [(ZnI_2)$_3$(TPT)$_2$]$_n$; [($ZnBr_2$)$_3$(TPT)$_2$]$_n$.(H_2O) and [($ZnBr_2$)(μ-Br)(ZnBr)(TPT)]$_n$; and, [($ZnCl_2$)(μ-Cl)(ZnCl)(TPT)]$_n$ respectively, on heating. On probing, they found that even the isostructural MOFs exhibited the different topology at higher temperature, which was hypothesized to be due to the bond strength of the Zn–X. They reported that these networks cannot be synthesized directly by using the reactants. Hence, they concluded that the initial arrangement of the interpenetrated structure is the main factor that triggers the reaction trajectory. However, the

structural information is retained by the amorphous phase and hence carried over to a metastable to form a more stable structure (Fig. 4.13).

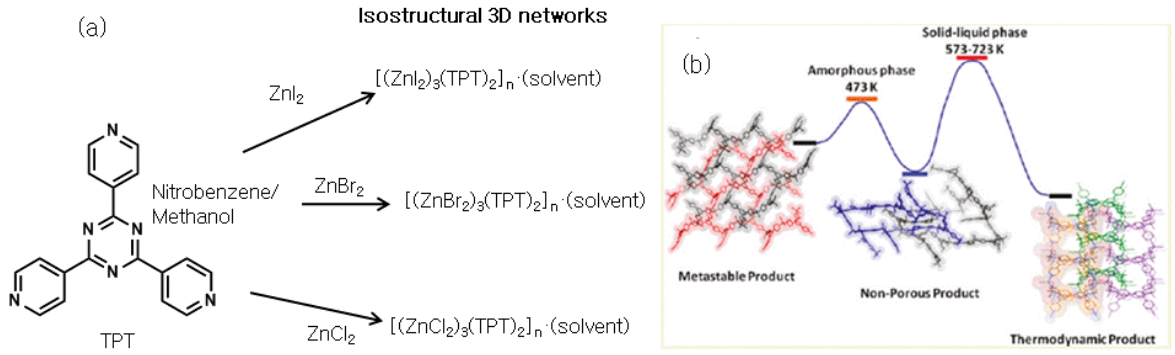

Fig. 4.13: (a) Schematic representation of porous isostructural coordination networks and (b) representation of the pathway to new design new class of material on heating

The MOFs functionalization achieved by the means of anions or groups like –F, $–NH_2$, –OH, –COOH [41-42] etc., in case of several MOFs, MILs and ZIFs was fruitful for the improved H_2 and CO_2 adsorption capacities. In other words, the MOF functionalization accomplished via ligand functionalization or anions has imparted the stabilities as well as hydrocarbon storage abilities to the MOFs. Some related literatures of gas adsorption have been discussed below.

Zhang et al. [43] reported the synthesis of a series of MOFs that has been constructed via ligand-functionalization strategy (Fig. 4.14). The authors systematically studied the series of MOFs with variation in functionalization on the ligand by performing

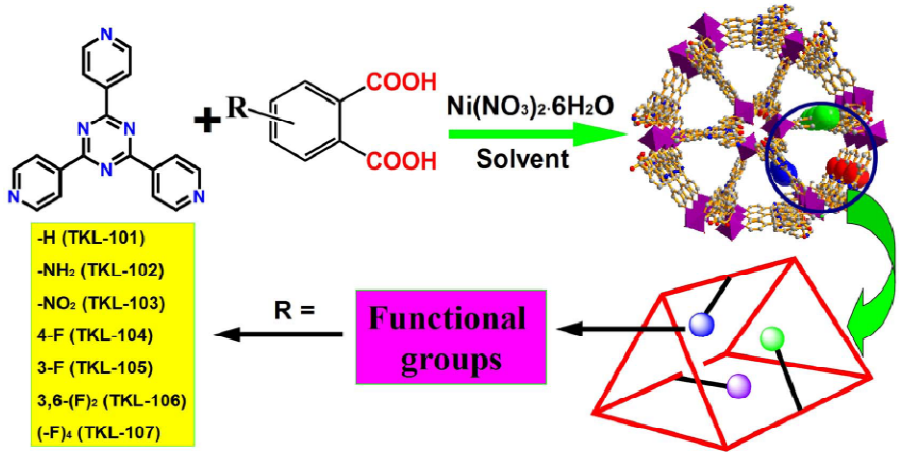

Fig. 4.14: General route for the synthesis of functionalized MOFs

adsorption study at low and high pressure. They observed that the ligand functionalized with fluorine resulted in the stable framework with significantly higher capacities towards H_2/CO_2, the same was well confirmed by theoretical studies of these MOFs structures. Hence, they suggested the MOF functionalized with fluorine group on its ligand can be used to construct mixed matrix membranes, displaying great potential for the application of CO_2 separation.

Pachfule et al. [44] solvothermally synthesized the 3D MOFs using ligands 4-(1H-tetrazole-5-yl)benzoic acid (4-TBA) and 2-fluoro-4-(1H-tetrazole-5-yl)benzoic acid (2F-4-TBA) with Cu(II) as a metal precursor. They observed that the high adsorption capacity for N_2, H_2, and CO_2 at 1 atm pressure for all highly porous resulted MOFs. The adsorption study revealed that fluorinated MOF showed less adsorption as compare to non-fluorinated. Therefore, they suggested that increment in adsorption of H_2 with fluorination is not a general phenomenon but it is structure directed (Fig. 4.15). Furthermore, theoretical study revealed that the directed fluorine atoms inside the pores of the MOF cause steric hindrance and hence resulted in the less adsorption of H_2.

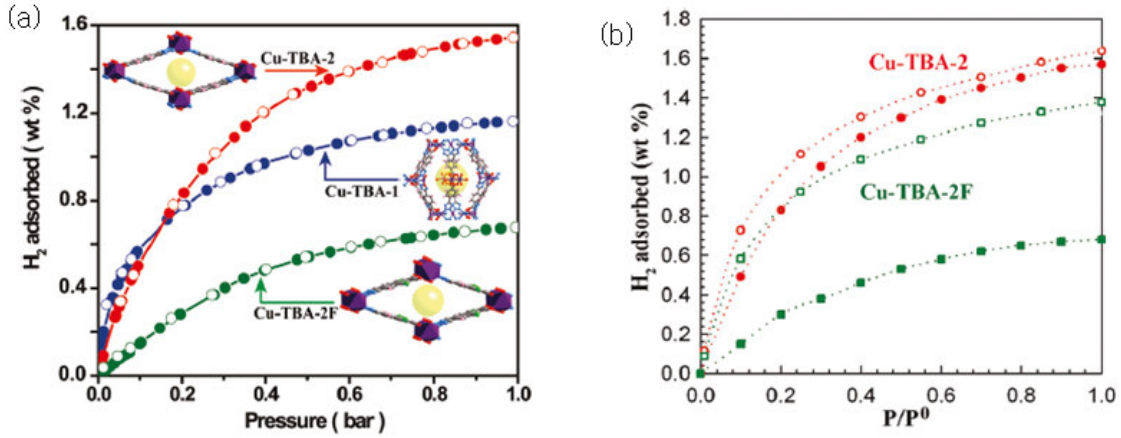

Fig. 4.15: (a) H_2 adsorption isotherms below 1.0 bar for Cu-TBA-1 (blue), -2 (red), and -2F (green) at 77 K and (b) simulated adsorption isotherms and H_2 adsorption sites in non-fluorinated and fluorinated MOFs

Dorofeeva et al. [45] reported the synthesis of 2D porous coordination polymer $[Fe_2NiO(Piv)_6(L1)]_n$ and discrete molecule $[\{Fe_2NiO(Piv)_6\}_8\{L2\}_{12}]$, possessing nanocube structure formed by using trinuclear building block, $\{Fe_2NiO(Piv)_6\}$ (Piv= pivalate) and, two ligands such as pseudo-D_3h ligand, tris-(4-pyridyl)pyridine (L1) and C_{2v} ligand, 4-(N,N-

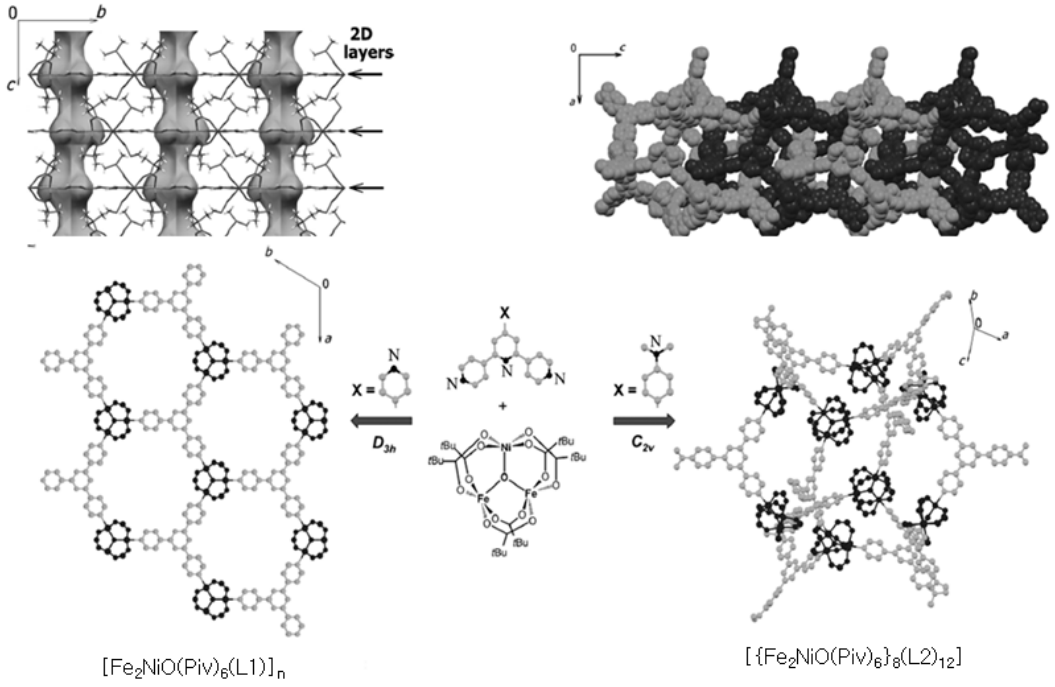

Fig. 4.16: Synthetic schematic representation of 2D porous coordination polymer $[Fe_2NiO(Piv)_6(L1)]_n$ and discrete molecule $[\{Fe_2NiO(Piv)_6\}_8(L2)_{12}]$ with their crystal structure

dimethylamino)phenyl-2,6-bis(4-pyridyl)pyridine (L2) (Fig. 4.16). They observed that the nanocube structure possesses infinite catenated chains, held together by hydrogen-bonding interactions. Moreover, they carried out N_2 and H_2 adsorption study for 2D porous coordination polymer and noticed that it absorbed significant quantities of N_2 and H_2 at 78 K (S_{BET}= 730 m^2g^{-1}, H_2 sorption capacity: 0.9% by weight at 865 Torr). Subsequently, the system collapsed on desolvation of the crystal structure.

Ma et al. [46] reported isostructural lanthanide microporous MOFs synthesized in DMSO by using trigonal-planar ligand, 4,4',4"-*s*-triazine-2,4,6-triyl-tribenzoate (TATB) and nitrate salts of various lanthanides, Ln such as Dy^{3+}, Er^{3+}, Y^{3+}, Yb^{3+}. On structural data analysis, they detected that the four isostructural MOFs exhibited square-planar $Ln_4(\mu_4–H_2O)$ cluster as the secondary building unit (SBU) and resulted in doubly interpenetrated (8,3)-connected nets. They explained that the pore size in MOFs was restricted due to interpenetration, therefore, it showed the potential application of separation of H_2 and O_2 over N_2 and CO (Fig. 4.17).

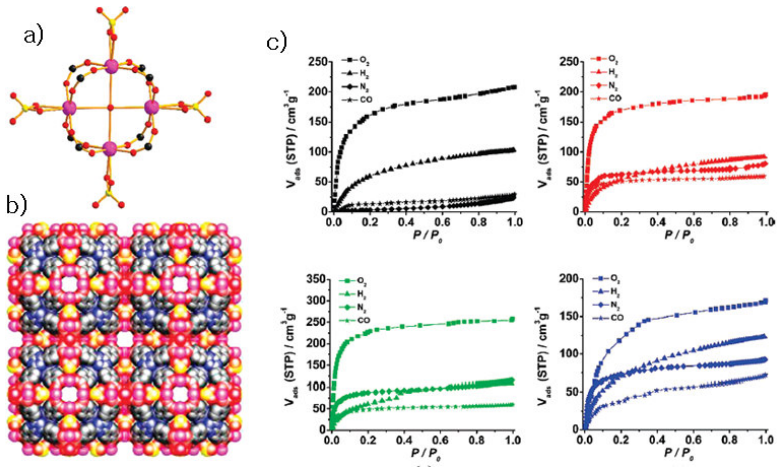

Fig. 4.17: (a) Structures of MOFs (Dy^{3+}, Er^{3+}, Y^{3+}, Yb^{3+}); (b) space-filling packing of activated sulfate-bridging doubly interpenetrated (8,3)-connected net and (c) O_2, H_2, N_2, and CO adsorption isotherms for four isostructural MOFs at 77 K

Rowsell et al. [47] studied the H_2 adsorption isotherm for isoreticular MOFs (IRMOFs) measured at 77 K up to a pressure of 1 atm and correlated them with their structural features. They used the ligand functionalized with –Br, $–NH_2$, –OH, thiophene analogue, etc., on the phenylene link of IRMOF-1 (MOF-5). They examined the effect of functionalization and organic domain linked to the ligand on the low pressure H_2 gas adsorption property of MOFs. On probing the adsorption isotherm, they found that the functional group has shown the minor effect on the adsorption of non-catenated MOFs regardless of large disparity in the pore volume of the resulted MOFs in contrast to catenated MOFs (Fig. 4.18). They also showed that the replacement of the groups containing coordinatively unsaturated metal sites with the metal oxide units resulted in greater H_2 uptake.

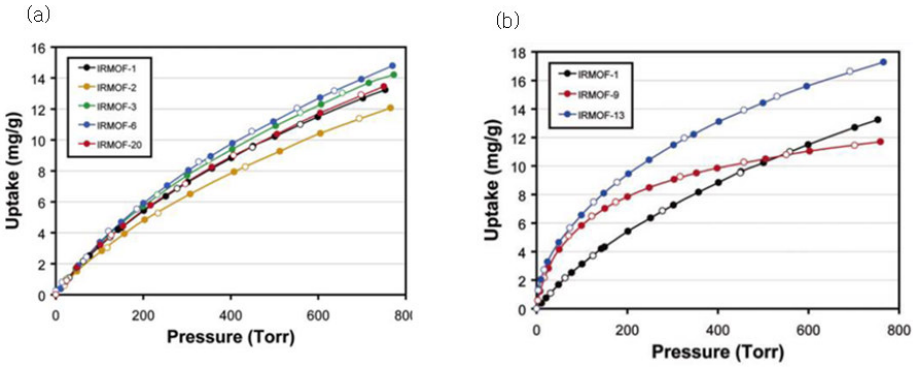

Fig. 4.18: Comparison of H_2 adsorption isotherms for (a) noncatenated IRMOFs and (b) catenated IRMOFs and IRMOF-1 measured at 77 K

Literature survey revealed that there are various reports on formation supramolecular assembly of phosphonic acid and pyridyl based ligands. But there is no report on the assembly formed by flexible phosphonic acid with pyridyl analogues. The conformational flexible triphosphonic acid with six ionisable hydrogens present on its three phosphonic groups, raises its chance to exist in various deprotonated form. Hence, it was envisaged that the flexible phosphonic acid can adopt various conformations in presence of different pyridyl analogues.

This chapter has dealt with the supramolecular reaction of flexible triphosphonic acid with several *N*-heterocyclic ditopic pyridyl based ligands. It was envisaged that conformational change in the ligand may exhibit polymorphism in the system. Construction of some polymorphs and pseudo-polymorphs of conformationally flexible triphosphonic acid was attempted and examined the interactions and synthons involved in the system. Moreover, the solid state transformation of one polymorph to another was also achieved via single-crystal-to-single-crystal transformation. Additionally, isostructural porous 2D MOFs were synthesized but still these MOFs exhibited tunable pore size with respect to the functionality. On the other hand, the impact of CO_2 adsorption has been showcased on tuning the dimensions of the channel due to the presence of different anions, which has not been reported earlier.

Result and discussion:

The inclusion of the flexible $–CH_2$ linker between the aromatic ring and $–PO_3H_2$ moiety in the phosphonic acid could lead to different relative organization for the phosphonic groups on either side of the phenyl ring [48]. Consequently, this results in the establishment of different conformations of triphosphonic depending on the relative dispositions of the phosphonic acids moieties. All possible conformations are shown in scheme 4.1.

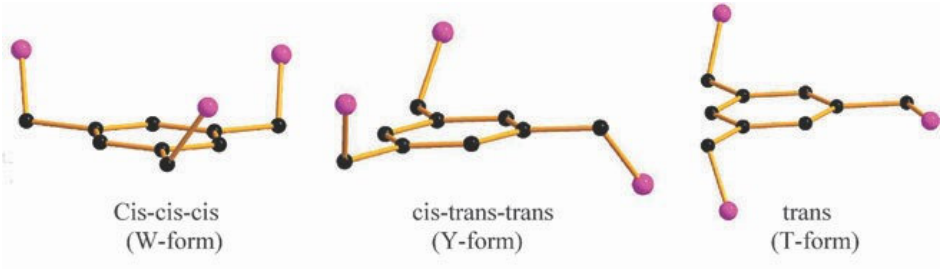

Scheme 4.1: Possible conformations for tripodal phosphonic acid

The supramolecular reaction between tripodal phosphonic acid i.e., ((2,4,6-trimethylbenzene-1,3,5-triyl)tris(methylene))triphosphonic acid (H_6TPA) and a variety of ditopic pyridine analogues such as 2,2'-bipyridine ($^{2,2'}BPy$), 4,4'-bipyridine ($^{4,4'}BPy$), 1,10-phenanthroline (Phen) and 4,2':6',4''-terpyridine (Terp) produced six molecular salts [$H_5TPA^-.H^{2,2'}BPy^+$] (**4a**), [$(H_4TPA^{2-})_2.(H_2{}^{4,4'}BPy^{2+})_2.H_2O$] (**4b**), [$H_4TPA^{2-}.H_2TPA^{4-}.(H_2{}^{4,4'}BPy^{2+})_3.(H_2O)_8$] (**4c**), [$H_5TPA^-.HPhen^+.(H_2O)_5$] (**4d**), [$H_5TPA^-.HPhen^+.MeOH$] (**4e**) and [$H_5TPA^-.H_4TPA^{2-}.H_3Terp^{3+}.S$] (**4f**) in high yields by using supramolecular approach (Scheme 4.2), where S in **4f** is squeezed solvent molecule.

Suitable crystals for single crystal X-ray analysis were grown from different solvents like methanol, dimethylformamide (DMF), water. The crystallographic data for **4a**-**4f** has been displayed in Table 4.1 - 4.6, whereas selected bond distances and bond angles are listed in Table 4.16.

In the complexes **4a**-**4f**, the conformational flexible TPA showed different orientation depending upon the ditopic ligands used and the solvent present in the lattice of the system. Hence, columns of TPA adopted five different packing **motifs I**-**V** (Fig. 4.41). While in **4e**, Phen molecules are present in between the tapes formed by TPA. On probing the salts **4a**-**4f**, it was found that the supramolecular networks are sustained by various synthons **I**-**IV** as displayed in scheme 4.3.

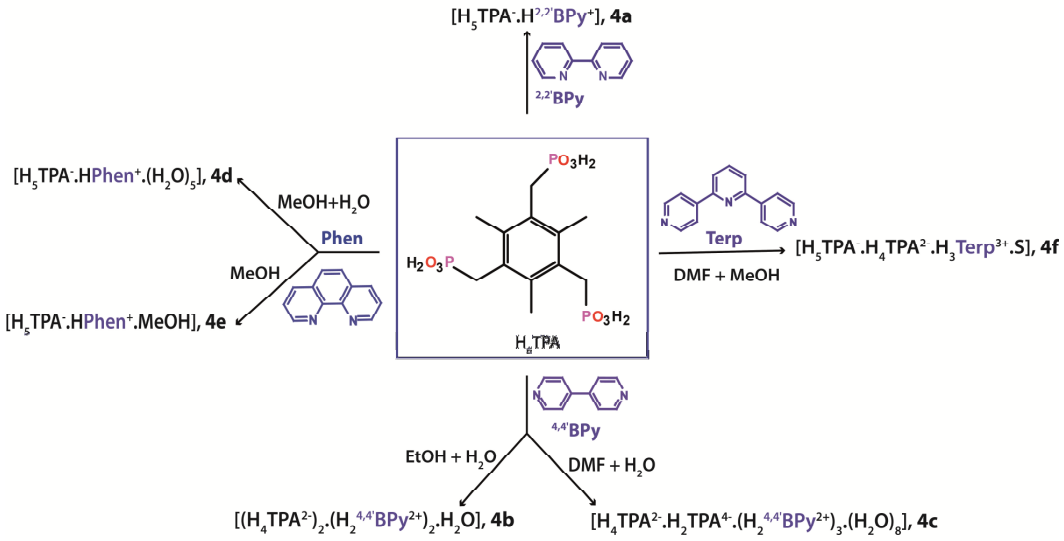

Scheme 4.2: Synthetic representation of salts **4a**-**4f**

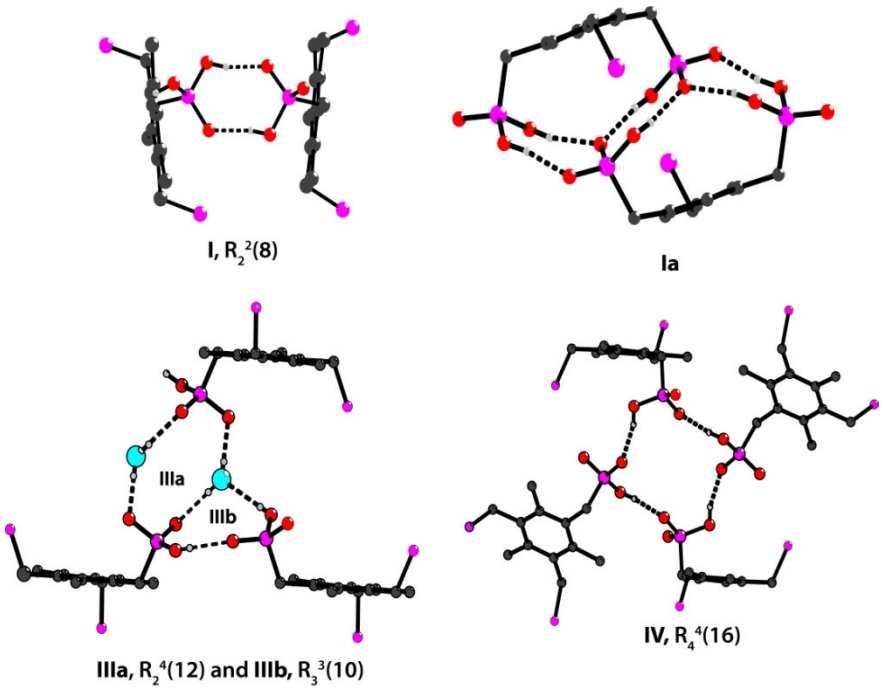

Scheme 4.3: Synthons **I-IV** observed in molecular salts **4a**-**4f**

Crystal structure of [$H_5TPA^-.H^{2,2'}BPy^+$] (4a):

Single-crystal X-ray analysis showed the transfer of proton from triphosphonic acid to $^{2,2'}$BPy, hence it disclosed the presence of one molecule each of triphosphonate (H_5TPA^-) and $^{2,2'}$BPy cation in its asymmetric unit (Fig. 4.19). Interestingly, the *cis*-form of H_5TPA^- molecule interacts with another H_5TPA^- molecule, therefore it resulted in the formation of three

consecutive dimers **Ia** via various O–H···O interactions (O6–H6E···O2, 1.719 Å; O4–H4E···O1, 1.791 Å; O3–H3E···O1, 1.746 Å) (Scheme 4.3). The pair of glued H_5TPA^- molecules is further extended to connect another pair of H_5TPA^- molecules in all four directions via O8–H8E···O5, 1.699 Å, which ends in the formation of 2D corrugated sheet of H_5TPA^- molecules in *bc*-plane (Fig. 4.20). Furthermore, this sheet is embellished with $^{2,2'}$BPy molecules above and below the sheet through N–H···O interaction (N2–H2D···O9, 1.825 Å). The attribute of TPA molecules to adopt many conformations that led to the variety of its hydrogen-bonded motif due to its flexibility in the molecule. Hence, salt **4a** displays **motif I** (Fig. 4.21).

Crystal structure of $[(H_4TPA^{2-})_2.(H_2^{4,4'}BPy^{2+})_2.H_2O]$ (4b):

Salt **4b** crystallized in triclinic system, *P*-1 space group and formed by the transfer of two proton from each triphosphonate anion to $^{4,4'}$BPy as confirmed by the bond length of P–O^-. The asymmetric unit consisted of two molecules each of triphosphonate and $^{4,4'}$BPy anions along with one water molecule (Fig. 4.22).

It was found that the chain of H_4TPA^{2-} molecule runs along *a*-axis and forms trimer synthon **IIIb** via various O–H···O interactions (O13–H13E···O11, 2.127 Å; O12···O19, 2.664 Å; O15···O19, 2.616 Å) with water molecule. Further, this chain is fastened together by the same chain along *c*-axis and formed a tape via a heterotetramer synthon **IIIa** (O19···O14, 2.395 Å) with two water molecules (Fig. 4.23). These tapes composed of H_4TPA^{2-} and water molecules linked with another tape along *b*-axis via another triphosphonate molecule involve various O–H···O interactions (O5–H5E···O9, 1.759 Å; O10–H10E···O2, 1.766 Å; O3–H3E···O11, 1.838 Å) and consequently, resulted in the formation of hydrogen bonded cavity, terminated by water molecules (Fig. 4.24). It may be noted that it was not possible to add hydrogen atoms on water molecule due to disorder in the system; hence, the water molecules are isolated. The framework is embellished by $^{4,4'}$BPy above and below the framework via N–H···O interactions (N2–H2D···O16, 1.791 Å; N1–H1D···O7, 1.767 Å) and corresponds to a **motif II** (Fig. 4.25).

Crystal structure of $[H_4TPA^{2-}.H_2TPA^{4-}.(H_2^{4,4'}BPy^{2+})_3.(H_2O)_8]$ (4c):

Salt **4c** crystallized in monoclinic system, *C2/c* space group with two molecules of triphosphonate anion and three molecules of $^{4,4'}$BPy cations along with eight water molecules in its asymmetric unit (Fig. 4.26). A phosphonate molecule form a dimer **I** via O–H···O interactions

(O8–H8E···O16, 1.827 Å; O17–H17E···O9, 1.720 Å) with another phosphonate molecule, which on the other end linked with $^{4,4'}$BPy molecule involving N–H···O interactions (N2–H2D···O13, 1.756 Å; N1–H1D···O2, 1.728 Å).

Due to presence of number of donors and acceptors atoms, an array of various N–H···O, O–H···O and π···π interactions resulted in the formation of hydrogen bonded porous supramolecular framework (Fig. 4.27) through synthons **I** and **IIIb** in *ab*-plane. However, the $^{4,4'}$BPy molecules are involved above and below the framework through π···π interaction between π-electron cloud of $^{4,4'}$BPy and triphosphonate anion (3.923 Å) and also between two $^{4,4'}$BPy's (3.565 Å). Similarly here, it was not possible to add hydrogen atoms on water molecules present in the lattice. The 1D column formed along *c*-axis holds cluster of water molecules in it and subsequently, the framework represents to be **motif III** (Fig. 4.28).

Crystal structure of [H_5TPA^-.$HPhen^+$.$(H_2O)_5$] (4d):

The asymmetric unit of salt **4d** is comprised of one molecule each of H_5TPA anion and HPhen cation along with five water molecules (Fig. 4.29) produced from the mixture of methanol and water (1:2). The triphosphonate in *cis*-mode forms three consecutive dimers as observed in **4a** (O6–H6E···O7, 1.772 Å; O8–H8E···O7, 1.772 Å; O4–H4E···O9, 1.694 Å) (Fig. 4.30).

These dimers are linked in all directions via O–H···O interaction (O3–H3E···O5, 1.723 Å) resulting in a 2D sheet formation in *ac*-plane. Further, these sheets stacked over one other but the neighbor sheet masked the cavities formed by the 2D neighbor sheet of H_5TPA^-. These inter-sheet interactions involve distinct O–H···O interactions connected through water molecules (O2···O12, 2.737 Å; O8-H8E···O7, 1.772 Å; O9···O10, 2.792; O5···O14, 2.982 Å; O5···O13, 2.807 Å; O14···O12, 2.566 Å) (Fig. 4.31) (Note: Due to failure in addition of H atoms on water molecule caused by the disorder, the interactions O–H···O is shown as O···O). These water molecules are placed at the corner of the hydrogen bonded cavity formed along *b*-axis. While, the $HPhen^+$ molecules are laid at the centre of the channel formed, interacting via N2–H2D···O2; 1.938 Å and hence, the resulted framework represents **motif IV** (Fig. 4.32).

Crystal structure of [H_5TPA^-.$HPhen^+$.MeOH] (4e):

Single crystal X-ray analysis revealed that it is composed of one molecule each of H_5TPA^- anion, $HPhen^+$ cation and a methanol molecule (Fig. 4.33) produced from the mixture of

methanol and water but in the different ratio (1.5:0.5). In **4e**, the phosphonate anion in *cis-trans* mode forms three consecutive dimers via O–H···O interaction (O6–H6E···O9, 1.697 Å; O8–H8E···O9, 1.799 Å; O4–H4E···O7, 1.783 Å) (Fig. 4.34).

Structural analysis disclosed that each of these fused dimers linked to the adjacent fused dimers (O3–H3E···O5, 1.741 Å) resulting in the formation of 2D sheet of H_5TPA^- along *b*-axis (Fig. 4.35). However, the $HPhen^+$ and methanol molecules are linked through intermolecular interactions (N2–H2D···O1, 1.929 Å; O10–H10E···O1, 1.979 Å) to the 2D sheet and lie in between them, which further directed the formation of 3D layered supramolecular network in *ac*-plane (Fig. 4.36).

Crystal structure of [$H_5TPA^-.H_4TPA^{2-}.H_3Terp^{3+}.S$] (4f):

Salt **4f** crystallized in $P2_1/c$ space group, monoclinic system with one molecule of Terp cation and two molecules of TPA anions in its asymmetric unit (Fig. 4.37). In salt **4f**, the phosphonate anions are arranged along *a*-axis via O–H···O interaction (O2–H2E···O5; 1.707 Å) and these chains are further linked to another chain of phosphonate by means of heterotetramer synthon **IV** involving O–H···O interaction (O16–H16E···O7, 1.652 Å; O18–H18E···O8, 1.712 Å) (Fig. 4.38) formed a tape. The resulted tape is further extended to *c*-axis using dimerisation (O12–H12E···O4, 1.724 Å; O6–H6E···O10, 1.794 Å). Hence, an array of O–H···O interactions led to the formation of a sheet through dimerisation in *bc*-plane (Fig. 4.39). Subsequently, an assemblage of O–H···O, N–H···O and π···π interactions generated the **motif V**, while H_3Terp^{3+} are arranged vertically via N–H···O interactions above and below the framework (Fig. 4.40). It may be noted that it was not possible to model the solvent molecule due to the disorder. Thus, the share of electron density was rejected by applying SQUEEZE treatment from PLATON program [49], and was tentatively found to be a DMF molecule with the help of TGA and elemental analysis.

Single-crystal-to-single-crystal transformation:

Remarkably, molecular complex involving H_6TPA and $^{4,4'}BPy$ showed polymorphism as they exist in two forms **4b** and **4c**. Moreover, the one form has been successfully synthesized from another via SC-SC transformation.

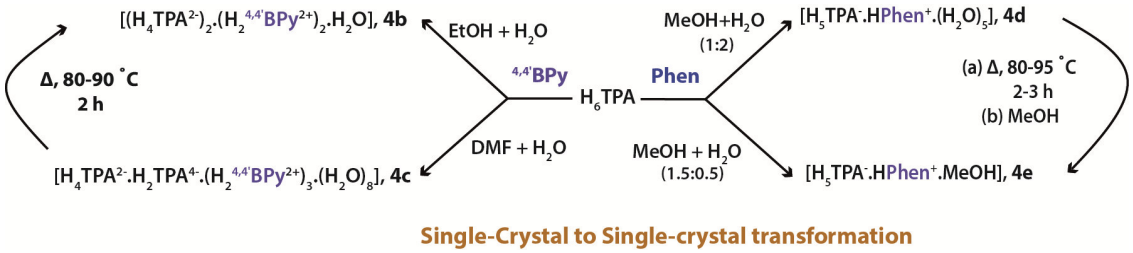

Scheme 4.4: Illustration of single crystal to single crystal transformation in salts **4b**-**4e**

It was envisioned that the as-synthesized crystals of **4c** was heated at 80-90 °C for 2 hrs (Scheme 4.4) and resulted in the formation of salt **4b** as confirmed by single-crystal XRD. Similarly, in molecular complex of H_6TPA with Phen can be considered as parent molecules, which in different ratio of same organic solvents afforded an organic solvent induced single crystal *viz*., salts **4d** (H_2O) and **4e** (MeOH). Additionally, one form can be transformed into another via SC-SC transformation. Similarly here, the salt **4d** heated around 80-95 °C for 2-3 hrs. Hence, water molecules were removed earlier on heating and the resulted compound was soaked in methanol, which furnished salt **4e** as confirmed by single-crystal XRD and powder XRD (Fig. 4.42). Although salts **4d** and **4e** exhibited same space group, but both illustrated different supramolecular networks depending upon the solvent molecule used [50], as former manifested the porous hydrogen bonded framework while latter represented the layered structure.

Metal Organic Frameworks (MOFs)

Many researchers have been attracted towards the formation of 3D rigid porous frameworks [51-52]. In contrast to the significant research on 3D rigid porous frameworks, it is surprising that little investigation on the third generation of soft materials has been undertaken in MOFs. In addition to these pyridyl based co-crystals, a newly synthesized pyridyl based ligand was also endeavored for the construction of MOFs. Known research is largely limited to the tripodal linkers like 2,4,6-tris(4-pyridyl)-1,3,5-triazine. Therefore, Cd^{2+}/Co^{2+}/Zn^{2+}/Eu^{2+} MOFs based on multiple Lewis basic sites (pyridine nitrogen's) i.e., polytopic ligand with three pyridyl donors and two methoxy, *viz.* 4'-(3,4-**dim**ethoxy**p**henyl)-4,2':6',4''-**t**erpyridine, **dmpt** (**4g**) were synthesized. The crystallographic data of dmpt has been summarized in Table 4.7. Recently, MOFs based on the same backbone of dmpt have been reported in the literature, wherein construction of two microporous cadmium based MOFs using 4-(4-carboxyphenyl)-2,2':4',4''-terpyridine ligand under different reaction conditions has been performed [38].

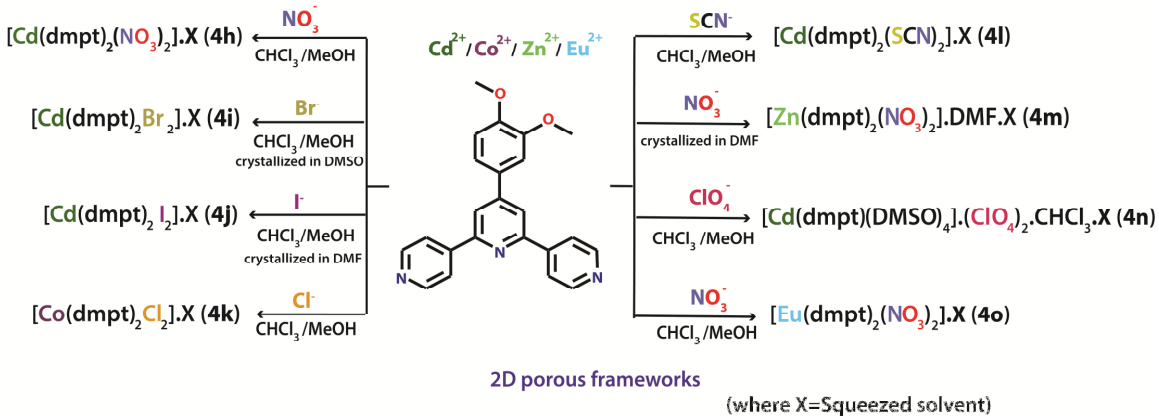

Scheme 4.5: Synthetic representation of MOFs **4h**-**4o**

In the present work of the study, $-NO_3$, $-ClO_4$, various halides (–Cl, –Br, –I) and pseudo-halide (SCN) have been used as the anions to facilitate the construction of eight 2D MOFs: $[Cd(dmpt)_2(NO_3)_2].X$ (**4h**), $[Cd(dmpt)_2Br_2].X$ (**4i**), $[Cd(dmpt)_2I_2].X$ (**4j**), $[Co(dmpt)_2Cl_2].X$ (**4k**), $[Cd(dmpt)_2(SCN)_2].X$ (**4l**), $[Zn(dmpt)_2(NO_3)_2].DMF.X$ (**4m**), $[Cd.dmpt.(DMSO)_4].(ClO_4)_2.CHCl_3.X$ (**4n**) and $[Eu(dmpt)_2(NO_3)_2].X$ (**4o**), in order to observe the impact of different anions on the dimensions of the channel and eventually on the adsorption of CO_2 gas (Scheme 4.5) where X= squeezed solvent. All MOFs are isomorphous, except **4l** and **4n**, exhibited the same topology with 2D binodal net and are characterized by single crystal X-ray diffraction technique. Although the molecular formula, unit cell parameters and the framework obtained for **4l** are same as for other MOFs but space group for **4l** is *P*-1 and *C*2/*c* for other MOFs. Notably, the structures reported here, except **4m**-**4n**, have number of features in common such as space group, nearly same unit cell parameters with same structure; but differs in dimensionality of channels. On the other hand, MOFs **4m**-**4n** exhibited different unit cell parameters and space group i.e., $P2_1/c$ and *P*-1 respectively. Besides, the resulting products are stable in air at ambient temperature and insoluble in common solvents such as water, alcohol, and acetonitrile. But, they are soluble in hot DMF or DMSO, therefore single crystal can also be obtained from its solution. The different synthetic methods for these MOFs are the evident for the stability of these compounds. The crystallographic data for MOFs, **4h**-**4o** has been displayed in Table 4.8-4.15.

Single crystal X-ray diffraction study revealed that all metal complexes **4h**-**4k**, **4m** and **4o** are isomorphic metal organic frameworks (IMOFs), belonging to monoclinic system with space group *C*2/*c* whereas **4m** exhibited same structure but with different space group i.e., $P2_1/c$.

Therefore, the structure of $[Cd(dmpt)_2(NO_3)_2]$ (**4h**) has been described here representatively. The asymmetric unit of these MOFs is consisted of one ligand, one monovalent anion (X = NO_3^-, Cl^-, Br^-, I^-), and one metal center lying on a crystallographic two-fold axis as demonstrated in Fig. 4.44 (**4h**), Fig. 4.51 (**4i**), Fig. 4.55 (**4j**), Fig. 4.59 (**4k**), Fig. 4.67 (**4m**) and Fig. 4.75 (**4o**). In each case, metal ion exhibited a six coordinated distorted octahedral geometry crowned with the N_4X_2 donor set, bonding from one exo-bidentate ligand and remaining two coordinating sites are occupied by the monodentate anions in trans-fashion. The coordination environment around the M(II) atom is displayed in Fig. 4.45 (**4h**), Fig. 4.52 (**4i**), Fig. 4.56 (**4j**), Fig. 4.60 (**4k**) and Fig. 4.68 (**4m**). However, in case of **4o**, Eu(II) exhibited eight coordinated geometry and bound to four nitrogen atoms each of four dmpt ligands and two bidendate nitrates (Fig. 4.76). The average bond distances, M(II)–N_1(Lewis base pyridyl), M(II)–N_2(Lewis base pyridyl) and M(II)–X in complexes **4h**-**4k**, **4m** and **4o** lie in the range of 2.220-2.410 Å, 2.296-2.483 Å and 2.291-2.880 Å, respectively, which are in good agreement with the previous studies [53-54]. It has been observed that the average M(II)–X bond lengths layout an increasing trend with the increase in size of the anion. The X–M–X' angle is perfect 180°, whereas the N–M–N angle around the M center ranges from 87.1° to 92.8°. Analysis of the crystal packing notified that each dmpt ligand binds to two M(II) via the two peripheral pyridyl donors, leaving the inner pyridyl unbound. On the other hand, each M(II) in turn connects four dmpt fragments, resulting in a two dimensional (2D) framework.

Coordination from both sides of the bidendate ligand extended the structure to one dimensional *zig-zag* chain along *ab*-plane. The twisting of the infrastructure of the ligand invoking the propagation of the clutch members of undulating chains at an angle of 102.7° along *ac*-plane (Fig. 4.46), which give rise to rhombohedral entity with metal site at the corners, can be treated as a secondary building unit (SBU) (Fig. 4.43). Hence, it resulted in the 2D architecture (Fig. 4.47 (**4h**), Fig. 4.53 (**4i**), Fig. 4.55 (**4j**), Fig. 4.61 (**4k**), Fig. 4.69 (**4m**) and Fig. 4.77 (**4o**)). The arrangement of the neighboring 2D layers results in the interdigitation of the layers. It was examined that the third arm in the ligand fetches two adjacent methoxy on the phenyl group acting as the pendant, plays a crucial role in further stabilizing the framework by offering the extension of 2D framework to 3D extended supramolecular solid architecture (Fig. 4.49 (**4h**), Fig. 4.54 (**4i**), Fig. 4.58 (**4j**), Fig. 4.62 (**4k**), Fig. 4.70 (**4m**) and Fig. 4.78 (**4o**)) with the help of $\pi\cdots\pi$ stacking ($\approx$ 4.244 and 3.899 Å) (Fig. 4.48) between the two inter-pendant groups in case of

MOFs **4h**-**4m**. However, in case of **4o**, the interlayer π-π stacking between central and peripheral pyridine ring (3.975 Å); central pyridine ring and the pendant ring (4.470 Å) has been displayed in Fig. 4.78. The selected bond lengths are given in Table 4.17-4.20 (**4h**-**4k**), Table 4.22 (**4m**) and Table 4.24 (**4o**). Additionally, some non–classical C–H···O and N–H···O interactions [55] have also been sighted in all MOFs to construct the 3D solid architecture as displayed in Table 4.25. The scrutiny of the 3D supramolecular framework enlightened that each M(II) center is linked to four different M(II) atoms via the four ligands to result in a 2D rhombohedral grid in the *c*-plane [39]. In the Cd_4 rhombus, the Cd–Cd distance through the bridging ligands found to be 13.6 Å (avg.), while the diagonal Cd–Cd separations are 11.6 (avg.) and 21.5 Å (avg.) (the average internal angles of the rhombus are 52.4 and 127.6°) (Fig. 4.50). The next layer of 2D rhombohedral grid is displaced along the *b*-axis, so that the 2D rhombohedral grids form ABAB pattern along the crystallographic *c*-axis and generated a 1D channel. Though the propagation of molecules in MOF **4m** is same but it displayed a disorder in coordinated nitrate anion. Hence, the framework manifested two dimensional channels along *a*- and *b*-axis accommodated by the DMF molecules (Fig. 4.69 and 4.70). Albeit, these MOFs are isostructural, but differ in the channel dimensions to some extent in all the cases – **4h** (6.5 X 6.6 $Å^2$), **4i** (8.1 X 7.4 $Å^2$), **4j** (7.0 X 6.9 $Å^2$), **4k** (6.7 X 6.5 $Å^2$), **4m** (9.7 X 7.5 $Å^2$) and **4o** (8.3 X 8.0 $Å^2$), which might be displayed by the virtue of flexibility of the framework (Table 4.26). Notably, the 1D column possesses alternate opening and closing pores along *c*-axis (Fig. 4.81). Moreover, the special feature of the structure is the directed anions inside the channel, which might selectively tune the adsorption property. It may be noted that the solvent molecule in all MOFs were highly disordered and no satisfactory disorder model could be accomplished, thus, the share of partial solvent electron densities was rejected by the SQUEEZE program in PLATON. Thereby, the solvents are tentatively designated based on TGA as well as the squeeze results i.e., one $CHCl_3$ molecule each in **4h**, **4k**; two $CHCl_3$ molecules in **4o**; one molecule of DMSO in **4i** and, one molecule DMF each in **4j** and **4m** respectively. On the other hand, the solvent-accessible volume and void volume for all MOFs are estimated by the PLATON program have been tabulated in detail (see Table 4.26). Topology analysis has led to the better understanding of the sophisticated 2D architecture, which details that the incorporated metal(II) ion can be considered as a 4-connnected node and the resulting structure exhibited a 2D uninodal 4^4-**sql** topology [56] (Fig. 4.80).

Crystal structure of $[Cd(dmpt)_2(SCN)_2].X$ (4l):

Single-crystal X-ray diffraction revealed that complex **4l**, crystallized in the triclinic space group, *P*-1. There are two crystallographically independent Cd^{2+} ions in the asymmetric unit (Fig. 4.63). The asymmetric unit consisted of two different conformational ligands showing drastic change in the torsion angle between central ring and the pendant varying from 2.66 to 22.47°. The local coordination geometry around each Cd^{2+} center is depicted in Fig. 4.64. The Cd1and Cd2 atoms are all coordinated by four nitrogen atoms of the pyridyl group from distinct bidentate dmpt and the axial position is engaged by SCN anions resulting in distorted octahedral coordination geometry. The average bond distance Cd1(II)–N1(Lewis base pyridyl), Cd1(II)–N5(Lewis base pyridyl), Cd(II)–N3(Lewis base pyridyl), Cd(II)–N7(Lewis base pyridyl) lie in the range of 2.388-2.419 Å. The N–Cd–N angles around the M center range from 87.6° to 92.3° building the equatorial plane of the octahedral geometry. However, the apical SCN^- ion is bound to Cd(II) through N atom with average Cd–N(SCN), N–C and C–S bond distances of 2.286, 1.143 and 1.626 respectively. These bond distances, in addition to bond angles of Cd1–N8–C48 and N8–C48–S2 of 172.08° and 177.21° respectively, are typical of a SCN^- ion bound to a metal through N atom and are in good agreement with the previous studies [53]. Despite of these, the second SCN group coordinated to Cd2 has different conformation as compare to the one coordinated to Cd1. The bond angles of Cd2–N4–C47 and N4–C47–S1 are 146.49° and 178.78° respectively. Both of these SCN groups are arranged in such a manner that they are orthogonal to each other. Nevertheless, complex **4l** has similar structural features such as metal-coordination environments, network topologies, and π···π interactions as discussed earlier. The propagation of molecules is similar as in MOF **4a**. Consequently, it led to the formation of similar 2D coordination network with SCN anions protruding towards the pore (Fig. 4.65). The selected bond lengths are given in Table 4.21, additionally, it also showed non–classical C–H···S interactions along with some C–H···O interactions as shown in Table 4.25. On analysis of extended 3D supramolecular framework (Fig. 4.66), it was found that the Cd–Cd distance through the bridging ligand, the diagonal Cd–Cd distance and the internal angles are nearly similar to that of **4a**. The MOF **4l** displayed the 1D channel dimension of 7.6 X 4.3 $Å^2$ occupied with SCN anion coordinated from Cd(II) and solvent molecules. While, the solvent molecules were highly disordered and hence, solvent electron densities were rejected by the SQUEEZE

program in PLATON, thereby, the solvents are tentatively assigned based on TGA as well as the squeeze results i.e., two $CHCl_3$ molecules.

Crystal structure of $[Cd.dmpt.(DMSO)_4].(ClO_4)_2.CHCl_3.X$ (4n):

Single crystal X-ray study revealed that MOF **4n**, crystallized in triclinic system, *P*-1 space group possess large non-interpenetrated rectangular cavities (*ca.* 13.9 X 6.4 $Å^2$). The large cavities residing ClO_4^- anions, $CHCl_3$ molecules, some unresolved disordered solvent molecule and coordinated DMSO molecules from the cationic framework. It is comprised of one dmpt, one metal ion, four coordinated DMSO molecules along with two molecules of ClO_4^- in order to balance the cationic framework in the asymmetric unit (Fig. 4.71).

The Cd(II) ion displays octahedral geometry by linking to four equatorial DMSO molecules and two axial dmpt molecules through N-atoms (Fig. 4.72). Likely in aforementioned MOFs, the Cd^{2+} ion coordinated by bidentate ligand from both sides extends the structure to 1D *zig-zag* chain but there is no propagation of another chain as the another site of Cd^{2+} has been blocked by DMSO molecules. The same *zig-zag* chain runs parallel along *a*-axis by the virtue of π···π interaction. Likewise here, the central pyridine ring remains unbound and the pendent group of the ligand is found to be primarily accountable for extending the 2D framework to 3D framework by π···π interaction (4.052 Å) between π-electron cloud of central pyridine ring from one layer and π-electron cloud of pendent ring of neighboring layer (Fig. 4.73). Thereafter, it exhibited the big hydrogen bonded rectangular cavities (Fig. 4.74), residing the encapsulated ClO_4^- anion and $CHCl_3$ molecules, which manifested C–H···O (anion) interaction with the ligand present in the cationic framework. The selected bond lengths for MOF **4n** are given in Table 4.23. Additionally, it also showed some non-classical Cl···O along with C–H···O interactions (Table 4.25). The MOF **4n** displayed the rectangular cavities of dimension *ca.* 13.9 X 6.4 $Å^2$ with solvent accessible volume and packing index of 521 $Å^3$ and 62.9 % respectively. Due to disorder, it was difficult to model solvent molecules hence the remaining unknown electron density was removed by treating the molecule with SQUEEZE in PLATON program. The solvents molecules are though tentatively designated based on TGA as well as the squeeze results i.e., two $CHCl_3$ molecules. Thus, the resulted 1D column possess the uncoordinated ClO_4^- anions, resolved and some unresolved $CHCl_3$ molecule and coordinated DMSO from Cd(II).

Refine_special_details

Thermal displacement parameters of some atoms such as C15, C11, O4, N4 and O5 were constrained by using EADP and SIMU in compound **4h**. On the other hand, in compounds **4i**-**4k**, only EADP constraint was used on atoms C12 and C11; N3 and C20; N3, C22, O1, C20, C17 and C18 respectively for a better configuration on the structure.

In compound **4h**-**4o**, the whole structure is slightly disordered, and that is the reason that the ADPs are elongated. It was deemed that the distortion in the structure is due to static disorder. Though, at low temperature, a better signal to noise ratio (higher I/sigma) was achieved, which led to much better agreement factors, despite, this distortion remained persistent. Similarly, in **4h**, **4m** and **4o**, the ADPs of nitrate are elongated due to the static disorder. It is worth noting that in case of MOF **4o**, the disorder was noticed in the nitrate anion coordinated to Eu(II). Due to the disorder, the oxygen O3-O5 of the nitrate anion occupied two positions with the site occupancy of 0.64:0.36, 0.80:0.20 and 0.57:0.43 respectively.

Platon squeeze details

The attempt of modeling the solvent molecule was ineffectual while solving the structure. Hence, the electron density was removed by SQUEEZE routine in PLATON to remove the solvent molecules from the pores of MOF **4h**-**4o**. According to the TGA analysis and squeeze results, the asymmetric unit of **4h**, **4k** consisted of one $CHCl_3$ molecule each whereas two $CHCl_3$ molecules were present in **4l**, **4n** and **4o**. On the other hand, the asymmetric unit of MOF **4i** is comprised of one DMSO molecule and, one molecule of DMF was found to be present in **4j** and **4m** in the pore.

IR, PXRD and thermogravimetric analysis

The appearance of C−N stretching bands at 1590−1599 and 1600−1662 cm^{-1} in the IR spectrum of **4h**-**4o** suggested the presence of free and coordinated pyridyl ring respectively. The characteristic absorption band with medium intensity of anions *viz*. NO_3^-, Cl^-, I^-, Br^-, SCN^- and ClO_4^- emerged at 1517, 820, 679, 665, 2070 and 1060 cm^{-1}, respectively. In order to study the bulk property of eight MOFs, PXRD measurements of MOFs **4h**-**4o** were carried out to validate whether the crystal structures are the actual model of their respective bulk materials (Fig. 4.82) and it was found that the peaks for synthesized compounds are in good agreement with the simulated one. To examine the thermal stability of **4a**-**4n**, TG analyses were carried out and it

flourished that MOFs **4h**-**4m** shows almost similar stability behavior towards thermal decomposition due to their isostructural nature.

It was analyzed that all triphosphonate salts were stable almost upto 250-260 °C. Among salts **4a**-**4f**, salts **4d**-**4f** have almost same stability as their framework starts decomposing at 260 °C. Initial mass loss in salt **4d** corresponds to the consecutive loss of two and three water molecules with mass loss of 5.7 and 9.2 % in the range of 110-210 °C. Later, mass loss around 270 °C relates to the loss of the organic fraction of the phosphonic acid. In case of salts **4e**-**4f**, the first mass loss of 6.2 % corresponds to the release of methanol molecule around 110-120 °C in former whereas in latter, the mass loss of 7.5 % accounts for the release of DMF molecule around 140-150 °C. In salts **4a**-**4c**, the framework was stable in the range of 230-250 °C. The initial loss of 2.8 % in **4b** corresponds to the loss of one water molecule and consecutive two mass losses of 3.5 % and 8.8 % accounts for loss of two and six water molecules around 90-180 °C in **4c** (Fig. 4.83).

On the other hand, all seven MOFs (**4h**-**4n**) were stable upto 500 °C due to similar structural properties. The primarily mass loss attributed to the loss of extra framework residual solvent molecules present in their respective lattices. The next mass loss indicates the loss of the organic component of the MOF.

In **4h**-**4n**, there is an initial loss of 11.4 % and 12.1 % corresponds to one $CHCl_3$ each in MOF **4h** and **4k**. The mass loss of 20.9 % manifested the loss of two molecules of $CHCl_3$ present in salt **4l**, however, the mass loss of 7.2 % and 7.4 % represented the loss of one DMF molecule each in **4j** and **4m**. In MOF **4i**, the mass loss of 8.3 % features the loss of one DMSO molecule. In contrast, MOF **4n** clearly showed two successive mass losses of 18.5 % and 29.7 % indicated the loss of two $CHCl_3$ molecules and four coordinated DMSO molecules respectively, nearly around 90 °C and 260 °C.

Adsorption Study

In last few decades, the variation in CO_2, N_2 gas adsorption was studied widely for functional MOFs [57] which protrude free functional groups towards the cavities. Finally, in order to analyze the effect of anions on the gas adsorption properties of the MOFs **4h**-**4m** and **4o**, the CO_2 gas uptake analysis was carried out. From single crystal X-ray diffraction analysis, it is apparent that the compounds **4h**-**4o** have 2D architecture with guest molecules occupying the pores/interlayer spacing and their pore sizes are comparable with kinetic diameters of N_2 and

CO_2. The N_2 adsorption isotherms performed on the compounds **4h**-**4m** and **4o** showed that these compounds are non-porous to nitrogen. The probable reason for the non-porous behavior with respect to N_2 may be due to their pore sizes being less or comparable with the kinetic diameter of nitrogen (3.65 Å). In spite of non porous nature of **4h**-**4m** and **4o** towards nitrogen, further studies have been made to explore their porosity by CO_2 adsorption as these molecules have lower kinetic diameter (CO_2 = 3.30 Å) than N_2. The CO_2 uptake studied at 273 K for **4h**-**4m** and **4o** showed an adsorption of 49.5, 39.8, 5.7, 22.6, 47.9, 25.3 and 50.6 cc/g of CO_2, respectively, as the pressure reaches to 1 bar. The framework in **4o** with Eu(II) ions though show the high packing index of 50.6 % but relatively display the highest CO_2 adsorption among all MOFs. It might be due to donor-acceptor affinity found between the Lewis acidic Eu(II) and the CO_2 molecules. It may be noted that due to an abortive task of modeling the disorder nitrate anion in MOF **4m** even at low temperature data collection. The solvent accessible void and the packing index were calculated tentatively using platon. On the other hand, the ClO_4^- anions in the pores of the MOF **4n** may possibly interrupt the adsorption of gas.

As shown in Fig. 4.84 and 4.85, the trends for CO_2 adsorption study are observed as $-NO_3$ > −Br > −Cl > −I, as per difference in electronegativity values from **4h** > **4i** > **4k** > **4j**. The two-dimensional architecture of **4h**-**4m** and **4o** holds considerable pore sizes on all compounds which favors the CO_2 uptake. The trend exposed in the CO_2 uptake is primarily due to polarization of the anions protruding towards the cavities and the space available to the solvent (solvent accessible void). The higher CO_2 uptake observed in case of **4h** and **4o**, as $-NO_3$ is polar group and more polarizing, which may be responsible for more CO_2 adsorption. Among all halogen and pseudo-halogen anions, SCN^- anion in **4l** apparently showed higher adsorption due to its polarizing group. It has more electron density followed by −Br in **4i**, which showed the higher adsorption than −Cl and −I as in this case it possess high solvent accessible volume (581 $Å^3$). However in case of **4j**, it displayed less CO_2 adsorption due to the comprehensible reflection of less polarized −I group. Hence, it was concluded that the polarizing group is mainly responsible for the adsorption in addition to the presence of solvent accessible void. Although N_2 and CO_2 have almost similar kinetic diameters but in case of N_2 adsorption, quadrupole interactions of N_2 remains lower than thermal energy at very lower temperature (77 K), which probably blocks the pore openings. While the elevated quadrupole interactions of CO_2 compared to the thermal energy in the case of CO_2 adsorption at 273 K, which does not block the windows

of pore openings [58], favors the uptake of CO_2 (273 K) over N_2 (77 K) in all the compounds. The CO_2 uptake shown by these compounds is moderate though, but the trends in these uptakes observed are interesting, which mostly depends on the anions present in the MOFs for the interaction with adsorbing gaseous molecules.

Summary:

In order to attain the complete knowledge of interaction between flexible phosphonic acid and ditopic ligand, six salts **4a**-**4f** of flexible phosphonate have been produced. Owing to the flexible arms present on the phosphonic acid, columns of TPA adopted five different packing **motifs I**-**V**. The salts **4b** and **4c** in presence of H_2O molecules showed polymorphism and manifests two different **motifs II** and **III**. Notably, among complexes **4a**-**4f**, **4a** and **4d** represents *cis*-conformation of TPA, rest all show *trans*-conformation of TPA. Therefore, it illustrated that TPA showed different orientation depending upon the ditopic ligands used. In case of **4d**, a hydrogen bonded chain is generated by triphosphonic and water via O–H···O interaction along *a*-axis whereas in case of its polymorph **4c**, hydrogen bond between triphosphonic acid and water resulted in a continuous chain of water and one of the −OH of the phosphonic acid. It has been anticipated that the latter complex allows the continuous proton transfer in the infinite chain of phosphonic and water molecules, thereafter, it might show proton conductivity.

Noticeably, complex of H_6TPA with Phen and $^{4,4'}$BPy can be employed as a pioneer in various organic solvents for its rational synthesis via single-crystal-to-single-crystal transformation. These salts were constructed directly in different solvents and the flexible nature of the phosphonic acid allows the system to produce these salts from solid to solid synthesis via SC-SC transformation.

The conformational flexible polytopic pyridine based ligands have appealing structure properties for the generation of soft porous materials, thereby, it was envisaged that the anions can be responsible (since the ligand is neutral) for the tuning of pore size of MOFs. Therefore, it can be used as absorber for selective gases. Herein, the polytopic pyridine based ligand has been modified by introducing two methoxy groups on the pendant of the ligand with conformationally flexibility in order to implement our objective to engineer the porous MOFs. It was found that the organic ligand with methoxy groups protruding into the framework pores of the coordination framework offered the potential to tune the adsorption properties with change in anions.

Single crystal X-ray diffraction study revealed that all metal complexes **4h**-**4k**, **4m** and **4o** are isomorphic metal organic frameworks (IMOFs), belonging to monoclinic system. They possess similar structural features such as metal-coordination environments, network topologies, π···π interactions and exhibits a 2D uninodal of 4^4-**sql** topology with slightly tuned cavity. In complexes **4h**-**4o** except in **4n**, [[$M(dmpt)_2(A)_2$]·X] (where A = anion, X = squeezed solvent) coordination monomer acts as the building block, building the 2D layer and is further piled up via Vander Waal interactions into three-dimensional (3D) framework. Thereby, the effect of weak interactions on structural dynamics of the systems has also been studied. On the other hand, the MOF **4n** displayed the large rectangular cavities of dimension *ca.* 13.9 X 6.4 $Å^2$. The 1D column formed possess the uncoordinated ClO_4^- anions, $CHCl_3$ molecule and coordinated DMSO from Cd(II). Furthermore, the impact of different anions present in the porous isomorphous MOFs has been studied on gas adsorption study. On analysis, it was demonstrated that the sorption study was affected with the change in anions directing inside the pores. Albeit, the CO_2 uptake shown by the MOFs is modest, still the trends is mostly dependent on the variation of anions present in the MOFs for the interaction with adsorbing gaseous molecules and also depend upon the solvent accessible void volume for particular MOF.

Table 4.1: Crystal Data and Collection Details of [$H_5TPA^-.H^{2,2'}BPy^+$] (4a)

Emprical formula	$C_{22}H_{29}N_2O_9P_3$
Formula weight	558.38
Crystal system	Monoclinic
Space group	$P2_1/n$
a/ Å	11.770(3)
b/ Å	13.614(3)
c/ Å	15.227(4)
α/ ^{o}	90
β/ ^{o}	94.76(12)
γ/ ^{o}	90
V / Å^3	2431.5(10)
Z	4
D_{calc} (g cm^{-3})	1.525
μ/mm^{-3}	0.302
θ range/ ^{o}	2.01 - 26.48
Reflections collected	4943
Independent reflections	3686
Parameters/ Restraints	333/0
GOF (F^2)	1.272
R_1; wR_2 [I>2σ(I)]	0.0588; 0.1893
R_1; wR_2 (all data)	0.0804; 0.2030
$\Delta\rho_{max}$; $\Delta\rho_{min}$	0.588; -0.847

Table 4.2: Crystal Data and Collection Details of $[(H_4TPA^{2-})_2.(H_2^{4,4'}BPy^{2+})_2.H_2O]$ (4b)

Emprical formula	$C_{44}H_{58}N_4O_{19}P_6$
Formula weight	1132.76
Crystal system	Triclinic
Space group	*P*-1
a/ Å	11.283(5)
b/ Å	13.939(6)
c/ Å	18.496(8)
α/ ^{o}	102.88(2)
β/ ^{o}	90.87(2)
γ/ ^{o}	95.39(2)
V / Å^3	2821.4(2)
Z	2
D_{calc} (g cm^{-3})	1.333
μ/mm^{-3}	0.262
θ range/ ^{o}	1.67 - 26.41
Reflections collected	11482
Independent reflections	8707
Parameters/ Restraints	688/6
GOF (F^2)	1.009
R_1; wR_2 [I>2σ(I)]	0.0481; 0.1450
R_1; wR_2 (all data)	0.0638; 0.1566
$\Delta\rho_{max}$; $\Delta\rho_{min}$	0.885; -0.713

Table 4.3: Crystal Data and Collection Details of $[H_4TPA^{2-}.H_2TPA^{4-}.(H_2^{4,4'}BPy^{2+})_3.(H_2O)_8]$ (4c)

Emprical formula	$C_{54}H_{66}N_6O_{26}P_6$
Formula weight	1400.95
Crystal system	Monoclinic
Space group	*C*2/*c*
a/ Å	36.770(4)
b/ Å	18.634(2)
c/ Å	20.682(2)
α/ ^{o}	90
β/ ^{o}	117.34(4)
γ/ ^{o}	90
V / Å^3	12588.0(2)
Z	8
D_{calc} (g cm^{-3})	1.479
μ/mm^{-3}	0.260
θ range/ ^{o}	1.86 - 26.60
Reflections collected	12892
Independent reflections	5720
Parameters/ Restraints	842/18
GOF (F^2)	1.052
R_1; wR_2 [I>2σ(I)]	0.1334; 0.3381
R_1; wR_2 (all data)	0.2531; 0.4126
$\Delta\rho_{max}$; $\Delta\rho_{min}$	0.959; -0.501

Table 4.4: Crystal Data and Collection Details of $[H_5TPA^-.HPhen^+.(H_2O)_5]$ (4d)

Emprical formula	$C_{24}H_{31}N_2O_{14}P_3$
Formula weight	664.42
Crystal system	Monoclinic
Space group	$P2_1/n$
a/ Å	11.410(4)
b/ Å	16.663(6)
c/ Å	16.175(7)
α/ ^{o}	90
β/ ^{o}	104.32(2)
γ/ ^{o}	90
V / Å^3	2980.0(2)
Z	4
D_{calc} (g cm^{-3})	1.481
μ/mm^{-3}	0.271
θ range/ ^{o}	2.21 - 28.40
Reflections collected	7452
Independent reflections	5285
Parameters/ Restraints	405/9
GOF (F^2)	1.039
R_1; wR_2 [I>2σ(I)]	0.0583; 0.1723
R_1; wR_2 (all data)	0.0827; 0.1937
$\Delta\rho_{max}$; $\Delta\rho_{min}$	0.837; -0.622

Table 4.5: Crystal Data and Collection Details of [H_5TPA^-.$HPhen^+$.MeOH] (4e)

Emprical formula	$C_{25}H_{33}N_2O_{10}P_3$
Formula weight	614.44
Crystal system	Monoclinic
Space group	$P2_1/n$
a/ Å	16.793(8)
b/ Å	9.886(4)
c/ Å	17.370(8)
α/ ^{o}	90
β/ ^{o}	103(1)
γ/ ^{o}	90
V / Å^3	2810.1(2)
Z	4
D_{calc} (g cm^{-3})	1.452
μ/mm^{-3}	0.271
θ range/ ^{o}	1.52 - 25.00
Reflections collected	4419
Independent reflections	3444
Parameters/ Restraints	371/0
GOF (F^2)	1.574
R_1; wR_2 [I>2σ(I)]	0.0487; 0.1463
R_1; wR_2 (all data)	0.0657; 0.1614
$\Delta\rho_{max}$; $\Delta\rho_{min}$	0.411; -0.519

Table 4.6: Crystal Data and Collection Details of [$H_5TPA^-.H_4TPA^{2-}.H_3Terp^{3+}.S$] (4f) (squeezed)

Emprical formula	$C_{42}H_{60}N_4O_{19}P_6$
Formula weight	1110.78
Crystal system	Monoclinic
Space group	*C*2/*c*
a/ Å	9.790(4)
b/ Å	18.657(7)
c/ Å	26.945(11)
α/ ^{o}	90
β/ ^{o}	92.63(2)
γ/ ^{o}	90
V / Å^3	4917.0(3)
Z	4
D_{calc} (g cm^{-3})	1.402
μ/mm^{-3}	0.292
θ range/ ^{o}	1.33 - 28.39
Reflections collected	12151
Independent reflections	5800
Parameters/ Restraints	610/0
GOF (F^2)	1.123
R_1; wR_2 [I>2σ(I)]	0.0709; 0.1769
R_1; wR_2 (all data)	0.1506; 0.2033
$\Delta\rho_{max}$; $\Delta\rho_{min}$	0.406; -0.482

Table 4.7: Crystal Data and Collection Details of dmpt (4g)

Emprical formula	$C_{23}H_{19}N_3O_2$
Formula weight	369.41
Crystal system	Triclinic
Space group	*P*-1
a/ Å	9.468(14)
b/ Å	10.433(17)
c/ Å	10.742(17)
α/ ^{o}	67.34(9)
β/ ^{o}	73.25(9)
γ/ ^{o}	85.91(9)
V / Å^3	936.8(3)
Z	2
D_{calc} (g cm^{-3})	1.310
μ/mm^{-3}	0.085
θ range/ ^{o}	2.12 - 26.42
Reflections collected	10452
Independent reflections	3579
Parameters/ Restraints	255/0
GOF (F^2)	0.912
R_1; wR_2 [I>2σ(I)]	0.0457; 0.1282
R_1; wR_2 (all data)	0.0751; 0.1539
$\Delta\rho_{max}$; $\Delta\rho_{min}$	0.155; -0.172

Table 4.8: Crystal Data and Collection Details of $[Cd(dmpt)_2(NO_3)_2].X$ (4h) (squeezed)

Emprical formula	$C_{47}H_{38}CdN_8Cl_4O_{10}$
Formula weight	1129.08
Crystal system	Monoclinic
Space group	*C2/c*
a/ Å	24.603(5)
b/ Å	11.964(3)
c/ Å	18.426(4)
α/ °	90
β/ °	114.57(1)
γ/ °	90
V / Å^3	4933.3(2)
Z	4
D_{calc} (g cm^{-3})	1.313
μ/mm^{-3}	0.504
θ range/ °	1.82 - 26.42
Reflections collected	41014
Independent reflections	5034
Parameters/ Restraints	297/0
GOF (F^2)	0.975
R_1; wR_2 [I>2σ(I)]	0.0486; 0.2081
R_1; wR_2 (all data)	0.0573; 0.2238
$\Delta\rho_{max}$; $\Delta\rho_{min}$	1.151; -0.940

Table 4.9: Crystal Data and Collection Details of $[Cd(dmpt)_2Br_2].X$ (4i) (squeezed)

Emprical formula	$C_{48}H_{44}CdBr_2N_6O_5S$
Formula weight	1089.18
Crystal system	Monoclinic
Space group	*C2/c*
a/ Å	24.885(11)
b/ Å	11.925(6)
c/ Å	18.044(8)
α/ °	90
β/ °	113.46(3)
γ/ °	90
V / Å^3	4912.2(4)
Z	4
D_{calc} (g cm^{-3})	1.367
μ/mm^{-3}	2.116
θ range/ °	1.78 - 20.08
Reflections collected	23824
Independent reflections	2315
Parameters/ Restraints	270/0
GOF (F^2)	1.023
R_1; wR_2 [I>2σ(I)]	0.0346; 0.1199
R_1; wR_2 (all data)	0.0417; 0.1254
$\Delta\rho_{max}$; $\Delta\rho_{min}$	1.064; -1.613

Table 4.10: Crystal Data and Collection Details of $[Cd(dmpt)_2I_2].X$ (4j) (squeezed)

Emprical formula	$C_{49}H_{45}CdI_2N_7O_5$
Formula weight	1178.15
Crystal system	Monoclinic
Space group	*C2/c*
a/ Å	25.611(7)
b/ Å	11.566(3)
c/ Å	18.539(6)
α/ °	90
β/ °	114.34(10)
γ/ °	90
V / Å^3	5003.7(3)
Z	4
D_{calc} (g cm^{-3})	1.467
μ/mm^{-3}	1.714
θ range/ °	1.75 - 26.40
Reflections collected	31991
Independent reflections	5122
Parameters/ Restraints	270/0
GOF (F^2)	0.809
R_1; wR_2 [I>2σ(I)]	0.0311; 0.1106
R_1; wR_2 (all data)	0.0406; 0.1178
$\Delta\rho_{max}$; $\Delta\rho_{min}$	1.024; -1.284

Table 4.11: Crystal Data and Collection Details of $[Co(dmpt)_2Cl_2].X$ (4k) (squeezed)

Emprical formula	$C_{47}H_{39}CoN_6Cl_5O_4$
Formula weight	988.05
Crystal system	Monoclinic
Space group	*C2/c*
a/ Å	24.484(18)
b/ Å	11.890(8)
c/ Å	18.110(13)
α/ °	90
β/ °	114.56(4)
γ/ °	90
V / Å^3	4795.3(6)
Z	4
D_{calc} (g cm^{-3})	1.203
μ/mm^{-3}	0.514
θ range/ °	1.83 - 26.42
Reflections collected	36341
Independent reflections	4874
Parameters/ Restraints	270/0
GOF (F^2)	1.168
R_1; wR_2 [I>2σ(I)]	0.0630; 0.1875
R_1; wR_2 (all data)	0.1087; 0.2007
$\Delta\rho_{max}$; $\Delta\rho_{min}$	0.818; -0.758

Table 4.12: Crystal Data and Collection Details of $[Cd(dmpt)_2(SCN)_2].X$ (4l) (squeezed)

Emprical formula	$C_{50}H_{40}CdN_8O_4S_2Cl_6$
Formula weight	1206.16
Crystal system	Triclinic
Space group	*P*-1
a/ Å	11.817(2)
b/ Å	13.439(3)
c/ Å	18.201(4)
α/ °	110.60(10)
β/ °	92.50(10)
γ/ °	113.87(10)
V / Å^3	2415.1(9)
Z	2
D_{calc} (g cm^{-3})	1.330
μ/mm^{-3}	0.589
θ range/ °	1.22 - 28.40
Reflections collected	42342
Independent reflections	12051
Parameters/ Restraints	575/0
GOF (F^2)	0.841
R_1; wR_2 [I>2σ(I)]	0.0309; 0.0940
R_1; wR_2 (all data)	0.0404; 0.1015
$\Delta\rho_{max}$; $\Delta\rho_{min}$	0.887; -0.768

Table 4.13: Crystal Data and Collection Details of $[Zn(dmpt)_2(NO_3)_2].DMF.X$ (4m) (squeezed)

Emprical formula	$C_{55}H_{59}ZnN_{12}O_{15}$
Formula weight	1193.51
Crystal system	Monoclinic
Space group	$P2_1/c$
a/ Å	13.244(13)
b/ Å	7.884(9)
c/ Å	24.674(3)
α/ ^{o}	90
β/ ^{o}	91.64(6)
γ/ ^{o}	90
V / Å^3	2575.5(5)
Z	2
D_{calc} (g cm^{-3})	1.463
μ/mm^{-3}	0.558
θ range/ ^{o}	2.22 - 28.45
Reflections collected	31632
Independent reflections	6437
Parameters/ Restraints	362/0
GOF (F^2)	1.430
R_1; wR_2 [I>2σ(I)]	0.1461; 0.4027
R_1; wR_2 (all data)	0.2208; 0.4414
$\Delta\rho_{max}$; $\Delta\rho_{min}$	3.606; -1.610

Table 4.14: Crystal Data and Collection Details of [Cd.dmpt.$(DMSO)_4$].$(ClO_4)_2$.$CHCl_3$.X (4n) (squeezed)

Emprical formula	$C_{34}H_{46}CdN_3Cl_{11}O_{14}S_4$
Formula weight	1351.39
Crystal system	Triclinic
Space group	*P*-1
a/ Å	8.738(11)
b/ Å	16.762(19)
c/ Å	17.658(2)
α/ ^{o}	102.05(6)
β/ ^{o}	100.58(5)
γ/ ^{o}	100.35(5)
V / Å^3	2421.5(5)
Z	2
D_{calc} (g cm^{-3})	1.526
μ/mm^{-3}	0.959
θ range/ ^{o}	2.54 - 28.39
Reflections collected	11461
Independent reflections	8809
Parameters/ Restraints	545/0
GOF (F^2)	0.925
R_1; wR_2 [I>2σ(I)]	0.0774; 0.2146
R_1; wR_2 (all data)	0.0962; 0.2321
$\Delta\rho_{max}$; $\Delta\rho_{min}$	2.612; -2.440

Table 4.15: Crystal Data and Collection Details of $[Eu(dmpt)_2(NO_3)_2].X$ (4o) (squeezed)

Emprical formula	$C_{48}H_{40}EuN_8Cl_6O_{10}$
Formula weight	1253.56
Crystal system	Monoclinic
Space group	*C2/c*
a/ Å	24.691(2)
b/ Å	11.929(12)
c/ Å	18.509(17)
α/ ^{o}	90
β/ ^{o}	114.72(4)
γ/ ^{o}	90
V / Å^3	4952.4(8)
Z	4
D_{calc} (g cm^{-3})	1.361
μ/mm^{-3}	1.327
θ range/ ^{o}	2.07 - 28.29
Reflections collected	6134
Independent reflections	4834
Parameters/ Restraints	327/0
GOF (F^2)	1.104
R_1; wR_2 [I>2σ(I)]	0.0716; 0.2408
R_1; wR_2 (all data)	0.0810; 0.2567
$\Delta\rho_{max}$; $\Delta\rho_{min}$	1.370; -1.610

Table 4.16: Non-covalent interactions for 4a-4f (Å and ^{o})

D-H···A	d(D-H)	d(H-A)	d(D-A)	<(DHA)>	Symmetery codes
[H_5TPA^{-}.$H^{2,2'}BPy^{+}$] (4a)					
N2–H2D···O9	0.860(5)	1.825(4)	2.585(4)	146.3	-x+1/2,+y+1/2,-z+1/2+1
O8–H8E···O5	0.819(3)	1.699(5)	2.476(6)	157.6	-x+1/2,+y+1/2,-z+1/2+1
O4–H4E···O1	0.820(3)	1.791(3)	2.586(4)	162.9	-x+1,-y,-z+2
O7–H7E···O3	0.820(3)	1.915(2)	2.705(4)	161.3	-x+1,-y,-z+2
O6–H6E···O2	0.820(3)	1.719(3)	2.508(4)	160.8	-x+1,-y,-z+2
O3–H3E···O1	0.820(4)	1.746(8)	2.554(12)	168.0	-x+1,-y,-z+2
[$(H_4TPA^{2-})_2$.$(H_2^{4,4'}BPy^{2+})_2$.H_2O] (4b)					
N1–H1D···O7	0.861(2)	1.767(2)	2.625(3)	174.9	x+1,+y,+z
N2–H2D···O16	0.860(2)	1.791(2)	2.649(3)	175.3	-
N3–H3D···O12	0.859(2)	1.754(3)	2.611(4)	174.0	-x+1,-y+1,-z+1
N4–H4D···O1	0.864(35)	1.709(2)	2.572(4)	176.8	-x+1,-y+2,-z+1
O3-H3E···O11	0.820(2)	1.838(2)	2.654(3)	173.2	x-1,+y,+z
O4–H4E···O16	0.820(2)	1.758(3)	2.564(4)	167.5	-x+1,-y+1,-z
O5–H5E···O9	0.820(2)	1.759(3)	2.474(4)	140.0	-x+1,-y+2,-z
O10-H10E···O2	0.820(2)	1.776(2)	2.589(3)	176.8	x+1,+y,+z
O13–H13E···O11	0.820(3)	2.127(2)	2.564(3)	113.2	x-1,+y,+z
O14–H14E···O19	0.820(3)	2.318(3)	2.395(3)	85.3	-
O17–H17E···O7	0.820(2)	1.772(3)	2.561(4)	160.8	x+1,+y-1,+z

O15···O19	-	-	2.616(23)	-	-
O12···O19	-	-	2.664(24)	-	-

$[H_4TPA^{2-}.H_2TPA^{4-}.(H_2^{4,4'}BPy^{2+})_3.(H_2O)_8]$ (4c)

N1–H1D···O2	0.858(12)	1.728(9)	2.568(15)	165.5	x-1/2,+y-1/2,+z
N2–H2D···O13	0.860(12)	1.756(8)	2.609(14)	171.9	-x+2,-y+1,-z
N3–H3D···O15	0.860(11)	1.701(9)	2.545(14)	166.6	x-1,+y,+z
N4–H4D···O11	0.861(11)	1.749(12)	2.564(17)	157.2	-x,y,1/2-z
N5–H5D···O1	0.858(12)	1.748(8)	2.567(13)	150.6	-
N6–H6D···O5	0.860(12)	1.730(9)	2.578(16)	168.8	-
O3–H3E···O19	0.820(9)	1.901(10)	2.613(13)	144.7	-1/2+x,1/2+y,z
O3–H3E···O11	0.820(2)	1.833(8)	2.675(12)	162.2	-
O8-H8E···O16	0.820(8)	1.827(8)	2.643(12)	172.6	x,1+y,z
O12–H12E···O7	0.819(9)	1.690(8)	2.468(13)	158.0	x,1-y,-1/2+z
O14–H14E···O16	0.820(9)	1.758(3)	2.564(4)	167.5	x,-y,-1/2+z
O1···O21	-	-	2.917(21)	-	-
O3···O25	-	-	3.866(13)	-	-
O4…O25	-	-	2.583(12)	-	-
O6···O25	-	-	2.615(13)	-	-
O10···O24	-	-	2.862(28)	-	-
O15···O19	-	-	2.757(14)	-	-
O15···O23	-	-	2.918(16)	-	-
O18…O19	-	-	2.556(13)	-	-

O21…O22	-	-	2.365(55)	-	-
O22···O26	-	-	2.374(50)	-	-
O23···O20	-	-	2.744(23)	-	-
$[H_5TPA^-.HPhen^+.(H_2O)_5]$ (4d)					
N2–H2D···O2	0.860(2)	1.938(2)	2.725(3)	151.5	x-1/2,-y+1/2+1,+z+1/2
O1–H1E···O11	0.819(3)	1.822(6)	2.515(7)	141.4	x+1/2+1,+y+1/2,-z+1/2
O3–H3E···O5	0.820(2)	1.723(2)	2.519(3)	163.0	x+1/2+2,+y+1/2,-z+1/2
O4-H4E···O9	0.819(2)	1.694(2)	2.480(3)	160.1	-x+2,-y+1,-z+1
O6–H6E···O7	0.820(2)	1.773(2)	2.578(3)	166.6	-x+2,-y+1,-z+1
O8–H8E···O7	0.820(2)	1.772(2)	2.577(3)	167.0	-x+2,-y+1,-z+1
O13–H14w···O5	0.925(70)	2.761(52)	2.781(44)	81.6	x-1/2,-y+1/2,+z+1/2
O13–H14w···O11	0.925(70)	1.999(58)	2.145(38)	86.1	-
O13–H14w…O10	0.925(33)	1.888(21)	2.463(29)	118.1	-
O2···O12	-	-	2.737(3)	-	-
O9···O10	-	-	2.792(1)	-	-
O10···O11	-	-	2.617(0)	-	-
O14···O13	-	-	2.111(0)	-	-
O14···O12	-	-	2.566(1)	-	-
$[H_5TPA^-.HPhen^+.MeOH]$ (4e)					
N2–H2D···O1	0.860(1)	1.929(1)	2.724(1)	153.1	x,+y,+z-1
O2–H2E···O7	0.820(1)	1.727(1)	2.543(1)	173.5	x,+y+1,+z

O3–H3E···O5	0.820(1)	1.741(1)	2.510(2)	155.5	x+1/2+1,+y+1/2, -z+1/2+1
O4–H4E···O7	0.820(1)	1.783(1)	2.549(2)	154.8	-x+2,-y,-z+2
O6–H6E···O9	0.820(1)	1.697(1)	2.496(2)	164.2	-x+2,-y,-z+2
O8–H8E···O9	0.820(1)	1.799(1)	2.617(1)	174.6	-x+2,-y,-z+2
$[H_5TPA^{-}.H_4TPA^{2-}.H_3Terp^{3+}.S]$ (4f)					
N1–H1D···O17	0.861(3)	1.741(3)	2.573(4)	161.8	-x+1,+y-1/2,-z +1/2
N3–H3D···O13	0.860(4)	1.876(2)	2.705(4)	161.1	x,+y-1,+z
O2–H2E···O5	0.820(2)	1.707(3)	2.507(4)	165.0	x+1,+y,+z
O6–H3E···O10	0.819(3)	1.794(3)	2.557(4)	154.2	-x+1,+y-1/2,-z +1/2
O9–H9E···O13	0.820(3)	1.703(2)	2.490(4)	160.0	-x+1,-y+1,-z+1
O11–H11E···O15	0.820(3)	1.759(3)	2.570(5)	158.5	x+1,+y,+z
O12–H12E···O4	0.819(2)	1.724(2)	2.520(3)	163.3	-x+1,+y+1/2,- z+1/2
O14–H14E···O1	0.820(3)	1.698(2)	2.501(4)	165.4	-x+1,-y+1,-z+1
O16–H16E···O7	0.820(3)	1.652 (3)	2.496(4)	165.7	-

*Note: Due to failure in addition of H atoms on water molecule disorder caused by the disorder, the interactions O–H···O is shown as O···O in case of salts **4b**-**4d**. Hence, the empirical formula of these salts does not include the H from water molecules.

Table 4.17: Bond distances and angles for MOF 4h (Å and °)

$[Cd(dmpt)_2(NO_3)_2].X$ (4h)			
Bond Distances			
$Cd1–N3^{\#1}$	2.375(3)	$Cd1–N3^{\#2}$	2.375(3)
Cd1–N1	2.391(3)	$Cd1–N1^{\#3}$	2.391(3)
Cd1–O3	2.388(4)	$Cd1–O3^{\#3}$	2.388(4)
Bond Angles			
N1–Cd1–O3	82.97(11)	$N3^{\#1}$–Cd1–N1	93.11(10)
$N1^{\#3}$–Cd1–$O3^{\#3}$	82.97(11)	$N3^{\#1}$–Cd1–$N1^{\#3}$	86.89(10)
$N3^{\#2}$–Cd1–N1	86.89(10)	N1–Cd1–$N1^{\#3}$	180.00(9)
N1–Cd1–$O3^{\#3}$	97.03(11)	O3–Cd1–$O3^{\#3}$	180.00(14)
$N1^{\#3}$—Cd1—O3	97.03(11)	$N3^{\#2}$–Cd1–$O3^{\#3}$	75.03(13)
$N3^{\#2}$–Cd1–$N1^{\#3}$	93.11(10)	$N3^{\#2}$–Cd1–O3	75.03(13)
$N3^{\#1}$–Cd1–$N3^{\#2}$	180.00(11)	$N3^{\#1}$–Cd1–$O3^{\#3}$	104.97(13)
$N3^{\#2}$–Cd1–O3	104.97(13)		

Symmetry codes: -0.5+x, 2.5-y, -0.5+z (#1); 0.5-x, -0.5+y, 0.5-z (#2); -x, 2-y, -z (#3)

Table 4.18: Bond distances and angles for MOF 4i (Å and °)

$[Cd(dmpt)_2Br_2].X$ (4i)			
Bond Distances			
$Cd1–N3^{\#1}$	2.399(5)	Cd1–N3	2.399(5)
$Cd1–N1^{\#1}$	2.487(6)	Cd1–N1	2.487(6)
$Cd1–Br1^{\#1}$	2.700(1)	Cd1–Br1	2.700(1)
Bond Angles			
$N3–Cd1–N1^{\#1}$	92.20(17)	$N3^{\#1}–Cd1–Br1$	90.75(12)
N3–Cd1–N1	87.80(17)	$N3^{\#1}–Cd1–Br1^{\#1}$	89.25(12)
$N3^{\#1}–Cd1–N1$	92.20(17)	$N3–Cd1–Br1^{\#1}$	90.75(12)
$N3^{\#1}–Cd1–N1^{\#1}$	87.80(17)	N3–Cd1–Br1	90.25(12)
$N1^{\#1}–Cd1–Br1^{\#1}$	88.86(12)	N1–Cd1–Br1	88.86(12)
$N1–Cd1–Br1^{\#1}$	91.14(12)	$N3^{\#1}–Cd1–N3$	179.99(17)
$N1^{\#1}–Cd1–Br1$	91.14(12)	$N1^{\#1}–Cd1–N1$	180.00(16)

Symmetry codes: 1-x, 2-y, -z (#1)

Table 4.19: Bond distances and angles for MOF 4j (Å and °)

$[Cd(dmpt)_2I_2].X$ (4j)			
Bond Distances			
Cd1–I1	2.880(1)	Cd1–I1$^{\#1}$	2.880(1)
Cd1–N3	2.426(3)	Cd1–N3$^{\#1}$	2.426(3)
Cd1–N1	2.560(3)	Cd1–N1$^{\#1}$	2.560(3)
Bond Angles			
N1–Cd1–I1	88.65(8)	N3$^{\#1}$–Cd1–I1$^{\#1}$	88.64(8)
N1—Cd1–I1$^{\#1}$	91.35(8)	N3$^{\#1}$–Cd1–I1	91.36(8)
N1$^{\#1}$–Cd1–I1$^{\#1}$	88.65(8)	N3–Cd1–N1	86.27(11)
N1$^{\#1}$–Cd1–I1	91.35(8)	N3$^{\#1}$–Cd1–N1	93.73(11)
N3$^{\#1}$–Cd1–N3	180.00(12)	N3$^{\#1}$–Cd1–N1$^{\#1}$	86.27(11)
N1$^{\#1}$–Cd1–N1	179.99(10)	N3–Cd1–N1$^{\#1}$	93.73(11)
I1–Cd1–I1$^{\#1}$	179.98(1)	N3–Cd1–I1	88.64(8)

Symmetry codes: 2-x, 1-y, 1-z (#1)

Table 4.20: Bond distances and angles for MOF 4k (Å and °)

$[Co(dmpt)_2Cl_2].X$ (4k)			
Bond Distances			
Co1–N2	2.297(6)	Co1–N2$^{\#1}$	2.297(6)
Co1–N3	2.203(3)	Co1–N3$^{\#1}$	2.203(3)
Co1–Cl1	2.430(2)	Co1–Cl1$^{\#1}$	2.430(2)
Bond Angles			
N3–Co1–N2	87.97(12)	N2$^{\#1}$–Co1–Cl1	92.12(9)
N3–Co1–N2$^{\#1}$	92.03(12)	N3–Co1–Cl1	89.86(9)
N3$^{\#1}$–Co1–N2$^{\#1}$	87.97(12)	N3$^{\#1}$–Co1–Cl1	90.14(9)
N3$^{\#1}$–Co1–N2	92.03(12)	N3$^{\#1}$–Co1–Cl1$^{\#1}$	89.86(9)
N2–Co1–Cl1	87.88(9)	N3–Co1–Cl1$^{\#1}$	90.14(9)
N2$^{\#1}$–Co1–Cl1$^{\#1}$	92.12(9)	N3–Co1–N3$^{\#1}$	179.98(13)
N2–Co1–Cl1$^{\#1}$	92.12(9)	Cl1–Co1–Cl1$^{\#1}$	180.00(4)
N2–Co1–N2$^{\#1}$	179.99(11)		

Symmetry codes: -x, -y, -z (#1)

Table 4.21: Bond distances and angles for MOF 4l (Å and °)

$[Cd(dmpt)_2(SCN)_2].X$ (4l)			
Bond Distances			
Cd1–N1	2.415(3)	Cd1–N1$^{\#1}$	2.415(3)
Cd1–N5	2.416(3)	Cd1–N5$^{\#1}$	2.416(3)
Cd1–N8	2.284(3)	Cd1–N8$^{\#1}$	2.284(3)
Cd2–N4	2.308(4)	Cd2–N4$^{\#2}$	2.306(3)
Cd2–N3	2.420(2)	Cd2–N3$^{\#2}$	2.419(2)
Cd2–N7$^{\#4}$	2.388(2)	Cd2–N7$^{\#5}$	2.388(2)
Bond Angles			
N8–Cd1–N1	89.34(7)	N8–Cd1–N1$^{\#1}$	90.66(7)
N8$^{\#1}$–Cd1–N1	90.66(7)	N8$^{\#1}$–Cd1–N1$^{\#1}$	89.34(7)
N1–Cd1–N5	87.66(6)	N1–Cd1–N5$^{\#1}$	92.34(6)
N1$^{\#1}$–Cd1–N5	92.34(6)	N1$^{\#1}$–Cd1–N5$^{\#1}$	87.66(6)
N8–Cd1–N5	88.17(7)	N8–Cd1–N5$^{\#1}$	91.83(7)
N8$^{\#1}$–Cd1–N5$^{\#1}$	88.17(7)	N8$^{\#1}$–Cd1–N5	91.83(7)
N4–Cd2–N7$^{\#3}$	92.40(7)	N4–Cd2–N7$^{\#4}$	87.60(7)
N4$^{\#2}$–Cd2–N7$^{\#3}$	87.60(7)	N4$^{\#3}$–Cd2–N7$^{\#4}$	92.40(7)
N7$^{\#4}$–Cd2–N3	88.16(6)	N7$^{\#3}$–Cd2–N3	91.84(6)
N7$^{\#4}$–Cd2–N3$^{\#2}$	91.84(6)	N7$^{\#3}$–Cd2–N3$^{\#2}$	88.16(6)
N4$^{\#2}$–Cd2–N3$^{\#2}$	89.63(7)	N4–Cd2–N3$^{\#2}$	90.37(7)

N4–Cd2–N3	89.63(7)	$N4^{\#}$–Cd2–N3	90.37(7)
$N1^{\#1}$–Cd1–N1	179.98(6)	$N7^{\#3}$–Cd2–$N7^{\#4}$	180.00(6)
$N8^{\#1}$–Cd1–N8	179.99(8)	$N5^{\#1}$–Cd1–N5	180.00(6)
$N3^{\#2}$–Cd2–N3	179.99(6)	N4–Cd2–$N4^{\#2}$	180.00(8)

Symmetry codes: 1-x, -y, -z (#1); 1-x, 2-y, 1-z (#2); 2-x, 2-y, 1-z (#3); -1+x, y, z (#4); 1+x, y, z (#5)

Table 4.22: Bond distances and angles for MOF 4m (Å and °)

$[Zn(dmpt)_2(NO_3)_2]$.DMF.X (4m)			
Bond Distances			
Zn1–O1	2.106(6)	Zn1–O1$^{\#1}$	2.106(6)
Zn1–N1	2.180(9)	Zn1–N1$^{\#1}$	2.180(9)
Zn1–N2	2.219(9)	Zn1–N2$^{\#1}$	2.219(9)
Bond Angles			
O1–Zn1–N2	91.36(27)	O1$^{\#1}$–Zn1–N2	88.64(27)
O1–Zn1–N2$^{\#1}$	88.64(27)	O1$^{\#1}$–Zn1–N2$^{\#1}$	91.36(27)
O1$^{\#1}$–Zn1–N1$^{\#1}$	87.79(26)	O1$^{\#1}$–Zn1–N1	92.21(26)
O1–Zn1–N1$^{\#1}$	92.21(26)	O1–Zn1–N1	87.79(26)
N1–Zn1–N2	84.04(26)	N1$^{\#1}$–Zn1–N2	95.96(26)
N1$^{\#1}$–Zn1–N2$^{\#1}$	84.04(26)	N1–Zn1–N2$^{\#1}$	95.96(26)
O1–Zn1–O1$^{\#1}$	180.00(26)	N1–Zn1–N1$^{\#1}$	180.00(26)
N2–Zn1–N2$^{\#1}$	179.99(27)		

Symmetry codes: 1-x, -y, 1-z (#1)

Table 4.23: Bond distances and angles for MOF 4n (Å and °)

[Cd.dmpt.$(DMSO)_4$].$(ClO_4)_2$.$CHCl_3$.X (4n)			
Bond Distances			
Cd1–N1	2.251(5)	Cd1–$N1^{\#2}$	2.251(5)
Cd1–O5	2.340(4)	Cd1–$O5^{\#2}$	2.340(4)
Cd1–O6	2.293(7)	Cd1–$O6^{\#2}$	2.293(7)
Cd2–O3	2.298(5)	Cd2–$O3^{\#1}$	2.298(5)
Cd2–N3	2.307(5)	Cd2–$N3^{\#1}$	2.307(5)
Cd2–O4	2.309(4)	Cd2–$O4^{\#1}$	2.309(4)
Bond Angles			
N1–Cd1–O5	86.11(12)	$N1^{\#2}$–Cd1–$O5^{\#2}$	86.11(12)
$N1^{\#2}$–Cd1–O5	93.89(12)	N1–Cd1–$O5^{\#2}$	93.89(12)
$N1^{\#2}$–Cd1–$O6^{\#2}$	91.24(14)	N1–Cd1–O6	91.24(14)
$N1^{\#2}$–Cd1–O6	88.76(14)	N1–Cd1–$O6^{\#2}$	88.76(14)
O3–Cd2–O4	86.93(16)	O3–Cd2–$O4^{\#1}$	93.07(16)
O6–Cd1–O5	85.03(17)	$O3^{\#1}$–Cd2–$O4^{\#1}$	86.93(16)
O6–Cd1–$O5^{\#2}$	94.97(17)	$O6^{\#2}$–Cd1–O5	94.97(17)
$O6^{\#2}$–Cd1–$O5^{\#2}$	85.03(17)	$O3^{\#1}$–Cd2–N3	94.18(14)
$O3^{\#1}$–Cd2–$N3^{\#1}$	85.82(14)	O3–Cd2–$N3^{\#1}$	94.18(14)
O3–Cd2–N3	85.82(14)	$N3^{\#1}$–Cd2–$O4^{\#1}$	91.48(12)
N3–Cd2–O4	91.48(12)	$N3^{\#1}$–Cd2–O4	88.52(12)

$O3^{\#1}$–Cd2–O4	93.07(16)	$N1^{\#2}$–Cd1–N1	179.99(14)
O3–Cd2–$O3^{\#1}$	180.00(16)	N3–Cd2–$N3^{\#1}$	180.00(13)
O6–Cd1–$O6^{\#2}$	179.99(15)	O5–Cd1–$O5^{\#2}$	180.00(14)
$O4^{\#1}$–Cd2–O4	180.00(12)		

Symmetry codes: -x, 1-y, 1-z (#1); 1-x, -y, -z (#2)

Table 4.24: Bond distances and angles for MOF 4o (Å and °)

$[Eu(dmpt)_2(NO_3)_2].X$ (4o)			
Bond Distances			
Eu1–O4	2.378(8)	Eu1–O4$^{\#1}$	2.378(8)
Eu1–N3	2.382(4)	Eu1–N3$^{\#1}$	2.382(4)
Eu1–N1	2.398(6)	Eu1–N1$^{\#1}$	2.398(6)
Eu1–N4$^{\#1}$	3.175(5)	Eu1–O3	3.207(24)
Bond Angles			
O4–Eu1–N1	82.60(18)	O4$^{\#1}$–Eu1–N1$^{\#1}$	82.60(18)
O4–Eu1–N1$^{\#1}$	97.40(18)	O4$^{\#1}$–Eu1–N1	97.40(18)
O4$^{\#1}$–Eu1–N3	74.46(19)	O4–Eu1–N3$^{\#1}$	74.46(19)
O4–Eu1–N3	105.54(19)	O4$^{\#1}$–Eu1–N3$^{\#1}$	105.54(19)
N3$^{\#1}$–Eu1–N1$^{\#1}$	86.96(11)	N3–Eu1–N1$^{\#1}$	93.04(11)
N3$^{\#1}$–Eu1–N3	180.00(12)	N3$^{\#1}$–Eu1–N1	93.04(11)
N3–Eu1–N1	86.96(11)	N3$^{\#1}$–Eu1–N4$^{\#1}$	86.99(12)
N3–Eu1–N4$^{\#1}$	93.01(12)	N1–Eu1–N4$^{\#1}$	92.33(10)
N1$^{\#1}$–Eu1–N4$^{\#1}$	87.67(10)	N1$^{\#1}$–Eu1–N1	179.99(9)
O4–Eu1–N4$^{\#1}$	160.40(16)	N1$^{\#1}$–Eu1–O3	79.14(27)
N3–Eu1–O3	70.48(43)	N3$^{\#1}$–Eu1–O3	109.52(43)
N4$^{\#1}$–Eu1–O3	158.04(41)	N1–Eu1–O3	100.86(27)
O4–Eu1–O4$^{\#1}$	179.99(22)	O4$^{\#1}$–Eu1–O3	139.20(41)

Symmetry codes: -x, -y, -z (#1)

Table 4.25: Non- classical interactions in MOFs 4h-4o

Interaction	Bond length (Å)	Symmetry codes
4h		
C14–H14(Py)···O2	2.710(5)	x,-y+2,+z-1/2
C15–H15(Py)···O1	2.503(4)	x,-y+2,+z-1/2
C22–H22A···O4	2.596(9)	x+1/2,-y+1/2+1,+z+1/2
N3···O3	2.901	-
4i		
C15–H15(Py)···O2	2.520(4)	x,-y+2,+z-1/2
C17–H17···Br1	2.832(1)	-x+1,+y,-z+1/2
4j		
C12–H12···I1	2.968(0)	-x+2,+y,-z+1/2
C17–H17(Py)···O2	2.528(3)	x,-y+1,+z+1/2
C21–H21(Py)···O1	2.688(4)	-x+1/2+1,-y+1/2+1,-z
C23–H23B···I1	3.079	-
4k		
C12–H12···Cl1	2.770(1)	-x,+y,-z+1/2
C17–H17(Py)···O2	2.564(3)	x,-y,+z-1/2
C23–H23(Py)···O1	2.622(5)	-x+1/2,-y+1/2,-z+1
4l		
C12–H12(Py)···S2	2.976(1)	x,+y+1,+z
C17–H17(Py)···S2	2.853(1)	x,+y+1,+z
C35–H35(Py)···O1	2.531(2)	-x+1,-y+1,-z
C46–H46C···S2	2.963(1)	-x+1,-y+1,-z+1
4m		
N3···O3	3.039	-
C21–H21···O5	2.461(27)	x-1,+y,+z
C23–H23(Py)···O5	2.538(29)	-x+1,+y-1/2,-z+1/2

C25–H25B···O4	2.370(19)	-x+1,-y,-z+1
C26–H26B···O4	2.561(18)	-x+1,-y,-z+1
4n		
Cl3···O7	2.942	-
C1–H1···O12	2.641(9)	-
C2–H2···O12	2.615(11)	-
C4–H4···O9	2.490(9)	x,+y-1,+z
C7–H7···O9	2.671(9)	x,+y-1,+z
C9–H9···O7	2.692(5)	-x+1,-y+1,-z+1
C12–H12···O7	2.542(6)	-x+1,-y+1,-z+1
C15–H15···O13	2.679(23)	-
C17–H17···O9	2.576(10)	x,+y-1,+z
C22–H22A···O7	2.629(7)	-x+1,-y+1,-z+1
C25–H25B···O8	2.567(12)	-
C26–H26B···O8	2.723(9)	x-1,+y,+z
C27–H27B···O11	2.711(12)	x-1,+y,+z
C27–H27C···O14	2.633(20)	-
C30–H30A···O2	2.418(4)	-x+1,-y,-z+1
C30–H30A···O1	2.603(4)	-x+1,-y,-z+1
C32–H32···O10	2.610(10)	-
C32–H32···O9	2.491(8)	-
4o		
C12–H12(Py)···O5	2.715(14)	-x,+y,-z+1/2
C12–H12(Py)···N4	2.653(4)	-x,+y,-z+1/2
C17–H17(Py)···O2	2.551(3)	x,-y,+z-1/2
C21–H21(Py)···O1	2.704(4)	-x+1/2,-y+1/2,-z+1

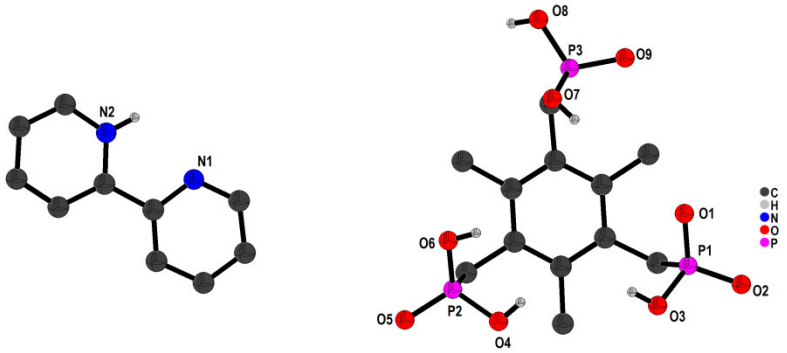

Fig. 4.19: Crystal structure of [$H_5TPA^-.H^{2,2'}BPy^+$] (**4a**). (C–H bonds are not shown for clarity)

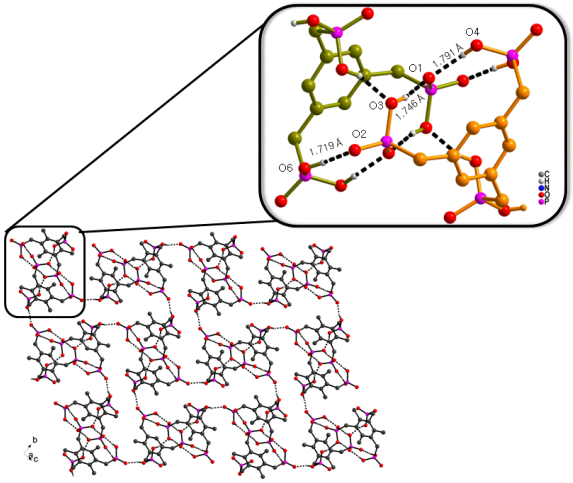

Fig. 4.20: Intermolecular interactions (O–H···O) involved between two triphosphonic acid arranged in *cis*-mode and 2D herringbone network of TPA in **4a**

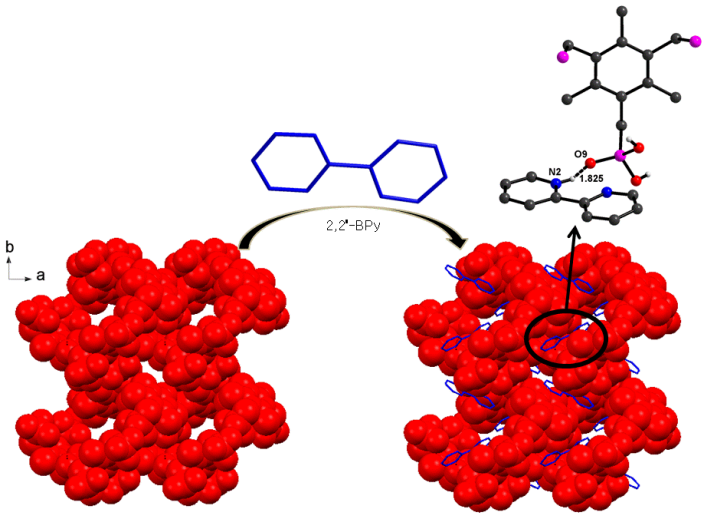

Fig. 4.21: View of 2D supramolecular network of TPA in space-fill representation with 2,2'-BPy interacted via N–H···O above and below the network and representing one of the motif i.e. **motif I** in *ab*-plane in **4a**

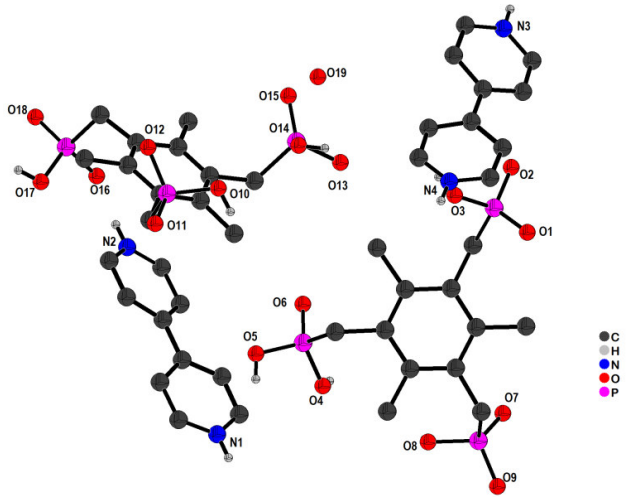

Fig. 4.22: Crystal structure of $[(H_4TPA^{2-})_2.(H_2^{4,4'}BPy^{2+})_2.H_2O]$ (**4b**). (C–H bonds are not shown for clarity)

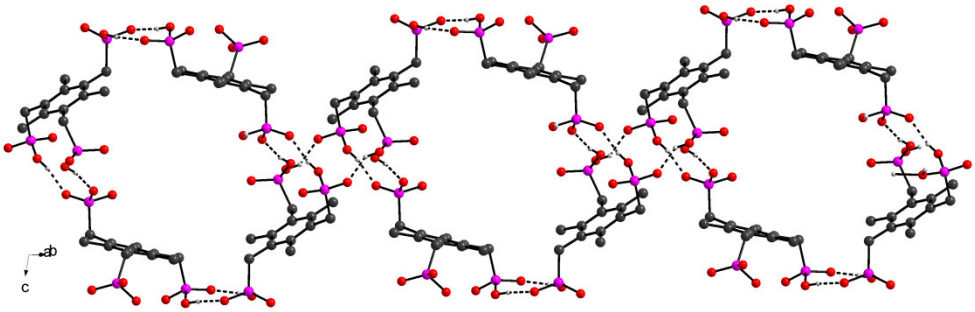

Fig. 4.23: Hydrogen bonded cavities formed by H_4TPA^{2-} along *bc*-plane in **4b**

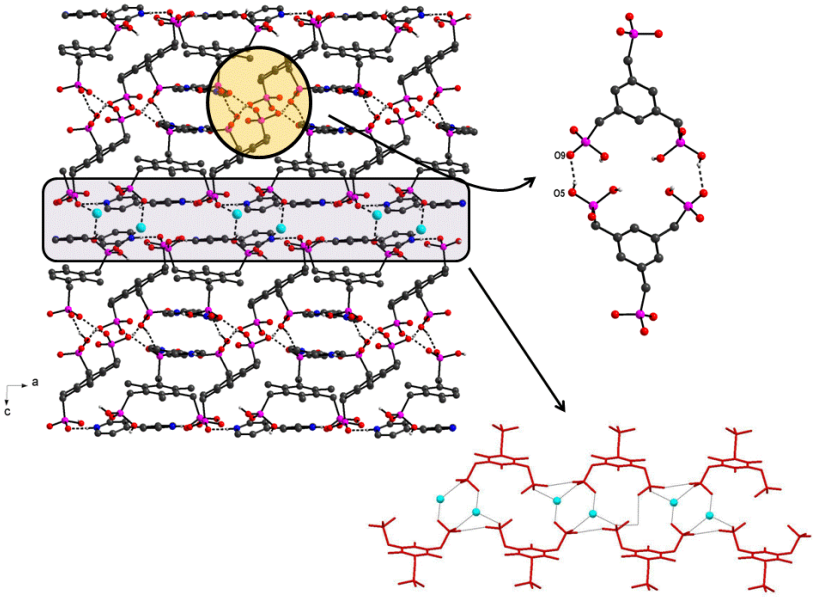

Fig. 4.24: 2D supramolecular framework with an array of O–H···O and N–H···O interactions involving a tape comprised of water and H_4TPA^{2-} molecule formed via synthons **IIIa** and **IIIb** in **4b**

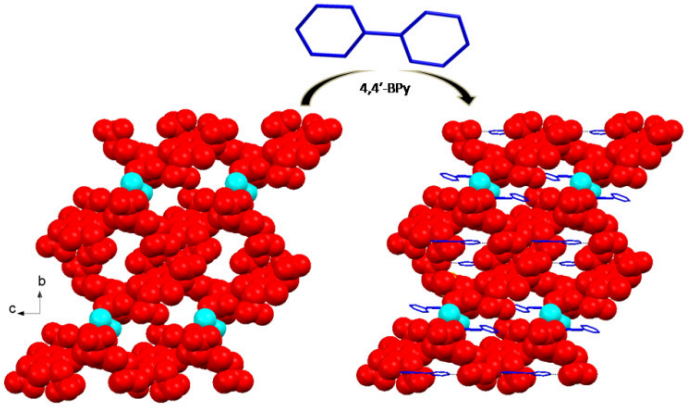

Fig. 4.25: View of 2D supramolecular network of H_4TPA^{2-} in space-fill representation along with water molecules in aqua color with 4,4'-BPy (in blue) interacted via N–H···O the network and representing one of the motif i.e. **motif II** in *bc*-plane for **4b**

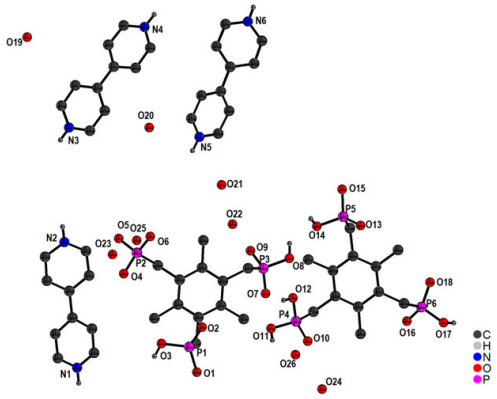

Fig. 4.26: Crystal structure of $[H_4TPA^{2-}.H_2TPA^{4-}.(H_2{}^{4,4'}BPy^{2+})_3.(H_2O)_8]$ (**4c**). (C–H bonds are not shown for clarity)

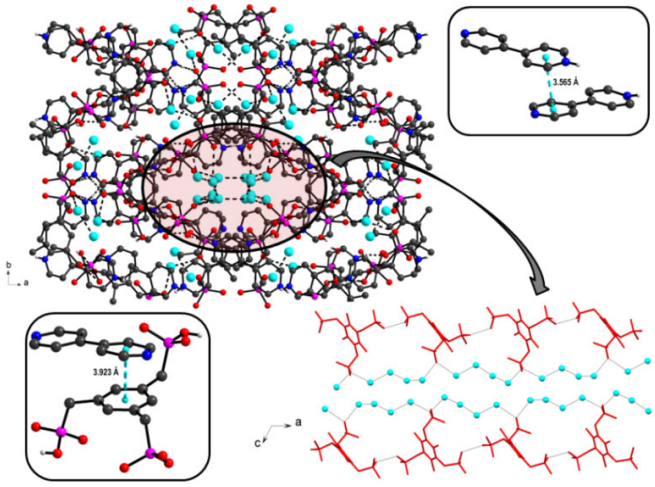

Fig. 4.27: Representation of 3D supramolecular hydrogen bonded cavity displaying 1D channel along *c*-axis, with continuous chain of water molecules (in aqua color) and TPA molecule in **4c**

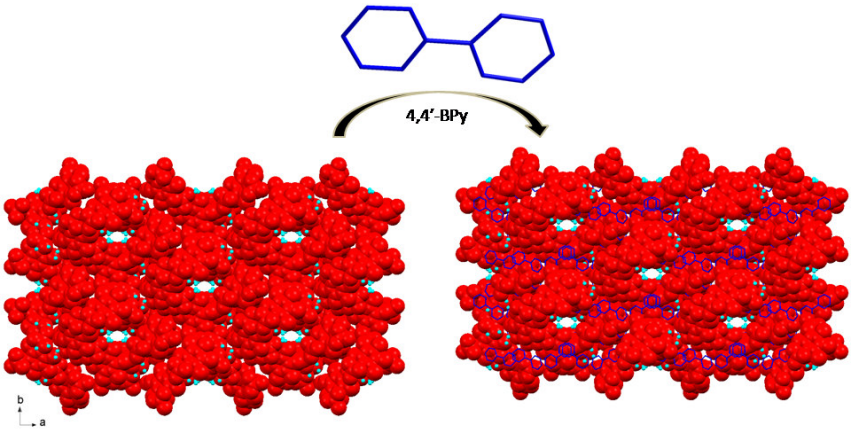

Fig. 4.28: Representation of 3D supramolecular hydrogen bonded porous framework of TPA (red color) and water molecule (aqua color) with 4,4'-BPy molecules lying above and below the framework and representing one of the motif i.e. **motif III** in **4c**

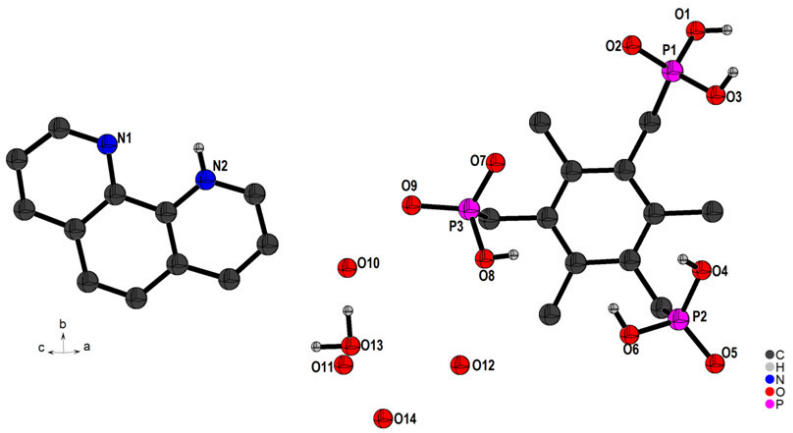

Fig. 4.29: Crystal structure of $[H_5TPA^-.HPhen^+.(H_2O)_5]$ (**4d**). (C–H bonds are not shown for clarity)

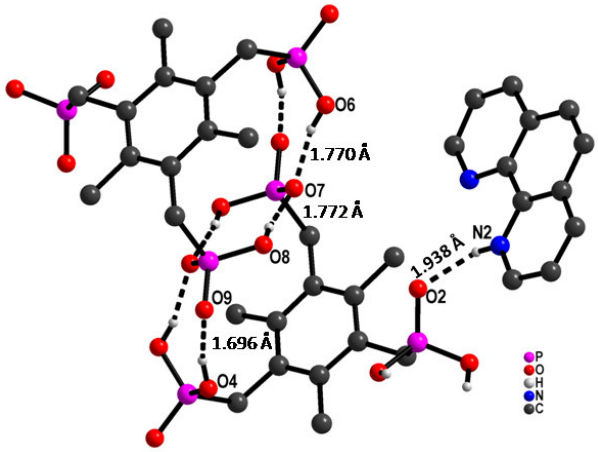

Fig. 4.30: Intermolecular non-covalent interaction involving various O–H···O and N–H···O interactions forming synthon **Ia** in salt **4d**

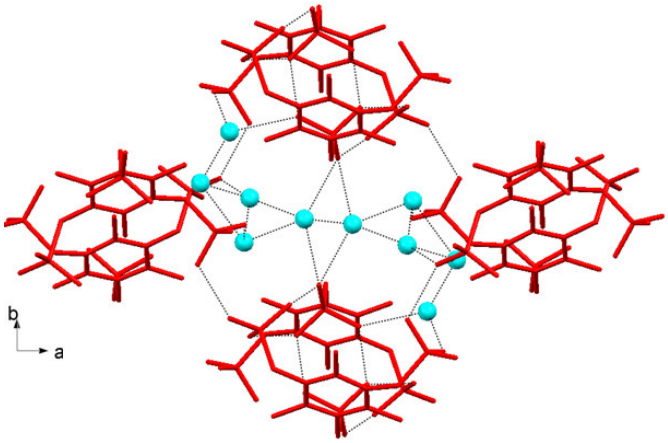

Fig. 4.31: Cluster of water molecules (aqua color) in the hydrogen bonded cavity formed by H_5TPA^- in *ab*-axis in **4d**

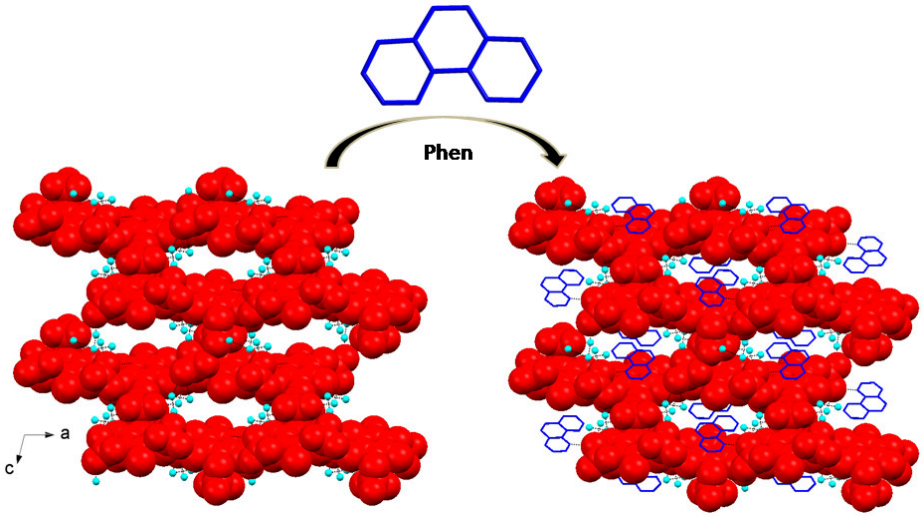

Fig. 4.32: 3D hydrogen bonded network formed by H_5TPA^- and $HPhen^+$ molecules interacting above and below the framework via N–H···O interaction; representing one of the motif i.e. **motif IV** in **4d**

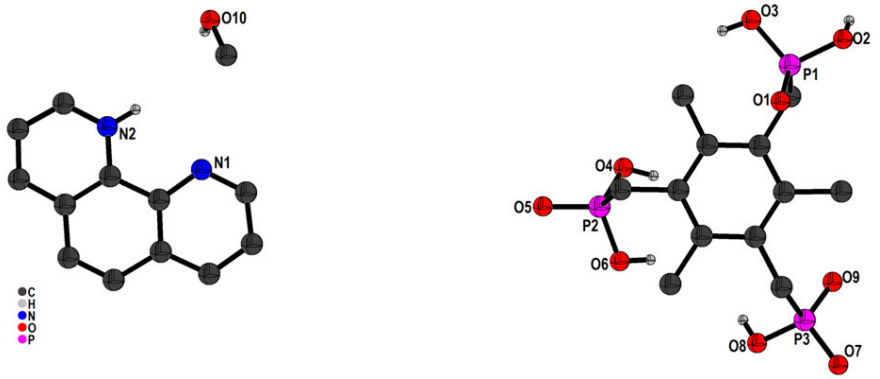

Fig. 4.33: Crystal structure of [H_5TPA^-.$HPhen^+$.MeOH] (**4e**). (C–H bonds are not shown for clarity)

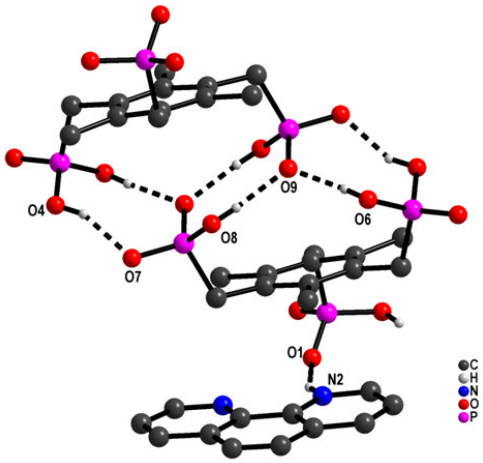

Fig. 4.34: Intermolecular non-covalent interaction involving various O–H···O and N–H···O interactions forming synthon **Ia** in salt **4e**

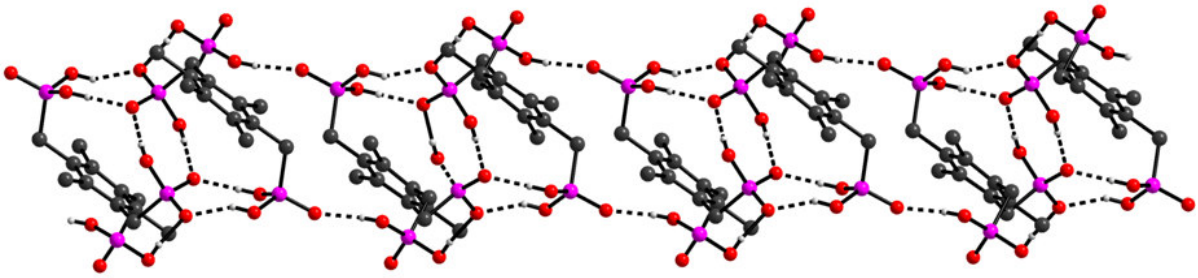

Fig. 4.35: 2D sheet formed by H_5TPA^- molecules via synthon formation **Ia** in **4e**

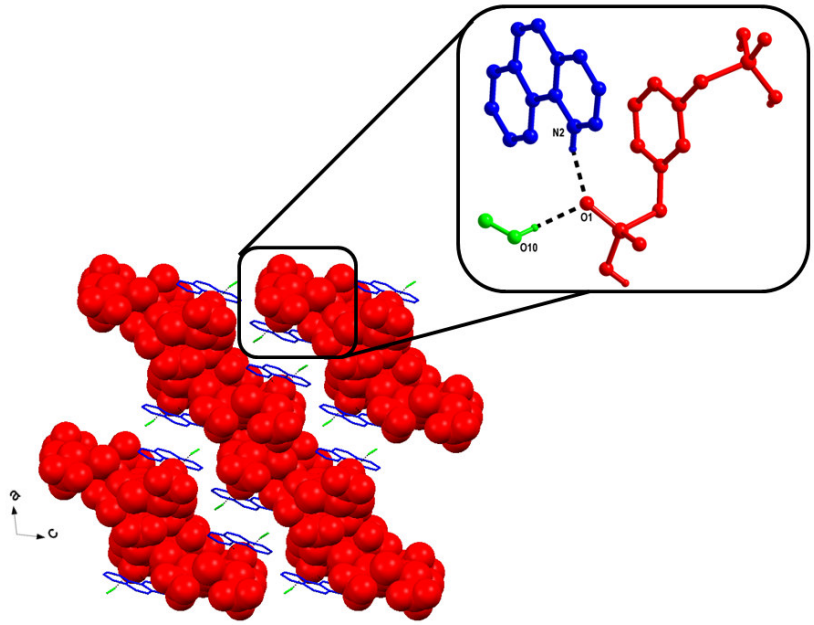

Fig. 4.36: 3D layered supramolecular network in *ac*-plane with 2D sheet of H_5TPA^- (in red color); $HPhen^+$ (blue color) and methanol (green color) molecules lying in between the sheets in **4e**

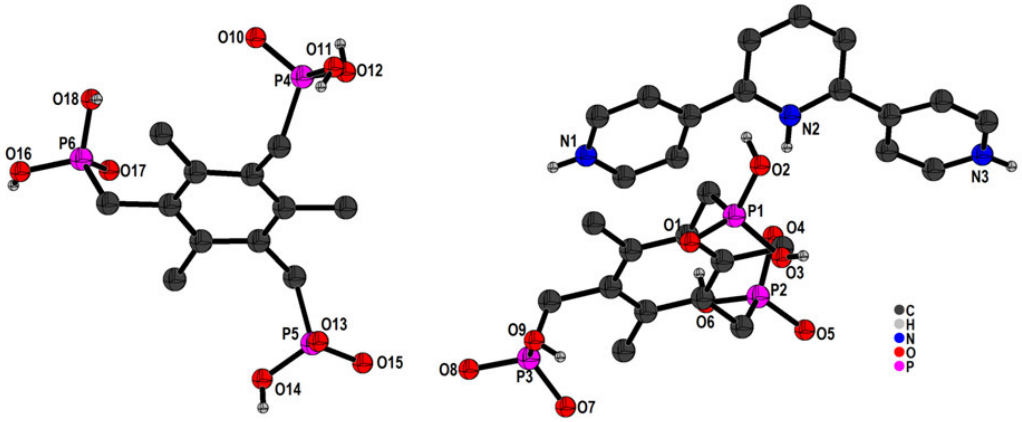

Fig. 4.37: Crystal structure of [$H_5TPA^-.H_4TPA^{2-}.H_3Terp^{3+}.S$] (**4f**). (C–H bonds are not shown for clarity)

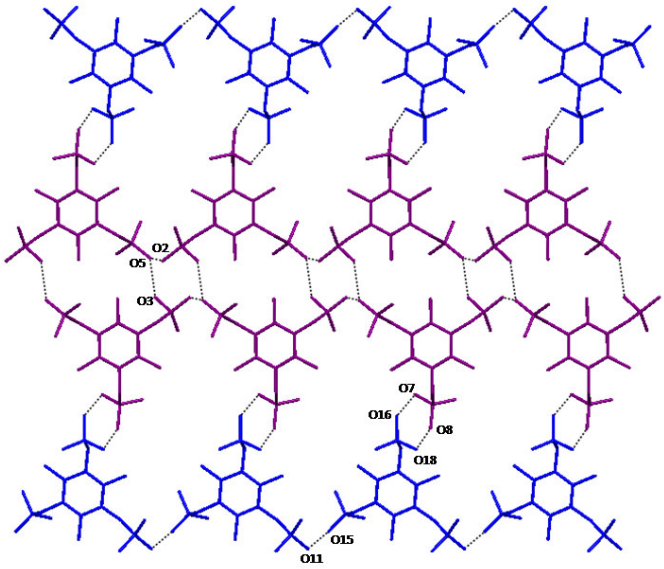

Fig. 4.38: 2D view of triphosphonate sheet formed via formation of synthon **IV** in **4f**

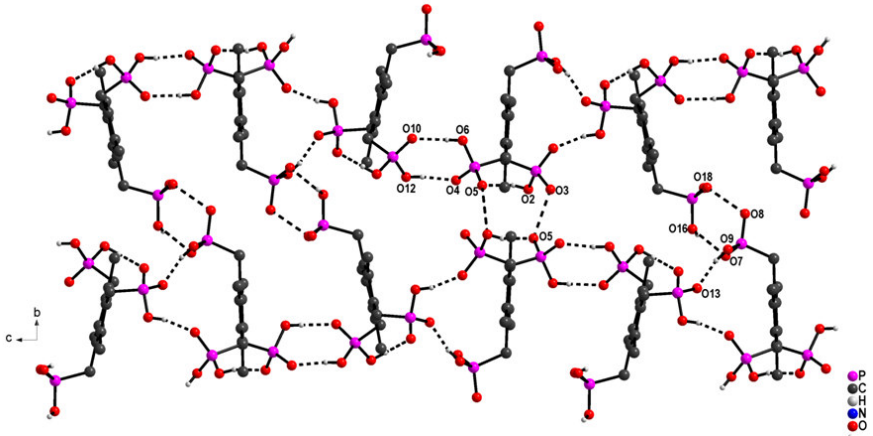

Fig. 4.39: 3D representation of TPA molecules involving an array of synthon **I** in *bc*-plane for salt **4f**

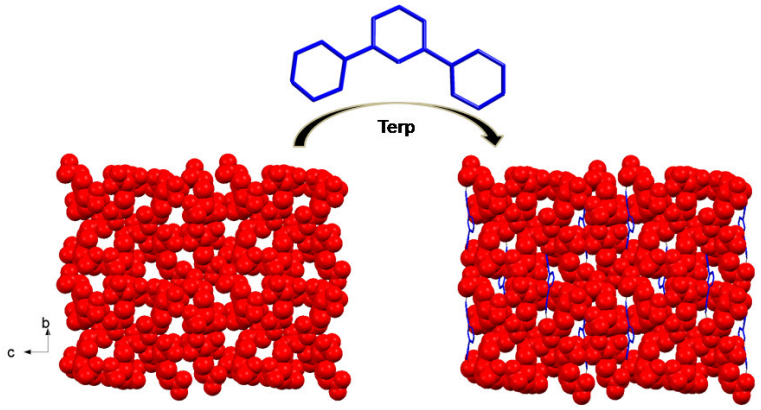

Fig. 4.40: 3D hydrogen bonded network formed by TPA molecules and Terp molecules interacting above and below the framework via N–H···O interaction representing one of the motif i.e., **motif V** in **4f**

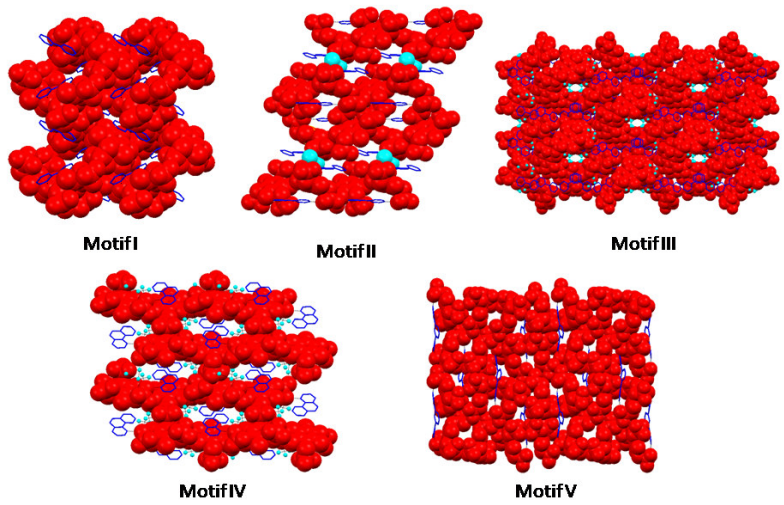

Fig. 4.41: Representation of motifs **I-V** adopted by columns of TPA in salts **4a-4f**

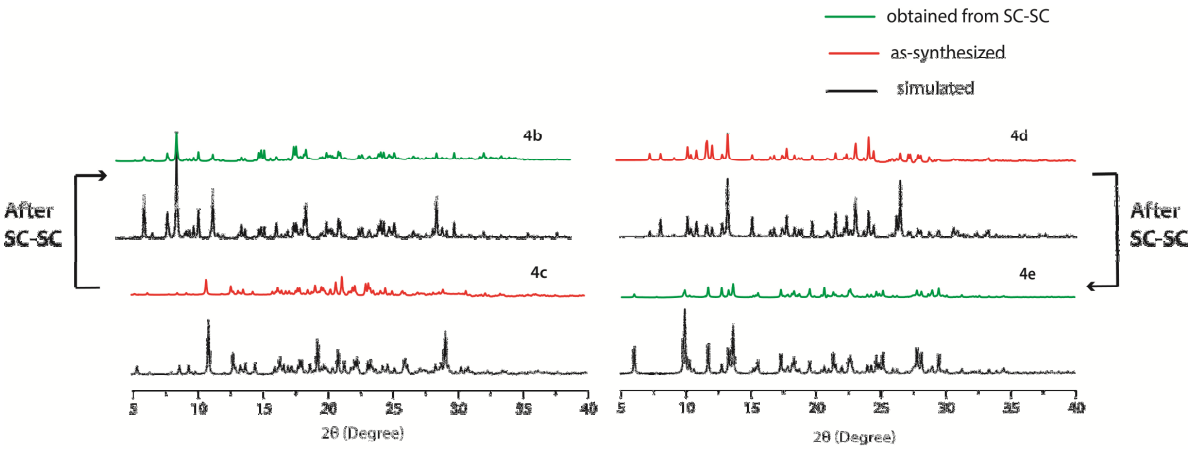

Fig. 4.42: PXRD pattern for salts **4b-4e** after SC-SC

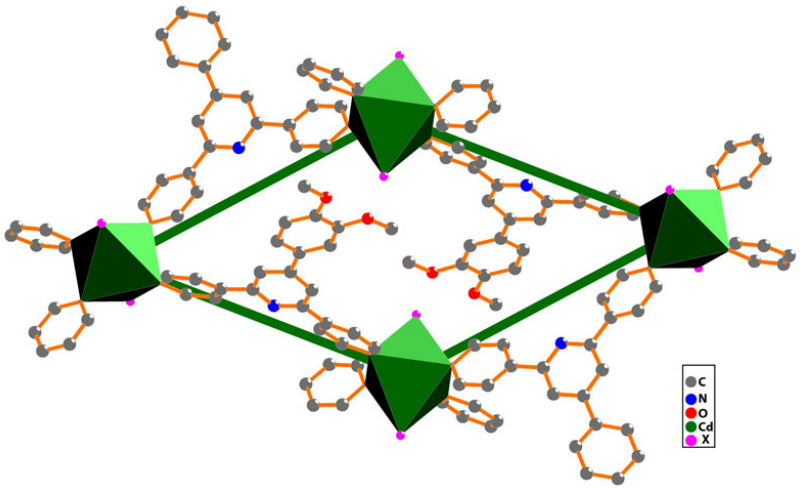

Fig. 4.43: Representation of secondary building unit (SBU) for **4h**-**4o** except in **4n**

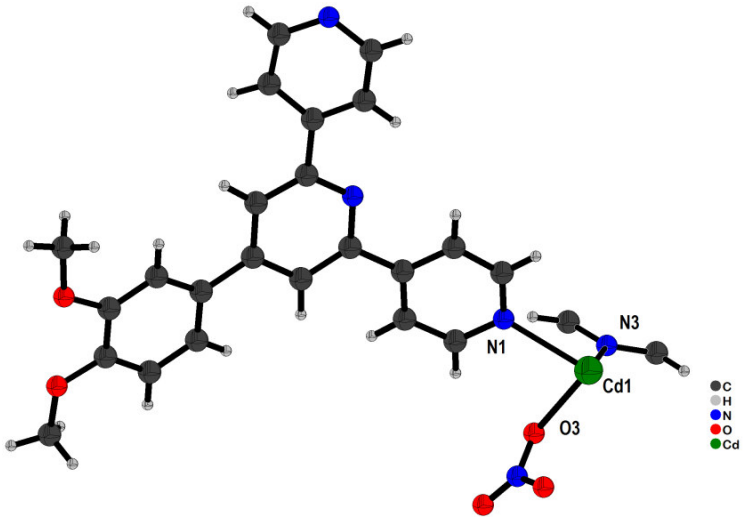

Fig. 4.44: Crystal structure of $[Cd(dmpt)_2(NO_3)_2].X$ (**4h**)

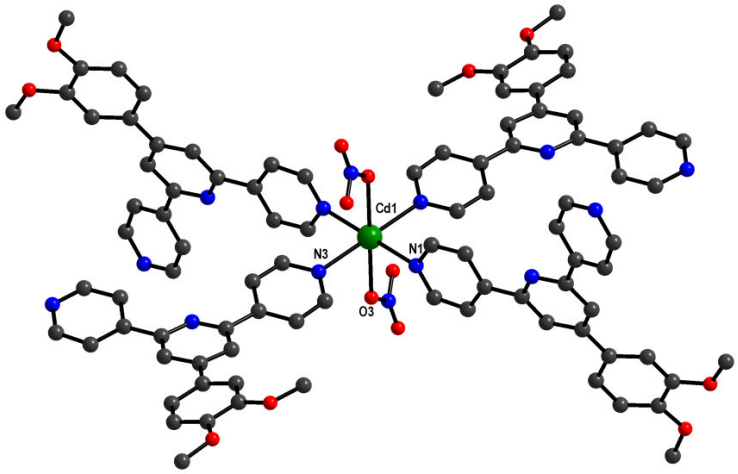

Fig. 4.45: Coordination environment around Cd center in **4h** (C–H bonds are not shown for clarity)

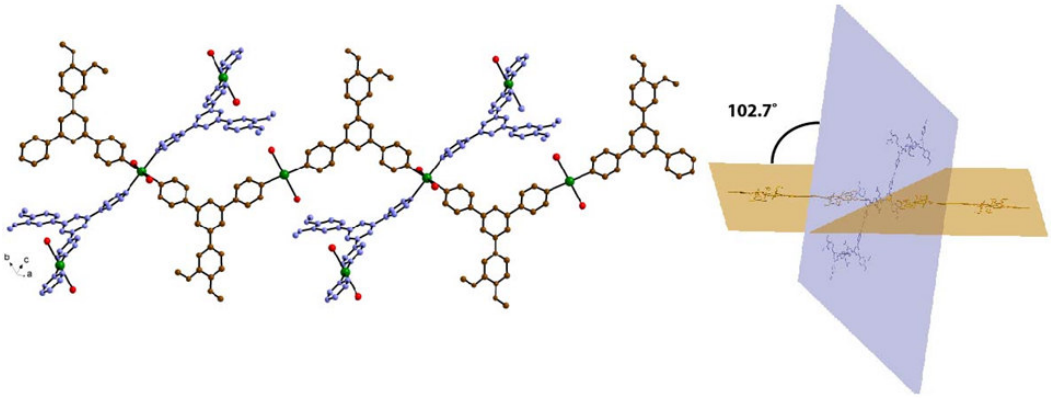

Fig. 4.46: View of 1D chain of metal and dmpt in *ab*-plane (brown colored chain), further extended in *ac*-plane (blue colored chain) at 102.7° with respect to brown one

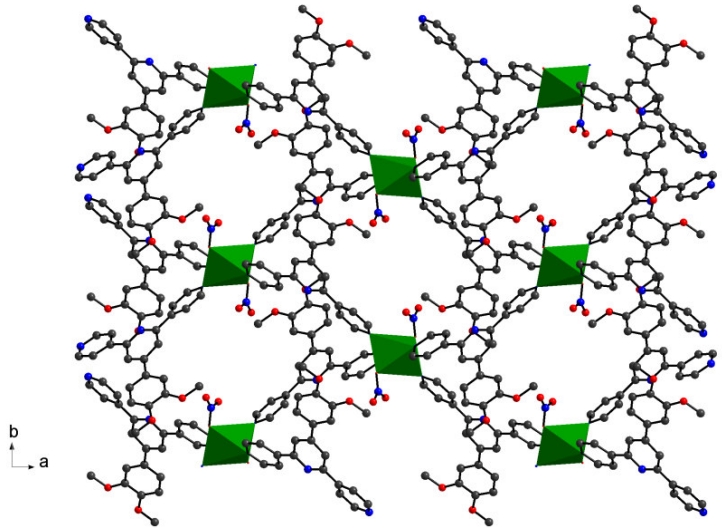

Fig. 4.47: View of 2D coordination network along *c*-axis in **4h**

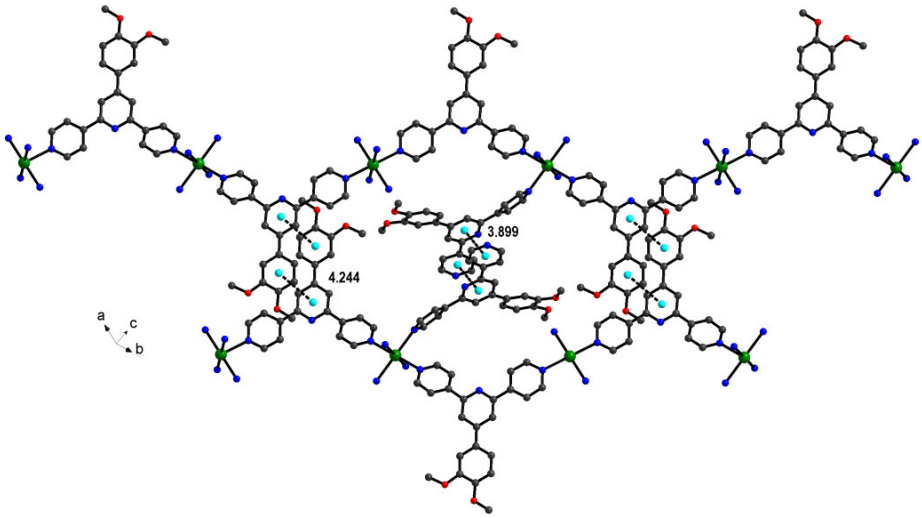

Fig. 4.48: Interlayer π-π stacking between central pyridine rings and between central ring and the pendant ring are 3.889 Å and 4.224 Å respectively

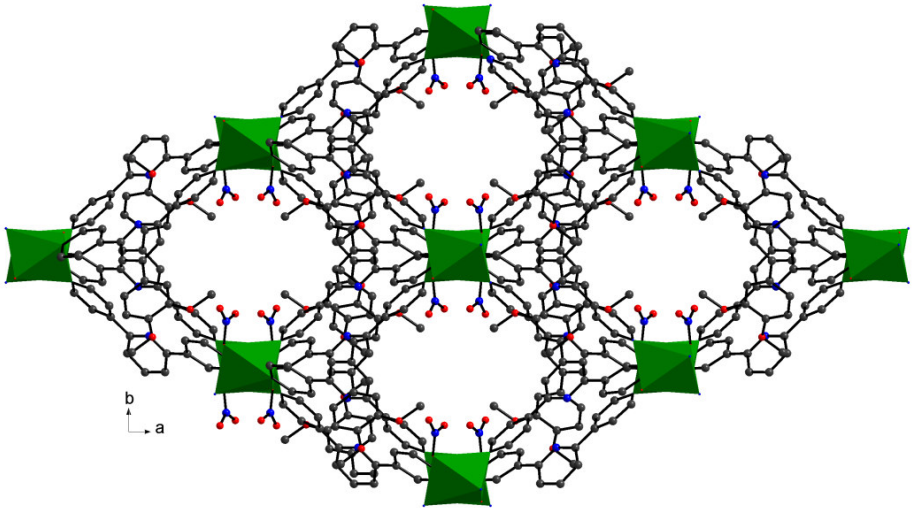

Fig. 4.49: Representation of 3D network in *ab*-plane for **4h**

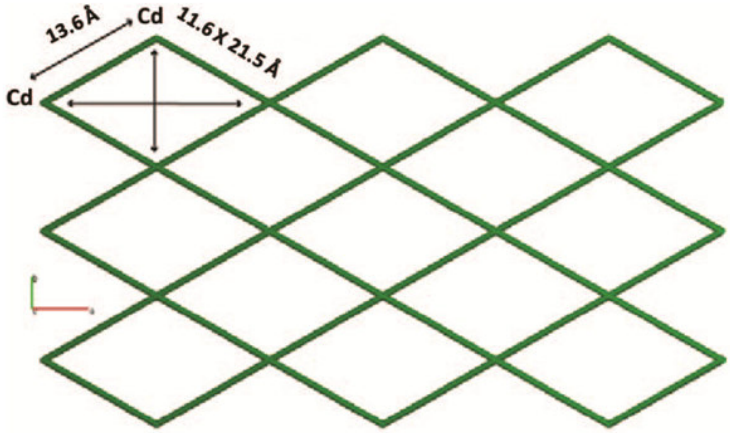

Fig. 4.50: View of Cd–Cd network in 2D framework along *c*-axis presenting the diagonal separation of Cd–Cd (11.6 X 21.5 Å) and Cd–Cd separation bridged by **dmpt** (13.6 Å)

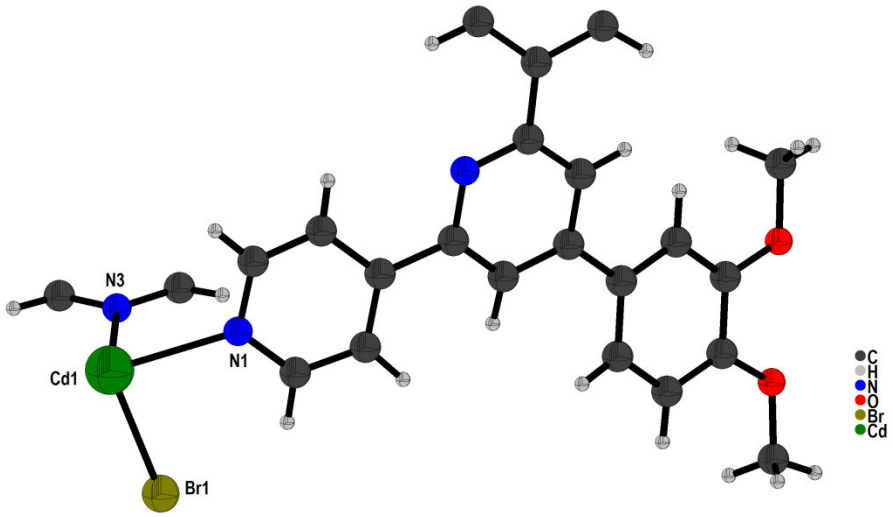

Fig. 4.51: Crystal structure of $[Cd(dmpt)_2(Br)_2].X$ (**4i**)

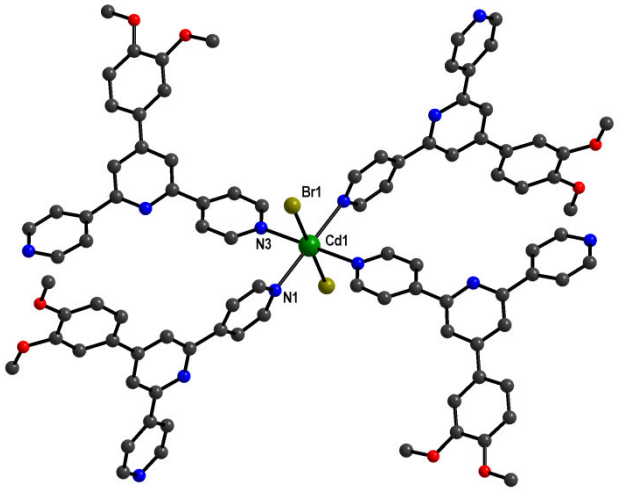

Fig. 4.52: Coordination environment around Cd center in **4i** (C–H bonds are not shown for clarity)

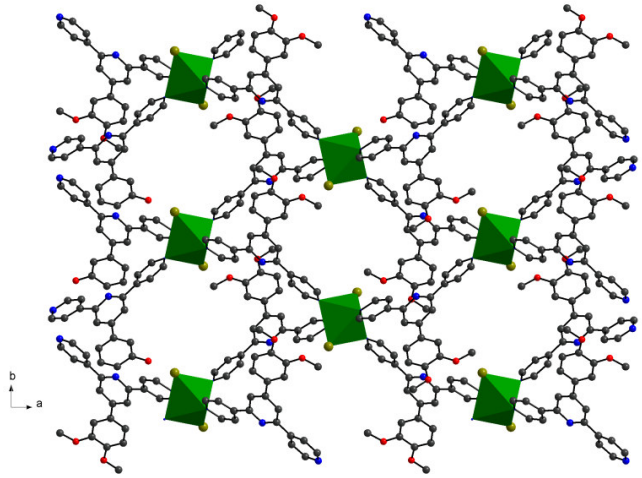

Fig. 4.53: View of 2D coordination network along *c*-axis in **4i**

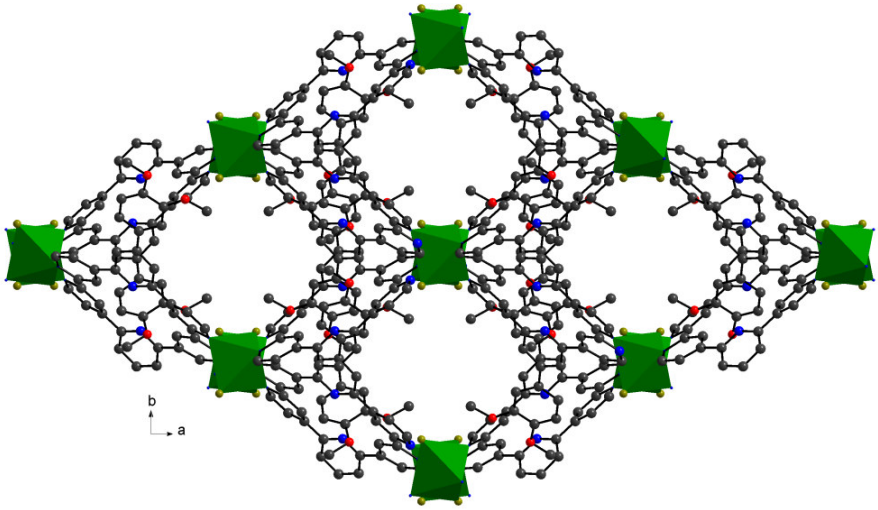

Fig. 4.54: Representation of 3D network in *ab*-plane for **4i**

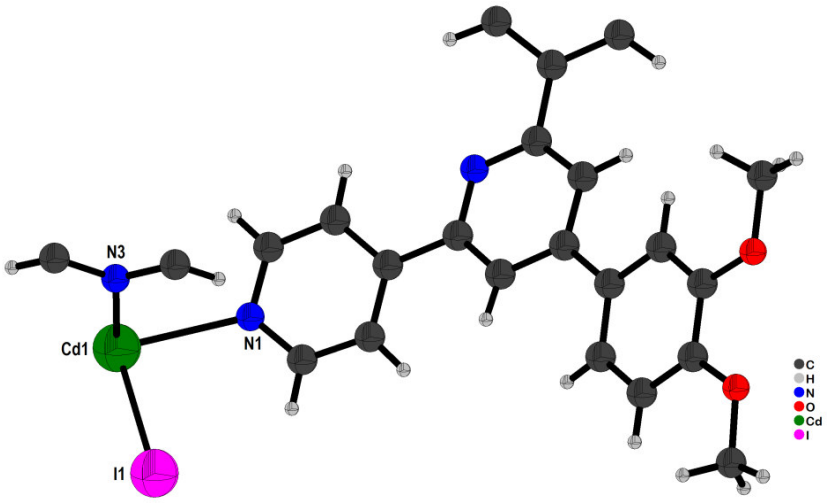

Fig. 4.55: Crystal structure of $[Cd(dmpt)_2(I)_2].X$ (**4j**)

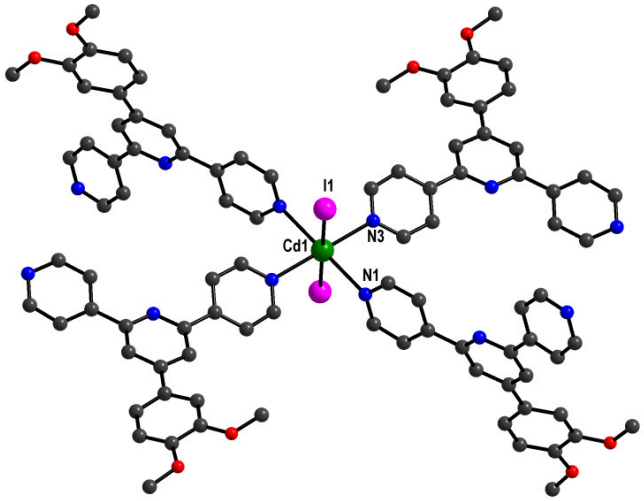

Fig. 4.56: Coordination environment around Cd center in **4j** (C–H bonds are not shown for clarity)

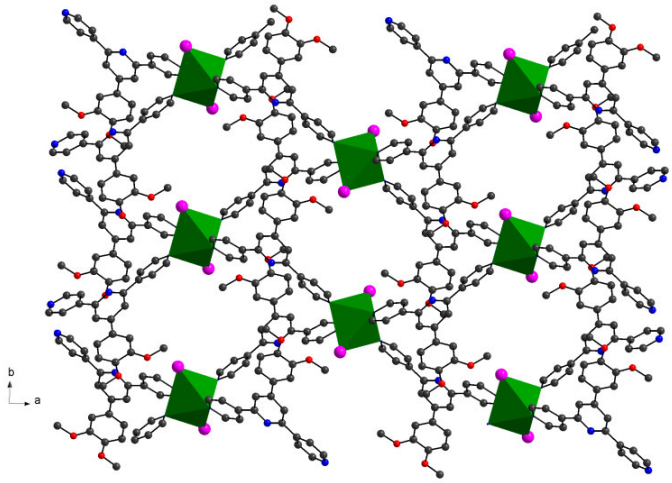

Fig. 4.57: View of 2D coordination network along *c*-axis in **4j**

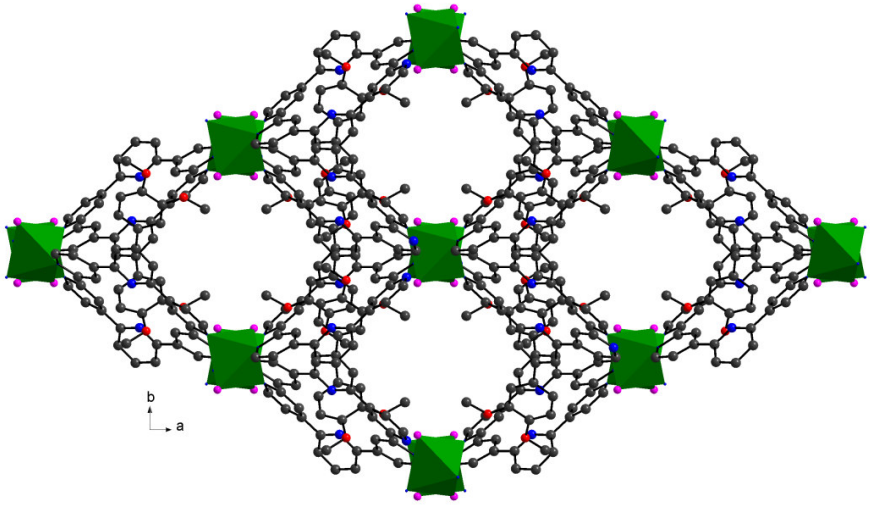

Fig. 4.58: Representation of 3D network in *ab*-plane for **4j**

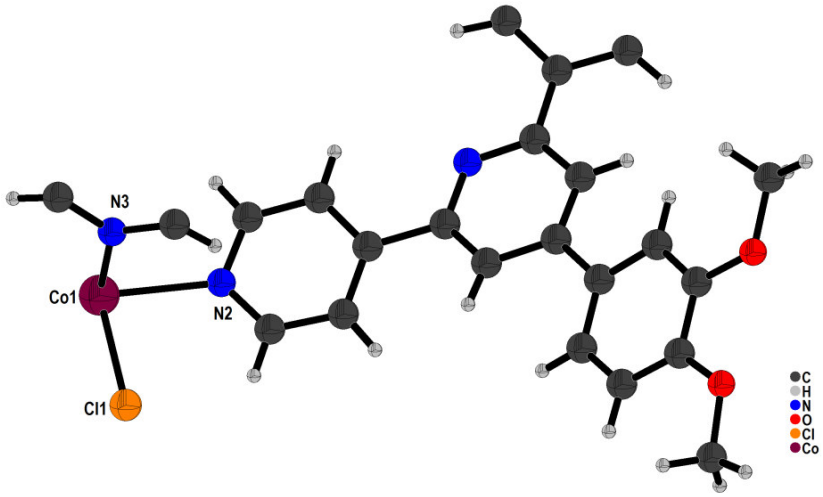

Fig. 4.59: Crystal structure of $[Co(dmpt)_2(Cl)_2].X$ (**4k**)

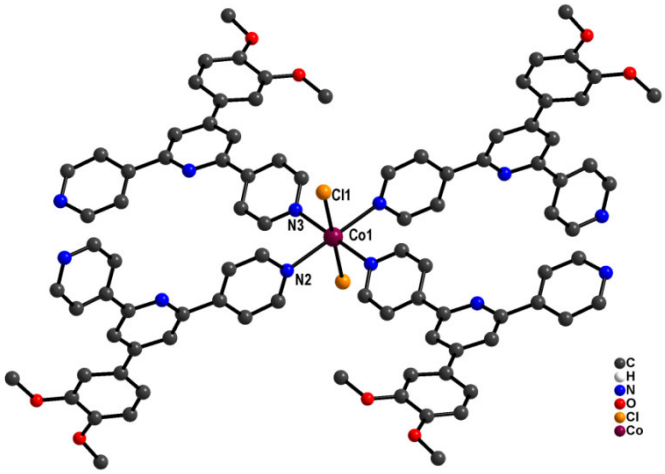

Fig. 4.60: Coordination environment around Co center in **4k** (C−H bonds are not shown for clarity)

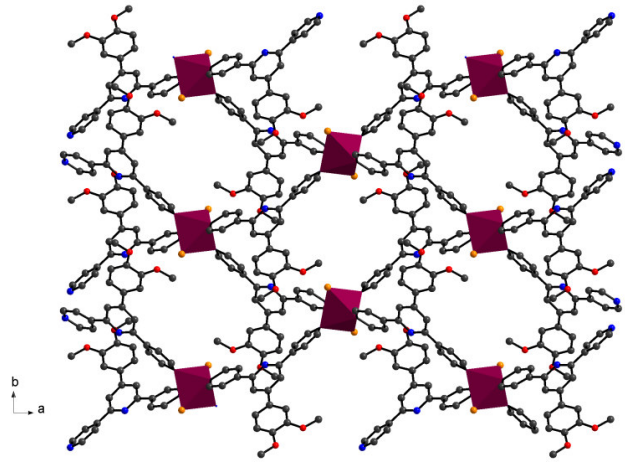

Fig. 4.61: View of 2D coordination network along *c*-axis in **4k**

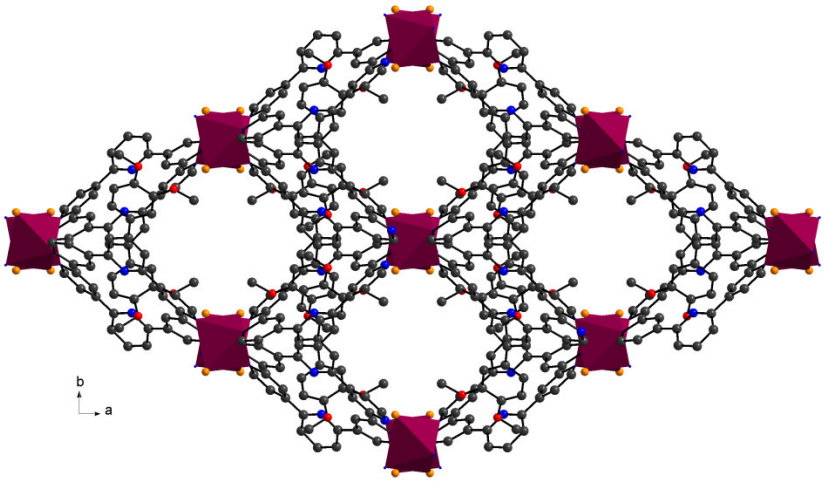

Fig. 4.62: Representation of 3D network in *ab*-plane for **4k**

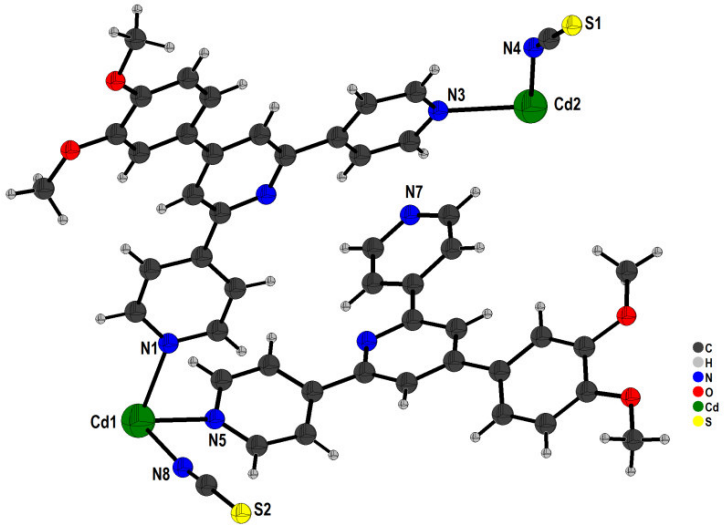

Fig. 4.63: Crystal structure of $[Cd(dmpt)_2(SCN)_2].X$ (**4l**). (C–H bonds are not shown for clarity)

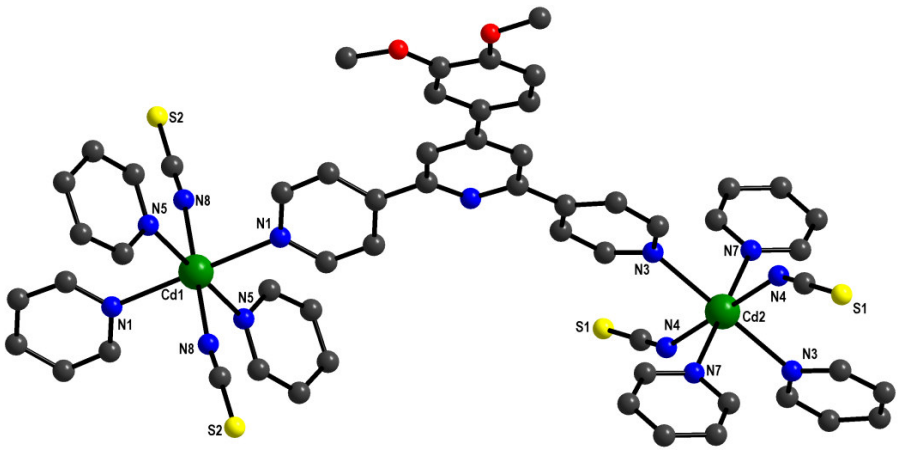

Fig. 4.64: Coordination environment around Cd center in **4l**

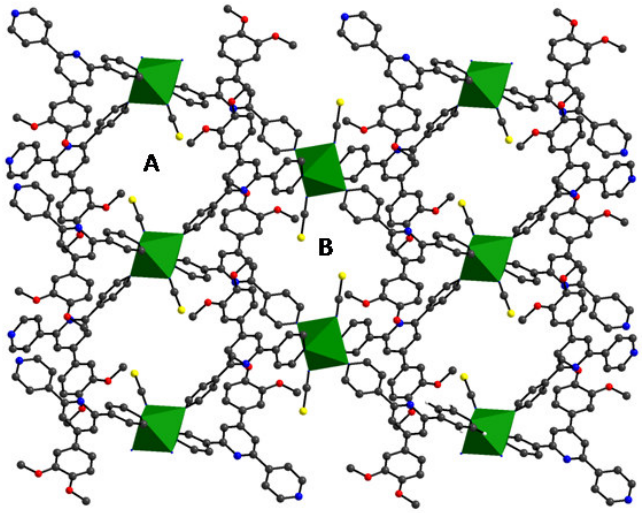

Fig. 4.65: View of 2D coordination network along *c*-axis with two cavities accommodating coordinated SCN in **4l**

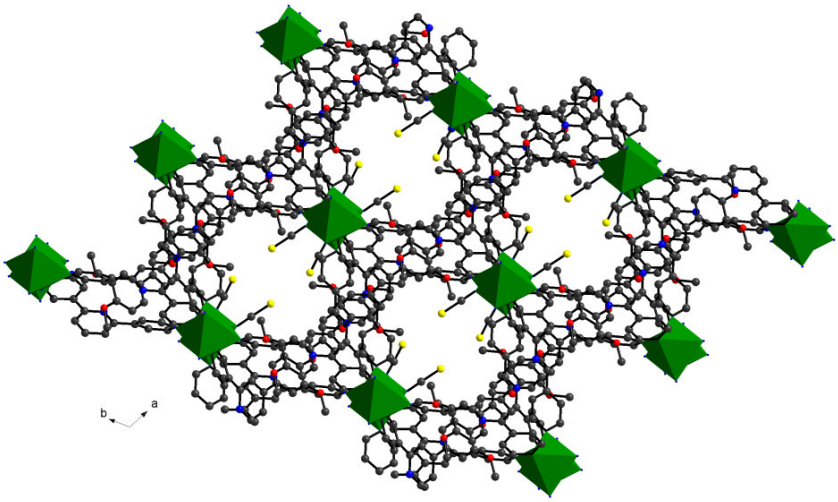

Fig.4.66: Representation of 3D network in *ab*-plane for **4l**

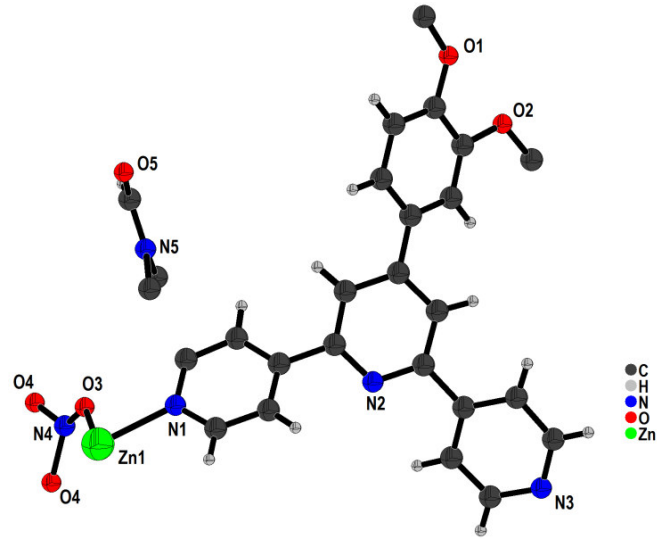

Fig. 4.67: Crystal structure of $[Zn(dmpt)_2(NO_3)_2].DMF.X$ (**4m**)

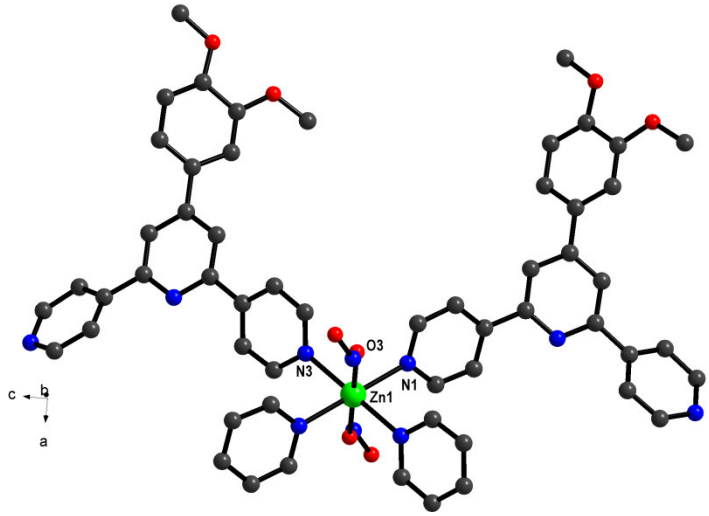

Fig. 4.68: Coordination environment around Zn center in **4m** (C−H bonds are not shown for clarity)

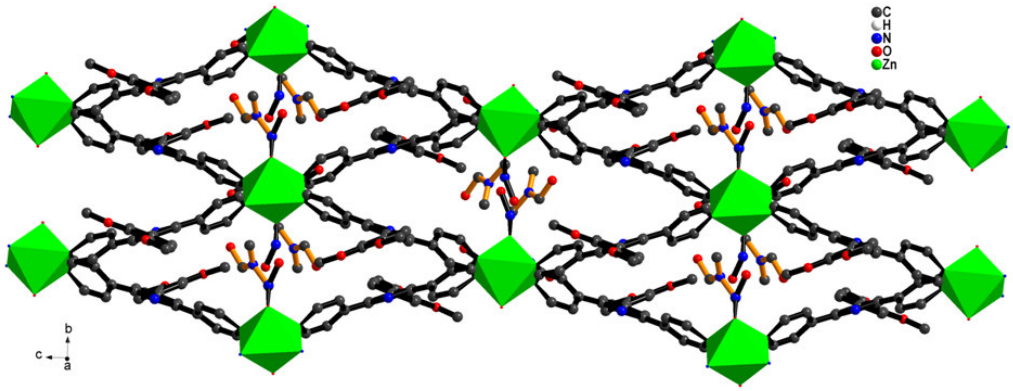

Fig. 4.69: 2D porous network; accommodating DMF molecules and nitrate ions protrude inside the cavity along *a*-axis, **4m**

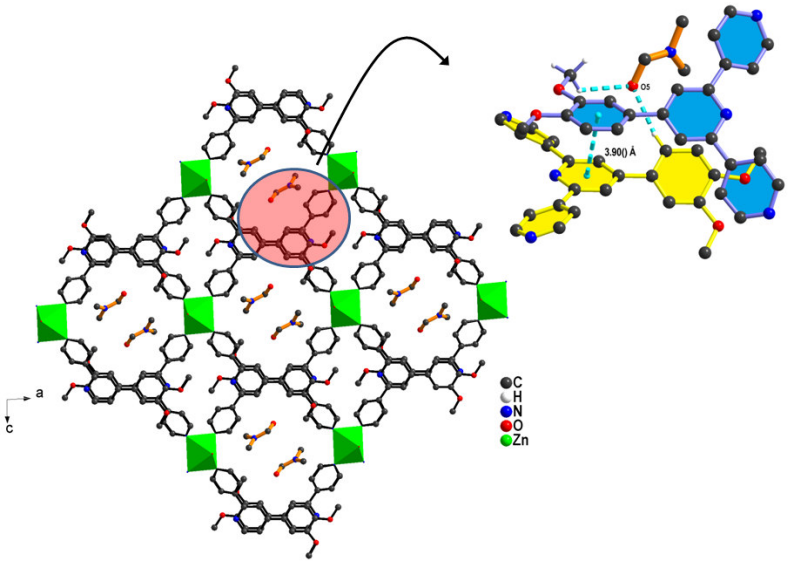

Fig. 4.70: 3D extended network via π···π interaction (3.900 Å) in **4m**

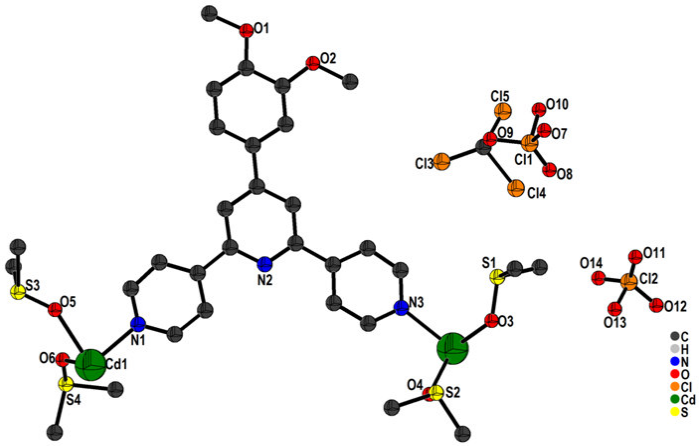

Fig. 4.71: Crystal structure of $[Cd.dmpt.(DMSO)_4].(ClO_4)_2.CHCl_3.X$ (**4n**). (C–H bonds are not shown for clarity)

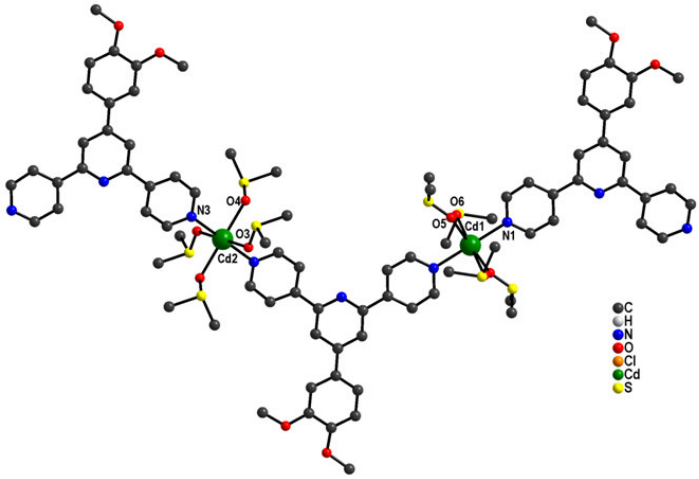

Fig. 4.72: Coordination environment around Cd center in **4n**

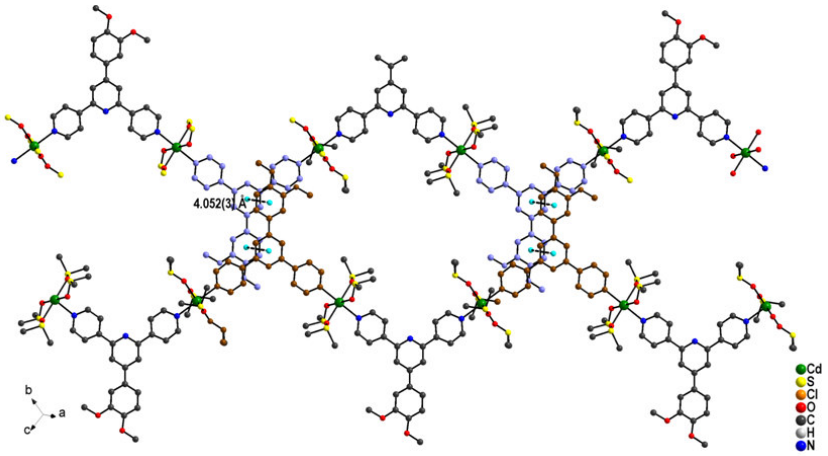

Fig. 4.73: Interlayer π-π stacking between central pyridine ring and the pendant ring (4.052 Å) in **4n**

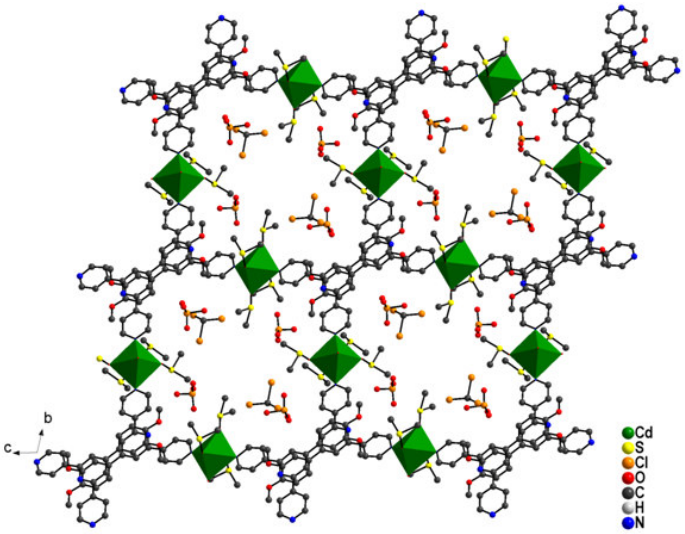

Fig. 4.74: Extended 3D porous MOF in **4n**

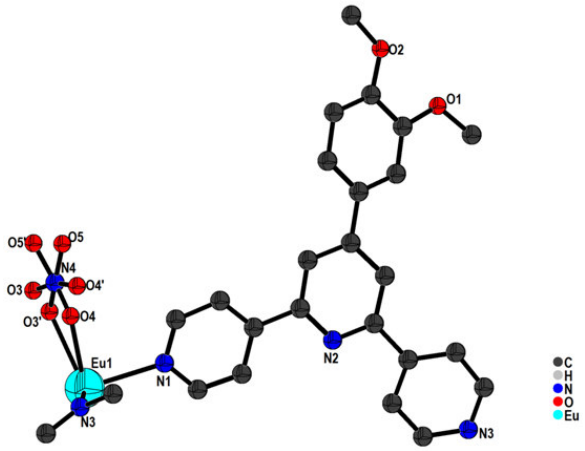

Fig. 4.75: Crystal structure of $[Eu(dmpt)_2(NO_3)_2].X$ (**4o**). (C−H bonds are not shown for clarity)

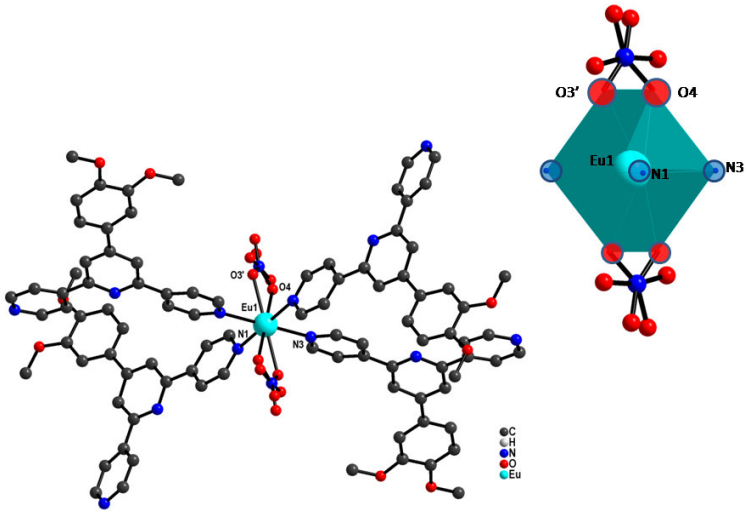

Fig. 4.76: Coordination environment around Eu center in **4o**

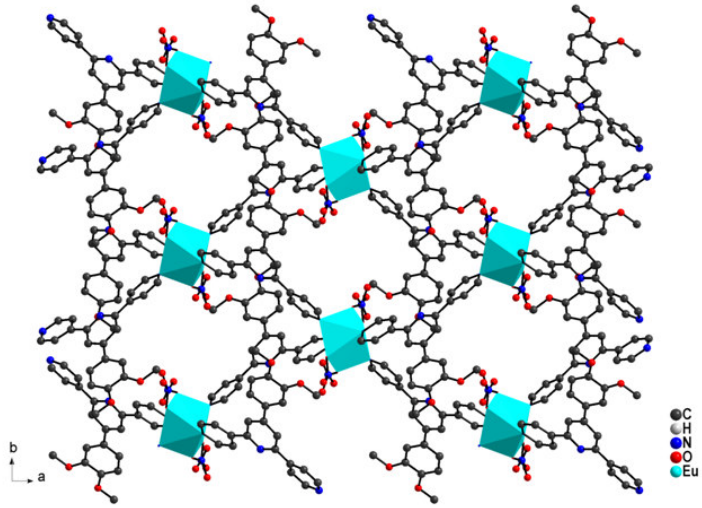

Fig. 4.77: View of 2D coordination network along *c*-axis in **4o**

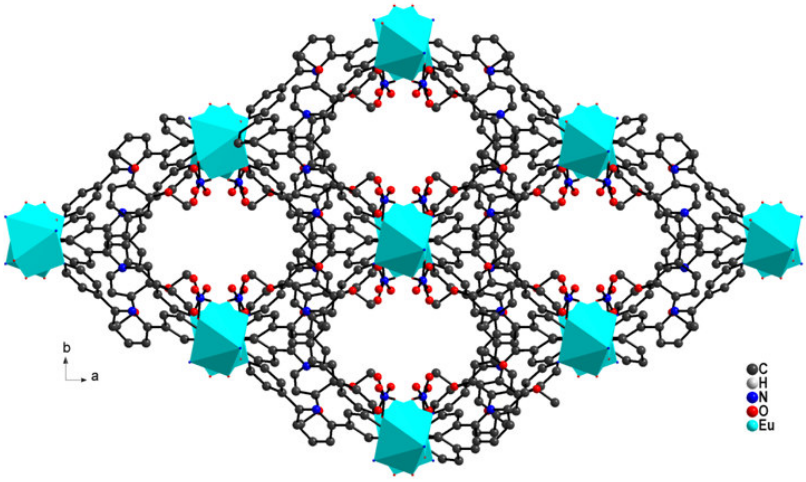

Fig. 4.78: Representation of 3D network in *ab*-plane for **4o**

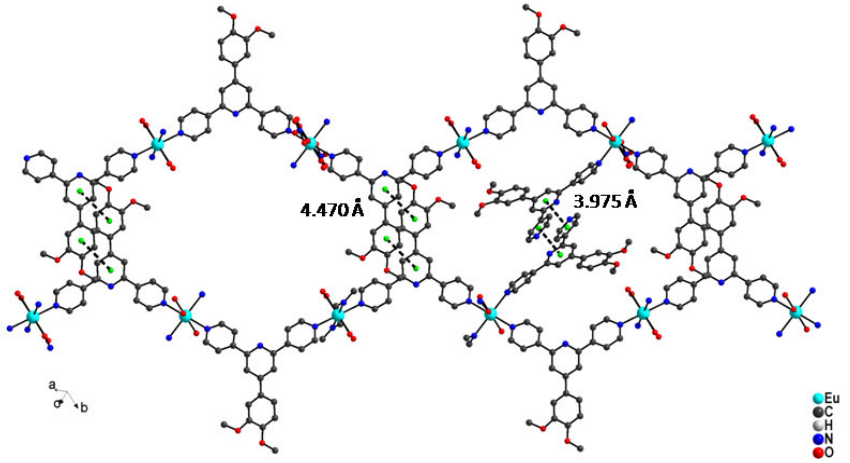

Fig. 4.79: Interlayer π-π stacking between central and peripheral pyridine ring (3.975 Å); central pyridine ring and the pendant ring (4.470 Å), **4o**

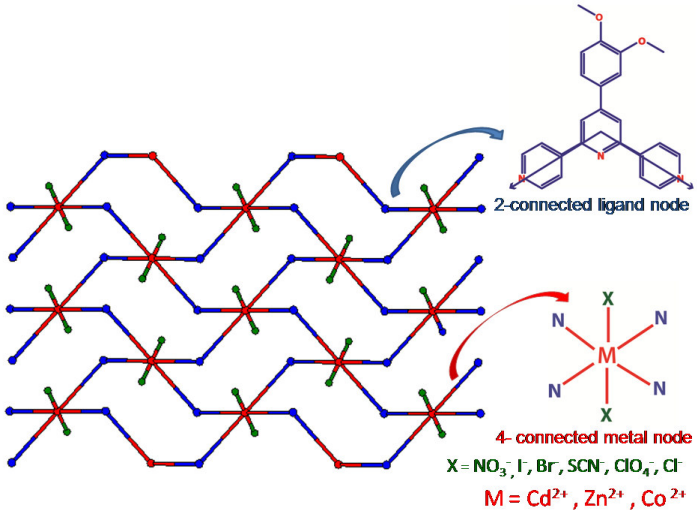

Fig. 4.80: Schematic representation of the (2,4)-connected network (red and blue nodes for the 4-connected M (II) centers and 2-connected ligand node, respectively

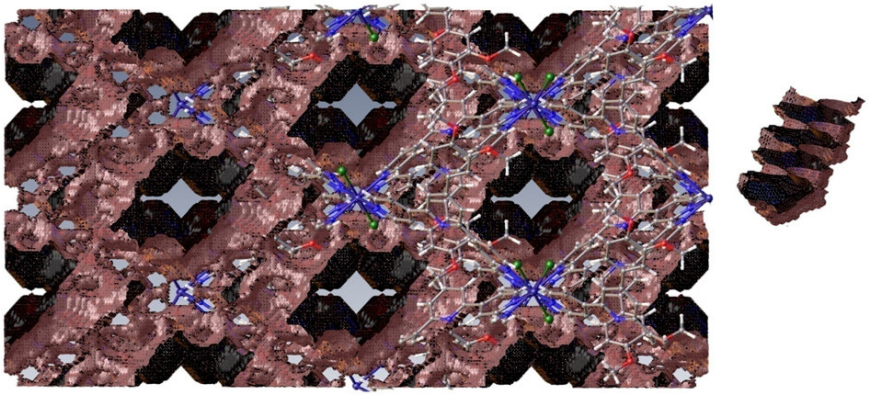

Fig. 4.81: Representation of voids in 3D framework and the cross-section of 1D channel displaying the shape of the channel

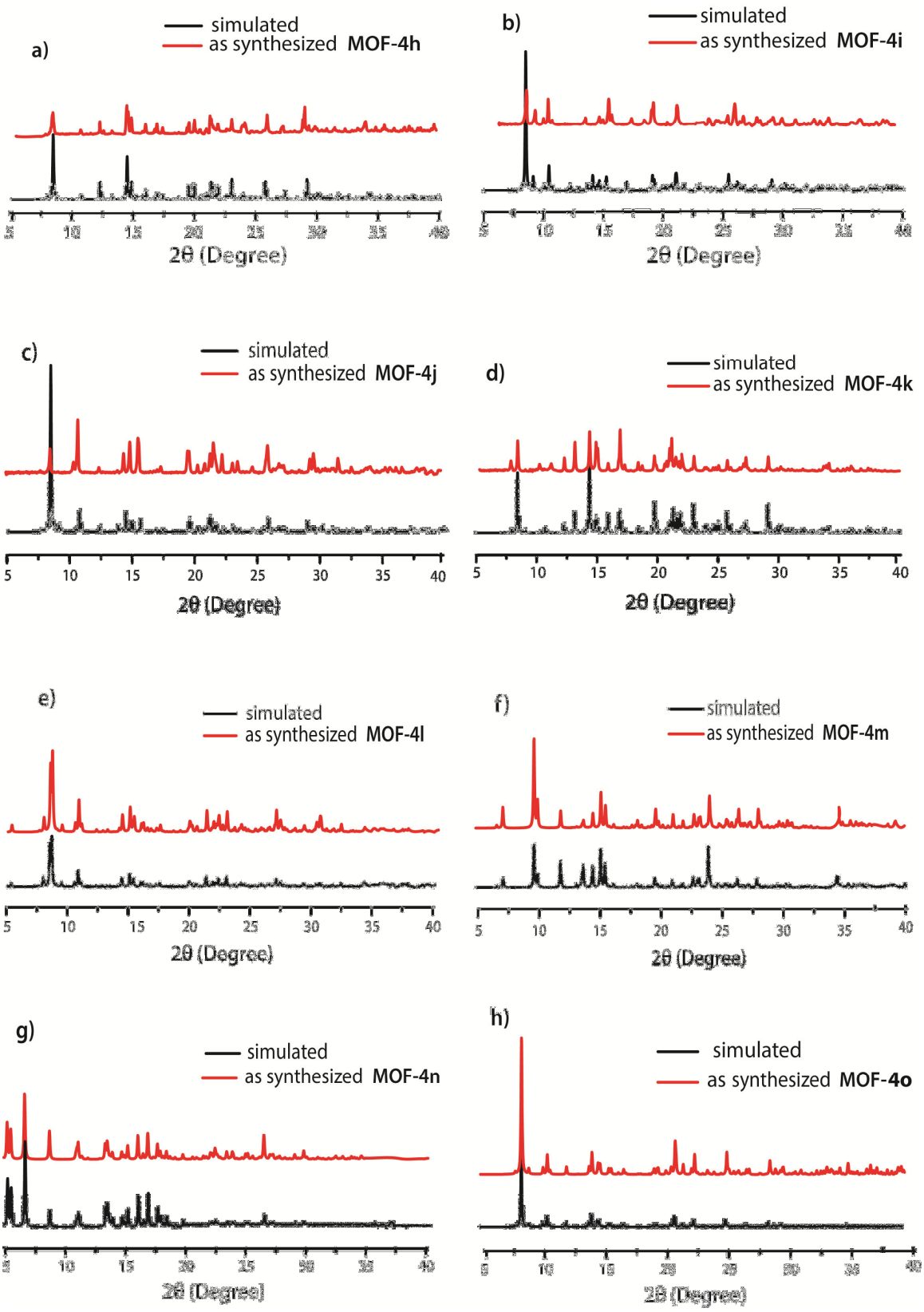

Fig. 4.82: PXRD pattern for MOFs **4h**-**4o**

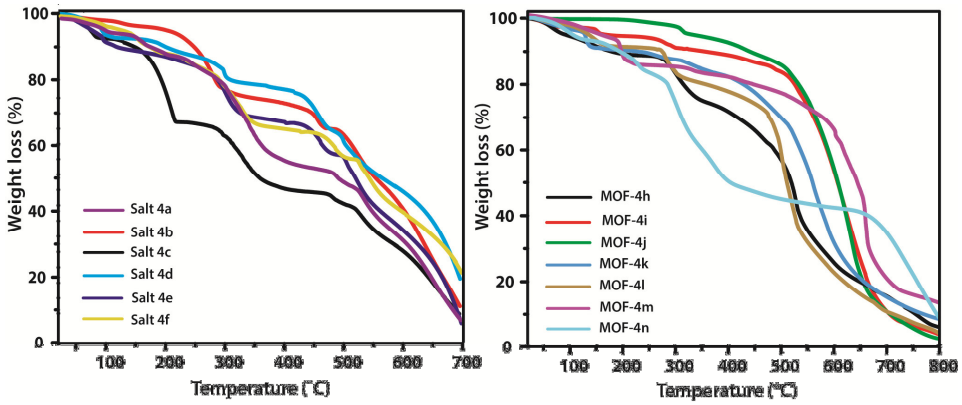

Fig. 4.83: Thermogravimetric curves for salts **4a-4f** and MOFs **4h-4n**

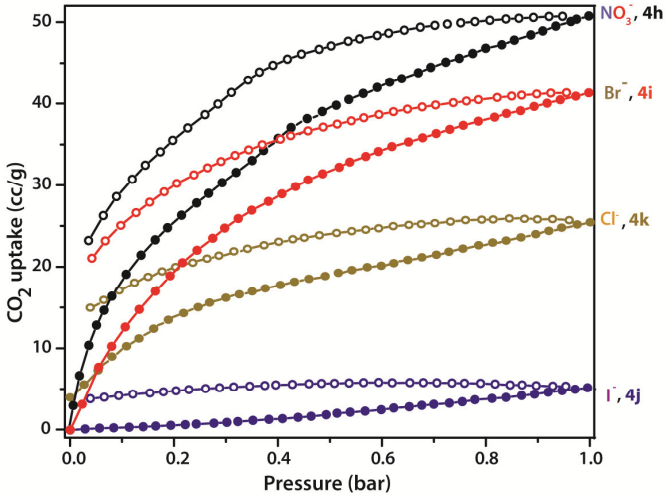

Fig. 4.84: CO_2 adsorption isotherms for MOFs **4h–4j**. Filled and open circles represent adsorption and desorption data, respectively

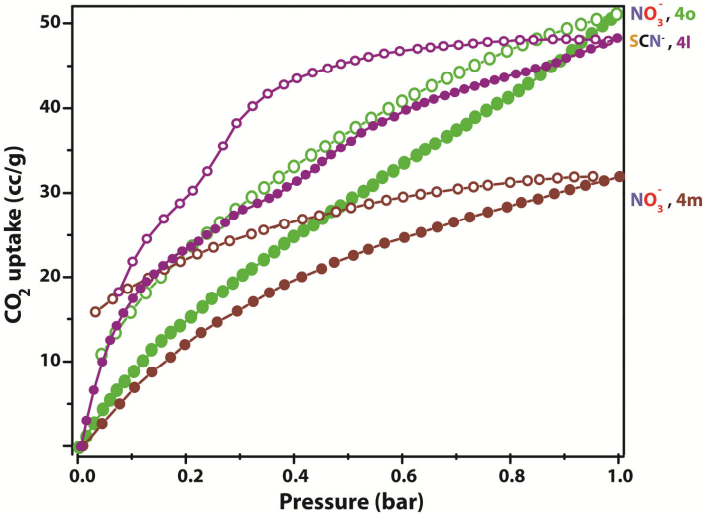

Fig. 4.85: CO_2 adsorption isotherms for MOFs **4l-4m** and **4o**. Filled and open circles represent adsorption and desorption data, respectively

Table 4.26: Summarizing the torsion angles between the rings of the ligand, dmpt:

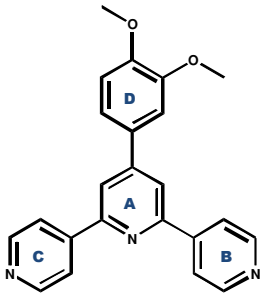

Compound	Torsion angle between A and B (°)	Torsion angle between A and C (°)	Torsion angle between A and D (°)	Torsion angle between C and B (°)
4g (dmpt)	-39.41	-6.36	-37.78	39.68
4h	16.90	-16.95	-15.91	3.65
4i	-17.20	21.30	18.96	0.13
4j	-17.72	21.44	17.18	4.70
4k	-20.39	25.93	17.97	6.48
4l	24.54	8.59	-3.63	27.98
4m	22.71	-15.08	38.54	49.18
4n	2.47	-6.71	-0.97	3.98
4o	20.64	-14.93	14.44	3.99

Table 4.27: Summarizing the pore details of 4h-4o

MOFs	Dimensions of the cavity (Å^2)	Solvent accessible void (Å^3)	Total potential per unit cell volume (Å^3)	Packing index (%)	CO_2 Adsorption (cc/g)
4h	6.5 X 6.6	504	4993.3	58.8	49.5
4i	8.1 X 7.4	581	4912.2	57.0	39.8
4j	7.0 X 6.9	573	5003.7	57.2	5.7
4k	6.7 X 6.5	573	4795.0	57.4	22.6
4l	7.6 X 4.3	391	2415.1	61.0	47.9
4m	9.7 X 7.5	139	2575.5	51.0	25.3
4o	8.3 X 8.0	510	4952.3	59.8	50.6

References:

1. Gibson, V. C., Redshaw, C. and Solan, G. A., "Bis(imino)pyridine: Surprisingly reactive ligands and a gateway to new families of catalysts", *Chem. Rev.*, **107**, 1745 (2007).
2. Seo, J. S., Whang, D., Lee, H., Jun, S. I., Oh, J., Jeon, Y. J. and Kim, K., "A homochiral metal-organic porous material for enantioselective separation and catalysis", *Nature*, **404**, 982 (2000).
3. Kawamichi, T., Inokuma, Y., Kawano, M. and Fujita, M., "Regioselecitive Huisgen cycloaddition within porous coordination networks", *Angew. Chem., Int. Ed.,* **49**, 2375 (2010).
4. Hennigar, T. L., MacQuarrie, D. C., Losier, P., Rogers, R. D. and Zaworotko, M. J., "Supramolecular isomerism in coordination polymers: Conformational freedom of ligands in $[Co(NO_3)_2(1,2\text{-bis}(4\text{-pyridyl})\text{ethane})_{1.5}]_n$", *Angew. Chem., Int. Ed.*, **36**, 972 (1997).
5. Constable, E. C., Dunphy, E. L., Housecroft, C. E., Neuburger, M., Schaffner, S., Schaper, F. and Batten, S. R., "Expanded ligands: Bis(2,2':6',2''-terpyridine carboxylic acid)ruthenium(II) complexes as metallosupramolecular analogues of dicarboxylic acids", *Dalton Trans.*, 4323 (2007).
6. Hathcock, D. J., Stone, K., Madden, J. and Slattery, S. J., "Electron donating substituent effects on redox and spin state properties of iron(II) bis-terpyridyl complexes", *Inorg. Chim. Acta*, **282**, 131 (1998).
7. Saitoh, A., Miyasaka, H., Yamashita, M. and Clerac, R., "Direct evidence of exchange interaction dependence of magnetization relaxation in a family of ferromagnetic-type single-chain magnets", *J. Mater. Chem.*, **17**, 2002 (2007).
8. Kitaura, R., Fujimoto, K., Noro, S.-I., Kondo, M., and Kitagawa, S., "A pillared-layer coordination polymer network displaying hysteretic sorption: $[Cu_2(pzdc)_2(dpyg)]n$ (pzdc= pyrazine-2,3-dicarboxylate; dpyg=1,2-di(4-pyridyl)glycol)", *Angew. Chem., Int. Ed.*, **114**, 141 (2002).
9. Chen, B., Wang, L., Xiao, Y., Fronczek, F. R., Xue, M., Cui, Y. and Qian, G., "A luminescent metal-organic framework with Lewis basic pyridyl sites for the sensing of metal ions", *Angew. Chem., Int. Ed.*, **48**, 500 (2009).
10. Graham, D., Faulds, K. and Smith, W. E., "Biosensing using silver nanoparticles and surface enhanced resonance Raman scattering", *Chem. Commun.*, **42**, 4363 (2006).

11. Campeau, L.-C., Rousseaux, S. and Fagnou, K., "A solution to the 2-pyridyl organometallic cross-coupling problem: Regioselective catalytic direct arylation of pyridine *N*-oxides", *J. Am. Chem. Soc.*, **127**, 18020 (2005).
12. Shattock, T. R., Arora, K. K., Vishweshwar, P. and Zaworotko, M. J., "Hierarchy of supramolecular synthons: Persistent carboxylic acid···pyridine hydrogen bonds in co-crystals that also contain a hydroxyl moiety", *Cryst. Growth Des.*, **8**, 4533 (2008).
13. Vishweshwar, P., Nangia, A. and Lynch, V. M., "Recurrence of carboxylic acid-pyridine supramolecular synthon in the crystal structures of some pyrazinecarboxylic acids", *J. Org. Chem.*, **67**, 556 (2002).
14. Alshahateet, S. F., Nakano, K., Bishop, R., Craig, D. C., Harris, K. D. M. and Scudder, M. L., "Co-crystalline hydrogen bonded solids based on the alcohol-carboxylic acid-alcohol supramolecular motif", *CrystEngComm*, **6**, 5 (2004).
15. Zhao, C., Sun, Q.-F., Hart-Cooper, W. M., DiPasquale, A. G., Toste, F. D., Bergman, R. G. and Raymond, K. N., "Chiral amide directed assembly of a diastereo- and enantiopure supramolecular host and its application to enantioselective catalysis of neutral substrates", *J. Am. Chem. Soc.*, **135**, 18802 (2013).
16. Steed, J. W., "Anion-tuned supramolecular gels: A natural evolution from urea supramolecular chemistry", *Chem. Soc. Rev.*, **39**, 3686 (2010).
17. Pihko, P. M., "*Hydrogen Bonding in Organic Synthesis*", John Wiley & Sons, New York, (2009).
18. Karunatilaka, C., Bučar, D.-K., Ditzler, L. R., Friščić, T., Swenson, D. C., MacGillivray, L. R. and Tivanski, A. V., "Softening and hardening of macro- and nano-sized organic co-crystals in a single-crystal transformation", *Angew. Chem., Int. Ed.*, **50**, 8642 (2011).
19. Jin, H., Plonka, A. M., Parise, J. B. and Goroff, N. S., "Pressure induced topochemical polymerization of diiodobutadiyne: A single-crystal-to-single-crystal transformation", *CrystEngComm*, **15**, 3106 (2013).
20. Sharma, C. V. K. and Clearfield, A., "Three-dimensional hexagonal structures from a novel self-complementary molecular building block", *J. Am. Chem. Soc.*, **122**, 4394 (2000).
21. Kong, D., McBee, J. L. and Clearfield, A., "Crystal engineered acid-base complexes with 2D and 3D hydrogen bonding systems using a bisphosphonic acid as the building block", *Cryst. Growth Des.*, **5**, 643 (2005).

22. Kong, D., Yao, J., Clearfield, A. and Zon, J., "Hydrogen-bonded structures formed from the reaction of 1,3,5-benzene-triphosphonic acid and adamantane", *Cryst. Growth Des.*, **8**, 2892 (2008).
23. Beckmann, J., Rüttinger, R. and Schwich, T., "1,3,5-Benzene-tri-*p*-phenylphosphonic acid. A new building block in supramolecular chemistry", *Cryst. Growth Des.*, **8**, 3271 (2008).
24. Kong D. and Clearfield, A., "Crystal-engineered three-dimensional hydrogen-bonding networks built with 1,3,5-benzenetri(phosphonic acid) and bipyridine synthons", *Cryst. Growth Des.*, **5**, 1767 (2005).
25. Mehring, M., "Two- and three-dimensional hydrogen-bonded networks built from 1,3,5-$[(HO)_2(O)P]_3C_6H_3$ and 4-(dimethylamino)pyridine", *Eur. J. Inorg. Chem.*, 3240 (2004).
26. Białek, M. J., Zaręba, J. K., Janczak, J. and Zoń, J., "Chains, layers, channels, and more: Supramolecular chemistry of potent diphosphonic tectons with tuned flexibility. The generation of pseudopolymorphs, polymorphs, and adducts", *Cryst. Growth Des.*, **13**, 4039 (2013).
27. Furukawa, H., Ko, N., Go, Y. B., Aratani, N., Choi, S. B., Choi, E., Yazaydin, A., Snurr, R. Q., O'Keeffe, M., Kim, J. and Yaghi, O. M., "Ultrahigh porosity in metal-organic frameworks", *Science*, **329**, 424 (2010).
28. Kundu, T., Sahoo, S. C. and Banerjee, R., "Variable water adsorption in amino acid derivative based homochiral metal organic frameworks", *Cryst. Growth Des.*, **12**, 4633 (2012).
29. Jiang, H.-L., Akita, T., Ishida, T., Haruta, M. and Xu, Q., "Synergistic catalysis of Au@Ag core−shell nanoparticles stabilized on metal-organic framework", *J. Am. Chem. Soc.*, **133**, 1304 (2011).
30. Yang, W., Davies, A. J., Lin, X., Suyetin, M., Matsuda, R., Blake, A. J., Wilson, C., Lewis, W., Parker, J. E., Tang, C. C., George, M. W., Hubberstey, P., Kitagawa, S., Sakamoto, H., Bichoutskaia, E., Champness, N. R., Yang, S. and Schröder, M., "Selective CO_2 uptake and inverse CO_2/C_2H_2 selectivity in a dynamic bifunctional metal-organic framework", *Chem. Sci.*, **3**, 2993 (2012).
31. Sumida, K., Rogow, D. L., Mason, J. A., McDonald, T. M., Bloch, E. D., Herm, Z. R., Bae, T.-H. and Long, J. R., "Carbon dioxide capture in metal-organic frameworks", *Chem. Rev.*, **112**, 724 (2012).

32. Li, X.-Z., Zhou, X.-P., Li, D. and Yin, Y.-G., "Controlling interpenetration in CuCN coordination polymers by size of the pendant substituents of terpyridine ligands", *CrystEngComm*, **13**, 6759 (2011).
33. Liu, C., Ding, Y.-B., Shi, X.-H., Zhang, D., Hu, M.-H., Yin, Y.-G. and Li, D., "Interpenetrating metal–organic frameworks assembled from polypyridine ligands and cyanocuprate catenations", *Cryst. Growth Des.*, **9**, 1275 (2009).
34. Inokuma, Y., Arai, T. and Fujita, M., "Networked molecular cages as crystalline sponges for fullerenes and other guests", *Nat. Chem.*, **2**, 780 (2010).
35. Murase, T., Nishijima, Y., and Fujita, M., "Cage-catalyzed knoevenagel condensation under neutral conditions in water", *J. Am. Chem. Soc*., **134**, 162 (2012).
36. Ikemoto, K., Inokuma, Y. and Fujita, M., "Diels–Alder via molecular recognition in a crystalline molecular flask", *J. Am. Chem. Soc*., **133**, 16806 (2011).
37. Kawamichi, T., Kodama, T., Kawano, M. and Fujita, M., "Single-crystalline molecular flasks: Chemical transformation with bulky reagents in the pores of porous coordination networks", *Angew. Chem., Int. Ed*., **47**, 8030 (2008).
38. Wen, L., Ke, X., Qiu, L., Zou, Y., Zhou, L., Zhao, J. and Li, D., "Assembly of two porous cadmium(II) frameworks: Selective adsorption and luminescent property", *Cryst. Growth Des.,* **12**, 4083 (2012).
39. Constable, E. C., Zhang, G., Housecroft, C. E., Neuburger, M. and Zampese, J. A., "Adding the second dimension with cadmium: Two-dimensional sheets assembled from cadmium(II) and 4'-phenyl-4,2':6',4''-terpyridine and locked by π-stacked interactions", *CrystEngComm*, **11**, 2279 (2009).
40. Martí-Rujas, J., Islam, N., Hashizume, D., Izumi, F., Fujita, M. and Kawano, M., "Dramatic structural rearrangements in porous coordination networks", *J. Am. Chem. Soc*., **133**, 5853 (2011).
41. Couck, S., Denayer, J. F. M., Baron, G. V., Rémy, T., Gascon, J. and Kapteijn, F., "An amine-functionalized MIL-53 metal-organic framework with large separation power for CO_2 and CH_4", *J. Am. Chem. Soc.*, **131**, 6326 (2009).
42. Dincă, M. and Long, J. R., "Strong H_2 binding and selective gas adsorption within the microporous coordination solid $Mg_3(O_2C\text{-}C_{10}H_6\text{-}CO_2)_3$", *J. Am. Chem. Soc.*, **127**, 9376 (2005).

43. Zhang, D.-S., Chang, Z., Li, Y.-F., Jiang, Z.-Y., Xuan, Z.-H., Zhang, Y.-H., Li, J.-R., Chen, Q., Hu, T.-L. and Bu, X.-H., "Fluorous metal-organic frameworks with enhanced stability and high H_2/CO_2 storage capacities", *Nature*, Scientific Reports **3**, Article number: 3312 (2013).
44. Pachfule, P., Chen, Y., Sahoo, S. C., Jiang, J. and Banerjee, R., "Structural isomerism and effect of fluorination on gas adsorption in copper-tetrazolate based metal organic frameworks", *Chem. Mater*., **23**, 2908 (2011).
45. Dorofeeva, V. N., Kolotilov, S. V., Kiskin, M. A., Polunin, R. A., Dobrokhotova, Z. V., Cador, O., Golhen, S., Ouahab, L., Eremenko, I. L. and Novotortsev, V. M., "2D porous honeycomb polymers versus discrete nanocubes from trigonal trinuclear complexes and ligands with variable topology", *Chem. Eur. J*., **18**, 5006 (2012).
46. Ma, S., Yuan, D., Wang, X.-S. and Zhou, H.-C., "Microporous lanthanide metal-organic frameworks containing coordinatively linked interpenetration: Syntheses, gas adsorption studies, thermal stability analysis, and photoluminescence investigation", *Inorg. Chem.*, **48**, 2072 (2009).
47. Rowsell, J. L. C. and Yaghi, O. M., "Effects of functionalization, catenation, and variation of the metal oxide and organic linking units on the low-pressure hydrogen adsorption properties of metal-organic frameworks", *J. Am. Chem. Soc.*, **128**, 1304 (2006).
48. Murugavel, R. and Singh, M. P., "One, two, and three methylene phosphonic acid groups ($–CH_2PO_3H_2$) on a mesitylene ring: Synthesis, characterization and aspects of supramolecular aggregation", *New J. Chem*., **34**, 1846 (2010).
49. Liu, G.-Z., Xin, L.-Y. and Wang, L.-Y., "Ancillary ligand-mediated syntheses and fluorescence properties of zinc(II) complexes based on flexible benzene dicarboxylic acid", *CrystEngComm*, **13**, 3013 (2011).
50. Felloni, M., Blake, A. J., Hubberstey, P., Wilson, C. and Schröder, M., "Solvent control of supramolecular architectures in 4,4'-bipyridyl-bridged copper(II) dipicolinate complexes", *Cryst. Growth Des*., **9**, 4685 (2009).
51. Lin, X., Telepeni, I., Blake, A. J., Dailly, A., Brown, C. M., Simmons, J. M., Zoppi, M., Walker, G. S., Thomas, K. M., Mays, T. J., Hubberstey, P., Champness, N. R. and Schröder, M., "High capacity hydrogen adsorption in Cu(II) tetracarboxylate framework materials: The

role of pore size, ligand functionalization, and exposed metal sites", *J. Am. Chem. Soc.*, **131**, 2159 (2009).

52. Du, M., Chen, S.-T. and Bu, X.-H., "$\{[Cd(bpo)(SCN)_2]\cdot CH_3CN\}_n$: A novel three-dimensional (3D) noninterpenetrated channel-like open framework with porous properties", *Cryst. Growth Des.*, **2**, 625 (2002).
53. Zhang, R.-H., "Rare Earth Element Chemistry (in Chinese)", *Tianjin Press of Science and Technology*, Tianjin, P.R. China, 40 (1987).
54. Desiraju, G. R. and Steiner, T., "*The Weak Hydrogen Bond in Structural Chemistry and Biology*", Oxford University Press, (1999).
55. Spek, A. L., "Single-crystal structure validation with the program *PLATON*", *J. Appl. Crystallogr.*, **36**, 7 (2003).
56. Ockwig, N. W., Delgado-Friedrichs, O., O'Keeffe, M. and Yaghi, O. M., "Reticular chemistry: Occurrence and taxonomy of nets and grammar for the design of frameworks", *Acc. Chem. Res.*, **38**, 176 (2005) and http://rcsr.anu.edu.au.
57. Pachfule, P., Das, R., Poddar, P. and Banerjee, R., "Structural, magnetic, and gas adsorption study of a series of partially fluorinated metal-organic frameworks (H*F*-MOFs)", *Inorg. Chem.*, **50**, 3855 (2011).
58. Amrouche, H., Aguado, S., Pérez-Pellitero, J., Chizallet, C., Siperstein, F., Farrusseng, D., Bats, N. and Nieto-Draghi, C., "Experimental and computational study of functionality impact on sodalite–zeolitic imidazolate frameworks for CO_2 separation", *J. Phys. Chem. C*, **115**, 16425 (2011).

Chapter 5

Experimental

Materials and methods:

All purchased chemicals were of highest grade and used without further purification. Preliminary treatment of solvents such as acetonitrile, dichloromethane, toluene, diethylether and tetrahydrofuran for its further purification was carried out [1]. Phenylphosphonic acid (H_2PPA), phosphonoacetic acid (H_2PAA), 3-phosphonopropionic acid (H_2PPRA), *tert*-butylphosphonic acid (H_2tBPA), etidronic acid (H_4EA), (1,4-phenylenebis(methylene))diphosphonic acid (H_4DPA), $Cd(ClO_4)_2.6H_2O$ (reagent grade), hydrogen bromide solution (33 wt% in acetic acid), mesitylene, triethylphosphite, 4-acetylpyridine, 2,2'-bipyridine ($^{2,2'}BPy$), 4,4'-bipyridine ($^{4,4'}BPy$) and anthracene were purchased from Aldrich chemical company, Germany. $CoCl_2.6H_2O$, $Cd(NO_3)_2.4H_2O$, $Zn(NO_3)_2.6H_2O$, $Eu(NO_3)_3.6H_2O$, $Cd(CH_3COO)_2.2H_2O$, $Cu(NO_3)_2.3H_2O$, potassium thiocyanate, sodium bromide, hydrazine hydrate (99%), acetylacetone, iodine, formaldehyde (37%), paraformaldehyde, sodium nitrite, acetic acid, sodium borohydride, phosphoryl chloride, 1,10-phenanthroline (Phen), 3,4-dimethoxybenzaldehyde, ammonia solution, phenol, 2-nitrophenol and 4-nitrophenol were purchased from S. D. Fine Chemicals, India. All manipulations were carried out in ambient atmosphere.

Caution: *Perchlorate salts are potentially explosive and should be handled carefully only in small amounts with appropriate precautions.*

Instrumentation:

The IR spectra were recorded as KBr pellets on a Thermo Nikolet Nexus FT-IR spectrometer. ^{1}H-NMR spectra were recorded on a Bruker AVANCE, 500.13 MHz spectrometer with tetramethylsilane (TMS) as the internal standard. C, H, and N elemental analyses were performed on an Elementar Vario ELIII analyzer. The powder X-ray diffraction (PXRD) data were collected on a Bruker Advanced D8 diffractometer using CuKα radiation. The TG analyses were carried out on Pyris Diamond thermogravimetry analyzer under air with a heating rate of 10 °C min^{-1}. The CO_2 adsorption measurement was carried out on Quantachrome gas sorption instrument.

X-ray crystallography:

The X-ray data on suitable crystals of the complexes were collected on a Bruker Kappa Apex four circle-CCD diffractometer using graphite monochromated MoKα radiation (λ = 0.71070 Å). Structure solution and refinement were done by direct method and developed by conventionally alternating cycles of least-squares refinement on SHELXTL program [2-3]. SAINT and SADABS software packages [4] were employed for data reductions and absorption corrections, respectively. All the non-hydrogen atoms were refined anisotropically. The hydrogen atoms were granted to hop on their respective parent atoms according to their positions generated theoretically and refined isotropically with fixed thermal factors.

Chapter 2

The 3,3',5,5'-tetramethyl-1H,1'H-4,4'-bipyrazole (BPz) [5] and methylenebis(3,5-dimethylpyrazole) (MBPz) [6] were synthesized as reported in the literature.

Synthesis of 2-bis(3,5-dimethyl-1H-pyrazol-4-yl)diazene, (BPaz)

To the mixture of acetylacetone (5.00 g, 50.00 mmol) and 50 mL of acetic acid, aqueous solution of sodium nitrite (5.00 g, 70.00 mmol) was added to the mixture at 5 °C. The reaction mixture was stirred for 3 hrs at room temperature. The mixture was diluted to 150 mL followed by the addition of hydrazine hydrate (30 mL). The resultant mixture was further allowed to stir overnight at room temperature. The resulted yellow precipitate was filtered and washed thoroughly with water. Yield: 8.50 g, 77%. IR (ν/cm^{-1}): 2913, 2323, 1604, 1580.

Synthesis of [(HPPA$^-$)$_2$.H$_2$BPz^{2+}] (2a)

A 3mL methanolic solution of BPz (0.19 g, 1.00 mmol) was added to a methanolic solution (2 mL) of phenylphosphonic acid (H_2PPA) (0.16 g, 1.00 mmol). The mixture was heated at 50 °C and stirred for 15 min. The resultant colorless solution was filtered and allowed to stand at room temperature. Colorless crystals of compound **2a** were obtained by slow evaporation of the resulted solution. Yield: 0.31 g, 62%. Elemental anal. calc. (%) for $C_{22}H_{28}N_4O_6P_2$: C, 52.18; H, 5.57; N, 11.06. Found: C, 52.63; H, 5.48; N, 11.28. IR (ν/cm^{-1}): 3189, 3076, 2300, 1821, 1604, 1431, 1140, 1031, 931, 753.

Synthesis of [HtBPA$^-$.HBPz$^+$] (2b)

Salt **2b** was prepared by the similar method as employed for **2a** by using BPz (0.19 g, 1.00 mmol) and *tert*-butylphosphonic acid (H_2tBPA) (0.14 g, 1.00 mmol) followed by the addition of few drops of water. Yield: 0.21 g, 67%. Elemental anal. calc. (%) for $C_{14}H_{25}N_4O_3P$: C, 51.21; H, 7.67; N, 17.06. Found: C, 51.43; H, 7.38; N, 17.18. IR (ν/cm^{-1}): 3273, 2966, 2324, 1967, 1571, 1473, 1301, 1005, 930, 647.

Synthesis of [(HPPRA$^-$)$_2$.H$_2$BPz^{2+}.(MeOH)$_2$.H$_2$O] (2c)

A 2 mL methanolic solution of BPz (0.19 g, 1.00 mmol) was added to acetonitrile solution (3 mL) of 3-phosphonopropionic acid (H_2PPRA) (0.17 g, 1.00 mmol) in place of phenylphosphonic acid. The mixture was stirred for 15 min and the resulted solution was kept for crystallization at low temperature. Colorless crystals of compound **2c** were obtained after 3 days by slow evaporation of the resulted solution. Yield: 0.37 g, 64%. Elemental anal. calc. (%) for $C_{18}H_{36}N_4O_{13}P_2$: C, 37.37; H, 6.27; N, 9.69. Found: C, 37.63; H, 6.12; N, 9.48. IR (ν/cm^{-1}): 3082, 2305, 1718, 1418, 1257, 1113, 1101, 789, 908, 623.

Synthesis of [H$_2$DPA^{2-}.(HBPz$^+$)$_2$.H$_2$O] (2d)

Salt **2d** was prepared by the similar method as employed for **2a** by using BPz (0.28 g, 1.50 mmol) and (1,4-phenylenebis(methylene))diphosphonic acid (H_4DPA) (0.27 g, 1.00 mmol) in ethanolic solution followed by the addition of few drops of water. Yield: 0.39 g, 59%. Elemental anal. calc. (%) for $C_{28}H_{42}N_8O_7P_2$: C, 50.60; H, 6.37; N, 16.86. Found: C, 50.83; H, 6.18; N, 16.68. IR (ν/cm^{-1}): 3346, 3201, 3074, 2921, 2305, 1731, 1616, 1510, 1418, 1263, 1117, 847, 799, 557.

Synthesis of [HPPA$^-$.H$_2$PPA.HMBPz$^+$.MBPz] (2e)

A 5 mL methanolic solution of MBPz (0.20 g, 1.00 mmol) was added to a methanolic solution (5 mL) of phenylphosphonic acid (H_2PPA) (0.16 g, 1.00 mmol) followed by the addition of few drops of water. The mixture was stirred for 1 hr at room temperature and the colorless crystals of compound **2e** were obtained by slow evaporation of the resulted solution. Yield: 0.37 g, 52%. Elemental anal. calc. (%) for $C_{34}H_{46}N_8O_6P_2$: C, 56.35; H, 6.40; N, 15.46. Found: C, 56.26; H, 6.53; N, 15.65. IR (ν/cm^{-1}): 3406, 3185, 1697, 1597, 1447, 1297, 1139, 1018, 932, 753, 696, 560, 531.

Synthesis of [$(HtBPA^-)_2.H_2MBPz^{2+}$.EtOH] (2f)

Salt **2f** was prepared by the similar method as employed for **2e** by using MBPz (0.20 g, 1.00 mmol) and *tert*-butylphosphonic acid (H_2tBPA) (0.28 g, 2.00 mmol) in ethanolic solution. Yield: 0.27 g, 53%. Elemental anal. calc. (%) $C_{21}H_{44}N_4O_7P_2$: C, 47.90; H, 8.42; N, 10.64. Found: C, 47.82; H, 8.59; N, 10.50. IR (ν/cm^{-1}): 3199, 3085, 2985, 2877, 2327, 1590, 1518, 1469, 1382, 1297, 1197, 996, 946, 839, 739, 653, 488.

Synthesis of [$HPAA^-$.$HMBPz^+$.MBPz.MeOH] (2g)

Salt **2g** was prepared by the similar method as employed for **2e** by using MBPz (0.20 g, 1.00 mmol) and phosphonoacetic acid (H_2PAA) (0.14 g, 1.00 mmol). Yield: 0.29 g, 51%. Elemental anal. calc. (%) for $C_{25}H_{41}N_8O_6P$: C, 51.72; H, 7.12; N, 19.30. Found: C, 51.85, H, 7.21; N, 19.42. IR (ν/cm^{-1}): 3192, 3134, 3078, 2927, 2856, 1726, 1583, 1518, 1433, 1290, 1146, 1061, 932, 867, 753, 589, 482.

Synthesis of [$HPPRA^-$.$HMBPz^+$] (2h)

Salt **2h** was prepared by the similar method as employed for **2e** by using MBPz (0.20 g, 1.00 mmol) and 3-phosphonopropionic acid (H_2PPRA) (0.17 g, 1.00 mmol). Yield: 0.16 g, 47%. Elemental anal. calc. (%) for $C_{14}H_{23}N_4O_5P$: C, 46.93; H, 6.47; N, 15.64. Found: C, 46.81; H, 6.39; N, 15.78. IR (ν/cm^{-1}): 3156, 3092, 2927, 2877, 2348, 1712, 1597, 1525, 1411, 1261, 1204, 1125, 1018, 932, 789, 739, 503.

Synthesis of [$H_2EA^{2-}.H_2MBPz^{2+}$.solvent] (2i)

A 2 mL ethanolic solution of MBPz (0.20 g, 1.00 mmol) was added to acetonitrile solution (2 mL) of etidronic acid (H_4EA) (0.21 g, 1.00 mmol) in hot condition. Colorless crystals of compound **2i** were obtained by slow evaporation of the resulted solution at room temperature. Yield: 0.15 g, 33%. Elemental anal. calc. (%) for $C_{15}H_{30}N_4O_8P_2$: C, 39.48; H, 6.63; N, 12.28. Found: C, 39.65; H, 6.45; N, 12.39. IR (ν/cm^{-1}): 3385, 2920, 2806, 2698, 1640, 1590, 1454, 1268, 1146, 1003, 925, 811, 746, 631, 517, 453.

Synthesis of [$H_2EA^{2-}.H_2MBPz^{2+}$] (2j)

Salt **2j** was prepared by the similar method as employed for **2e** but with the addition of 0.5 mL of DMSO in hot condition instead of acetonitrile. Yield: 0.20 g, 49%. Elemental anal.

calc. (%) for $C_{13}H_{24}N_4O_7P_2$: C, 38.05; H, 5.90; N, 13.66. Found: C, 38.18; H, 5.85; N, 13.59. IR (ν/cm^{-1}): 3373, 2812, 2780, 2543, 1691, 1512, 1354, 1212, 1198, 996, 911, 842, 798, 612, 598.

Synthesis of [H_3DPA^-.$(H_2DPA^{2-})_{0.5}$.H_2MBPz^{2+}.$(H_2O)_{0.4}$] (2k)

Salt **2k** was prepared by the similar method as employed for **2e** by using MBPz (0.20 g, 1.00 mmol) and (1,4-phenylenebis(methylene))diphosphonic acid (H_4DPA) (0.27 g, 1.00 mmol). Yield: 0.34 g, 28%. Elemental anal. calc. (%) for $C_{23}H_{34.8}N_4O_{9.4}P_3$: C, 45.24; H, 5.74; N, 9.17. Found: C, 45.69; H, 5.43; N, 9.34. IR (ν/cm^{-1}): 3399, 3192, 3134, 2920, 2355, 1597, 1511, 1425, 1368, 1297, 1268, 1125, 989, 939, 832, 746, 567, 482.

Synthesis of [H_2PPA.BPaz] (2l)

Co-crystal **2l** was prepared by the similar method as employed for **2e** by using BPaz (0.22 g, 1.00 mmol) and phenylphosphonic acid (H_2PPA) (0.24 g, 1.50 mmol) in ethanol. Pale yellow crystals of compound **2l** were obtained by slow evaporation of the resulted solution. Yield: 0.19 g, 53%. Elemental anal. calc. (%) for $C_{16}H_{21}N_6O_3P$: C, 51.06; H, 5.62; N, 22.33. Found: C, 51.22; H, 5.55; N, 22.20. IR (ν/cm^{-1}): 3382, 2747, 1900, 1594, 1497, 1435, 1325, 1150, 992, 754, 703.

Synthesis of [$(H_2tBPA)_2$.BPaz] (2m)

Co-crystal **2m** was prepared by the similar method as employed for **2l** by using *tert*-butylphosphonic acid (H_2tBPA) (0.28 g, 2.00 mmol) in ethanol followed by the addition of few drops of water. Yield: 0.27 g, 56%. Elemental anal. calc. (%) for $C_{18}H_{36}N_6O_6P_2$: C, 43.72; H, 7.34; N, 17.00. Found: C, 43.58; H, 7.54; N, 17.28. IR (ν/cm^{-1}): 3195, 2973, 2315, 1591, 1475, 1370, 1188, 1193, 997, 926, 772, 648.

Synthesis of [H_2DPA^{2-}.$(HBPaz^+)_2$.$(BPaz)_2$.DMSO.H_2O] (2n)

Salt **2n** was prepared by the similar method as employed for **2l** by using (1,4-phenylenebis(methylene))diphosphonic acid (H_4DPA) (0.40 g, 1.50 mmol) in ethanol followed by the addition of few drops of DMSO in hot condition. Yellow crystals of compound **2n** were obtained by slow evaporation of the resulted solution. Yield: 0.15 g, 51%. Elemental anal. calc. (%) for $C_{50}H_{68}N_{24}O_8P_2S$: C, 48.93; H, 5.58; N, 27.39; S, 2.61. Found: C, 48.74; H, 5.34; N, 27.48; S, 2.83. IR (ν/cm^{-1}): 3256, 3121, 2974, 2262, 1693, 1462, 1362, 1152, 990, 772, 626.

Chapter 3

Synthesis of [($HAPa^-$).($HBPz^+$).THF] (3a)

The *n*-butanolic and THF solution of H_2APa (0.41 g, 1.50 mmol) and BPz (0.29 g, 1.50 mmol) was heated and stirred for 15 mins. The resultant yellow solution was filtered and allowed to stand at room temperature. Yellow crystals of compound **3a** were obtained by slow evaporation of the resulted solution. Yield: 0.49 g, 62%. Elemental anal. calc. (%) for $C_{29}H_{35}N_4O_4P$: C, 65.16; H, 6.60; N, 10.48. Found: C, 65.37; H, 6.36; N, 10.67. IR (KBr, cm^{-1}): 3468, 3329, 2912, 2824, 2329, 1614, 1472, 1250, 1121, 834, 798.

Synthesis of [($HAPa^-$).($HBPz^+$).dioxane] (3b)

Salt **3b** was prepared by the similar method as employed for **3a** in dioxane followed by the addition of few drops of *n*-butanol. Yield: 0.52 g, 64%. Elemental anal. calc. (%) for $C_{29}H_{35}N_4O_5P$: C, 63.26; H, 6.41; N, 10.18. Found: C, 63.44; H, 6.23; N, 10.38. IR (KBr, cm^{-1}): 3490, 3250, 2978, 2854, 2398, 1598, 1410, 1301, 1250, 1172, 1098, 921, 823.

Synthesis of [($HAPa^-$).($HBPz^+$).benzene] (3c)

Salt **3c** was prepared by the similar method as employed for **3a** in benzene followed by the addition of few drops of *n*-butanol. Yield: 0.44 g, 55%. Elemental anal. calc. (%) for $C_{31}H_{33}N_4O_3P$: C, 68.87; H, 6.15; N, 10.36. Found: C, 68.56; H, 6.24; N, 10.44. IR (KBr, cm^{-1}): 3199, 3163, 3081, 2952, 2342, 1659, 1617, 1565, 1547, 1421, 1377, 1305, 1235, 1122, 1065, 1011, 933, 841, 727.

Synthesis of [($HAPa^-$).($HBPz^+$).thiophene] (3d)

Salt **3d** was prepared by the similar method as employed for **3a** in thiophene followed by the addition of few drops of *n*-butanol. Yield: 0.42 g, 52%. Elemental anal. calc. (%) for $C_{29}H_{31}N_4O_3PS$: C, 63.72; H, 5.72; N, 10.25. Found: C, 63.46; H, 5.52; N, 10.38. IR (KBr, cm^{-1}): 3263, 3068, 2990, 2250, 1648, 1523, 1480, 1348, 1261, 1121, 1058, 815, 750.

Synthesis of [($HAPa^-$).($HBPz^+$).nitromethane] (3e)

Salt **3e** was prepared by the similar method as employed for **3a** in nitromethane followed by the addition of few drops of *n*-butanol. Yield: 0.46 g, 59%. Elemental anal. calc. (%) for $C_{26}H_{30}N_5O_5P$: C, 59.65; H, 5.78; N, 13.38. Found: C, 59.32; H, 5.61; N, 13.21. IR (KBr, cm^{-1}): 3230, 3024, 2982, 2359, 1698, 1584, 1472, 1325, 1244, 1109, 1051, 958, 826, 758.

Synthesis of [$(HAPa^-)_2$.$(HBPz^+)_2$.nitrobenz.H_2O] (3f)

Salt **3f** was prepared by the similar method as employed for **3a** in nitrobenzene followed by the addition of few drops of *n*-butanol. Yield: 0.28 g, 36%. Elemental anal. calc. (%) for $C_{56}H_{59}N_9O_9P_2$: C, 63.21; H, 5.59; N, 11.85. Found: C, 63.19; H, 5.24; N, 11.62. IR (KBr, cm^{-1}): 3199, 3152, 3072, 2922, 2360, 1724, 1609, 1521, 1477, 1346, 1227, 1171, 1012, 948, 715.

Synthesis of [$(HAPa^-)_2$.$(HBPz^+)_2$.thiophenol] (3g)

Salt **3g** was prepared by the similar method as employed for **3a** in thiophenol followed by the addition of few drops of *n*-butanol. Yield: 0.31 g, 41%. Elemental anal. calc. (%) for $C_{56}H_{60}N_8O_6P_2S$: C, 64.98; H, 5.84; N, 10.82. Found: C, 64.79; H, 5.54; N, 10.65. IR (KBr, cm^{-1}): 3132, 3111, 3063, 2987, 2345, 1729, 1629, 1587, 1498, 1390, 1298, 1163, 1098, 934, 785.

Synthesis of [$(HAPa^-)_2$.$(HBPz^+)_2$.toluene] (3h)

Salt **3h** was prepared by the similar method as employed for **3a** in toluene followed by the addition of few drops of *n*-butanol. Yield: 0.32 g, 43%. Elemental anal. calc. (%) for $C_{57}H_{62}N_8O_6P_2$: C, 67.31; H, 6.14; N, 11.02. Found: C, 67.58; H, 6.34; N, 11.35. IR (KBr, cm^{-1}): 3199, 3078, 2928, 2819, 2372, 2330, 1619, 1574, 1545, 1418, 1344, 1309, 1252, 1168, 1142, 1011, 943, 884, 843, 753, 731, 694.

Synthesis of [$(HAPa^-)_2$.$(HBPz^+)_2$.*p*-cresol.H_2O] (3i)

Salt **3i** was prepared by the similar method as employed for **3a** in *n*-butanol with the addition of *p*-cresol (0.11 g, 1.00 mmol). Yield: 0.25 g, 32%. Elemental anal. calc. (%) for $C_{57}H_{62}N_8O_8P_2$: C, 65.26; H, 5.96; N, 10.68. Found: C, 65.48; H, 5.74; N, 10.45. IR (KBr, cm^{-1}): 3342, 3263, 2950, 2342, 1623, 1610, 1550, 1429, 1314, 1269, 1140, 1009, 976, 877, 765, 730, 691.

Synthesis of [$(HAPa^-)$.$(H_2BPz^{2+})_{0.5}$.phenol] (3j)

Salt **3j** was prepared by the similar method as employed for **3a** in phenol followed by the addition of few drops of *n*-butanol. Yield: 0.48 g, 35%. Elemental anal. calc. (%) for $C_{26}H_{26}N_2O_4P$: C, 67.67; H, 5.68; N, 6.07. Found: C, 67.34; H, 5.28; N, 6.27. IR (KBr, cm^{-1}): 3452, 3428, 3285, 2923, 2350, 1716, 1610, 1564, 1436, 1419, 1282, 1195, 1145, 1065, 991, 806, 761, 732, 681.

Synthesis of [$(HAPa^-)_2.H_2BPz^{2+}$.2-NP.*n*-butanol] (3k)

Salt **3k** was prepared by the similar method as employed for **3a** by using H_2APa (0.41 g, 1.50 mmol) and BPz (0.19 g, 1.00 mmol) in *n*-butanol with the addition of 2-nitrophenol (2-NP) (0.14 g, 1.00 mmol). Red crystals of compound **3k** were obtained by slow evaporation of the resulted solution. Yield: 0.36 g, 38%. Elemental anal. calc. (%) for $C_{50}H_{55}N_5O_{10}P_2$: C, 63.35; H, 5.85; N, 7.39. Found: C, 63.56; H, 5.54; N, 7.58. IR (KBr, cm^{-1}): 3661, 3204, 2404, 2330, 1663, 1614, 1531, 1418, 1315, 1246, 1120, 1059, 918, 835, 728.

Synthesis of [$(HAPa^-)_2.H_2BPz^{2+}$.4-NP.S] (3l)

Salt **3l** was prepared by the similar method as employed for **3a** by using H_2APa (0.41 g, 1.50 mmol) and BPz (0.19 g, 1.00 mmol) in *n*-butanol with the addition of 4-nitrophenol (4-NP) (0.14 g, 1.00 mmol). Red crystals of compound **3l** were obtained by slow evaporation of the resulted solution. Yield: 0.32 g, 34%. Elemental anal. calc. (%) for $C_{50}H_{55}N_5O_{10}P_2$: C, 63.35; H, 5.85; N, 7.39. Found: C, 63.50; H, 5.62; N, 7.51. IR (KBr, cm^{-1}): 3326, 3084, 2928, 2814, 2731, 2677, 2561, 2487, 2436, 1921, 1598, 1496, 1288, 1335, 1300, 1107, 936, 851, 729.

Synthesis of [$(HAPa^-)_2.(HBPz^+)_2.(H_2APa)_2.H_2O$] (3m)

Salt **3m** was prepared by the similar method as employed for **3a** by using H_2APa (0.54 g, 2.00 mmol) and BPz (0.19 g, 1.00 mmol) in ethanol with the addition of few drops of water. Yield: 0.39 g, 53%. Elemental anal. calc. (%) for $C_{80}H_{80}N_8O_{13}P_4$: C, 64.69; H, 5.43; N, 7.54. Found: C, 64.43; H, 5.67; N, 7.46. IR (KBr, cm^{-1}): 3468, 3066, 2968, 2398, 1649, 1418, 1362, 1062, 998, 824, 779, 748.

Synthesis:

Ethyl hydrogen (anthracen-9-ylmethyl)phosphonate, (3n) and (anthracen-9-ylmethyl)phosphonic acid, H_2APa:

To recrystallized 9-bromomethyl anthracene [7] (2.30 g, 8.50 mmol), triethylphosphite (1.45 g, 8.70 mmol) was added and the suspension was refluxed for 8 hrs at 150 °C. The reaction mixture was allowed to cool at room temperature and the volatiles were removed under vacuum. The resulted yellow solid in the mixture was filtered and recrystallized from methanol. Yield: 1.89 g, 68% as a yellow solid. ^1H NMR spectrum (DMSO-*d*6), d, ppm: 1.41 m (6H, CH_3); 3.47 d (2H, CH_2P); 4.22 m (4H, CH_2); 7.35 m (4H, ArH); 7.91 m (4H, ArH); 8.15 d (1H, ArH).

The resulted phosphonoester (1.48 g, 4.50 mmol) was allowed to undergo controlled acidic hydrolysis by refluxing in presence of 30 mL of 70% aqueous HCl for 14 hrs on a boiling water bath. The product **3n** was precipitated and washed with water after filtration. Yield 1.16 g, 86%. ^{1}H NMR spectrum (DMSO-*d*6), d, ppm: 1.30 m (3H, CH_3); 4.19 m (2H, CH_2); 4.44 d (2H, CH_2P); 7.37 m (4H, ArH); 7.92 m (4H, ArH); 8.15 d (1H, ArH); 11.96 s (1H, OH). Elemental anal. calc. (%) for $C_{17}H_{17}O_3P$: C, 68.00; H, 5.71. Found (%): C, 68.32; H, 5.54.

On the other hand, **H_2APa** was synthesized on further complete acidic hydrolysis of phosphonoester with 30 mL of 70% aqueous HCl for more than 24 hrs. The resulted precipitate was filtered and washed thoroughly with water. Yield 1.07 g, 88%. ^{1}H NMR spectrum (DMSO-*d*6), d, ppm: 4.42 d (2H, CH_2P); 7.37 m (4H, ArH); 7.92 m (4H, ArH); 8.15 d (1H, ArH); 11.96 s (2H, OH). Elemental anal. calc. (%) for $C_{15}H_{13}O_3P$: C, 66.18; H, 4.81. Found (%): C, 66.36; H, 4.64.

Synthesis of $[Cu_2(\mu_2\text{-}C_{15}H_{12}PO_3)_2(^{2,2'}BPy)_2(H_2O)_2]((NO_3)_2.X)$ (3o)

To the acetonitrile solution of $Cu(NO_3)_2.3H_2O$ (0.10 g, 0.41 mmol), **3n** (0.12 g, 0.41 mmol) and 2,2'-bipyridine (0.06 g, 0.41 mmol) were added followed by the addition of few drops of triethylamine in 1 mL methanol. The reaction mixture was stirred for 3 hrs. The precipitate was filtered and kept at room temperature for crystallization. After one week, green crystals of compound **3o** were found from the mother liquor. Yield: 0.20 g, 42%. Elemental anal. calc. (%) for $C_{56}H_{60}Cu_2N_6O_{14}P_2$: C, 54.68; H, 4.92; N, 6.83. Found: C, 54.38; H, 4.57; N, 6.99. IR (KBr, cm^{-1}): 3266, 2881, 2416, 2322, 2032, 1886, 1798, 1656, 1435, 1324, 1176, 1019, 936, 777, 720.

Synthesis of $[Cu_2(\mu_2\text{-}C_{15}H_{12}PO_3)_2(^{2,2'}BPy)_2(NO_3)_2]$.MeOH (3p)

The compound **3p** was synthesized from compound **3n**. The crystals of **3p** were harvested and washed with methanol. The crystals were allowed to heat under vacuum at 100 ºC for 12 hrs. Furthermore, the resulted compound was kept undisturbed in methanol for two days, resulted in compound **3p**. Elemental anal. calc. (%) for $C_{56}H_{56}Cu_2N_6O_{14}P_2$: C, 54.86; H, 4.60; N, 6.85. Found: C, 54.65; H, 4.41; N, 6.52. IR (KBr, cm^{-1}): 3386, 3242, 2925, 2645, 2495, 2027, 1982, 1892, 1747, 1602, 1316, 1043, 878, 771.

Chapter 4

The ((2,4,6-trimethylbenzene-1,3,5-triyl)tris(methylene))triphosphonic acid (H_6TPA) [ref. [48] from chapter 4] and 4,2':6',4''-terpyridine (Terp) [ref. [39] from chapter 4] were synthesized as reported in the literature.

Synthesis of [$H_5TPA^-.H^{2,2'}BPy^+$] (4a)

A 2 mL methanolic solution of 2,2'-bipyridine (0.16 g, 1.00 mmol) was added to ethanolic solution (2 mL) of ((2,4,6-trimethylbenzene-1,3,5-triyl)tris(methylene))triphosphonic acid, H_6TPA (0.40 g, 1.00 mmol) in hot condition. Colorless crystals of compound **4a** were obtained by slow evaporation of the resulted solution at room temperature. Yield: 0.34 g, 62%. Elemental anal. calc. (%) for $C_{22}H_{29}N_2O_9P_3$: C, 47.32; H, 5.23; N, 5.02. Found: C, 47.45; H, 5.54; N, 5.19. IR (KBr, cm^{-1}) (ν): 3297, 1580, 1246.

Synthesis of [$(H_4TPA^{2-})_2.(H_2^{4,4'}BPy^{2+})_2.H_2O$] (4b)

Salt **4b** was prepared by the similar method as employed for **4a** by using H_6TPA (0.40 g, 1.00 mmol) and 4,4'-bipyridine (0.16 g, 1.00 mmol) in ethanol followed by the addition of few drops of water in hot condition. Yield: 0.36 g, 64%. Elemental anal. calc. (%) for $C_{44}H_{60}N_4O_{19}P_6$: C, 46.57; H, 5.33; N, 4.94. Found: C, 46.26; H, 5.58; N, 4.75. IR (KBr, cm^{-1}): 3376, 1608, 1130.

Synthesis of [$H_4TPA^{2-}.H_2TPA^{4-}.(H_2^{4,4'}BPy^{2+})_3.(H_2O)_8$] (4c)

Salt **4c** was prepared by the similar method as employed for **4a** by using H_6TPA (0.40 g, 1.00 mmol) and 4,4'-bipyridine (0.16 g, 1.00 mmol) in DMF followed by the addition of few drops of water in hot condition. Yield: 0.30 g, 65%. Elemental anal. calc. (%) for $C_{54}H_{82}N_6O_{26}P_6$: C, 45.77; H, 5.83; N, 5.93. Found: C, 45.56; H, 5.63; N, 5.77. IR (KBr, cm^{-1}): 3386, 1634, 1234.

Synthesis of [$H_5TPA^-.HPhen^+.(H_2O)_5$] (4d)

Salt **4d** was prepared by the similar method as employed for **4a** by using H_6TPA (0.40 g, 1.00 mmol) and 1,10-phenanthroline (Phen) (0.18 g, 1.00 mmol) in methanol followed by water (MeOH:H_2O = 1:2) in hot condition. Yield: 0.41 g, 61%. Elemental anal. calc. (%) for $C_{24}H_{39}N_2O_{14}P_3$: C, 42.86; H, 5.85; N, 4.17. Found: C, 42.66; H, 5.98; N, 4.05. IR (KBr, cm^{-1}): 3371, 1624, 1180 cm^{-1}.

Synthesis of [H_5TPA^-.$HPhen^+$.MeOH] (4e)

Salt **4e** was prepared by the similar method as employed for **4a** by using H_6TPA (0.40 g, 1.00 mmol) and 1,10-phenanthroline (Phen) (0.18 g, 1.00 mmol) in methanol followed by water (MeOH:H_2O = 1.5:0.5) in hot condition. Yield: 0.40 g, 68%. Elemental anal. calc. (%) for $C_{25}H_{33}N_2O_{10}P_3$: C, 48.87; H, 5.41; N, 4.56. Found: C, 48.56; H, 4.98; N, 4.25. IR (KBr, cm^{-1}): 3370, 1629, 1134 cm^{-1}.

Synthesis of [H_5TPA^-.H_4TPA^{2-}.H_3Terp^{3+}.S] (4f)

Salt **4f** was prepared by the similar method as employed for **4a** by using H_6TPA (0.60 g, 1.50 mmol) and 4,2':6',4''-terpyridine (Terp) (0.23 g, 1.00 mmol) in methanol followed by DMF in hot condition. Yield: 0.47 g, 49%. Elemental anal. calc. (%) for $C_{42}H_{60}N_4O_{19}P_6$: C, 45.14; H, 5.44; N, 5.04. Found: C, 45.32; H, 5.28; N, 5.13. IR (KBr, cm^{-1}): 3366, 1646, 1180.

Synthesis of 4'-(3,4-**dim**ethoxy**p**henyl)-4,2':6',4''-**t**erpyridine (**dmpt) (4g)**

To the methanolic solution of 4-acetylpyridine (2.00 g, 17.00 mmol), 3,4-dimethoxybenzaldehyde (1.37 g, 8.20 mmol) and 15% aq. KOH solution (6 mL), added ammonia solution (60 mL). The reaction mixture was stirred at room temperature till the complete precipitation occurred (~ 48 hrs). The solid was collected by filtration, washed thoroughly with H_2O, and dried in vacuum over P_2O_5. Recrystallization from chloroform gave light yellow powder of dmpt. Yield: 0.51 g, 17%. Elemental anal. calc. (%) for $C_{23}H_{19}N_3O_2$: C, 74.78; H, 5.18; N, 11.37. Found: 74.62; H, 5.10; N, 11.29. IR (KBr, cm^{-1}): 3012, 3003, 1594, 1512, 1455, 1395, 1258, 1022, 920. ^1H NMR (500 MHz, $CDCl_3$): d (ppm) 8.76 (d, 4H), 8.06 (d, 4H), 7.96 (s, 2H), 7.32 (m, 1H), 7.20 (d, 1H), 7.03 (d, 1H), 3.84 (d, 6H).

Synthesis of [$Cd(dmpt)_2(NO_3)_2$].X (4h)

The methanolic solution of $Cd(NO_3)_2.4H_2O$ (0.15 g, 0.50 mmol) was layered onto the chloroform solution of the ligand, dmpt (0.18 g, 0.50 mmol). The pale yellow colored crystals grown on the walls of the vial were filtered, washed with water and chloroform. Yield: 0.11 g, 40%. Elemental anal. calc. (%) for $C_{47}H_{38}CdN_8Cl_4O_{10}$: C, 50.00; H, 3.39; N, 9.92. Found: C, 50.12; H, 3.31; N, 9.83. IR (KBr, cm^{-1}): 2898, 1603, 1599, 1517, 1310, 1256, 1154, 1016, 830.

Synthesis of $[Cd(dmpt)_2Br_2].X$ (4i)

To the methanolic mixture of $Cd(CH_3COO)_2.2H_2O$ (0.50 g, 1.30 mmol) and NaBr (0.14 g, 1.30 mmol), dmpt (0.36 g, 1.30 mmol) in chloroform was added and the mixture was stirred for 5 hrs. The resulting white precipitate was filtered and washed with water and chloroform. The complex **4i** was recrystallized from hot DMSO. Yield: 0.23 g, 36%. Elemental anal. calc. (%) for $C_{48}H_{44}CdBr_2N_6O_5S$: C, 52.93; H, 4.07; N, 7.72; S, 2.94. Found: C, 52.69; H, 4.68; N, 7.23; S, 2.65. IR (cm^{-1}): 2929, 1605, 1598, 1520, 1458, 1399, 1260, 1160, 1017, 828, 576.

Synthesis of $[Cd(dmpt)_2I_2].X$ (4j)

The compound **4j** was prepared by the similar method as employed for **4i** by using KI in place of NaBr. The complex **4j** was recrystallized from hot DMF. Yield: 0.27 g, 38%. Elemental anal. calc. (%) for $C_{49}H_{45}CdI_2N_7O_5$: C, 49.95; H, 3.85; N, 8.32. Found: C, 49.87; H, 3.54; N, 8.52. IR (cm^{-1}): 2910, 1604, 1511, 1407, 1320, 1254, 1143, 1021, 834, 665.

Synthesis of $[Co(dmpt)_2Cl_2].X$ (4k)

The compound **4k** was prepared by the similar method as employed for **4h** by using $CoCl_2.6H_2O$ (0.12 g, 0.50 mmol) in place of $Cd(NO_3)_2.4H_2O$. The pink colored crystals were filtered, washed thoroughly with water and chloroform. Yield: 0.09 g, 43%. Elemental anal. calc. (%) for $C_{47}H_{39}CoN_6Cl_5O_4$: C, 57.13; H, 3.98; N, 8.51. Found: C, 57.50; H, 3.62; N, 8.60. IR (KBr, cm^{-1}): 2917, 1662, 1594, 1506, 1391, 1319, 1253, 1152, 1015, 820, 673.

Synthesis of $[Cd(dmpt)_2(SCN)_2].X$ (4l)

The compound **4l** was prepared by the similar method as employed for compound **4i** by replacing NaBr with KSCN in the same molar ratio. The complex **4l** was recrystallized from hot DMF. Yield: 0.41 g, 53%. Elemental anal. calc. (%) for $C_{50}H_{40}CdN_8O_4S_2Cl_6$: C, 49.79; H, 3.34; N, 9.29; S, 5.32. Found: C, 49.53; H, 3.54; N, 9.48; S, 5.43. IR (cm^{-1}): 2928, 1682, 1534, 1512, 1334, 1321, 1263, 1134, 1098, 816, 790.

Synthesis of $[Zn(dmpt)_2(NO_3)_2]$ (4m)

The compound **4m** was prepared by the similar method as employed for compound **4h** by replacing $Cd(NO_3)_2.4H_2O$ with $Zn(NO_3)_2.6H_2O$ (0.15 g, 0.50 mmol). The colorless crystals were grown on the walls of the vial. Yield: 0.14 g, 48%. Elemental anal. calc. (%) for

$C_{55}H_{59}ZnN_{12}O_{15}$: C, 55.35; H, 4.98; N, 14.08. Found: C, 55.54; H, 4.73; N, 14.22. IR (cm^{-1}): 2890, 1611, 1589, 1521, 1314, 1265, 1144, 1023, 832.

Synthesis of $[Cd.dmpt.(DMSO)_4].(ClO_4)_2.CHCl_3.X$ (4n)

The compound **4n** was prepared by the similar method as employed for compound **4h** by using $Cd(ClO_4)_2.6H_2O$ (0.21 g, 0.50 mmol) instead of $Cd(NO_3)_2.4H_2O$. The colorless crystals were grown on the walls of the vial. Yield: 0.29 g, 43%. Elemental anal. calc. (%) for $C_{34}H_{46}CdN_3Cl_{11}O_{14}S_4$: C, 30.22; H, 3.43; N, 3.11; S, 9.49. Found: C, 30.54; H, 3.23; N, 3.32; S, 9.21. IR (cm^{-1}): 3021, 2984, 2354, 1699, 1554, 1323, 1211, 1123, 1087, 835, 620.

Synthesis of $[Eu(dmpt)_2(NO_3)_2].X$ (4o)

The compound **4o** was prepared by the similar method as employed for compound **4h** by using $Eu(NO_3)_2.6H_2O$ (0.19 g, 0.50 mmol) instead of $Cd(NO_3)_2.4H_2O$. The pale yellow crystals were grown on the walls of the vial. Yield: 0.17 g, 56%. Elemental anal. calc. (%) for $C_{48}H_{40}EuN_8Cl_6O_{10}$: C, 45.99; H, 3.22; N, 8.94. Found: C, 45.63; H, 3.33; N, 8.52. IR (cm^{-1}): 3468, 3118, 3049, 2838, 2779, 2495, 2422, 2017, 1598, 1515, 1463, 1409, 1354, 1328, 1262, 1215, 1162, 1018, 849, 812, 762.

Gas adsorption measurement:

For CO_2 adsorption measurement, the micro crystals of each MOF were soaked in 1:1 dry dichloromethane and methanol mixture for 12 hrs. Fresh 1:1 dry dichloromethane and methanol mixture was subsequently added, and the crystals were allowed to stay for an additional 48 hrs to remove coordinated and free solvates (DMF/$CHCl_3$) present in framework. The sample was dried under a dynamic vacuum ($<10^{-3}$ torr) at room temperature overnight. To remove traces of lattice solvent molecules still present in the framework, samples were heated at 60 °C for 12 hrs and 100 °C for 12 hrs under a dynamic vacuum.

References:

1. Perrin, D. D., Armarego, W. L. and Perrin, D. R., "Purification of laboratory chemicals" 2nd ed., *Pergamon*, New York (1980).
2. Sheldrick, G. M., "SHELXTL-NT-2000 version 6.12, reference manual", *University of Göttingen*, Göttingen, Germany.
3. Sheldrick, G. M., SADABS, *University of Göttingen*, Germany (1996).
4. Sheldrick, G. M., "Phase annealing in SHELX-90, direct methods for larger structures", *Acta Cryst.*, **A46**, 467 (1990).
5. Mosby, W. L., "The reactions of some 1:4-dicarbonyl systems with hydrazine", *J. Chem. Soc.*, 3997 (1957).
6. Kruger, P. E., Moubaraki, B., Fallon, G. D. and Murray, K. S., "Tetranuclear copper(II) complexes incorporating short and long metal–metal separations: Synthesis, structure and magnetism", *J. Chem. Soc*., *Dalton Trans*., 713 (2000).
7. Bullpit, M., Kitching, W., Doddrell, D. and Adcock, W., "Substituent effect of the bromomethyl group. Carbon-13 magnetic resonance study", *J. Org. Chem*., **41**, 760 (1976).